

Development of hot-wire welding process for butt joint of thick steel plate

(厚鋼板突合せ継手のホットワイヤ溶接技術の開発)

March, 2021

Somchai Wonthaisong

Department of Mechanical Science and Engineering
Graduate School of Engineering
Hiroshima University

Abstract

The improvement of efficiency in the welding process is strongly demanded, especially in the large-scale ship construction field, since the total welding length exceeds several hundred kilometres. Presently, the thick steel plate has been employed for welding. Which strongly has the demand for high strength, quality, and property of weld metal. In those parts, shapes and sizes of shipbuilding's structures have been fabricated by the welding process. There are essential as well as necessary about high joint efficiency, low fabrication costs, and economical methods. The importance of welding of thick steel sheets that have to use both of the appropriate techniques and parameters. In order to get the product with the required features under employing high-current arc welding especially high-current CO₂ arc welding, tandem CO₂ arc welding, and submerged arc welding. Submerged arc welding (SAW) is an arc welding process that uses a consumable wire as an electrode. It has significant advantages of higher productivity, more stable arc, and no spatters compares with other welding processes.

Although, these welding processes have been developed and applied to increase the deposition rate, and productivity. It can achieve higher efficiency than the conventional arc welding process. They still have the problems, such as difficulty in optimizing welding conditions, small tolerances in welding conditions on an actual construction site, which affected to secure joint strength from a decrease in HAZ toughness and is difficult to control the joint properties.

In the proposed welding process, hot-wire CO₂ arc welding technology was developed for the high-efficiency and low-heat-input CO₂ arc-welding process for thick steel plates of 20 and 36-mm. The butt joint was welded by the combinations of hot-wire feeding speed and welding current. It was investigated the stabilities within the molten pool for determining the optimum condition and founding the main factor which affected the molten metal precedence. For hot-wire double lasers welding method was performed with the thick steel plate of 20-mm. It was able to decrease the deposition rate of weld metal using the stable laser combination with total laser power of 12 kW.

Firstly, the development of the high-efficiency welding process for 20-mm thick steel plate using hot-wire CO₂ arc welding method was performed in two passes that were completely fulfilled. Sound beads without any defects were achieved under the conditions with a deposit ratio above 1.0 (Fulfilled weld). The deposition capability for each combination of the welding current and hot-wire feeding speed depended on the stable arc molten pool from feeding the total filler wire of hot wire and its. Therefore, obtained conditions were the welding current of 350A and hot-wire feeding speed of 7.5 m/min, 400 A and 5 m/min, 450 A and 5 m/min, and 500 A and 5 m/min, respectively. The dilution ratio and HAZ width became smaller due to molten pool temperature deduced by the hot-wire feeding, and the welding current decreased. The Vickers hardness average of weld metal was reduced when heat input was increased from adjusting the step welding current up increased. The sound beads were evaluated the mechanical properties, which were performed by Charpy impact test,

tensile test, and bending test. Those test results complied with the standard value and without any defects when they were investigated.

Second part, hot-wire CO₂ arc welding process was applied with 36-mm thickness for finding the optimized conditions in each pass. The total volume of the combination of CO₂ wire and hot wire could be filled on the bead width, which was determined after finishing the previous pass. Therefore, filling the weld metal on each pass achieved under the appropriately groove-shape size and stability of molten pool. The obtained conditions of the butt joint can increase the high-efficiency welding by feeding the higher hot wire in welding with the wider bead width. The mechanical properties were evaluated by Charpy impact, tensile, and bending test. The results found that the welded joint properties met the standard requirements. Also, adjusting the welding speed could increase the welding time. Still, it cannot improve the hardness and toughness of weld metal due to the decreased heat input from changing the welding speed, which affected to cooling rate within the molten pool.

Finally, to study the hot-wire laser welding method for narrow-gap joint of 20-mm thickness, in the first part was researched using both of stable laser beams with total laser power of 12 kW. The optimal condition, the molten pool formation and joint creation were generated by using the stable laser beam combination of 32x2 mm and 26x2 mm, beam position arrangement on the bottom side, and welding speed of 0.4 m/min. The welded joint properties, the tensile strength met the requirement of the specification. The results of Charpy impact tests, the absorbed energy of weld metal and fusion line zone showed adequate values over 47 J at 0°C. For the second part, the optimum welding condition used for investigating the molten pool formation using the weaving head system was the combination of laser beam of 32x2.5 mm and 25x2.4 mm, and angle of fixed and weaving head as 30° and 10°. While weaving width of 0.65 mm was used. The achieved weld bead was evaluated of joint property with Charpy impact test according to the standard requirement. In some cases, the Charpy impact test result still had some lack of fusion from investigating the fracture surface and directions of the test specimen. The toughness results of notch location at weld metal and fusion line zone showed a low mean value even though it was used the weaving head system. An essential idea of this problem, using a high laser power on the bottom side of the weld groove can troubleshoot the occurred imperfection.

Table of Contents

Chapter 1	Introduction.....	1
1.1	Research background.....	1
1.2	Objectives and construction of the thesis.....	2
Chapter 2	Literature review.....	5
2.1	Introduction.....	5
2.2	Investigation of high-efficiency butt welding for high tensile strength steel using hot-wire MAG welding.....	5
2.3	Development status of narrow-gap welding	8
2.4	Laser beam welding and hot wire method.....	12
2.5	Hot-wire laser welding process for butt joint of thick steel plate	15
2.5.1	Novel single-pass vertical welding process using hot-wire laser for thick steel plate	15
2.5.2	Effects of joint parameters on narrow gap welding for high-strength steel plate using hot-wire laser welding process.....	16
2.5.3	Welding of thick steel plate by hybrid laser-arc welding.....	17
Chapter 3	Development of the high-efficiency welding technology for thick steel plate using hot-wire CO ₂ arc welding process.....	19
3.1	Introduction.....	19
3.2	Introduction of hot-wire CO ₂ arc welding method and its equipment.....	19
3.3	Preliminary experiment to investigate ability in multi-pass joining by using hot-wire CO ₂ arc welding process	22
3.3.1	Materials and specimen used.....	22
3.3.2	Geometric calculation of number of passes for filling V-shaped groove before welding.....	23
3.3.3	Proper hot-wire current.....	26
3.3.4	Experimental procedure.....	28
3.3.5	Macroscopic method and calculation of power consumption.....	30
3.3.6	Result and discussion of capability of hot-wire CO ₂ arc welding..	33
3.3.6.1	Capability of hot-wire CO ₂ arc welding for thick steel plate.....	33
3.3.6.2	Effects of welding conditions on weld bead properties...	37
3.3.6.3	Reduction of power consumption and arc time.....	39
3.4	Optimization of welding conditions for thick plate joining.....	40
3.4.1	Materials and specimen.....	41
3.4.2	Experimental setup and welding conditions.....	42
3.4.3	Microstructural characterization and mechanical properties.....	44
3.4.4	Geometric calculation of two passes welding.....	44
3.4.5	Result and discussion.....	46

3.4.5.1	Optimization of wire feeding speed combination for CO ₂ arc welding and hot-wire.....	46
3.4.5.2	Weldment properties.....	51
3.5	Summary.....	58
Chapter 4	Investigation of welding phenomena and optimization of hot-wire CO₂ arc welding process for 36-mm heavy-thick steel plate.....	60
4.1	Introduction.....	60
4.2	Effects of groove shape on molten metal precedence.....	61
4.2.1	Materials and specimen used.....	61
4.2.2	Experimental procedure.....	63
4.2.3	Result and discussion.....	64
4.3	Optimization of multi-pass welding conditions for 36-mm heavy-thick joint.....	69
4.3.1	Materials and specimen used.....	69
4.3.2	Experimental procedure.....	71
4.3.3	Macro specimen preparation and Initial measurements of weld metal.....	75
4.3.4	Results and discussions.....	76
4.3.4.1	Influence of hot-wire feeding speed on molten pool phenomena.....	76
4.3.4.2	Effects of groove-shape size on melting metal flow in molten pool.....	77
4.3.4.3	Evaluation of joint properties.....	82
4.4	Optimization of welding conditions for faster welding speed.....	89
4.4.1	Introduction.....	89
4.4.2	Predictions of heat input and additional material volumes under various welding speeds.....	90
4.4.3	Specimens and welding conditions.....	90
4.4.4	Joint creation using appropriate welding conditions.....	101
4.4.5	Results and discussion.....	103
4.4.5.1	Property evaluations of the butt joint.....	104
4.5	Summary.....	108
Chapter 5	Development of hot-wire double lasers welding method for thick steel plate.....	109
5.1	Introduction.....	109
5.2	Materials and specimen used.....	110
5.3	Experimental procedure and equipment.....	111
5.4	Investigation of molten pool formation and joint creation using stable laser beam combination.....	114

5.4.1	Fundamental investigation of molten pool formation and joint creation using stable laser beam combination of 23x2 mm and 17x2 mm.....	115
5.4.1.1	Welding conditions.....	115
5.4.1.2	Results and discussion.....	117
5.4.2	Effects of stable laser beam combination on molten pool formation and joint creation.....	121
5.4.2.1	Welding conditions.....	121
5.4.2.2	Results and discussion.....	125
5.4.3	Joint creation using stable laser beam combination of 32x2 mm and 26x2 mm and evaluation of joint properties.....	129
5.4.3.1	Welding conditions.....	129
5.4.3.2	Results and discussion.....	130
5.5	Investigation of molten pool formation and joint creation using weaving and stable laser beam combination.....	138
5.5.1	Materials and specimen used.....	138
5.5.2	Welding conditions.....	139
5.5.3	Results and discussion.....	145
5.5.3.1	Molten pool and bead formations.....	145
5.5.3.2	Evaluation of joint properties.....	151
5.6	Summary.....	154
Chapter 6	Summary and future work.....	155
	Acknowledgements.....	157
	Reference.....	158
	Published or summited papers in regard to this thesis.....	167
	Presentations.....	168

Chapter 1

Introduction

1.1 Research background

In large-scale ship construction, there is strong demand for improvements in productivity, and quality especially in the welding process for the thick steel plates [1, 2] such as weather deck, machinery space, store side tank, cargo space, and others. It is important to design the structures to minimize the manufacturing costs with high-efficiency welding. Recently, the conventional welding process and multiple arc submerged arc welding (SAW) are widely employed on the long joint of inner bottom plates of cargo ships as shown in Fig. 1.1.

New welding processes have been developed and their conditions have been optimized to improve welding efficiency without a large increase of a heat input in order to maintain joint qualities and properties. In addition, new steel plates and filler wires have been developed and applied to maintain or improve joint properties under the much higher heat input condition for the higher welding efficiency [4-8].



Fig. 1.1 Photos of submerged-arc welding (SAW) and shipbuilding industry.
(Image courtesy of Tsuneishi shipbuilding Co., Ltd.) [3].

In the welding stage for thick steel plates using the high-productivity process such as high-current CO₂ arc welding, tandem CO₂ arc welding, and submerged arc welding, it is very important to select the appropriate welding processes and welding parameters in order to achieve the high efficiency and the required joint features [9-16]. Submerged arc welding (SAW) is an arc welding process which uses a consumable wire as an electrode [17]. A blanket of granular and fusible flux is used for shielding from atmospheric contamination and obtaining refined action of the slag during SAW [9]. SAW has significant advantages of higher productivity, more stable arc, and no spatters compared with other welding processes [18]. However, the flat position and flat plates are required for thick steel plates welding with the stable weld quality and high deposition rate [19].

The CO₂ gas shielded one-side welding process using two electrodes is one of the high-efficiency welding process employing a large arc current on both electrodes arranged in tandem along the welding direction. This single-pass efficient welding process has been developed for thick steel plates of 12-22 mm, and the process has not adversely affected the joint properties because of its lower heat input [20]. The cable welding wire (CWW) CO₂ welding is the newly developed process using the cable-type solid-welding wires. It can increase the deposition rate and own the ability to improve the high efficiency, quality, and low consumption of the welding production as well. [21-22].

New welding processes, such as gas–tungsten arc welding (GTAW), gas–metal arc welding (GMAW), SAW, and laser welding, in combination with hot-wire feeding have been developed and applied to improve productivity in manufacturing fields other than shipbuilding [23-31]. Welding phenomena and optimization of hot-wire feeding conditions have been investigated for the GTAW process. It has been suggested that the hot-wire current must be appropriately controlled to heat the tip to its melting point to achieve stable welding phenomena and higher efficiency. It has also been clarified that the deposited volume, i.e., hot-wire feeding speed, can be controlled independently of the arc current as the main heat source. Improvement in efficiency has been investigated for GMAW processes using CO₂ gas and a mixed gas (Ar+CO₂). From previous investigations, it was expected that combining hot-wire feeding with the welding process has potential to achieve both high efficiency and low heat input.

1.2 Objectives and construction of the thesis

The main objective of this research to develop the high-efficiency welding technology for thick steel plate joining using the hot-wire system which has the advantages not only in terms of efficiency, but also in terms of cost and joint characteristics for many industries, especially for a large-scale ship construction. CO₂ arc welding is generally used in many industries especially in the large-scale shipbuilding industry because of its economic efficiency and process efficiency. However, there are difficulties such as a very narrow tolerance of welding conditions

and the inability to obtain stable welding phenomena when aiming for higher efficiency using conventional CO₂ arc welding. In addition, the deteriorations of the joint quality and properties occur due to the higher heat input especially in high-efficiency welding for thick steel plates.

On the other hand, the novel welding process, which can decrease dramatically the heat input and improve the process efficiency, is strongly demanded in the large-scale shipbuilding industry. Laser welding and laser-arc hybrid welding have been attracted and studied. These laser processes have already been applied especially for thin-steel plates joining such as the automobile industry. However, there are many problems in the application for thick-steel plate joining such as the higher cost because of a high-power laser oscillator, a very small tolerance of a joint gap because of a small laser spot for deep penetration, uncontrollable joint properties because of a high dilution, cracking during welding, and so on.

In this study, 20-mm and 30-mm thickness steel plates were selected as the target materials for hot-wire CO₂ arc welding and hot-wire double lasers welding processes since these thick steel plates are widely used for the large-scale ship structures. Figure 1.2 shows the flow chart of the construction of the thesis.

Chapter 1 discusses the background of research as well as the objective and construction of the thesis.

Chapter 2 reviews the theoretical background, related information and present researches on welding of the butt joint of thick steel plates and high-efficiency welding processes, etc. In addition, narrow-gap welding and an innovative welding method of hot-wire laser welding processes are discussed.

Chapter 3 is to develop the high-efficiency welding technology using hot-wire CO₂ arc welding method for thickness 20-mm steel plate. The first part was investigated the deposition capability for each combination of welding current and hot-wire feeding speed. In the second part, sound filled joints were performed under the optimal welding conditions and evaluated the mechanical properties evaluation for thick plate joining.

In Chapter 4 carry out by using CO₂ hot-wire welding process for 36-mm heavy-thick steel plate. The welding condition was based on the results of the above trials in the Chapter 3. In this Chapter, the obtained conditions are optimized to achieve a deposit ratio in each pass where was combined between hot-wire feeding speed and its volume. Finally, sound filled joints were investigated the cross-section and evaluated the joint properties of long weld bead in a practical welding.

In Chapter 5, improvement of novel welding process using hot-wire double lasers method for the thick steel plate of 20-mm was presented in the narrow gap joint. The combination of double laser oscillators with total laser power of 12 kW, both diode lasers were used with a hot-wire system. In this Chapter was studied the feasibility using stable laser beam combination for molten pool formation, and joint

creation and applying weaving, and stable laser beam combination. Finally, cross-sectional observation of the obtained condition was investigated and evaluated the joint properties.

Finally, the conclusions of this thesis are summarized in chapter 6.

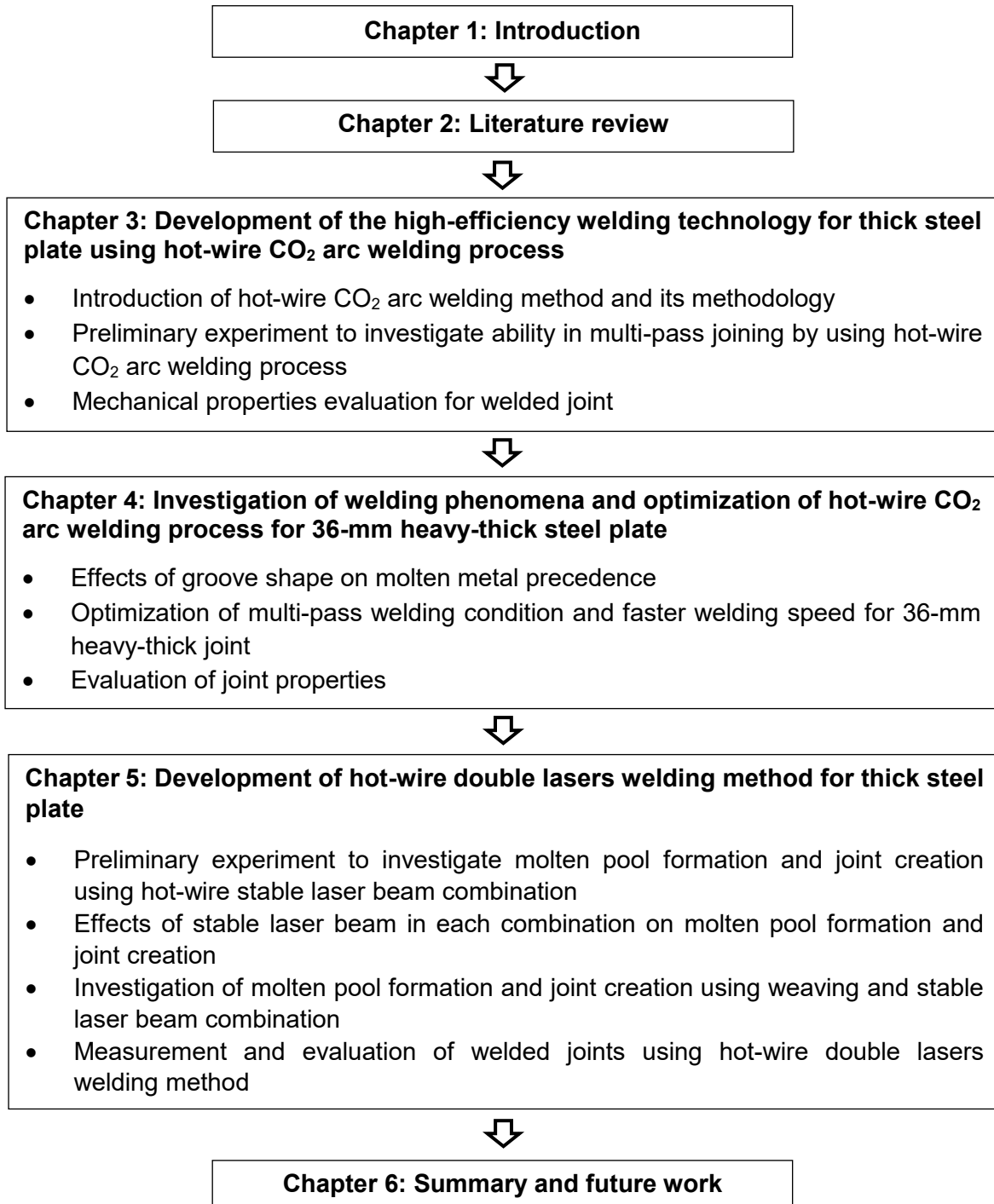


Fig. 1.2 Construction of the thesis.

Chapter 2

Literature review

2.1 Introduction

This chapter discusses the theoretical background, related research and present researches on the high-efficiency welding process in the large-scale ship construction field. The improvement of productivity, process flexibility and quality of welded joint is strongly demanded especially for thick steel plates using hot-wire CO₂ arc welding method. In addition, it is applied with hot-wire laser welding method on the narrow-gap joint and compared about the welding capabilities of both processes by the welding technology using hot wire.

2.2 Investigation of high-efficiency butt welding for high tensile strength steel using hot-wire MAG welding

Construction of machinery industry has applied a thickness of 8~25 mm of steel plate approximately which has a rate of deposited metal weight about 3~5% in total weight as a large time spent in operation. Welding process improvements by shortening of weldment, there are strongly demanded to increase weld deposition efficiency, high-efficient production, flexibility and quality of welded joint in a large-scale construction. Hence, MAG welding process has been employed for thick steel plate which is easy to ensure amount of deposited metal. For tandem arc welding and two arcs are simultaneously welded by two welding wires. They have been devised by simply increasing arc current to add amount of weld metal and can be fed the filler wire, or welded with an electrodes using a relatively low arc current [32]. Therefore, application of hot-wire MAG welding method to high tensile strength steel plate, which can control a welding consumables and hardly increase amount of heat input as shown in a schematic diagram of MAG welding, tandem arc welding, and hot-wire MAG welding in Fig. 2.1.

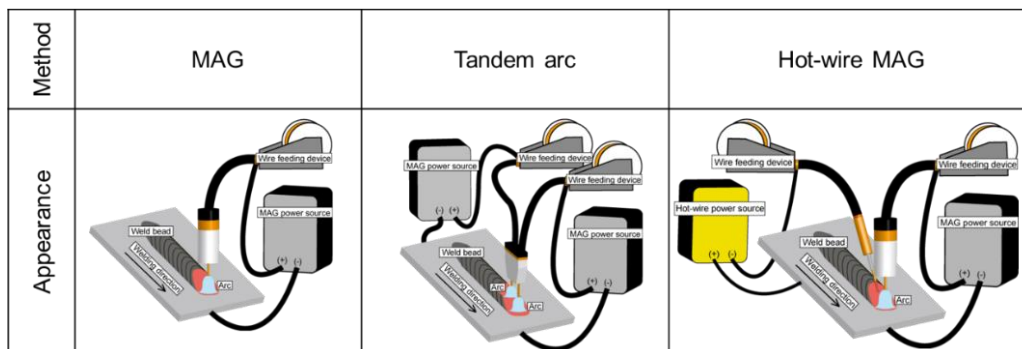


Fig. 2.1 Outline of welding method [33].

Hot-wire MAG welding method is a combination of hot-wire system and MAG welding method in which the hot wire is electrically heated through a positive direct current electrode and is conformable to base on joule heating's principle. It is applied to use with a molten pool of MAG welding process as shown in Fig. 2.2.

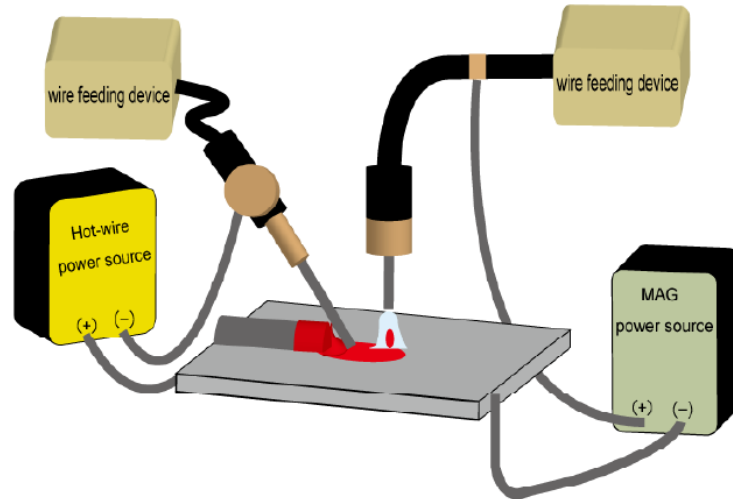


Fig. 2.2 System of hot-wire MAG welding method [33].

There are many studies regarding the hot-wire MAG welding process which carried out bead on plate welding to consider a basic penetration depth and thermal influence on hot-wire MAG welding system. The bead appearances and cross-sections as shown in Figs. 2.3 and 2.4, it clearly can be seen that as the hot-wire feeding speed and arc current are high. The increase of deposited volume of weld metal increase almost linearly with both relationships of welding condition. Conversely, the deposit ratio of weld metal from the increase of hot-wire feeding affects to decreasing the penetration depth due to the increased weld metal impede the transmission of the heat of arc. The results find that a reduction of penetration depth is shallower than welding without the hot-wire feeding when is compared with the hot-wire feeding speed of 10 and 15 m/min as shown the relationships in each condition in Fig. 2.5 [34].

Chapter 2 Literature review

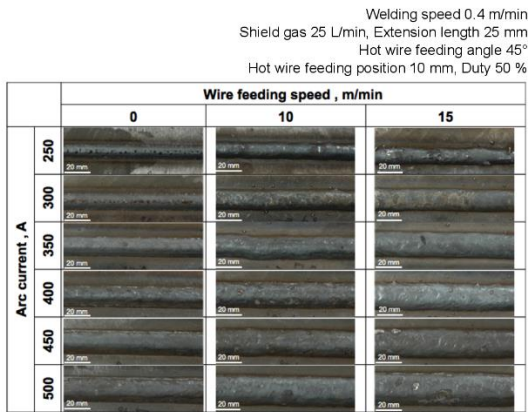


Fig. 2.3 Appearance of weld bead [34].

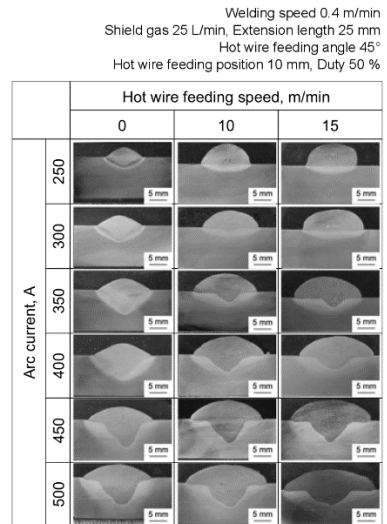


Fig. 2.4 Cross-section of weld bead [34].

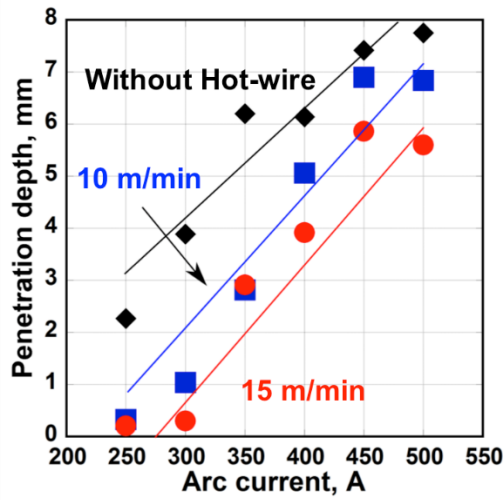


Fig. 2.5 Relationships between arc current and penetration depth [34].

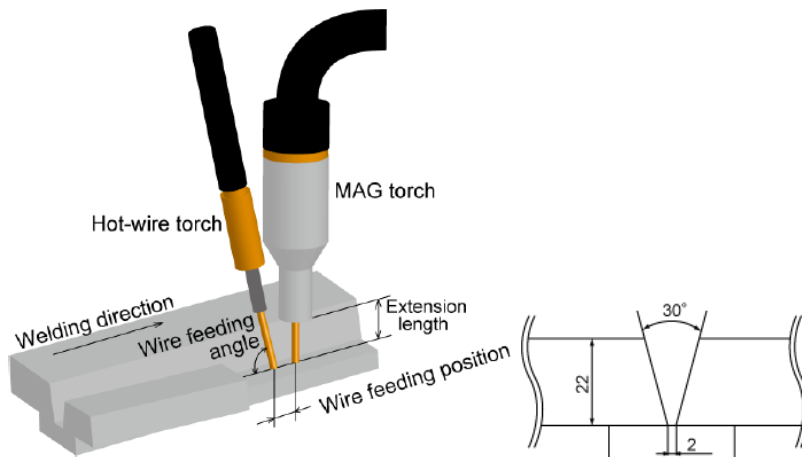


Fig. 2.6 Schematic illustration of hot-wire MAG welding method [34].

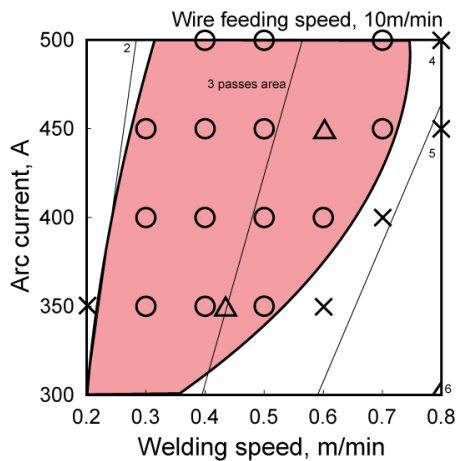


Fig. 2.7 Adequate welding condition [34].

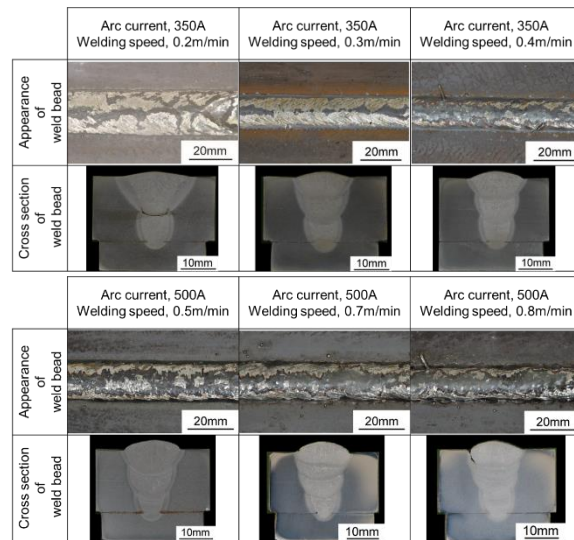


Fig. 2.8 Appearance of weld bead and cross-section [34].

Figure 2.6 shows the hot-wire MAG welding method for welding in V-groove shape which is used the combination between each arc current and welding speed while hot-wire feeding speed is fixed on the second pass for 22-mm thickness. Figure 2.7 shows the estimated result when the welding current is varied as 350~500 A on welding speed of 0.2~0.7 m/min respectively and hot-wire feeding speed is fixed as 10 m/min. This result shows that the arc current affects the number of passes on each welding speed, as shown in the adequate welding condition on red area. For example; the results of bead appearance and cross-section, which are carried out in each arc current and welding speed as shown in Fig. 2.8. Therefore, it is confirmed that the hot-wire MAG welding method can increase the double deposited volume of weld metal when compares with a conventional MAG welding process [34].

2.3 Development status of narrow-gap welding

Developments of the narrow-gap welding technology have been applied to join heavy, and thick sections in large structures. These technologies have the advantages to serve industrial requirements in both weld quality and productivity for instance, increased productivity, reduced distortion and reduced residual stress [35-38].

Preparations of a small groove joint is a slightly U-shaped or parallel sidewall, which is the directly related advantage as shown in Fig. 2.9. A single of double V-groove joint preparation is used in a traditional welding method normally with larger angle or a groove angle of 30° [35-36]. The narrow-gap welding for a thick plate leads to a small amount of weld metal and less time than traditional welding processes.

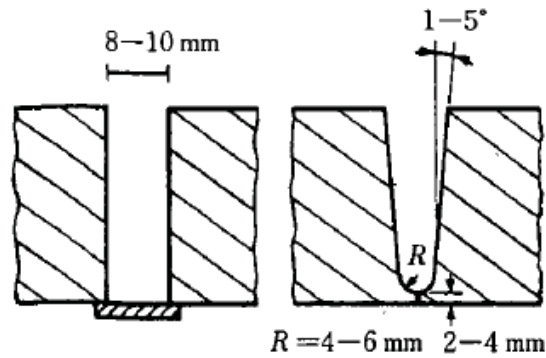
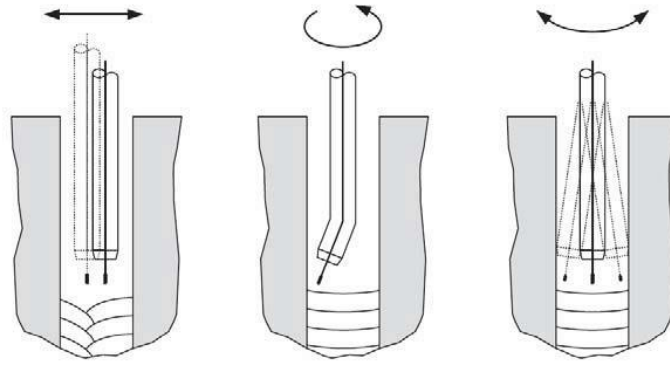


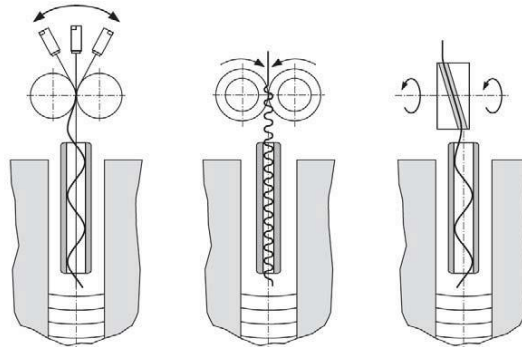
Fig. 2.9 Typical narrow-gap joint [39].

Narrow-gap welding (NGW) is widely used in international welding industries, which was first recognized in the USSR by Dudko, et al. [37], Meister and Martin [38] additionally improved the method in the United States in 1966. The development of this method is proposed to increase the high efficiency of deposited volume of weld metal by reducing the filler wire in a thick plate welded joint. The welding processes generally applied in a narrow-gap joint are GMAW, SAW, and GTAW. Electro gas and electro slag welding are used in some applications [40-43]. In addition, study of laser and laser arc hybrid welding, it is practically used [44-46]. Furthermore to welding method with a narrow groove, variety of approaches to fill the welding wire have been developed because they can achieve a sound bead such as a filler wire feeding technique, number of electrodes, and arcing manipulation, etc. Applications of electro slag and electro gas welding are used with a narrow gap joint in order to weld a thick steel plate especially in railway welding which is long vertical joint [47]. This method can achieve a high-quality welds by single-pass welding only, which has formations and defects. Infallibility of edge preparations is not required. Nevertheless, such a process encourages to very high dilution in the base metal and persuades a coarse grain structure in the heat affected zones (HAZ), and weld metal which obtain in low toughness without post weld heat treatment.

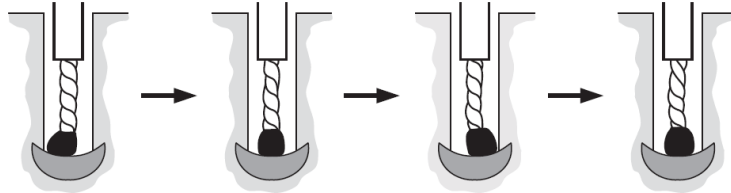
NG-GMAW (Narrow-gap welding using GMAW) is one of the most widely applied specifically in Japan [47]. It can give a high ability to weld in all positions with a low weld metal hydrogen content and a shielding gas is needed. An increase of higher productivity can achieve from a deposition rates tremendously by continuously feeding wire and more electrodes. In order to achieve a welding quality, proper melting of the sides of the joint is assured by a specially designed torch that fits into a narrow gap, while the welding arc will be alternately moved to the right and left of the weld groove. Having a different techniques of the feeding wire movement mainly applied as shown in Fig. 2.10. However, the innate defects related to lack of sidewall fusion, arc instability to magnetic fields and spattering build-up, which must be seriously considered [39, 43, 48-49]. Consequently, the range of appropriate welding parameters to obtain a high-quality weld is somewhat limited and highly skilled welder is required.



(a) NG-GMAW process variants - oscillation of straight fed wire.



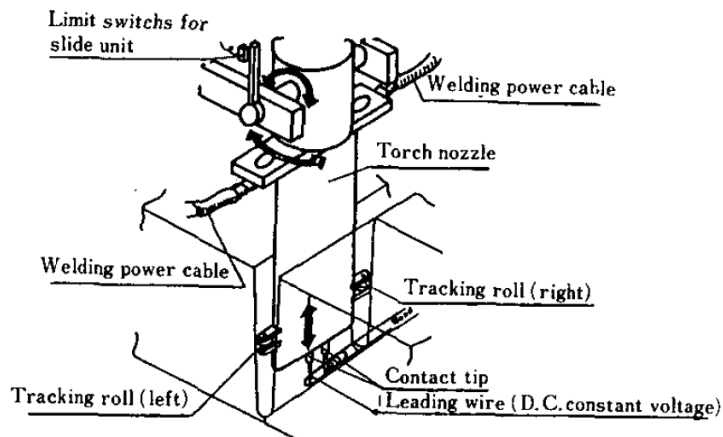
(b) NG-GMAW process variants - corrugation of wire to achieve oscillation.



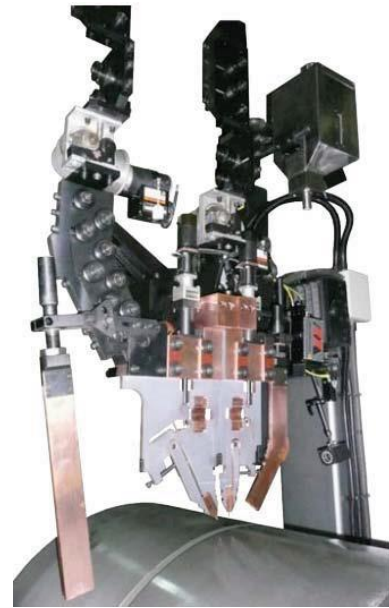
(c) TWISTARC NG-GMAW variant.

Fig. 2.10 Types of movement of the melting wire in NG-GMAW [39, 50].

NG-GMAW and SAW are compared with a narrow gap (NG-SAW) giving the higher deposition rates, and main advantages to overpower an inadequate fusion of sidewall and porosity. The wider tolerance of welding conditions to achieve a dependable welding joint is an attractive benefit for practicable use. NG-SAW method wants a suitable flux to produce gases and slag to protect the molten pool and arc. Compounding elements in the flux can be filled into the weld pool for improving weld metal properties as shown in Fig. 2.11. However, such application is ordinarily limited in the flat position. Furthermore, and major drawback is the difficulty of slag removal, which can give the defects like slag inclusions [47, 51-53].



(a) Schematic illustration of NG-SAW [39].



(b) Tandem twin wire SAW welding head and ancillary equipment [54].

Fig. 2.11 Narrow-gap SAW welding.

Likewise to NG-SAW, electro slag welding can give a high heat input due to this process still affects to grain growth on HAZ and reduced strength. Presently, narrow-gap GTAW process has been improved, and has the advantages such as no slag, no spatter, and high-quality weld metal in all welding positions. This process can control the heat input, wire feeding rate, and greater melting on a groove sidewall of butt joints, which there is the potential to relieve incomplete fusion defects. This process is mostly used in a high strength low alloy steel, titanium, and stainless steel as shown in Fig. 2.12.

The combination between NG-GTAW and hot-wire system as presented in Fig. 2.13 has been developed and is an attractive alternative for a need to increase deposition rate, which can control heat input independently. Achieved welding would be protected by a good shielding gas, which the arc reaches the weld groove of the joint that is the key point [50, 55-57]. Because of a small gap preparation of weld bead and the limitation of size, and electrode torch heads, which have the different techniques of electrode handling developed to obtain a nice weld quality as displayed in Fig. 2.14. However, a complicated equipment and special electrode torch head are needed due to the limited accessibility to preparation for a narrow-gap welding.

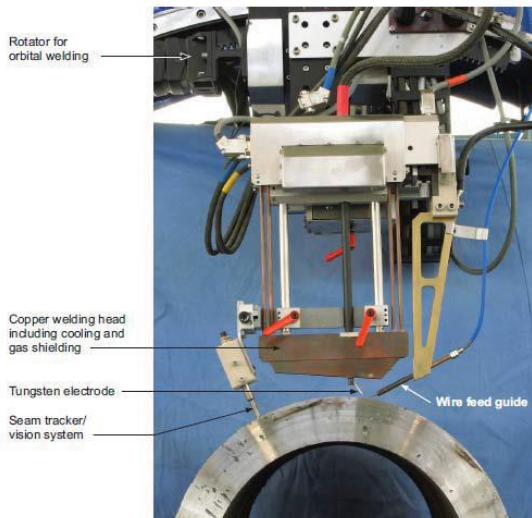


Fig. 2.12 Typical Narrow-gap GTAW welding with an orbital torch. [Image courtesy of Polysoude]

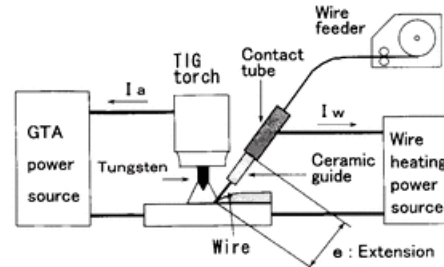


Fig. 2.13 Basic of Hot-wire GTAW [50].

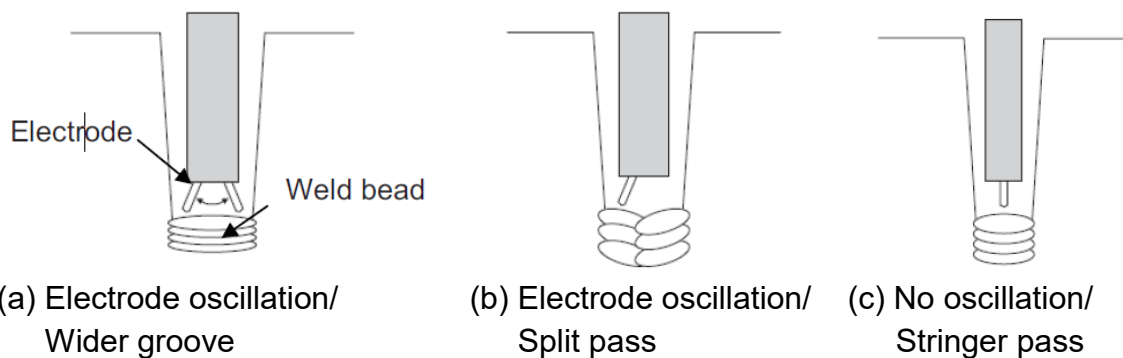


Fig. 2.14 Handle modes of welding electrode and weld pass in NG-GTAW [57].

For other processes can be applied for narrow-gap welding such as laser and hybrid laser-arc welding are interesting processes [44-46]. Even though these processes provides any advantages such as the high energy density, high welding speed, i.e., this process has the potential to generate defects and weld spatter of arcing as well

2.4 Laser beam welding and hot wire method

Laser beam welding (LBW) is a welding method applying a laser to joint pieces of metal or thermoplastic. The LBW gives extremely concentrating power density of laser spot which results in deep weld bead and narrow gap, high-speed welding, less distortion, low dilution and small HAZ that is a low heat input welding process. Furthermore, enough power density can form the keyhole using for deep penetration

with welding thick plates in several weld passes [58-61]. An angle and position with LBW on horizontal and vertical direction can effect to more defects of pores and undercuts that are difficult to success a sound weld joint due to action of gravity [62-64].

Hot wire method, principle of initially generating heat in feeding a filler wire is shown a sequential steps as illustrated in Fig. 2.15 [65]. At first step, the energization distance is determined between a work piece and a copper contact tip. Then the filler wire is fed through the copper contact tip until it touches the workpiece which there is negative electrode. The flow of electric current through a fed filler wire, which receives from copper contact tip directly and is complete with a closed loop circuit of the joule heating law. The heat occurred, it is generated under having a value of electrical resistance is high in the filler wire while a defocus laser beam operates a charge to contribute the volume of thermal volumetric energy in the hot wire in excess of the melting temperature slightly [66]. Accordingly, a complete molten pool is obtained by using low heat energy among feeding the hot wire at a rear laser beam and the hot wire is put into the molten pool continuously. For example; temperature distributions on filler wire to effect of wire current, at wire current of 121 A obtains a lower temperature than the current of 133 A [67]. Increasing the weld metal, that is added by the hot wire into the molten pool and it can increase the deposited volume of weld metal depending on wire feeding speed. In order to increase welding and reduce heat input, which it is observed the welding phenomena during welding from combination between GTAW and hot-wire feeding as shown in Fig. 2.16 [67-69].

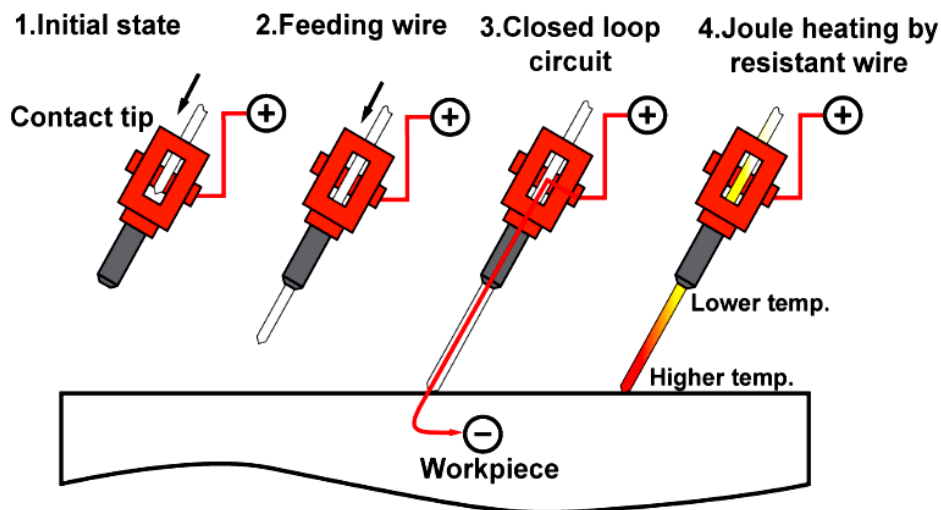


Fig. 2.15 Schematic layout of a hot-wire system.

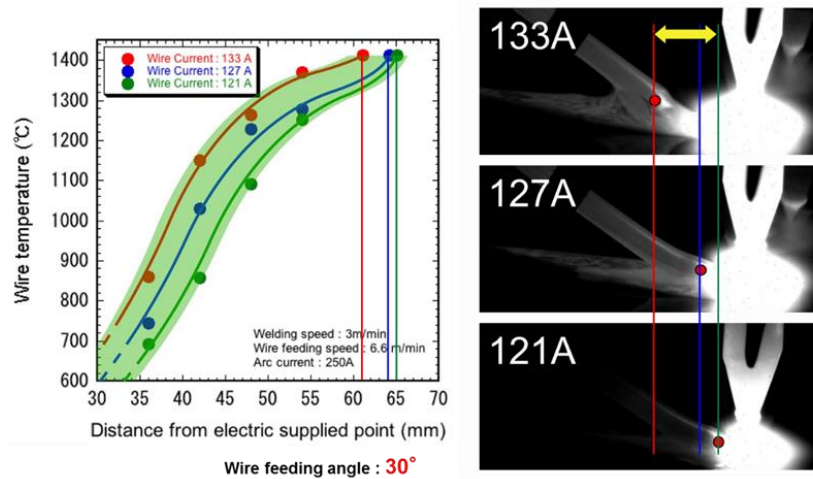


Fig. 2.16 Effect of wire current on temperature distributions of filler wire.

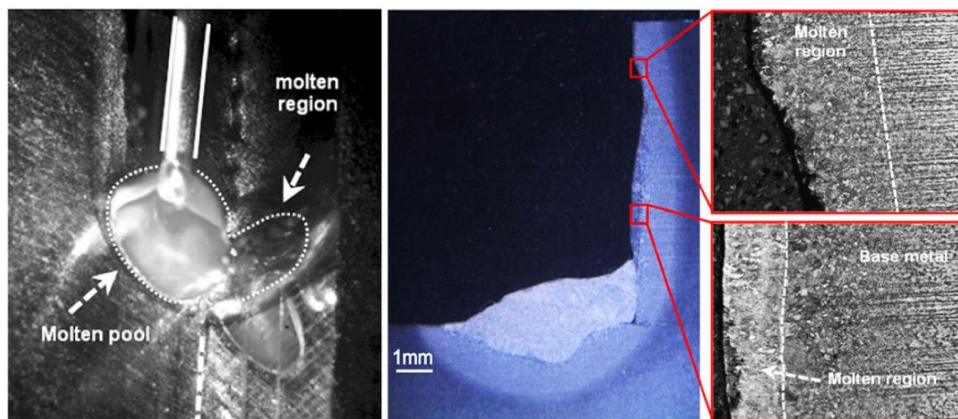


Fig. 2.17 Effect of laser beam reflection welded by a laser with a hot-wire feeding.

Hot-wire laser welding process is a combination of laser irradiation and hot-wire feeding. It has been investigated by in-situ observation with a high-speed camera during which laser beam welding on a basis of independently controlling melting between the hot wire and base metal as shown the result in Fig. 2.17. The high-speed image and cross-section, it is observed the melting phenomena of the groove wall and molten pool surface by reflected laser beam. This is outstanding evidence showing that the energy of scattering laser irradiation can increase the penetration depth at the groove side-wall and create the molten pool for the hot-wire feeding in narrow-gap welding [70-71]. Increasing deposition rate, reducing laser power and heat input can improve an application in many kinds of welding fields which has been examined such as the fillet welded joints of medium-thick plate for shipbuilding and bridge [72-73], lap joint of the high tensile/ultra-high tensile strength steels with a wider gap for an automobile body [74], and welding in a narrow-gap joint to reduce large shrinkage, residual stress and welding deformation.

2.5 Hot-wire laser welding process for butt joint of thick steel plate

2.5.1 Novel single-pass vertical welding process using hot-wire laser for thick steel plate

New single-pass vertical welding method is proposed to reduce the heat input and laser power as shown in Fig. 2.18. Preliminary investigations in welding phenomena by combining a diode laser with a large rectangular beam spot and hot-wire feeding system were performed on steel plates. In addition, the important factors were investigated experimentally, namely laser power, weaving of laser beam spot, gap width, laser irradiating angle, etc. [75-78].

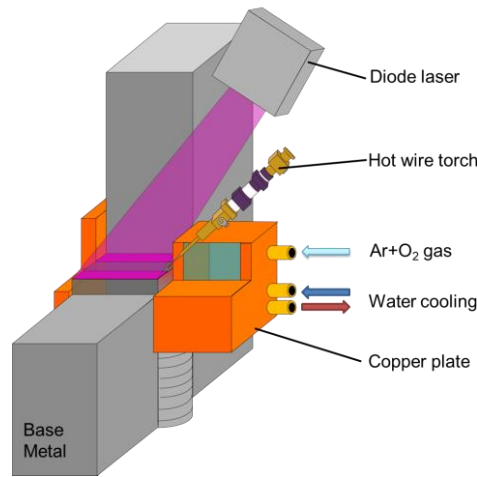


Fig. 2.18 Illustration of single-pass vertical welding using hot-wire laser.

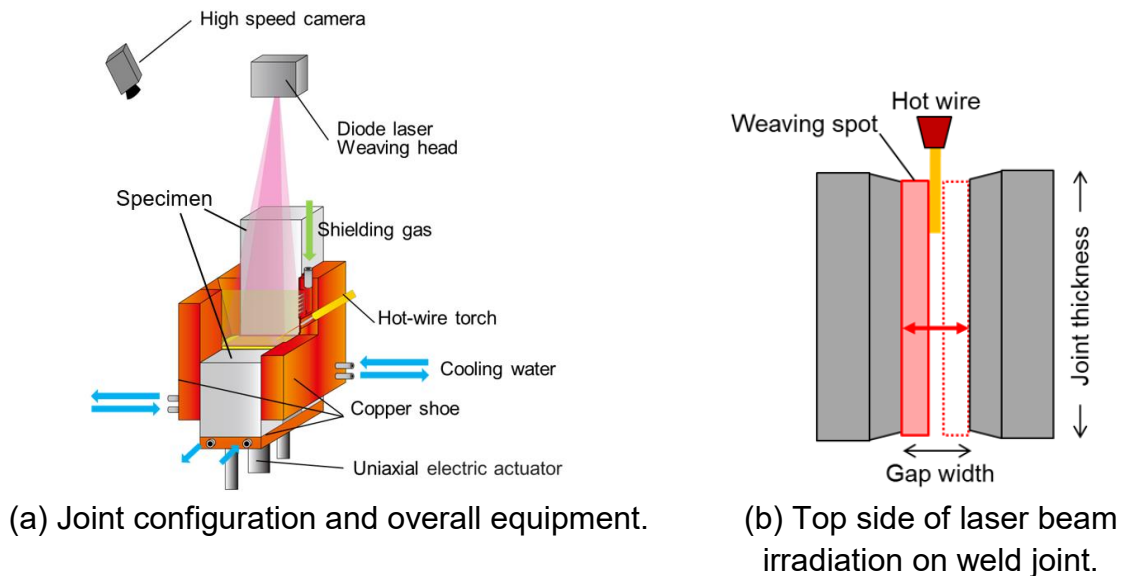


Fig. 2.19 Apparatuses of hot-wire laser single-pass vertical welding using the weaving system through on weld groove [79].

Sittisak (2019) studied the use of laser spot size and its motion by a weaving system for a vertical welding process, the schematic layout as shown in Fig. 2.19. The results find that the laser beam irradiation is controlled by the weaving system with applying the narrow beam having the high power density. It can optimize the laser power to keep the molten pool and to melt the base metal especially the combination of a weaving system and high-edge energy type [79].

2.5.2 Effects of joint parameters on narrow gap welding for high-strength steel plate using hot-wire laser welding process

Narrow-gap welding for high-strength steel plate of 12-mm thickness is performed under various conditions such as the welding speed, groove width, weaving width, and rectangular laser beam dimension to obtain a high quality, high efficiency joints without any defects. Hot-wire laser welding process is used as shown in Fig. 2.20 to succeed a sound weld joint with testing of mechanical properties [80-81].

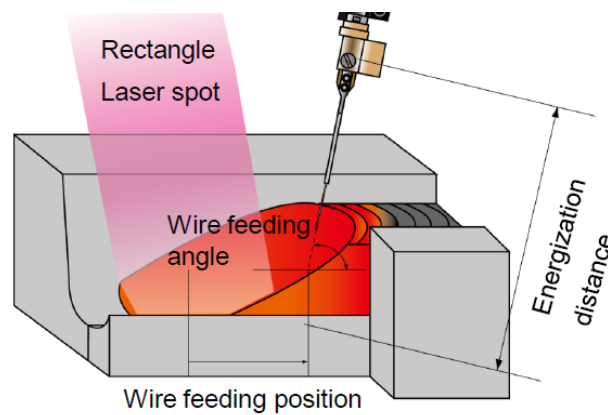


Fig. 2.20 Schematic diagram of hot-wire laser welding [82].

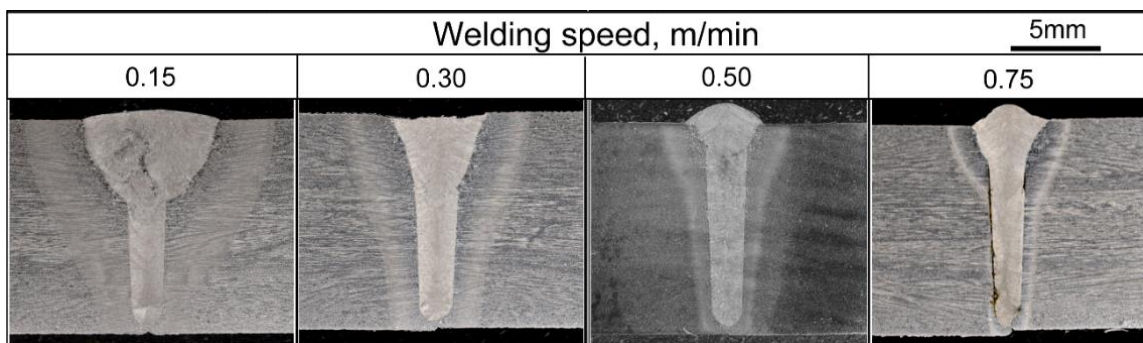


Fig. 2.21 Cross-sections of HT780 bead [82].

This results find that using the laser weaving width of 0.62 mm and welding speed of 0.5 m/min can minimize a fusion defects from investigating a cross-section of weld bead as shown in Fig. 2.21 when is compared with each welding speed. Due to the weaving width of laser beam is suitable to irradiation on sidewall and bottom side under laser power of 6 kW sufficiently. The obtained butt joint is examined a HAZ width where can be suppressed by changing a welding speed. The toughness of welded part is confirmed by Charpy impact test according to a specification requirement [82].

2.5.3 Welding of thick steel plate by hybrid laser-arc welding

The developments of materials manufacture have been under a higher requirements of welding technology and power consumption. The variations of hybrid laser-arc welding process such as laser-GMA, laser-plasma, laser-TIG, etc. are a combination of laser welding with traditional welding method. These process can increase a high productivity, efficiency, deep penetration and welding quality, and small heat affected zone (HAZ) [83-87].

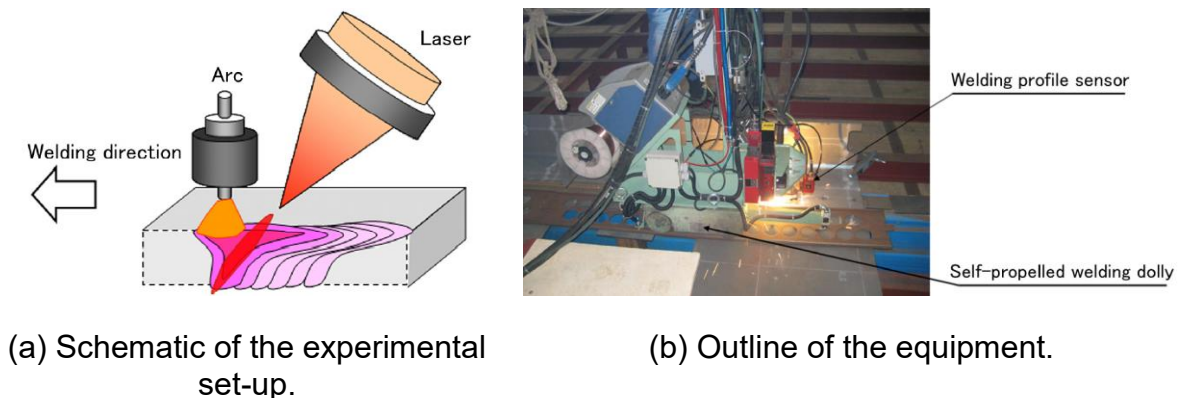


Fig. 2.22 Illustration of hybrid laser-arc welding [87].

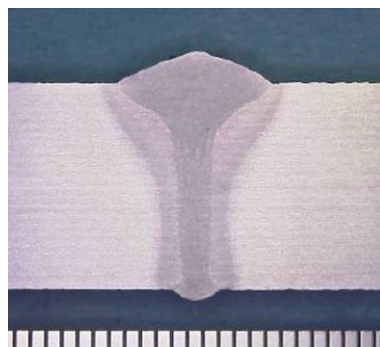


Fig. 2.23 Bead cross-section profile [87].

MHI (2010) reports about the industrial use of hybrid laser-arc welding in general commercial ships. This process is a combination of laser welding with traditional TIG welding as shown in Fig. 2.22. It has been developed and established a novel welding process in application for reduction of welding deformation.

For example, this welding method was applied to actual ships for butt joint of 13-mm thin steel plates or less in thickness as shown the bead cross-sectional profile using hybrid laser-arc welding in Fig 2.23. The results find that this process can reduce deformation after welding by using low-heat welding. The mechanical property of weld metal was carried out to evaluate the toughness property by Charpy impact test. It met the standard requirement and is sufficient for application to actual ships [87].

Chapter 3

Development of the high-efficiency welding technology for thick steel plate using hot-wire CO₂ arc welding process

3.1 Introduction

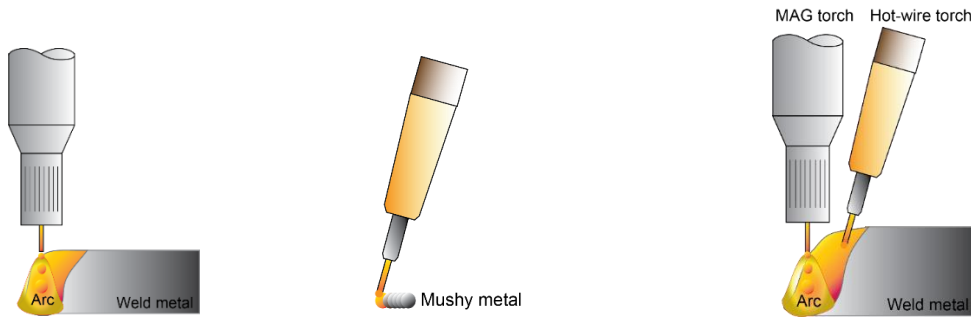
Generally, the high-current CO₂ arc welding process is suitable for joining the thick steel plate. The conventional arc welding processes require the high heat consumption to increase the deposition rate and their productivity. However, the influence of heat input can deteriorate the properties both of the weld metal and the adjacent of weld metal known as the heat affected zone (HAZ). In the HAZ, the metallurgical structure probably changes which mean its directly affect their mechanical properties.

In this chapter, the methodology of welding by using the high-efficiency welding technology is presented. The aim of experiment is increasing the productivity of 20-mm thickness steel plate. The combination of the CO₂ arc welding process and the hot-wire system were investigated with a solid wire as filler metal. Due to the different size of a filler wire diameter, the trial experiment was done to figure out the optimum welding current, hot-wire current, and hot-wire feeding speed for each filler wire diameter.

The single v-groove butt joints were prepared. The arc behavior was observed by a high-speed camera. The macroscopic testing was performed to investigate the dilution ratio, measure the HAZ width, and observe the shape of weld profile. The hardness testing was also performed to investigate the effect of the heat input for the comparison with the result from a conventional arc welding process.

3.2 Introduction of hot-wire CO₂ arc welding method and its equipment

This initial chapter explains the conceptual idea of the combination between CO₂ arc welding process and hot-wire method. The recently developed hot-wire CO₂ arc welding system as illustrated in Fig. 3.1(c) is the hybrid welding system with the combination between conventional CO₂ arc welding as shown in Fig. 3.1(a) and hot-wire system as shown in Fig. 3.1(b). In the proposed system, the hot-wire torch is set up behind the welding torch and provides heated filler material.



(a) CO₂ arc welding. (b) Hot-wire system. (c) Hot-wire CO₂ arc welding system.

Fig. 3.1 Schematic illustration of hot wire CO₂ arc welding process.

Figure 3.2 shows the power sources used in the experiment. The constant voltage power source (Panasonic; YD-5 0 0 CL4 TA2) is used as CO₂ arc welding power source (Fig. 3.2(a)). Shielding gas of pure carbon dioxide (100% CO₂) was used for this process with a constant 25 L/min gas flow rate.

The inverter power source (Babcock Hitachi; IV1320) shown in Fig. 3.2 (b) was used as the hot-wire power source. A filler wire for hot wire is electrically heated through a positive-direct current base on Joule heating's principle. The heated additive material up to just below its melting point is fed into the molten pool from backward. The heated additive material is melted perfectly by the excess heat from the molten pool as exhibits in Fig. 3.2.



(a) MAG welding power source.



(b) Hot-wire machine.

Fig. 3.2 Hot-wire CO₂ arc welding equipments.

Figure 3.3 shows the schematic illustration of the whole experimental system. The welding system was synchronized and controlled by PC, and all welding data (welding current, welding voltage, hot-wire current, hot-wire voltage, both wire feeding speeds) were acquired into PC.

The high-speed camera (NAC; HX-7) was used to record welding phenomena on all welding experiments, and the shooting parameters is shown in Table 3.1. The clearly recorded movies was used to discuss the welding phenomena around the weld pool.

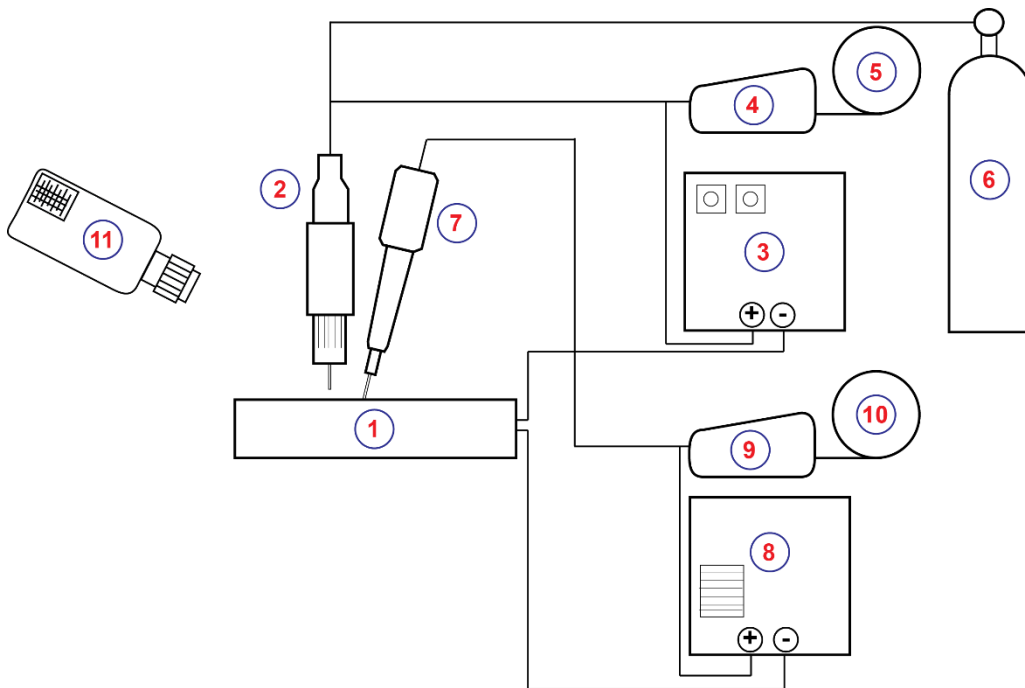


Fig. 3.3 Hot-wire CO₂ arc welding system; (1) Workpiece, (2) CO₂ arc welding torch, (3) CO₂ arc welding power source, (4) CO₂ arc welding wire feeding unit, (5) CO₂ arc welding filler wire, (6) Shielding gas (CO₂), (7) Hot-wire torch, (8) Hot-wire power source, (9) Hot-wire feeding unit, (10) Hot-wire filler metal and (11) High-speed camera.

Table 3.1 Observation conditions.

Camera	HX-7
Frame rate, fps	500
Shutter speed	1/1000
Diaphragm	32
Frame size	1280×1024
Filter	Band pass filter of 980 ± 5nm

3.3 Preliminary experiment to investigate ability in multi-pass joining by using hot-wire CO₂ arc welding process

3.3.1 Materials and specimen used

KE36 steel plates with dimensions of 20^t×50^w×200^l mm were used as a base metal. The butt joint with a V-shaped groove having its angle of 30 degree, and a root gap of 4 mm was employed. The schematic illustration of the specimen is shown in Fig. 3.4. Filler wire of JIS Z3312 YGW11 of 1.2 mm diameter for CO₂ arc welding was used on the first and second pass. JIS Z3312 YGW11 of 1.6 mm diameter for hot-wire on the second pass was used. Chemical compositions of the base metal and filler wires are shown in Table 3.2 and Table 3.3. The standard requirements of mechanical properties for the base metal and welded parts are shown in Table 3.4.

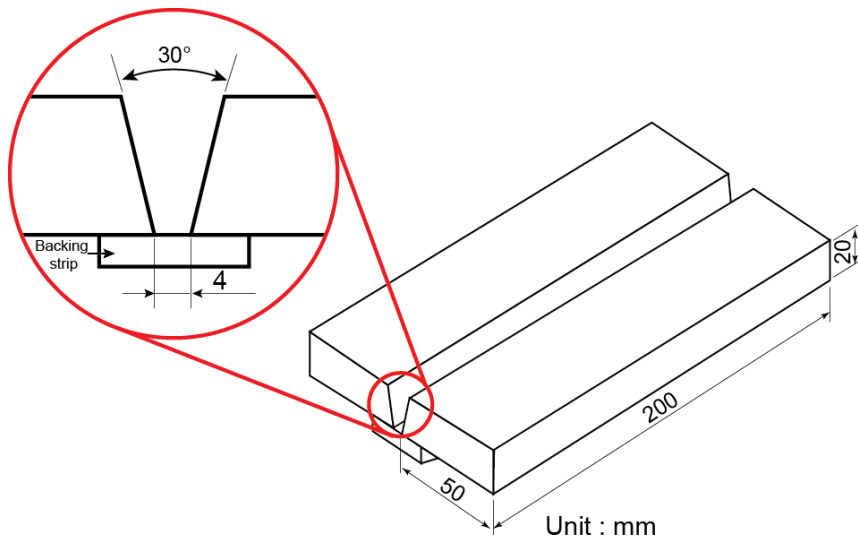


Fig. 3.4 Specimen of experiment.

Table 3.2 Chemical composition of base material.

Element	C	Si	Mn	P	S	Cu	Ni	Cr
Base metal (KE36)	0.12	0.2	1.21	0.14	0.04	0.01	0.01	0.02

Table 3.3 Chemical composition of filler wire.

Filler wire	C	Si	Mn	P	S	Cu	Ti	Zr
JIS Z3312 YGW11	0.02 ~ 0.15	0.40 ~ 1.00	1.00 ~ 1.60	0.03 or less	0.03 or less	0.50 or less	Ti + Zr : 0.02~0.15	

Table 3.4 Target values in mechanical properties.

Grade	Target properties			
	TS (MPa)	YP (MPa)	EL (%)	vE ₀ (J)
KE36	490~620	≥ 355	≥ 21	≥ 34 (Ave.) ≥ 24 (Each)

3.3.2 Geometric calculation of number of passes for filling V-shaped groove before welding

The number of passes required for filling the V-shaped groove shown in Fig. 3.4 was estimated based on the fed material volume calculated by both of filler wire feeding speeds from CO₂ arc welding and hot-wire feeding. The welding speed of 0.3 m/min and welding current for the first pass of 300 A were set as the basic welding conditions for the fundamental investigation in this study. The welding current for the second pass was varied from 300 to 400 A and the filler wire feeding speed was also varied from 12.7 to 19.9 m/min as shown in Table 3.5.

Figure 3.5 shows the estimated number of passes on the combination of filler wire feeding speeds from CO₂ arc welding and hot-wire feeding under the basic conditions of the welding speed of 0.3 m/min and welding current for the first pass of 300 A. The hot-wire feeding speed was varied from 0 to 15 m/min for the calculation as shown in Fig. 3.5. It became clear from the estimated results that the hot-wire feeding speed of 10 m/min for the welding current of 400A, 15 m/min for 350 and 300 A were needed on the most efficient process by two passes.

Figure 3.6 shows the estimated results when the welding speed was varied from 0.2 to 0.8 m/min on each hot-wire feeding speed of 0, 5, 10 and 15 m/min respectively. These results show that the hot-wire feeding speed affects largely on the number of passes on each welding speed for filling the groove. Although the higher hot-wire feeding speed can reduce dramatically the number of passes, the evaluation of stable welding phenomena without any defects must be needed.

Table 3.5 Welding current and measured wire feeding speed of CO₂ arc welding.

Welding current (Setting up), A	300	350	400
Welding current (Measurement), A	322 ~ 330	375 ~ 398	438 ~ 454
Arc voltage, V	31	38	41
CO ₂ wire feeding speed, m/min	12.7	16.3	19.9

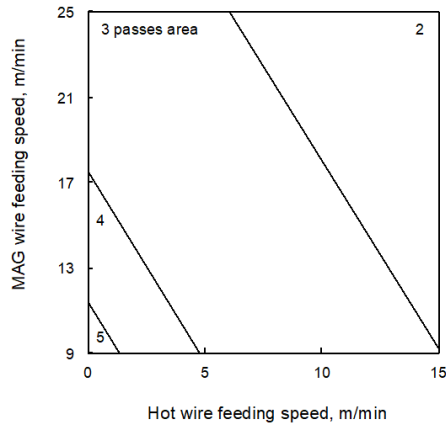
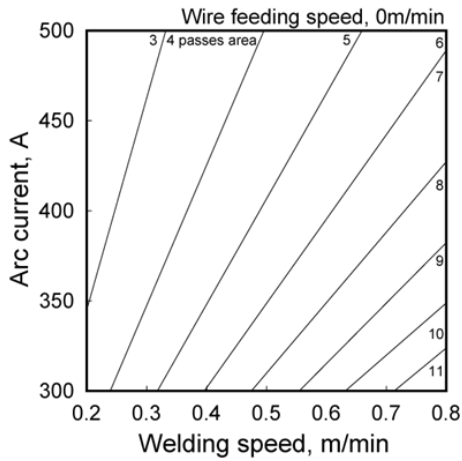
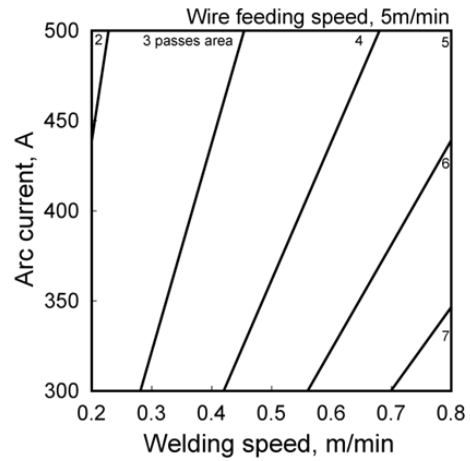


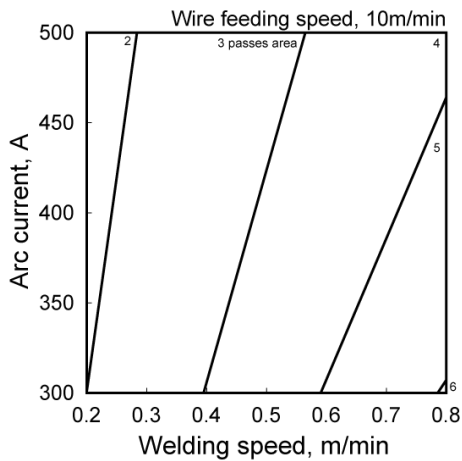
Fig. 3.5 Estimated number of passes for filling V-shaped groove, (Welding speed: 0.3 m/min, Welding current on first pass: 300 A).



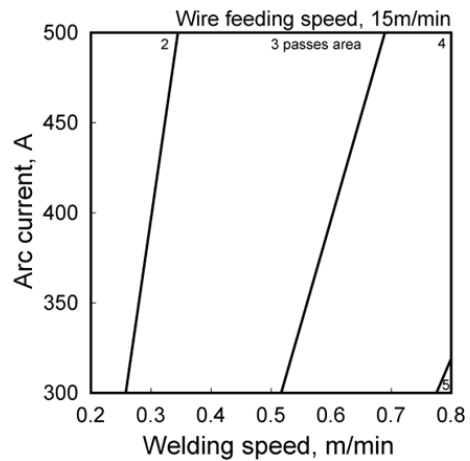
(a) Hot-wire feeding speed: 0 m/min.



(b) Hot-wire feeding speed: 5 m/min.



(c) Hot-wire feeding speed: 10 m/min.



(d) Hot-wire feeding speed: 15 m/min.

Fig. 3.6 Estimated number of passes for filling V-shaped groove, (Welding current on first pass: 300 A).

On Gas Metal Arc Welding (GMAW) including CO₂ arc welding, the power source having DC constant voltage characteristic is generally used. The arc voltage and filler wire feeding speed are set as constant values during welding by using this power source, in other word, the welding current changes inevitably to keep the constant filler wire feeding speed.

The actual measured welding current on each setting welding current was shown in Table 3.5 and Fig. 3.7. The variation of 10~20 A was obtained on the actual welding current measured during welding on a bead on plate and in the V-shaped groove. On the other hand, the constant arc voltage was measured during both welding on the bead on plate and in the groove.

Figure 3.8 shows the measured wire feeding speed of CO₂ arc welding and arc voltage on each setting welding current. The stable wire feeding speed depended on the setting welding current was confirmed on the used welding power source.

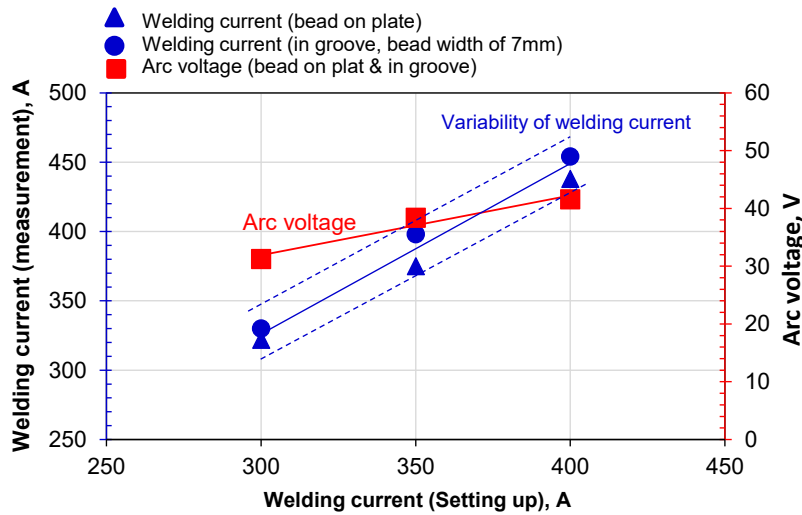


Fig. 3.7 Measured welding current and arc voltage on each setting welding current.

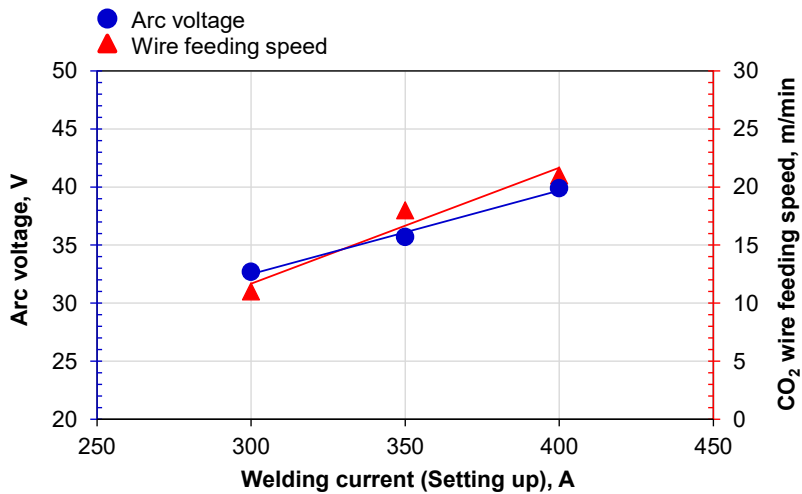


Fig. 3.8 Measured wire feeding speed of CO₂ arc welding and arc voltage on each setting welding current.

3.3.3 Proper hot-wire current

Before the series investigations of hot-wire CO₂ arc welding, the proper hot-wire current depended on the feeding speed on three types of filler wire diameters was investigated by bead-on plate welding. Three types of experiments were performed to obtain the effects of an arc heat input (welding current: 300 A) and CO₂ arc welding torch angle on the proper hot-wire current. Figure 3.9(a) shows the experimental setup of hot-wire feeding without arc, (b) shows the set-up of hot-wire feeding with arc and 0° torch angle having the distance of 7 mm between filler wire tips of CO₂ arc welding and hot-wire, (c) shows the set-up of hot-wire feeding with arc and 15° torch angle having the distance of 3 mm.

Figure 3.10 shows the measured optimum hot-wire current of the three types of filler wire diameters on the three types of experimental conditions. The almost same results of measured proper hot-wire current can be seen in Fig. 3.10, in other word, the filler wire tip temperature fed from hot-wire system can be controlled independently from the arc heat input. In addition, Stable melting phenomena of hot-wire during testing was observed in high-speed camera observation on all conditions.

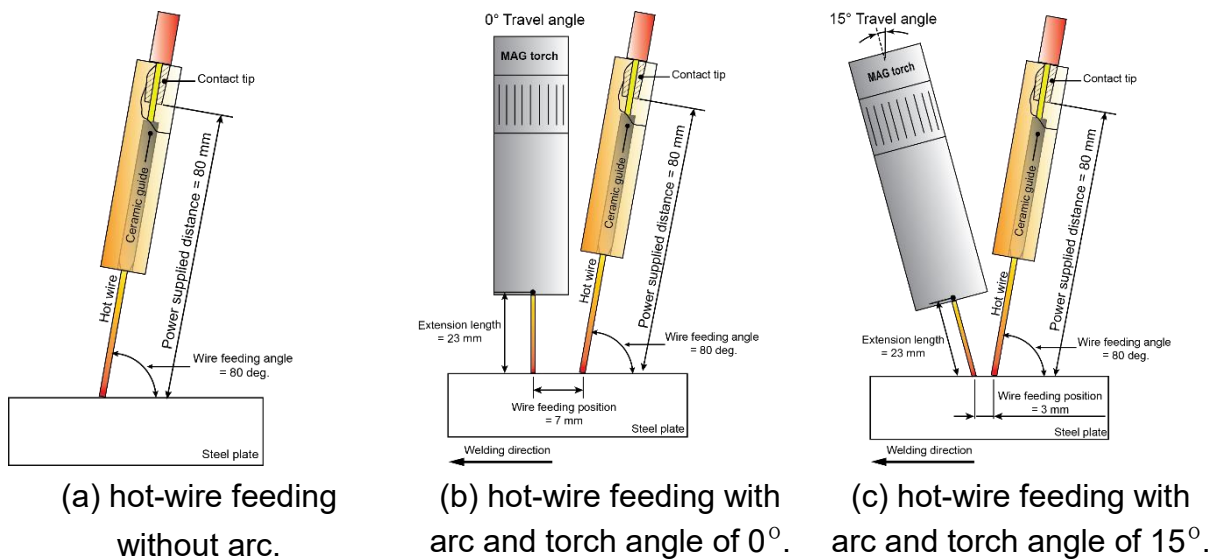


Fig. 3.9 Schematic illustrations of experimental setup for investigation of proper hot-wire current.

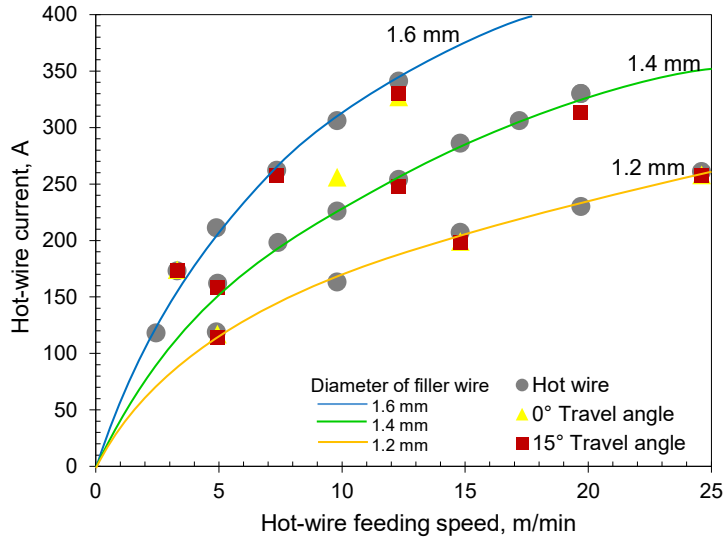


Fig. 3.10 Measured proper hot-wire current.

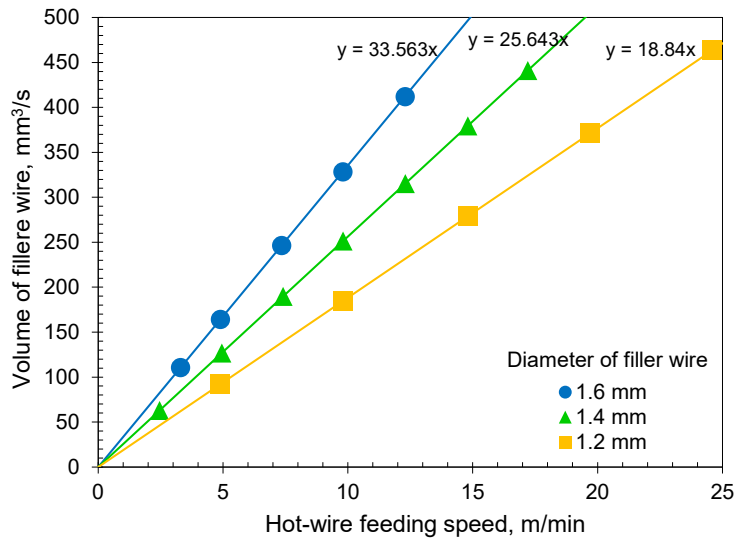


Fig. 3.11 Deposition volume.

Figure 3.11 shows the deposition volume from hot-wire feeding on each filler wire diameter. The results found that the deposition volume increases when the filler wire diameter becomes bigger at same filler wire feeding speed. In other words, the smaller wire diameter needs the higher wire feeding speed to keep the same deposition volume. However, it is also found from Fig. 3.10 that the smaller filler wire diameter can decrease the wire current compared with the larger filler wire diameter. Therefore, it is important to select the proper wire diameter according to the limitation of the filler wire feeding speed and hot-wire power supply.

3.3.4 Experimental procedure

Schematic illustrations and appearance of the experimental set-up, schematic illustration of the weaving method and the welding conditions are shown in Fig. 3.12, Fig. 3.13 and Table 3.6, respectively. The first pass was welded by CO₂ arc welding without hot-wire feeding, and then the second pass was welded by CO₂ arc welding with hot-wire feeding.

The hot wire was fed at a distance of 7 mm back from the wire tip of the CO₂ arc welding. The welding speed was fixed at 0.3 m/min for both passes. A welding current of 300 A and voltage of 31 V were used for the first pass. The wire-feeding speed of CO₂ arc welding was 12.7 m/min at a welding current of 300 A. On the second pass, the welding current and wire-feeding speed of the CO₂ arc welding were changed from 300 to 400 A and 12.7 to 19.9 m/min, respectively; the hot-wire feeding speed on the second pass varied from 0 to 15 m/min. The hot-wire current was set to heat the filler wire tip to near its melting point.

The weaving width on the first pass welding was set at 4 mm same as the root gap. On the second pass, it was set at 7 mm decided from the bead width at the top side of the first pass. High-speed imaging was performed to observe the stabilities of the arc, molten pool, and hot-wire feeding during welding.

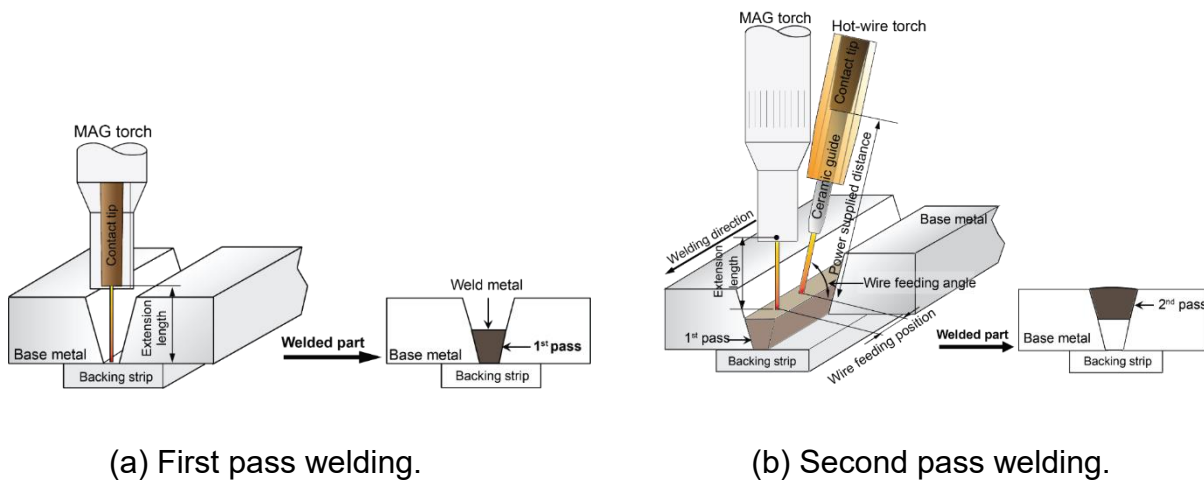
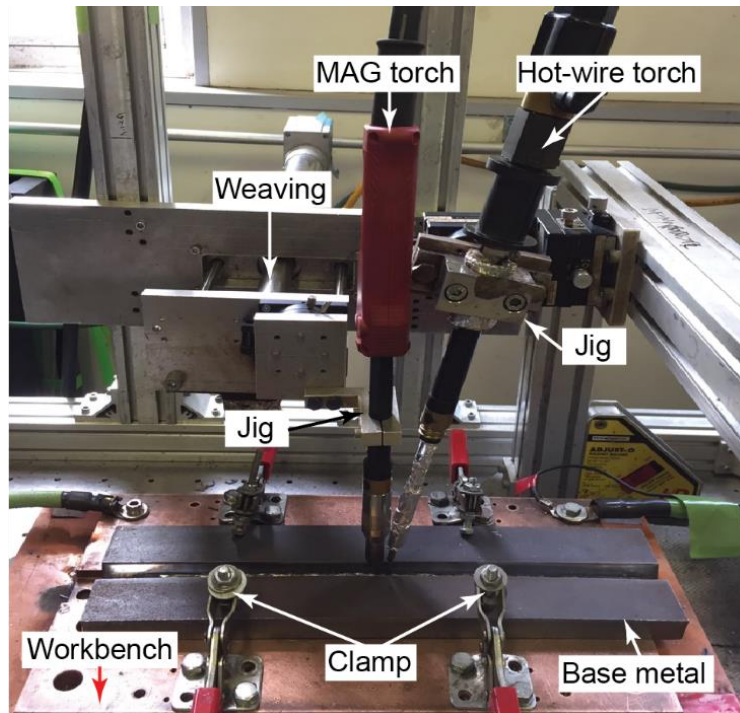
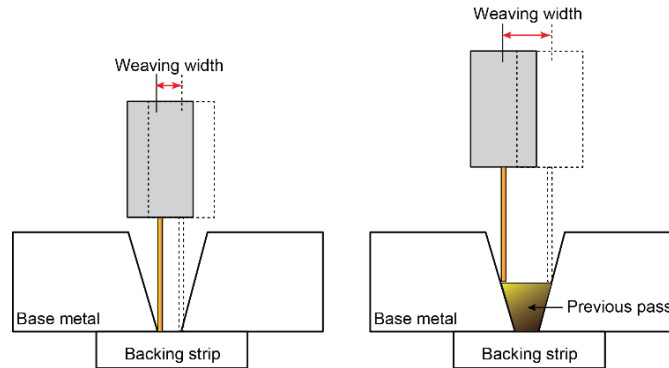


Fig. 3.12 Appearance of experimental set-up.



(c) Equipments for experiment.

Fig. 3.12 Appearance of experimental set-up (continued).



(a) 1st pass welding. (b) 2nd pass welding.

Fig. 3.13 Weaving width.

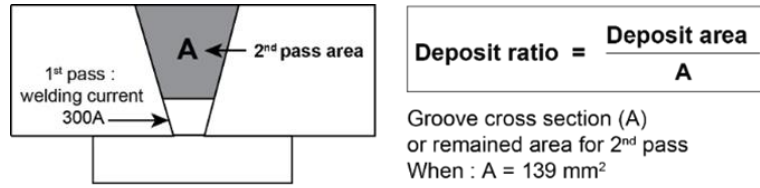
Table 3.6 Welding conditions.

CO ₂ arc welding conditions					
Pass No.	1	2			
Welding speed, m/min	0.3	0.3			
Welding current (Setting), A	300	300	350	400	
Arc voltage, V	31	31	38	41	
Wire feeding speed, m/min	12.7	12.7	16.3	19.9	
Area of weld metal, mm ²	48	48	61	75	
Volume of filler wire, mm ³ /s	239	239	296	375	
Wire diameter, mm	1.2	1.2			
Shielding gas (100%CO ₂), l/min	25	25			
Extension length, mm	23	22			
Weaving width, mm	4	7			
Hot-wire conditions					
Wire feeding speed, m/min	/	0	5	10	15
Area of weld metal, mm ²		0	33	67	100
Volume of filler wire, mm ³ /s		0	167	335	502
Wire current, A		0	208	298	384
Wire diameter, mm		1.6			
Wire feeding angle, degree		70			
Wire feeding position, mm		7			
Power supplied distance, mm		90			
Duty, %		50			

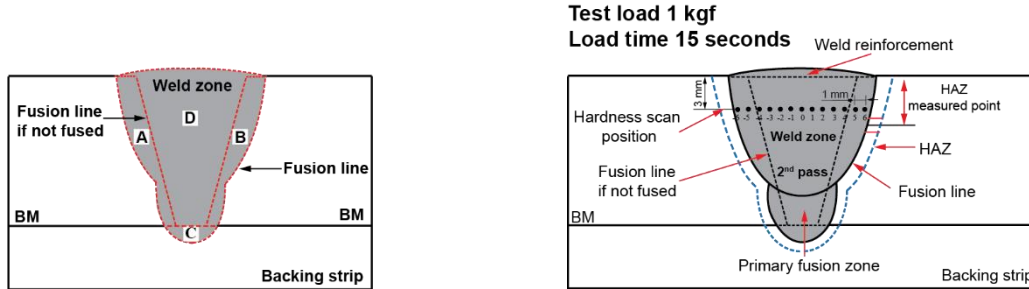
3.3.5 Macroscopic method and calculation of power consumption

After welding, the weld beads were cut at the central part and the cross-section was prepared for macroscopic observations. All cross-sections were polished by waterproof emery papers from P100 to P3000 and by 6 μ m and 1 μ m diamond pastes. Then, they were etched with a 3 % Nital acid solution.

Weld beads were evaluated by cross-sectional observation, deposit ratio and dilution ratio, as shown in Figs. 3.14(a) and (b). A deposit ratio of 1.0 means that the groove area was fully filled by deposited metal in the two passes. The heat-affected zone (HAZ) width and hardness distribution were also measured on the cross-section, as shown in Fig. 3.14(c).



(a) Deposit ratio.



(b) Dilution ratio.

(c) HAZ and Vickers hardness.

Fig. 3.14 Measurement methods for weld metal.

The weld profile was observed from the cross-sectional area. The deposit ratio, which means the ratio of deposited metal volume and the groove volume on the second pass, was calculated as shown in Fig. 3.14(a). The dilution ratio was calculated by equation (1) using the measured determination on the cross-section as shown in Figure 3.14

$$\%Dilution = \frac{A+B+C}{A+B+C+D} \times 100 \quad \dots\dots (1)$$

Where;

- A, B and C are the melted substrate cross-sectional area,
- D is the deposited filler metal cross-sectional area.

The Vickers hardness distribution was measured across the top side of the weld part on the cross-section, as shown in Fig. 3.14(c) using the testing load of 9.8 N and the load time of 15 s. The Vickers hardness defined by the following formula in equation (2) was calculated from the average value of the diagonal lengths of the indentation. The hardness distribution was measured along the line under 3 mm from the plate surface with 1 mm intervals.

$$HV = 0.1892 \times \frac{F}{d^2} \quad \dots\dots (2)$$

Where;

- HV is Vickers hardness,
- F is Load (N),
- d is Average diagonal length of indentation (mm).

The power consumption and arc time were calculated by the welding current, arc voltage, hot-wire current and hot-wire voltage measured during welding. The power consumption is described by a unit of 10 mm welding length when the groove is completely filled. For comparison, the power consumption of the conventional CO₂ arc welding method was calculated using the welding conditions used in the actual shipbuilding construction.

Examples of the welding current, arc voltage, hot-wire current and hot-wire voltage are shown in Fig. 3.15. All welding parameters were measured by a data acquisition system under 5000 Hz intervals. The calculation method of the power consumption and the welding conditions of the conventional CO₂ arc welding method are shown in Table 3.7 and Table 3.8.

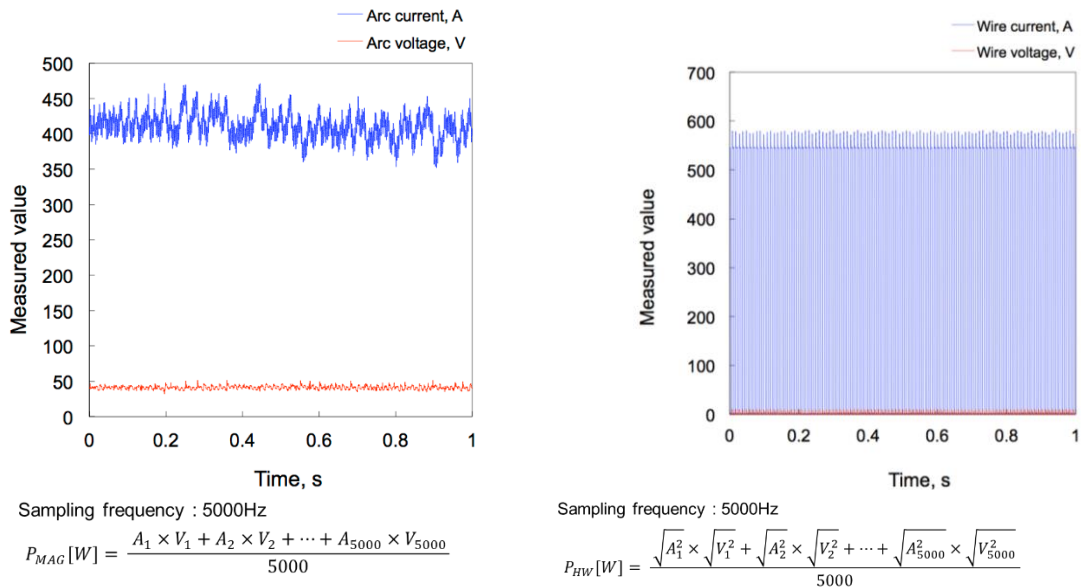


Fig. 3.15 Examples of welding current, arc voltage, hot-wire current and hot-wire voltage measured during welding.

Table 3.7 Calculation method of power consumption in each pass.

Pass No.	P _{MAG} , kW	P _{HW} , kW	
1 st pass	P ₁	P ₂	(P ₁ + P ₂) × $\frac{10}{\text{Welding speed, mm/sec}}$ +
2 nd pass	P ₃	P ₄	(P ₃ + P ₄) × $\frac{10}{\text{Welding speed, mm/sec}}$ +
3 rd pass	P ₅	P ₆	(P ₅ + P ₆) × $\frac{10}{\text{Welding speed, mm/sec}}$ +
4 th pass	P ₇	P ₈	(P ₇ + P ₈) × $\frac{10}{\text{Welding speed, mm/sec}}$ =
			Total power consumption, kJ

Table 3.8 Welding conditions of conventional CO₂ arc welding method.

Thickness (mm)	Angle	Welding method	Pass	Pole	Arc current (A)	Arc voltage (V)	Welding speed (cm/min)
20	40° (Gap : 6)	CO ₂ semi-automatic	1	-	160	24	20
			2	-	340	36	35
			3	-	340	36	30
		NS one side MAG	4	L	480	40	23
				T	460	40	

3.3.6 Result and discussion of capability of hot-wire CO₂ arc welding

3.3.6.1 Capability of hot-wire CO₂ arc welding for thick steel plate

The setting welding current and wire feeding speed of the CO₂ arc welding are used in the following figures. Figure 3.16 shows the deposition capability for each combination of welding current and hot-wire feeding speed. Only welding current condition of 350 A was applied for the hot-wire feeding speed of 15 m/min since unstable molten pool formation on the welding current of 300 A and excess volume of weld metal on the welding current of 400 A were observed under the hot-wire feeding speed of 15 m/min. The increase in volume caused by an increase of 100 A in welding current was about 27 mm², as shown in Fig. 3.17. Although the deposited volume increased on increasing the welding current, the heat input and arc pressure also increased and spattering became worse. In contrast, the volume increases for hot-wire feeding at 5~15 m/min were about 33~100 mm², as shown in Fig. 3.17. It became clear that hot-wire feeding could increase the deposited volume more efficiently without an increase of arc pressure and spatters, while minimizing the increase in heat input, compared with the effect of increasing the welding current.

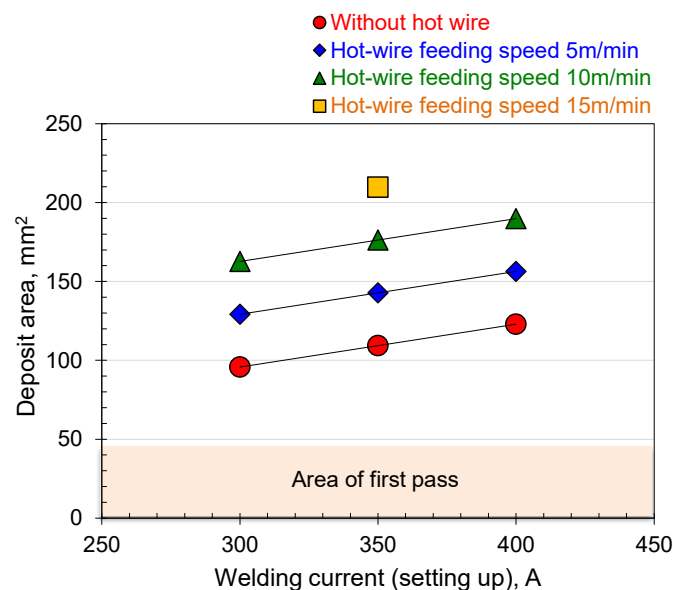


Fig. 3.16 Relationship between deposited volume and welding current.

The objective in this study is the dramatic improvement of welding process efficiency for joining of thick steel plates by applying the hot-wire method, therefore the ability to fill the groove only by two passes for the butt joint of 20-mm thick plates is estimated based on the volume of additional filler materials from CO₂ arc welding and hot-wire feeding. The ability was evaluated using the deposit ratio (deposited metal volume/groove volume on the second pass) as described in Fig. 3.16. The first pass welding was conducted by CO₂ arc welding without hot-wire feeding with the constant welding current of 300 A.

Figure 3.17 shows the calculated deposit ratio for several combinations of welding current and wire feeding speeds for CO₂ arc welding with hot-wire feeding, as shown in Table 3.6. The upper right region, where the deposit ratio exceeded 1.0, indicated that the groove volume was properly filled by deposited metal in two passes. It is clear that hot-wire feeding can efficiently improve the deposit ratio and spread the filled region with the deposit ratio over 1.0. For the experimental conditions shown in Table 3.6, two conditions achieved a deposit ratio above 1.0: the combinations of welding current and hot-wire feeding speed of 350 A (wire feeding speed of 16.3 m/min) and 15 m/min and 400 A (wire feeding speed of 19 m/min) and 10 m/min. Sound filled joints were expected to be obtained using these two combinations.

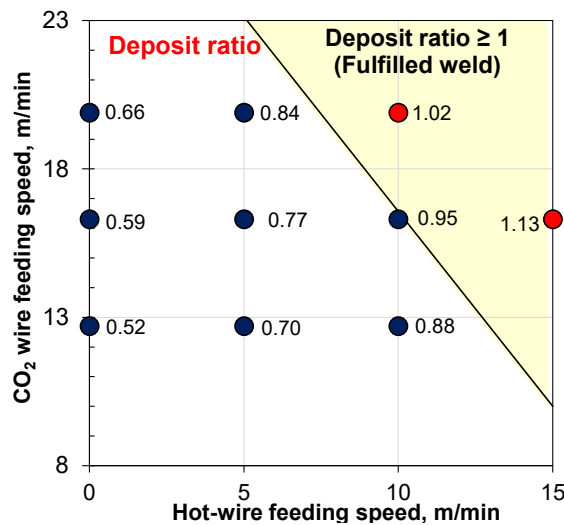


Fig. 3.17 Deposit ratio for the second pass.

Hot-wire welding on all welding conditions shown in Table 3.6 and Fig. 3.17 was performed to obtain the effect of hot-wire feeding on welding phenomena and weld part characteristics. Figure 3.18 shows bead appearances, cross-sections and high-speed images during welding of specimens welded under all welding conditions.

Stable molten pool, weld bead formations and stable hot-wire feeding without spattering were observed for all conditions on the high-speed videos. The sound bead appearances and sound penetration on the cross-section without any defects can also be seen in all conditions as shown in Fig. 3.18.

The increase of the weld metal volume with the increase of the hot-wire feeding speed can be clearly seen on the cross-sections of each welding current condition. On the welding current of 300 A, the estimated deposition ratio increases from 0.52 to 0.88 with the increase of hot-wire feeding speed from 0 to 10 m/min, as shown in Fig. 3.17. The cross-sectional photographs obtained from the actual experimental results shown in Fig. 3.18 clearly show the lack of weld metal. On the welding current of 350A, the estimated deposition ratio increases from 0.59 to 1.13 with the increase of hot-wire feeding speed from 0 to 15 m/min. The photographs show the clear lack of weld metal on hot-wire feeding speeds of 0 and 5 m/min, the slight lack of weld metal on 10 m/min, and the small excess weld metal on 15 m/min. On the welding current of 400A, the estimated deposition ratio increases from 0.66 to 1.02 with the increase of hot-wire feeding speed from 0 to 10 m/min. The photographs show the clear lack of weld metal on hot-wire feeding speeds of 0 and 5 m/min, and the small excess weld metal on 10 m/min. All test results are good agreement with the estimated results shown in Fig. 3.17.

It can be said from the above results that the hot-wire CO₂ arc welding has much potential to fill the groove of thick steel plate joint efficiently, and to reduce the number of passes without the increase of the welding current. It was also confirmed that the estimation method as shown in Fig. 3.17 could be useful for the selection of the welding condition before applying hot-wire CO₂ welding.

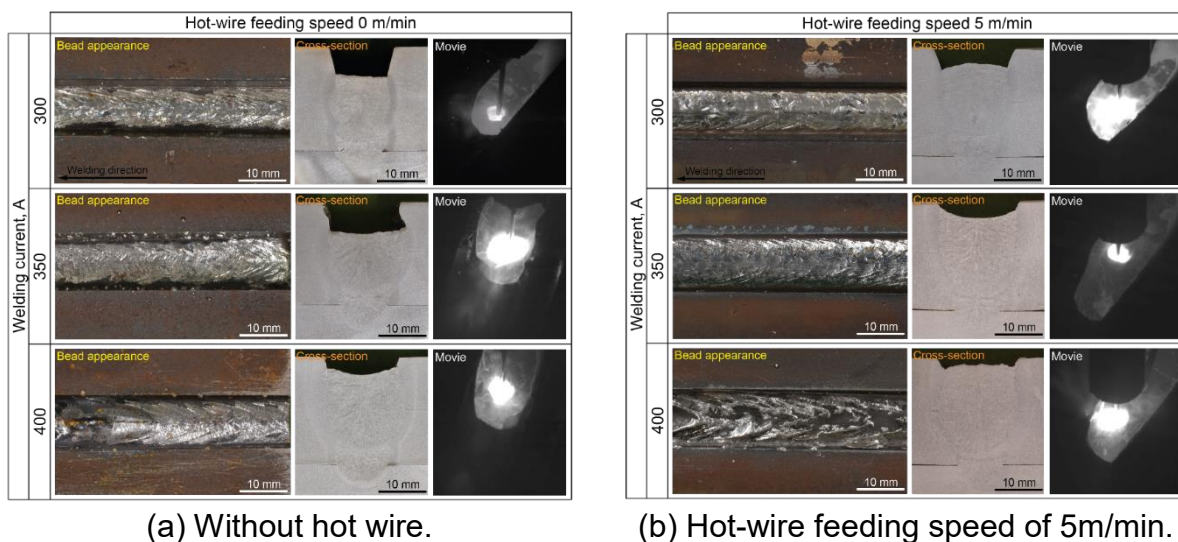
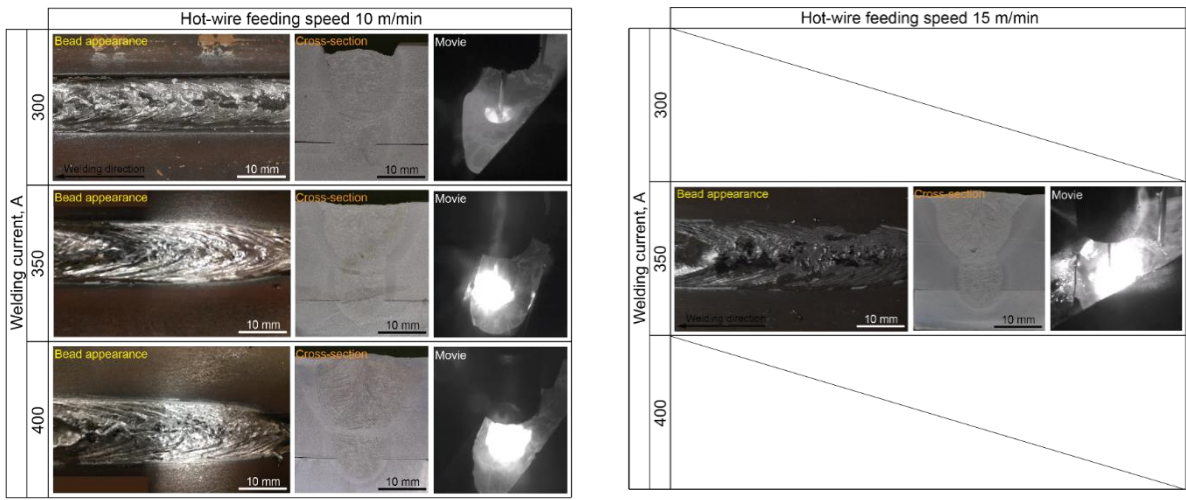


Fig. 3.18 Appearances of weld beads, cross-sections and molten pool images.



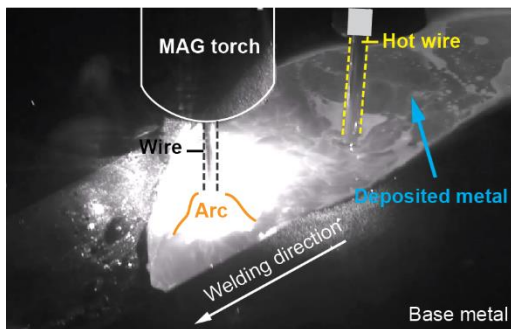
(c) Hot-wire feeding speed of 10 m/min.

(d) Hot-wire feeding speed of 15 m/min.

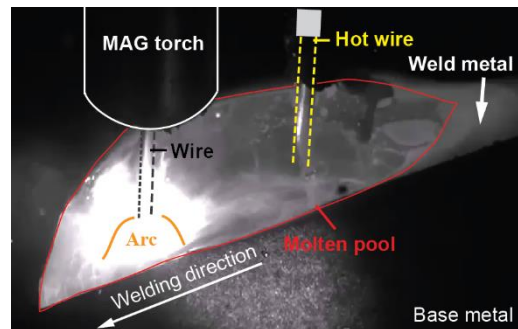
Fig. 3.18 Appearances of weld beads, cross-sections and molten pool images (continued).

Two welding conditions achieved a deposit ratio above 1.0: the combinations of welding current and hot-wire feeding speed of 350 A and 15 m/min and 400 A and 10 m/min on the actual hot-wire CO₂ arc welding as described above. The joint soundness and the welding stability were evaluated in detail.

Figure 3.19 shows an image from a high-speed video captured during actual welding with hot-wire feeding using these two conditions. It can be clearly seen from Fig. 3.19 that the hot-wire tip maintained a set distance from the arc, indicating that the hot wire was properly heated up to just below its melting point; extra heat input from the arc was not needed for hot-wire melting. And the weaving width of CO₂ arc welding torch suited the bead width of previous pass and melted groove edges properly.



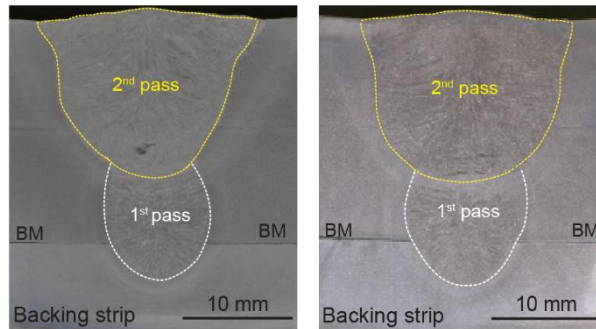
(a) 350A-15m/min.



(b) 400A-10m/min.

Fig. 3.19 High-speed camera images of molten pool.

Figure 3.20 shows the cross-sections obtained for the above two conditions with the estimated deposit ratio above 1.0. Proper penetrations and sound beads without any defects were obtained. A small volume of excess weld metal is also seen on both cross-sections, indicating that the deposit ratios on the actual cross-sections were just over 1.0. It can be said from these results that the hot-wire feeding speed, which means additional material volume, can be adapted for a welding current to obtain a sound bead and to avoid unstable welding phenomena and increase of heat input.



(a) 350A-15m/min. (b) 400A-10m/min.

Fig. 3.20 Cross-sections.

3.3.6.2 Effects of welding conditions on weld bead properties

The welded specimens of all welding conditions as shown in Table 3.6 and Fig. 3.18 were evaluated on the dilution ratio, HAZ width and Vickers hardness of weld metal to discuss the effect of welding conditions.

The summation of the wire feeding speeds for CO₂ arc welding and hot-wire feeding is used as a parameter in the following figures to clearly show the effects of hot-wire feeding on the weld bead properties and its capability on the welding conditions.

Figure 3.21 shows the relationship between the dilution ratio and total wire feeding speed. The dilution ratio without hot-wire feeding was very high, exceeding 50 % even when a welding current of 300 A was used. The dilution ratio decreased almost linearly with the increase of hot-wire feeding speed under all welding current conditions. The effect of hot-wire feeding on the dilution ratio became larger as the welding current became smaller: for example, dilution ratios for welding currents of 300, 350, and 400 A were 36 %, 46 %, and 51 %, respectively, when the hot-wire feeding speed was fixed at 5 m/min, and 34 %, 38 %, and 44 %, respectively, when the hot-wire feeding speed was fixed at 10 m/min. It is assumed that the ratio of deposited metal volume from hot-wire feeding to the volume from CO₂ arc welding mainly affected on the dilution ratio since the welding current affected largely on the melting volume of the base metal and the temperature of the deposited metal from

hot-wire feeding was just under its melting point. For the two conditions shown in Figs. 3.20 and 3.21, the dilution ratios were 29 % and 43 %. It became clear that hot-wire feeding could achieve a lower dilution ratio with a significant increase in deposited metal volume without an increase of welding current; in other words, the combination of hot-wire feeding and lower welding current lowered the dilution ratio by maintaining the same deposited metal volume as would be obtained under the higher welding current condition.

Figure 3.22 shows the relationship between HAZ width and total wire-feeding speed. The HAZ width widened with an increase of welding current when hot-wire feeding was not applied because the heat input from the arc and the deposited metal volume increased. In contrast, although the deposited metal volume significantly increased with increase of the hot-wire feeding speed, the HAZ width became linearly narrower. It is assumed that the molten pool temperature was lowered with the increase in ratio of the hot-wire feeding speed to the wire speed of CO₂ arc welding because the temperature of the deposited metal from hot-wire feeding was lower than that from CO₂ arc welding. The HAZ widths of the two conditions shown in Figs. 3.20 were 1.7 and 1.9 mm. Figure 3.22 shows that these two conditions achieved a narrow HAZ width, almost the same as that achieved by 300 A welding current without hot-wire feeding, with a doubling of the deposited metal volume. Hot-wire feeding was able to decrease the HAZ width with a significant increase in deposited metal volume, even if a relatively high welding current was employed.

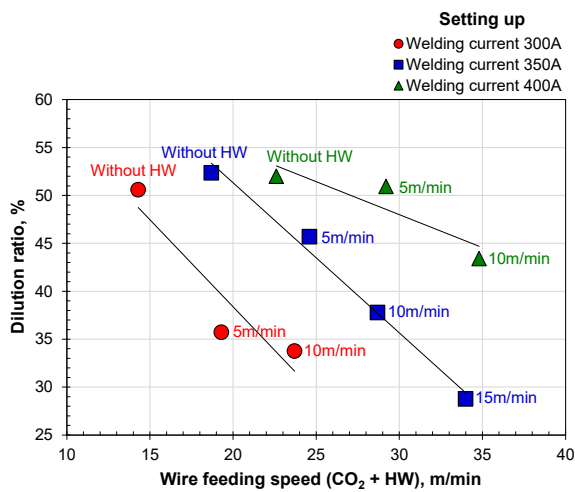


Fig. 3.21 Dilution ratio.

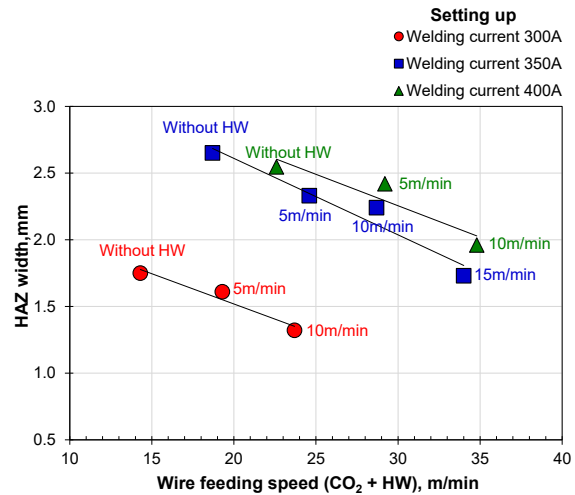


Fig. 3.22 HAZ width.

Figure 3.23 shows the Vickers hardness of weld metal used several combinations of welding current and wire feeding speed for CO₂ arc welding with hot-wire feeding. A higher welding current gave a higher wire feeding speed for CO₂ arc welding, i.e., a larger metal volume was deposited, but the weld metal hardness was lowered. In contrast, although an increase of hot-wire feeding speed gave a

larger volume of deposited metal, the weld metal hardness increased for each welding current condition. It is assumed that the higher hot-wire feeding speed created a lower molten pool temperature and higher cooling speed, thereby giving rise to higher hardness of the welded metal. It is suggested that a combination of higher hot-wire feeding speed and lower welding current should be selected to maintain weld metal hardness when high-efficiency welding is required.

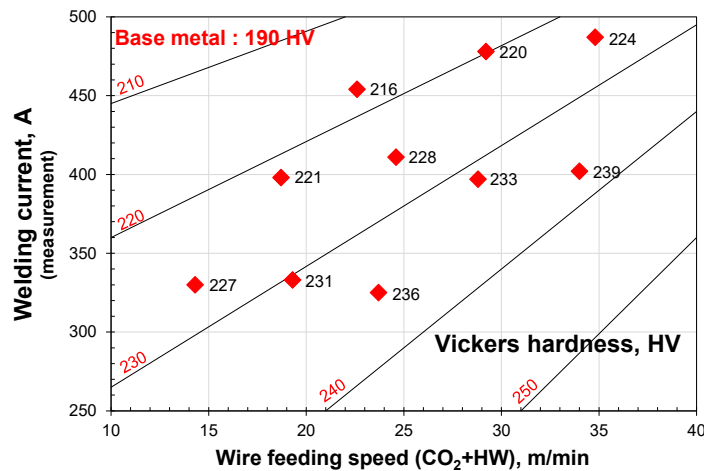


Fig. 3.23 Vickers hardness of weld metal.

3.3.6.3 Reduction of power consumption and arc time

Figure 3.24 compares the power consumption and arc time of hot-wire CO₂ arc welding and conventional CO₂ arc welding using a test sample having 400-mm length and the same thickness of 20-mm and groove shape as shown in Fig. 3.4. Hot-wire CO₂ arc welding was performed in two passes using the optimized conditions: 300 A welding current on the first pass; 400 A welding current and 10 m/min hot-wire feeding speed on the second pass, respectively. Conventional CO₂ arc welding was performed in four passes using conditions employed in actual shipbuilding: 160~460 A welding current and 0.2~0.33 m/min welding speed.

Figure 3.24(a) shows that the power consumption of 2,267 kJ achieved during hot-wire CO₂ arc welding was much lower than that of 4,221 kJ during conventional CO₂ arc welding. In this comparison, the application of hot-wire CO₂ arc welding improved the power consumption by 46 % reduction compared with that of conventional CO₂ arc welding. Figure 3.24(b) shows that the arc time of 160 s during hot-wire CO₂ arc welding was much shorter than that of 375 s during conventional CO₂ arc welding, representing an improvement by 57 % reduction.

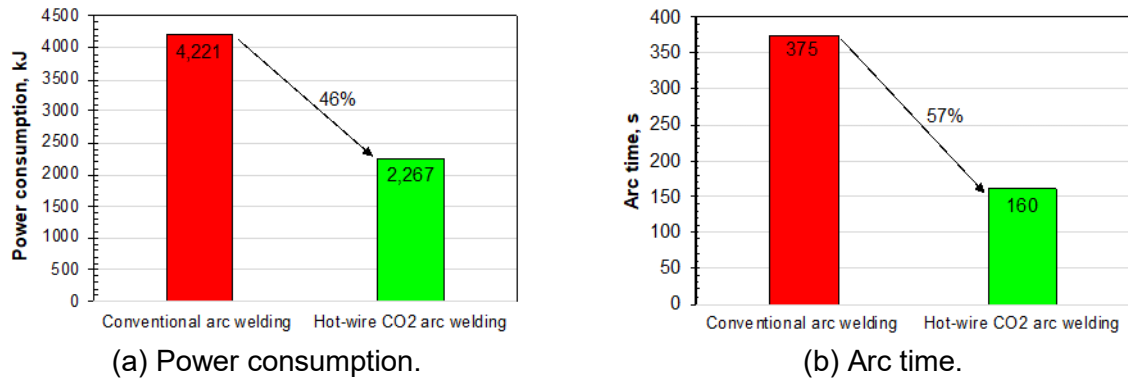
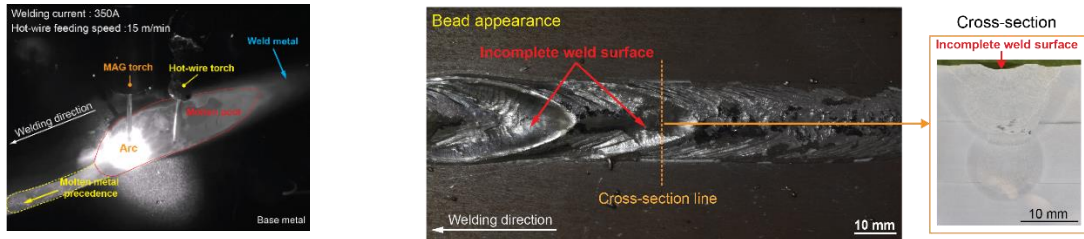


Fig. 3.24 Power consumption and arc time of hot-wire CO₂ arc welding in comparison with conventional arc welding.

Hot-wire CO₂ arc welding can significantly increase the deposition volume without the need to increase welding current and heat input. This advantage makes it possible to reduce the number of welding passes, i.e., from four to two in this research. A reduction in the number of passes can be expected to significantly improve welding time by reducing not only the arc time but also the setup time on an actual construction site.

3.4 Optimization of welding conditions for thick plate joining

According to the previous chapter, it was clearly confirmed that hot-wire CO₂ arc welding had the large potential to achieve both of the improvement of the process efficiency and proper joint properties with lower heat input. However, the unstable welding phenomena, which was a flow of molten metal preceding the molten pool (called molten metal precedence), was observed on a few welding conditions in high-speed observations during welding. This molten metal precedence made defects such as an unstable concave bead surface and incomplete fusion at the bottom of the second pass. The supporting evidences using the welding current of 350 A and hot-wire feeding speed of 15 m/min is shown in Fig. 3.25.



(a) Molten metal precedence. (b) Concave bead surface and incomplete fusion on cross-section.

Fig. 3.25 Examples of molten metal precedence and defects, (Welding current of the first pass: 300 A, second pass: 350 A, hot-wire: 15 m/min).

In this section, the welding currents both for the first pass and second pass were changed to achieve the more stable welding phenomena and the wider proper conditions to avoid molten metal precedence and any defects. The objective of this part was to obtain a sound joint using only two welding passes on a butt joint of 20 mm-thick steel plates with no defects or unstable welding phenomena using the developed hot-wire CO₂ arc-welding process. Detailed observations using a high-speed camera was used to analyze the molten pool flow during hot-wire CO₂ arc-welding. Optimization of the welding conditions was investigated by varying the hot-wire feeding speed and the welding current for the first and second pass. Cross-sectional observations and hardness measurements were used to investigate the effect of the hot-wire addition and the combination of the welding current and hot-wire feeding speed on the joint characteristics. Charpy impact tests, tensile tests and bending tests were also performed on the welded joint produced using the optimized welding conditions.

3.4.1 Materials and specimen

The 490-MPa-Class steel plate (NK-KE36) used as the base metal same as the previous part. The specimen used had the dimensions of 20 mm thickness, 250 mm width, and 400 mm length, as shown in Fig. 3.26. A butt joint with a V-shaped groove possessing an angle of 30° and a root gap of 4 mm was employed with a 9 mm-thick backing plate same as the previous experiments. A 1.2 mm-diameter filler wire of JIS Z3312 YGW11 was used on the first and second pass of the CO₂ arc welding, while a 1.6 mm-diameter filler wire of JIS Z3312 YGW11 was used for the CO₂ arc welding and hot-wire feeding on the second pass.

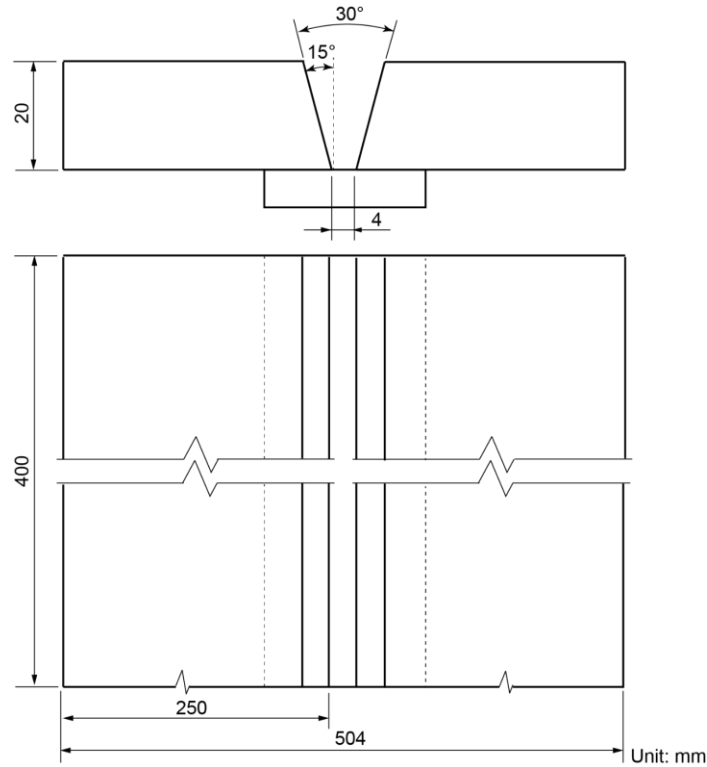


Fig. 3.26 Geometry of joint and specimen.

3.4.2 Experimental setup and welding conditions

Figure 3.27 schematically illustrates the experimental set-up for the first pass, second pass, where the welding conditions for the first and second pass are given in Table 3.9. The welding speed was fixed at 0.3 m/min for both the first and second pass. The first pass was welded by CO₂ arc welding without hot-wire feeding using a welding current of 300 or 400 A and a voltage of 31 or 41 V. The 1.2 mm-diameter wire was used for CO₂ arc welding on the first pass, where the wire feeding speed was 12.7 or 19.9 m/min at a welding current of 300 or 400 A, respectively.

The second pass was welded by CO₂ arc welding with hot-wire feeding. The welding current and voltage of CO₂ arc welding were varied from 300~500 A and from 31~42 V, respectively. For the CO₂ arc welding, the 1.2 mm-diameter wire was used during lower welding current conditions up to 400 A, and the 1.6 mm-diameter wire was used during higher welding current conditions over 400 A. The feeding speeds of the 1.2 and 1.6 mm-diameter wires were respectively varied from 12.7~19.9 m/min and from 9.7~11.7 m/min. In other words, the feeding volumes for the two wire diameters were varied from 241~376 mm³/s and from 326~393 mm³/s, respectively. The hot wire was fed at a distance 10 mm back from the wire tip of the CO₂ arc welding with a feeding angle of 70°. The hot-wire feeding speed was varied from 0 to 10 m/min; in other words, the feeding volumes were varied from 0~298 mm³/s for the 1.6 mm-diameter wire. The hot-wire current was set to sufficiently heat the filler wire tip to near its melting point.

The weaving width on the first pass welding was set at 4 mm same as the root gap. On the second pass, it was set at 7 mm decided from the bead width at the top side of the first pass as shown in Fig. 3.28.

High-speed imaging was used to observe the stabilities of the molten pool and the hot-wire feeding during welding. In particular, excessive molten metal flow to the front of the molten pool was observed during welding on the second pass with hot-wire feeding because the excessive molten metal flow created incomplete fusion on the boundary of two passes.

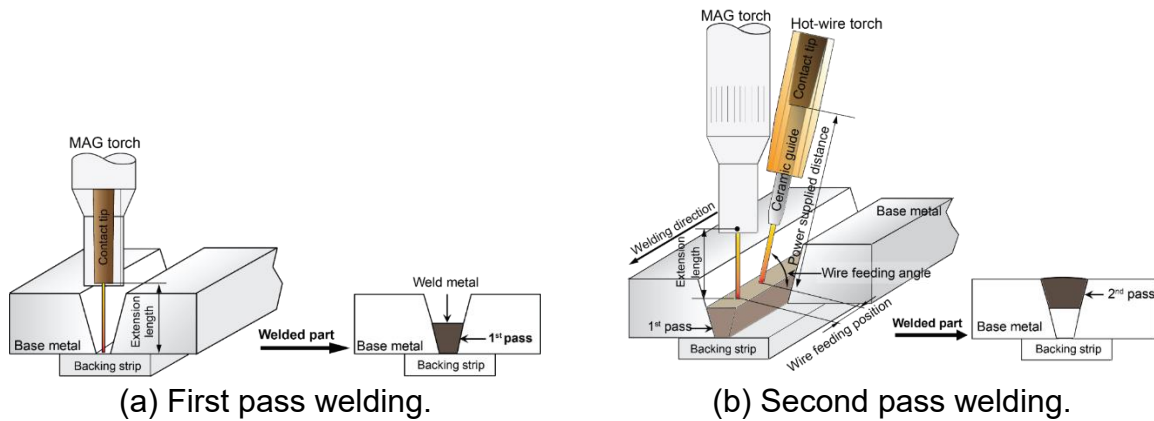


Fig. 3.27 Schematic illustrations of experimental set-up.

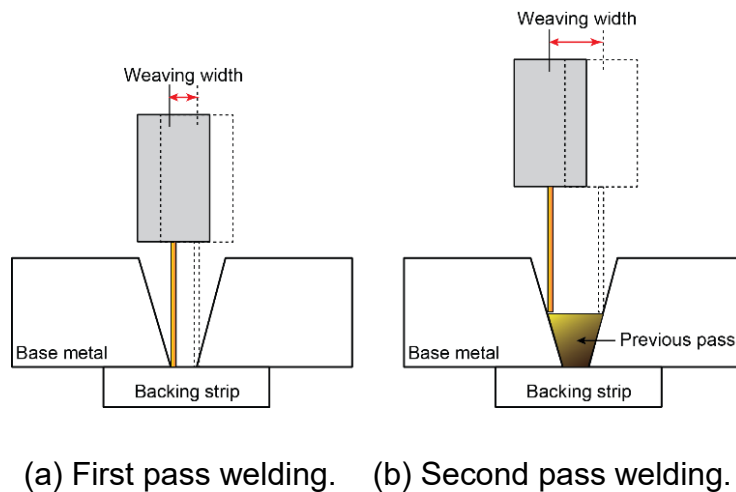


Fig. 3.28 Weaving method for CO₂ arc welding torch.

Table 3.9 Welding conditions.

CO ₂ arc welding conditions							
Pass No.	1		2				
Welding speed, m/min	0.3		0.3				
Welding current (Setting), A	300	400	300	350	400	450	500
Arc voltage, V	31	41	31	38	41	39	42
Wire feeding speed, m/min	12.7	19.9	12.7	16.3	19.9	9.7	11.7
Volume, mm ³ /s	241	376	241	297	376	326	393
Wire diameter, mm	1.2		1.2			1.6	
Shielding gas (100%CO ₂), l/min	25		25			25	
Extension length, mm	23		23			25	
Weaving width, mm	4		7			7	
Weaving frequency, Hz	3		3			3	
Hot-wire conditions							
Welding speed, m/min	/		0.3				
Wire feeding speed, m/min			0	5	7.5	10	
Volume, mm ³ /s			0	167	251	335	
Wire current, A			0	208	249	298	
Wire diameter, mm			1.6				
Wire feeding angle, degree			70				
Wire feeding position, mm			10				
Power supplied distance, mm			80				
Duty, %			50				

3.4.3 Microstructural characterization and mechanical properties

The welded joints made by using hot-wire CO₂ arc welding were prepared by standard techniques, which was described in the first part for the macroscopic preparation. The weld beads were evaluated via cross-sectional observations and the deposition ratio, where the weld metal hardness was measured along a line 3 mm from the plate surface on the cross-section. The weld joint properties were evaluated via a tensile test, a bending test and the Charpy impact test.

3.4.4 Geometric calculation of two passes welding

The deposit ratio, which is the ratio of the deposited metal volume to the groove volume on the second pass was calculated as shown in Fig. 3.29. A deposit ratio of 1.0 indicates that the groove area was fully filled by the deposited metal during the two passes. In this part, the welding current for the first pass was changed as 300 or

400 A to increase the tolerance for the selection of welding conditions as shown in Fig. 3.30.

The fill-up condition (deposit ratio ≥ 1.0) for the V-shaped groove can be estimated as shown in the yellow region for welding current 300~400 A (Fig. 3.31(a)), and the blue region for welding current 450~500 A in Fig. 3.31(b).

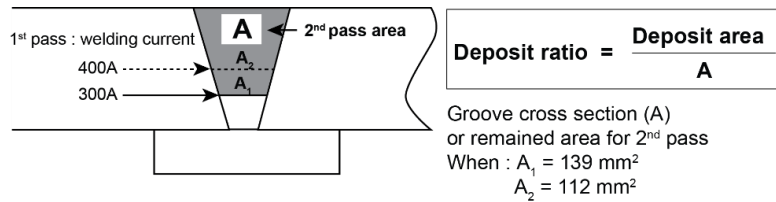
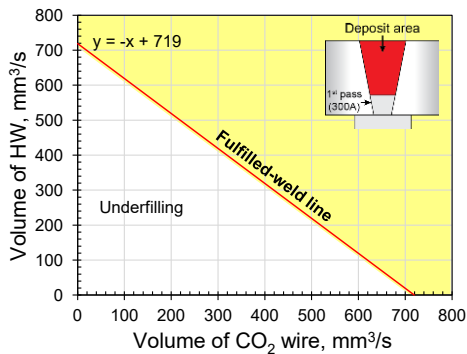
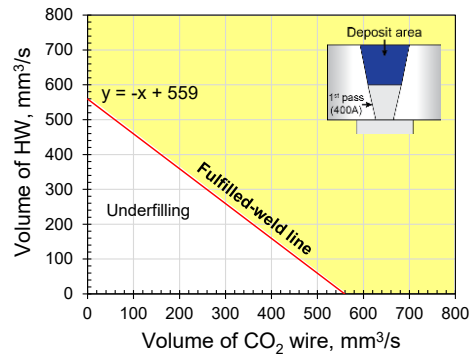


Fig. 3.29 Deposited area for second pass.

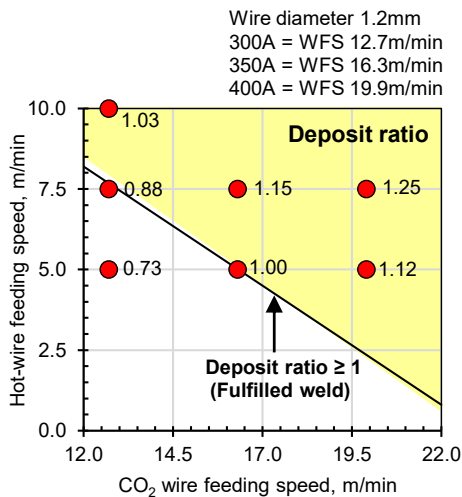


(a) First pass welding current of 300A.

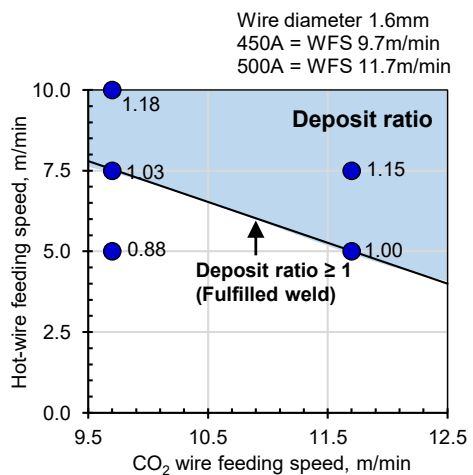


(b) First pass welding current of 400A.

Fig. 3.30 Deposited area for various combinations of wire feeding speeds during hot-wire feeding and CO₂ arc welding.



(a) Second pass welding current from 300 to 400 A.



(b) Second pass welding current from 450 to 500 A.

Fig. 3.31 Deposit ratio for various combinations of wire feeding speeds during hot-wire feeding and CO₂ arc welding on second pass.

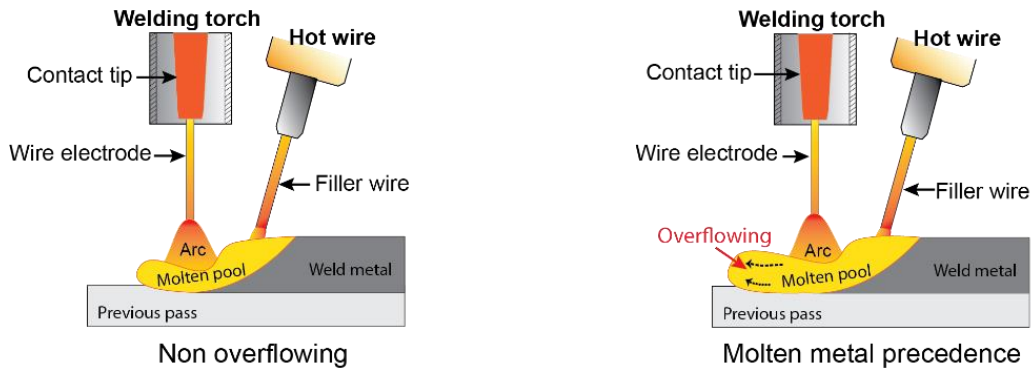
Figures 3.30 and 3.31 show the calculated deposit and area ratio for several combinations of wire feeding speeds for hot wire and CO₂ arc welding on the first pass welding current of 300 A and 400 A, respectively. Figure 3.31(a) shows the deposit ratio for welding current of 300~400 A using the 1.2 mm-diameter filler wire for CO₂ arc welding, and Fig. 3.31(b) show the ratio for welding current of 450~500 A using the 1.6 mm-diameter filler wire on the second pass. The upper right regions in all figures where the deposit ratio exceeded 1.0 signifies that the groove volume was adequately filled by the deposited metal with two passes. Thus, hot-wire feeding clearly has the capability of efficiently improving the deposition ratio and resulting in filled regions with deposition ratios over 1.0.

3.4.5 Result and discussion

3.4.5.1 Optimization of wire feeding speed combination for CO₂ arc welding and hot-wire

A flow of molten metal preceding the molten pool (molten metal precedence) was observed in high-speed observations during hot-wire CO₂ arc welding for several combinations of wire feeding speeds during hot-wire feeding and CO₂ arc welding. Figures 3.32 and 3.33 show schematic illustrations and examples of high-speed images during hot-wire CO₂ arc welding showing sound molten pool creation without molten metal precedence and molten metal precedence from the front and bottom of the molten pool, respectively.

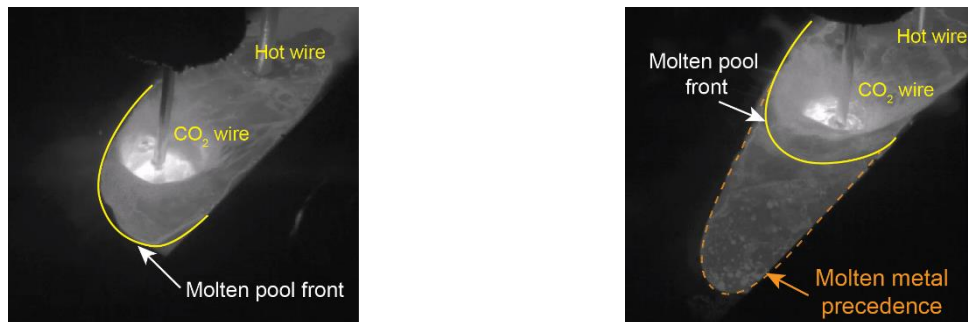
It can be clearly seen in Fig. 3.33(a) that the CO₂ arc creates an arc force just under the tip of the CO₂ arc welding wire that pushes down the molten pool surface. The hot-wire feeding is also clearly observed behind the CO₂ arc wire, where a 7.5 m/min feeding speed provides an adequate volume of additional material into the molten pool while the arc force of the 350 A welding current maintains a stable molten pool front with no molten metal precedence. However, excessive additional material volume with 10 m/min hot-wire feeding increases the molten pool height. This is especially the case at the front of the molten pool, whereupon the arc force of the 350 A welding current cannot maintain the stability of the molten pool front and induces molten metal precedence, as shown in Fig. 3.33(b). In addition, the molten metal precedence causes incomplete fusion at the bottom of the molten pool of the second pass.



(a) Stable molten pool without molten metal precedence.

(b) Unstable molten pool with molten metal precedence.

Fig. 3.32 Schematic illustrations of stability of molten pool and molten metal flow.



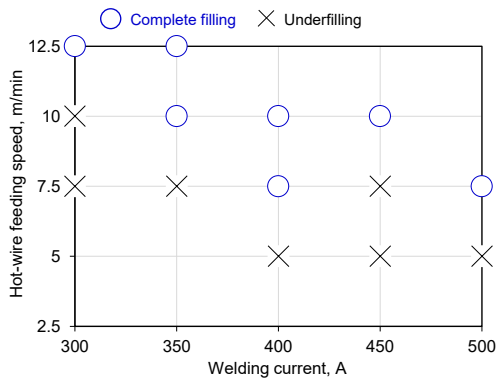
(a) Stable molten pool without molten metal precedence (7.5 m/min).

(b) Unstable molten pool with molten metal precedence (10 m/min).

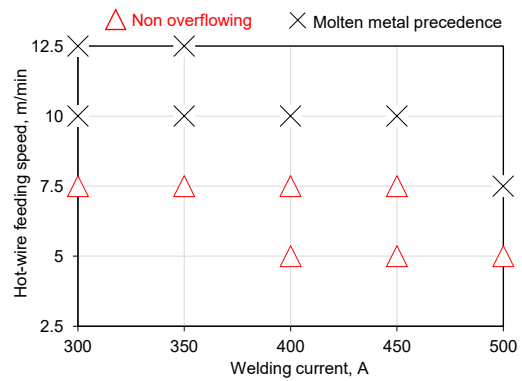
Fig. 3.33 High-speed images taken during second-pass welding using welding current of 350 A (wire feeding speed of 16.3 m/min) with hot-wire feeding speed of (a) 7.5 m/min, (b) 10 m/min.

Figures 3.34 and 3.35 show the results of the evaluations of the groove filling situation and molten metal precedence for various combinations of hot-wire feeding and CO₂ arc welding volumes on the first pass welding current of 300 and 400 A, respectively. The blue circle symbols and black cross symbols in Figs. 3.34(a) and 3.35(a) indicate the conditions for completely filling and underfilling, respectively. It is found that the hot-wire feeding speed for the completely filled groove decreases with the increase of the welding current in both welding current region of 300~400 A and 450~500 A. It is also clearly seen that the higher welding current of 400 A for the first pass can reduce the hot-wire feeding speed to obtain the completely filling condition.

The red triangle symbols and black cross symbols in Figs. 3.34(b) and 3.35(b) indicate the stable molten pool formation (non overflowing) without molten metal precedence and occurrence of molten metal precedence, respectively. Figure 3.36 shows the high-speed images captured during welding on all experimental combinations. It can be seen that the limitation of the hot-wire feeding speed to avoid molten metal precedence becomes smaller with higher welding current on the second pass both on the first pass welding current of 300 and 400 A.

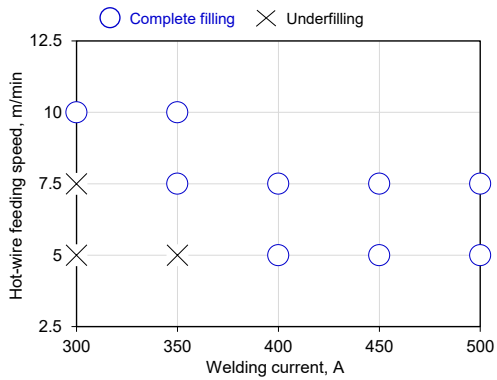


(a) Evaluation of groove filling.

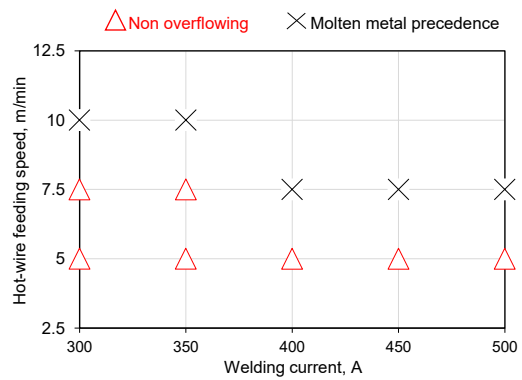


(b) Evaluation of molten metal precedence.

Fig. 3.34 Relationship between hot-wire feeding speed and each welding current, (First pass welding at welding current of 300 A).

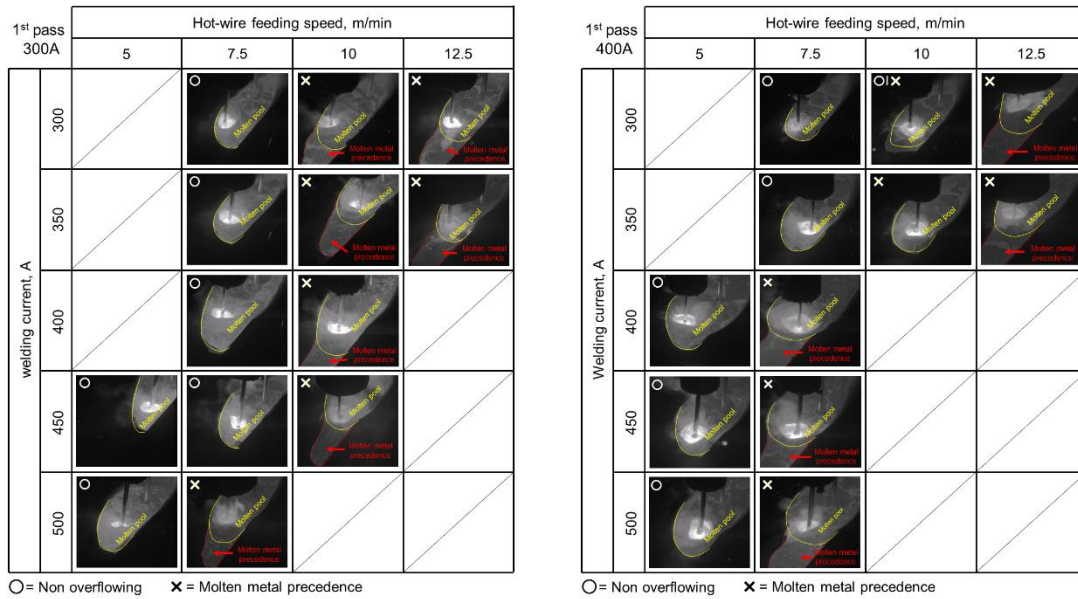


(a) Evaluation of groove filling.



(b) Evaluation of molten metal precedence.

Fig. 3.35 Relationship between hot-wire feeding speed and each welding current, (First pass welding at welding current of 400 A).



(a) First pass welding current of 300 A. (b) First pass welding current of 400 A.

Fig. 3.36 High-speed images captured during welding.

Only one suitable combination, which is the welding current for the second pass of 400 A and the hot-wire feeding speed of 7.5 m/min, achieved the completely filled sound joint and no molten metal precedence on the first pass welding current of 300 A as shown in Figs. 3.36. On the other hand, five suitable combinations, which are 300 A and 10 m/min, 350 A and 7.5 m/min, 400 A and 5 m/min, 450 A and 5 m/min, 500 A and 5 m/min, achieved the completely filled sound joint and no molten metal precedence on the first pass welding current of 400 A as shown in Figs. 3.37.

Figure 3.37 shows the results of the evaluations of the deposition ratio and molten metal precedence for various combinations of hot-wire feeding and CO₂ arc welding volumes. The bottom-left green region in Fig. 3.37 shows the conditions necessary for low metal deposition volumes under a low welding current and low hot-wire feeding speed. In this region where the deposition ratio is under 1.0, the groove volume was not adequately filled by the deposited metal in two passes, though a molten metal precedence was not observed and a stable molten pool front was maintained. The upper-right yellow region in Fig. 3.37 shows the conditions necessary for high metal deposition volumes under a high welding current and high hot-wire feeding speed. In this region where the deposition ratio exceeds 1.0, a molten metal precedence occurred and the stable molten pool front was not maintained, though the groove volume was adequately filled by deposited metal in two passes. The four conditions indicated by the blue symbols in Fig. 3.37 achieved a sufficient filling of the groove volume by two passes without molten metal precedence. These conditions provided an adequate volume of additional material via hot-wire feeding and could sufficiently fill the groove volume and avoid molten metal precedence at the corresponding welding current.

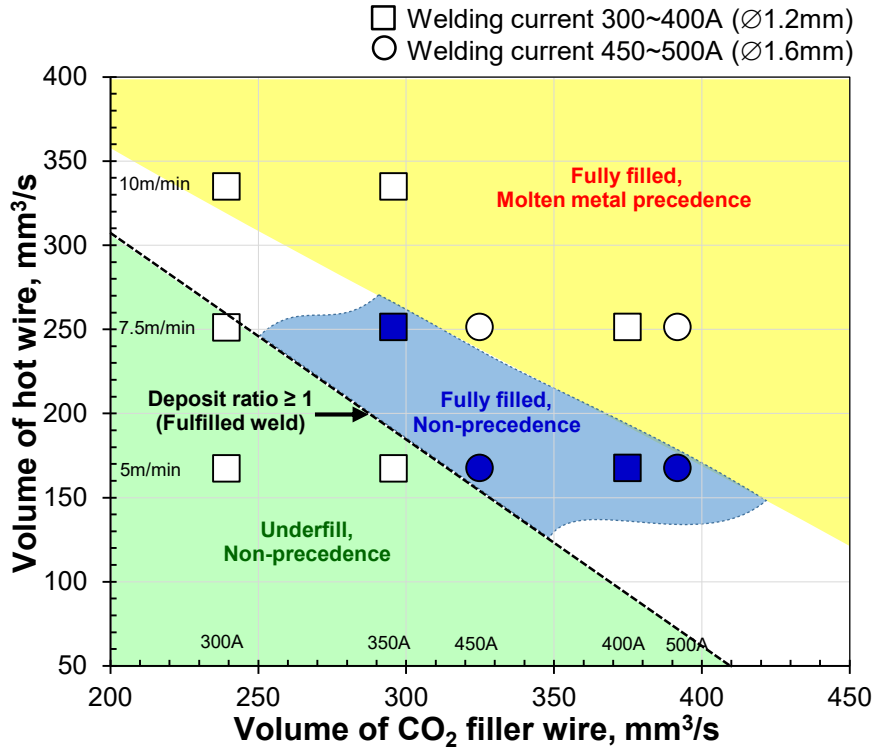
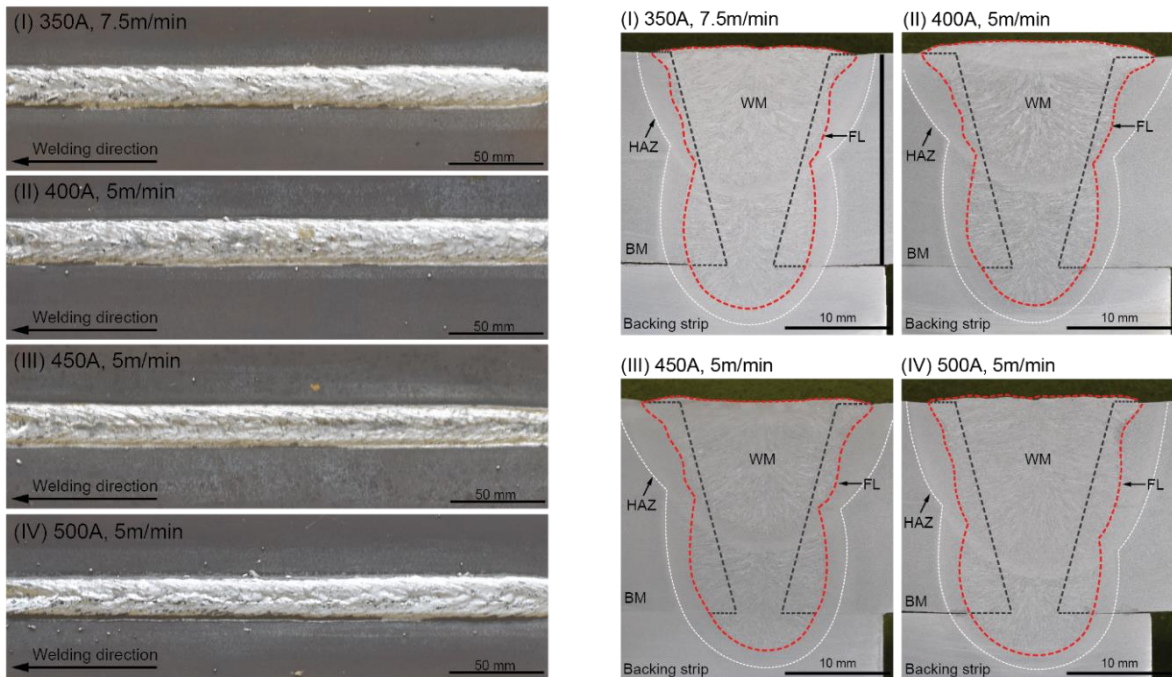


Fig. 3.37 Evaluated results of deposit ratio and molten metal precedence on combinations of hot-wire feeding and CO₂ arc welding volumes using first pass welding current of 400 A.



(a) Appearances of weld bead.

(b) Cross-section.

Fig. 3.38 Appearances of each welded parts at other welding currents.

Figure 3.38 shows the bead appearances and cross-sections obtained using the four suitable conditions exhibiting a deposition ratio greater than 1.0 with no molten metal precedence during welding (blue symbols in Fig. 3.37). Sound beads with no defects and only a small volume of excess weld metal were observed in all cross-sections. This was expected owing to the fact that the deposition ratios on the actual cross-sections were just over 1.0 (Fig. 3.38(b)).

3.4.5.2 Weldment properties

Figure 3.39 shows the relationship between the dilution ratio, HAZ width and heat input. The dilution ratio increases with the increase of the heat input by using the higher welding current as shown in Fig. 3.39(a). The HAZ width becomes wider with the increase of the heat input as shown in Fig. 3.39(b). It is found that the welding current affects largely on both of the dilution ratio and HAZ width during hot-wire CO₂ arc welding since the heat input from hot-wire feeding is much smaller than that from CO₂ arc welding. This means that the combination of the lower welding current and higher hot-wire feeding speed should be selected to obtain a small dilution ratio and narrow HAZ width with keeping deposited material volume.

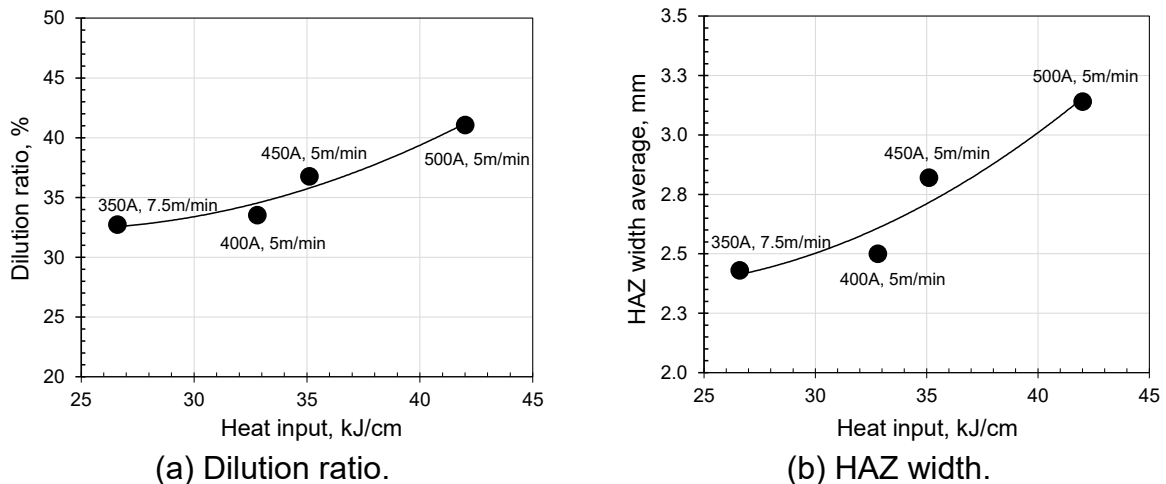


Fig. 3.39 Relationship of heat input and dilution ratio, HAZ width.

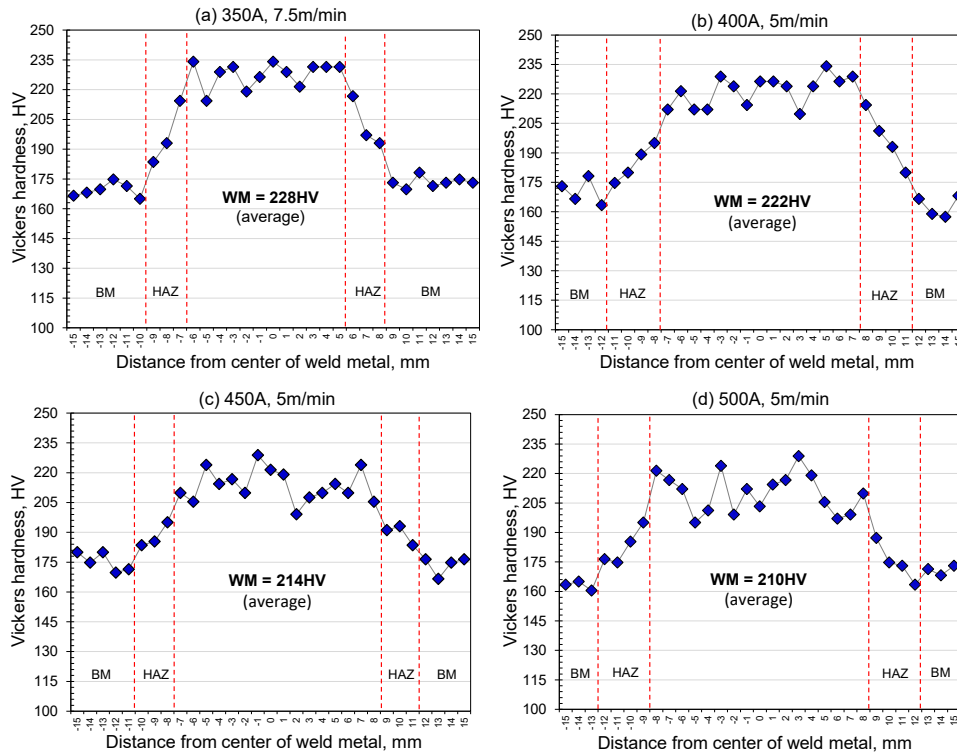


Fig. 3.40 Vickers hardness distributions across weldment on second pass.

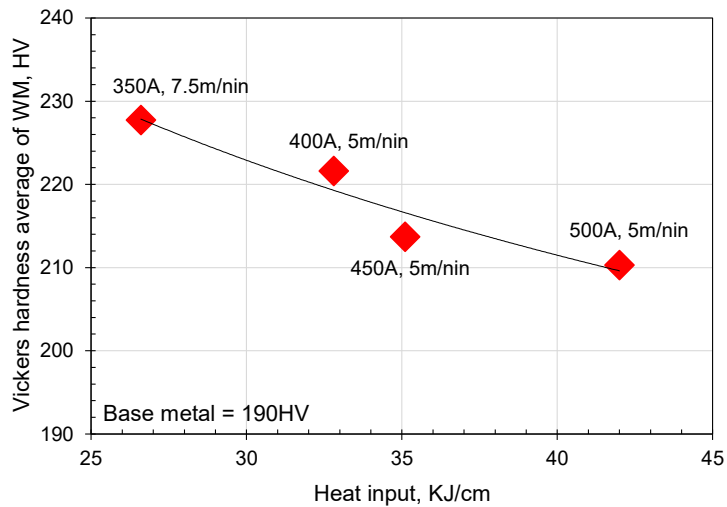


Fig. 3.41 Comparison of Vickers hardness of weld metals in each heat input.

The Vickers hardness distribution was measured on the second pass cross-section obtained by using four suitable conditions shown in Fig. 3.38. Figure 3.40 shows the measured hardness distributions on the four suitable conditions. It was found that the weld metal hardness were slightly higher than that of base metal, and the softening zone was very small on all four conditions.

Figure 3.41 shows the relationship between the Vickers hardness of the weld metal on the second pass and the heat input. It was also found that the conditions of a lower welding current and higher hot-wire feeding speed correspond with a higher hardness, while the conditions of a higher welding current and lower hot-wire feeding speed correspond with a lower hardness. An adequate weld metal hardness compared with the base material value of 190 HV were obtained with all four conditions even when a higher welding current of 500 A was applied. It is noted that the application of hot-wire feeding allows the use of lower welding currents while maintaining an adequate amount of deposited metal. In other words, the application of hot-wire feeding can achieve a lower heat input and avoid deterioration of weld metal hardness while maintaining process efficiency.

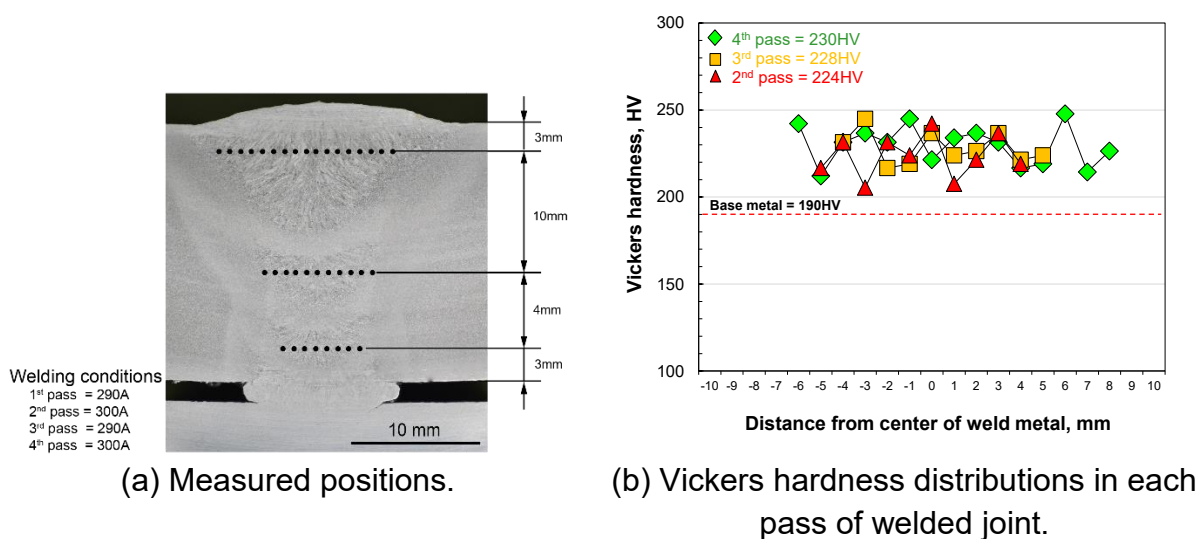


Fig. 3.42 Vickers hardness measurement for conventional CO₂ arc welding.

Figure 3.42 shows the joint cross-section using conventional CO₂ arc welding and Vickers hardness distributions in each passes on the cross-section. The average Vickers hardness of weld metal in each pass using conventional CO₂ arc welding is relatively high of 224~230 HV since the lower welding currents of 290-300A and four passes was employed for conventional CO₂ arc welding. Although the number of passes decreased from four to two, the efficiency increased dramatically and the power consumption decreased largely, the almost same hardness could be obtained using hot-wire CO₂ arc welding.

Figure 3.43 shows the schematic illustration of cut-off plan for tensile test and side bending test specimens in accordance with JIS Z 2201 No. 14 and JIS Z 2248, respectively. Tensile tests and side bending tests were carried out to evaluate the joint properties of the specimens welded by the four suitable conditions described above. Both of the tensile test and side bending test were performed on two

specimens cut from a single butt joint sample welded using one of the four conditions, where all four samples were tested.

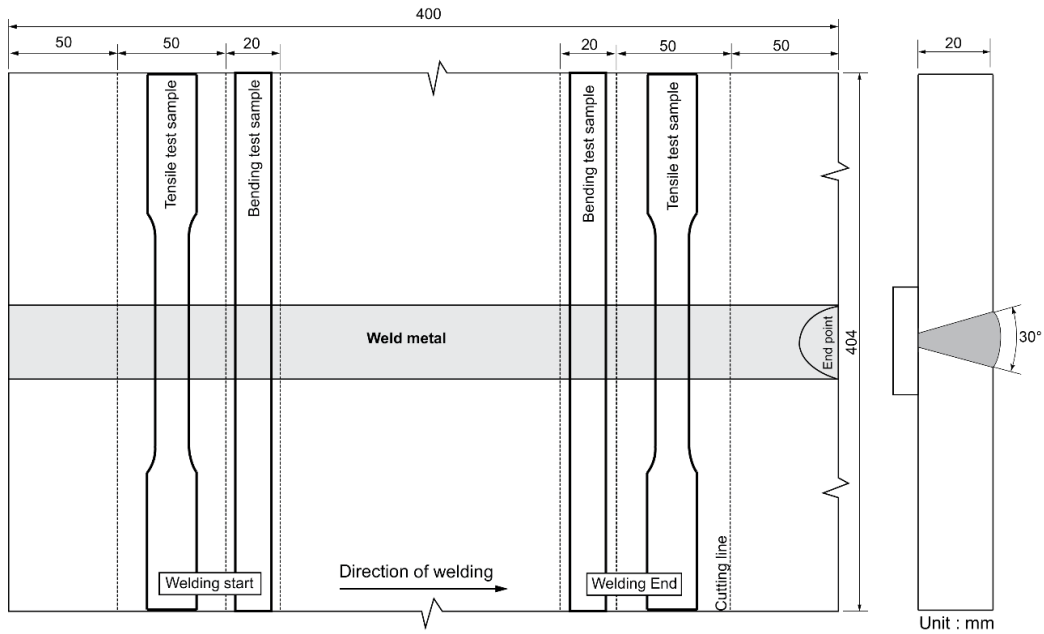


Fig. 3.43 Schematic illustration of cut-off plan for tensile test and side bending test specimens.

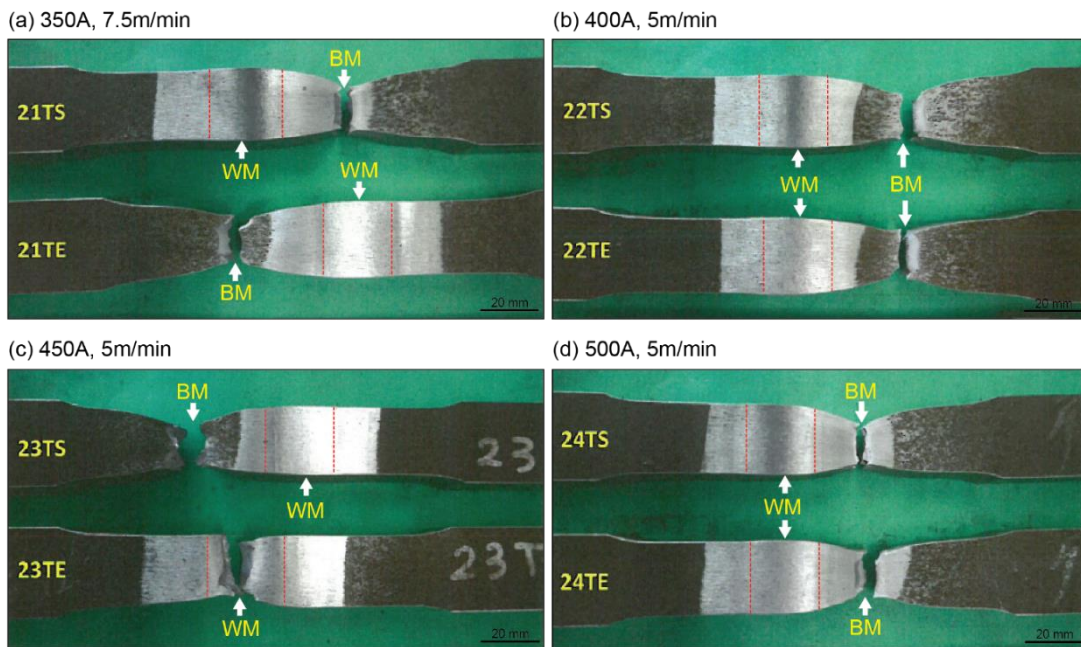


Fig. 3.44 Tensile test specimens after breaking.

Figure 3.44 shows the tensile test specimens after breaking, and Table 3.10 shows the tensile test results of the tensile strength and breaking position. It is clear from Fig. 3.44 that the breaking positions of seven of the specimens were located in the base metal region and one specimen broke at the edge of the weld metal. It can be also seen that all joints welded using the four suitable conditions achieved adequate tensile strength equivalent to that of the base material of 540 N/mm². The specimen that broke in the weld metal also exhibited an adequate tensile strength of 545 N/mm² compared with the value of the base material. It is assumed that an adequate tensile strength and fracture in the base metal can be obtained with appropriate weld metal hardness (Figs. 3.41 and 3.42) and suppression of softening of HAZ from a low heat input of the hot-wire CO₂ arc welding.

Table 3.10 Tensile test results.

Conditions	Tested position	Tensile strength [N/mm ²]	Breaking position
350A, 7.5m/min	Welding Start	536	Base metal part
	Welding End	536	Base metal part
400A, 5m/min	Welding Start	539	Base metal part
	Welding End	536	Base metal part
450A, 5m/min	Welding Start	536	Base metal part
	Welding End	545	Weld metal part
500A, 5m/min	Welding Start	538	Base metal part
	Welding End	540	Base metal part

*Tensile strength of base metal: 540N/mm²

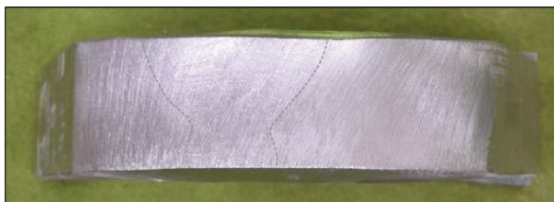
(a) 350A, 7.5m/min



(b) 400A, 5m/min



(c) 450A, 5m/min



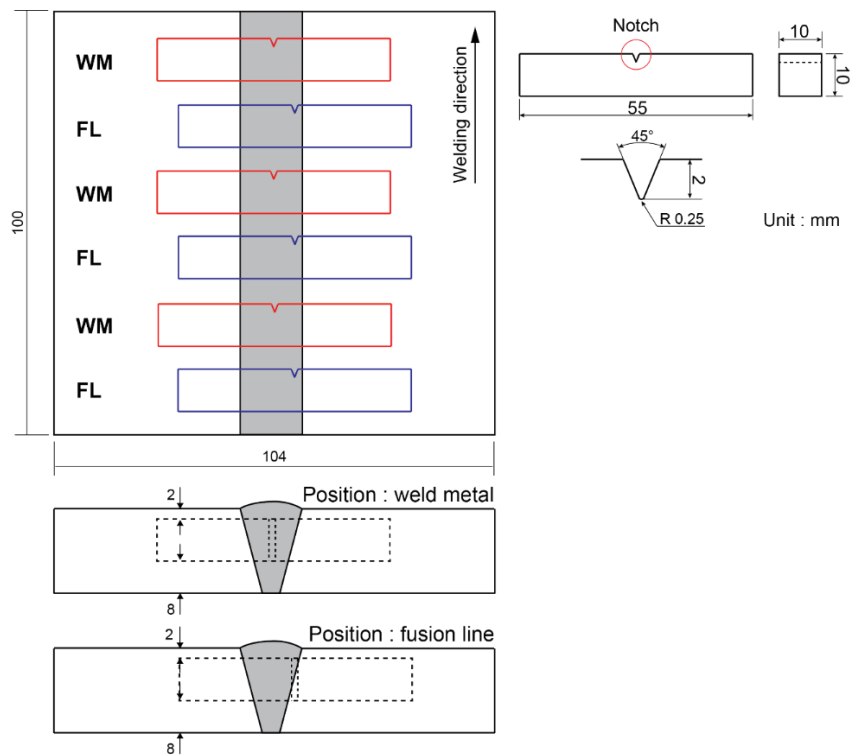
(d) 500A, 5m/min



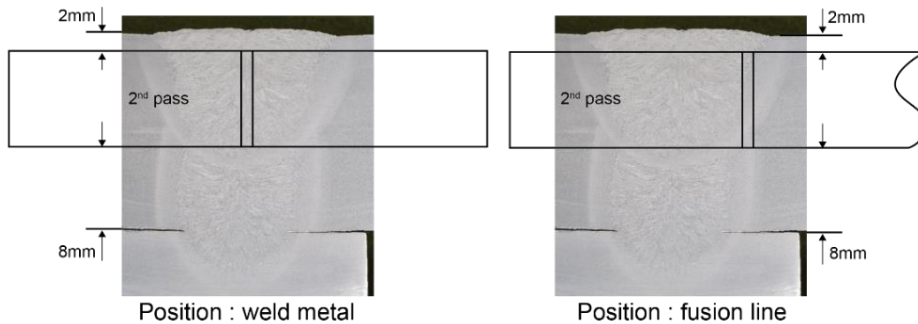
Fig. 3.45 Result of weld bead bending test.

Figure 3.45 shows the specimens welded by the four suitable conditions after performing transverse side bending tests. All specimens exhibited sound results with no defects and with breaking both on the weld metal region and the fusion line.

The Charpy impact test at 0°C using two kinds of specimens: one with its notch position at the weld metal and the other at the fusion line, were carried out to evaluate the toughness property. The V-notched specimens were cut-off from the joints welded using three suitable conditions as shown in Fig. 3.46 according to standard specimen size to be JIS Z 2242.



(a) Cutting plan.



(b) Test pieces and notch location.

Fig. 3.46 Preparing specimen for V-notch Charpy impact test.

Table 3.11 V-notch Charpy impact test results.

Conditions	Absorbed energy, J	
	Weld metal	Fusion line
400A, 5m/min	76.9	207.2
	66.6	199.5
	76.9	222.5
450A, 5m/min	159.4	-
	65.2	228.4
	99.9	-
500A, 5m/min	90.6	225.4
	86.0	194.7
	89.1	161.1

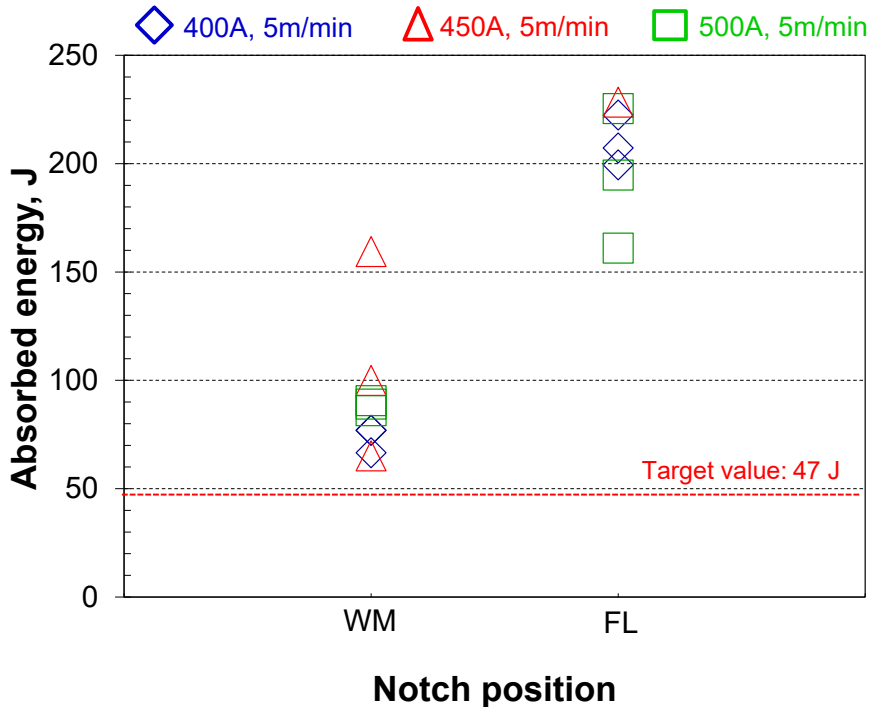


Fig. 3.47 Charpy impact test result.

Table 3.11 and Fig. 3.47 show the absorbed energy obtained from the Charpy impact test at 0°C for both notch positions. It is clearly seen in Fig. 3.47 that the absorbed energy both at the weld metal and the fusion line exhibit adequate values over 47 J at 0°C. The higher energy value at the fusion line was obtained because of the low heat input derived from the hot-wire feeding instead of the higher heat input via employing the higher welding current. It is also assumed that weld metal toughness can be improved by careful selection of the filler wire material for hot-wire feeding without changing the CO₂ arc welding conditions.

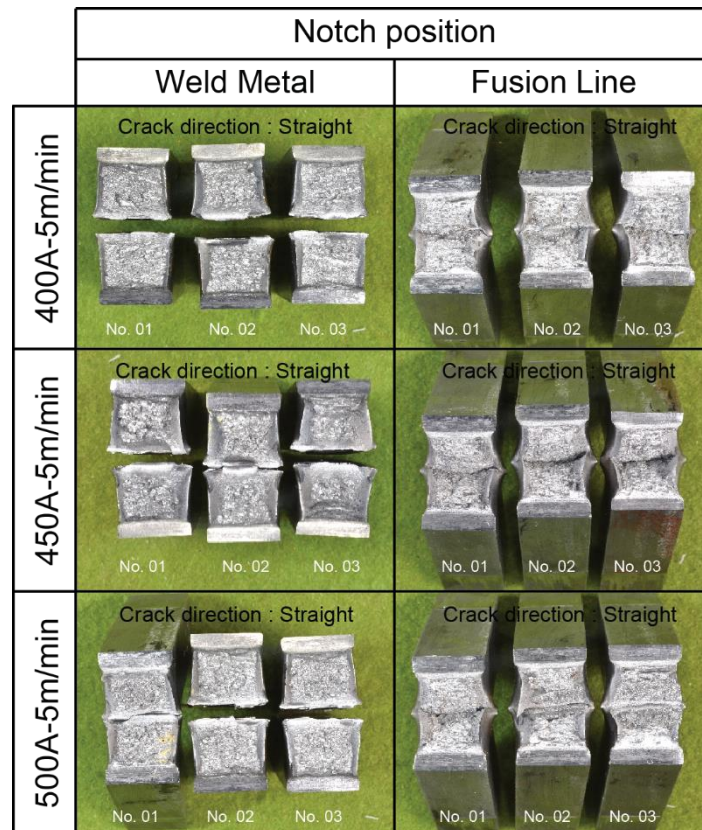


Fig. 3.48 Fracture surface and crack direction of test pieces.

The fracture surfaces of all specimens at weld metal, and fusion line are shown in Fig. 3.48. All specimens show a combined fracture surfaces with brittle and ductile fractures. The specimen cut-off from the fusion line shows the higher ratio of ductile fracture surface with the higher absorbed energy because of the low heat input derived from the hot-wire method. On the other hand, the toughness of weld metal can be improved by the adequate selection of filler metal for hot wire.

3.5 Summary

In first part of this chapter, preliminary experiments were performed to investigate the ability in multi-pass joining by using hot-wire CO₂ arc welding process for thick steel plate joints. Optimization of welding conditions using only two welding passes on the butt joint of 20-mm thickness steel plates was investigated using several combinations of hot-wire feeding speed and welding current. Cross-sectional observation was performed to investigate the effect of hot-wire addition and the combination of welding current and hot-wire feeding speed on the joint characteristics. The summary of the first part is as follows.

- (1) Efficient hot-wire addition at up to 15 m/min using a filler wire of 1.6 mm diameter could be achieved, using an appropriate current to heat the hot-wire tip up to its melting point, for several combinations of welding currents, giving stable welding phenomena.
- (2) A sound joint without any defects could be obtained in only two welding passes using the optimized welding conditions at a welding speed of 0.3 m/min.
- (3) Hot-wire addition can achieve a lower dilution ratio, narrower HAZ width, and higher weld metal hardness with a significant increase in deposited metal volume without an increase of welding current; in other words, the combination of higher hot-wire feeding speed and lower welding current resulted in much lower heat input while maintaining the same deposited metal volume as achieved using a higher welding current.
- (4) The proposed hot-wire CO₂ arc-welding process reduced power consumption by 46 % and arc time by 57 % compared with those of the conventional CO₂ arc-welding process on a butt joint of 20-mm thickness steel plates.

In the second part, optimization of welding conditions using only two welding passes on a butt joint of 20 mm-thick steel plates was investigated based on high-speed imaging for several combinations of welding current and hot-wire feeding speed. Cross-sectional observation and mechanical tests were performed to evaluate the joint properties. The conclusions are as follows:

- (1) Efficient hot-wire addition on the second pass was sufficient to fill the groove area with only two passes for each welding current, though molten metal precedence was observed via high-speed imaging for conditions with relatively high wire feeding speeds.
- (2) Optimized combinations of the welding current from 300~500 A and hot-wire feeding speed for a butt joint of 20 mm-thick plates at a welding speed of 0.3 m/min could be obtained after only two welding passes with no defects or molten metal precedence during welding.
- (3) The combination of lower welding current and higher hot-wire feeding speed achieved higher weld metal hardness. In addition, an adequate weld metal hardness could be obtained even at a higher welding current of 500 A because of the significant effect that the hot-wire addition exerted to decrease the heat input compared with conventional high-efficiency welding processes.
- (4) Sound properties as revealed by the Charpy impact test, tensile test, and transverse side bending test were obtained on welded joints created with the optimized combinations of welding current and hot-wire feeding speed.

Chapter 4

Investigation of welding phenomena and optimization of hot-wire CO₂ arc welding process for 36-mm heavy-thick steel plate

4.1 Introduction

In the Chapter 3, it was clearly found that hot-wire CO₂ arc welding had much potential to improve the efficiency without the large increase of a heat input. A few suitable combinations of the welding current and hot-wire feeding speed were obtained for a butt joint with the V-shaped groove on 20-mm thick steel plate by using only two passes. The adequate joint properties were also achieved on the sound joints. However, a flow of molten metal preceding the molten pool (molten metal precedence) was observed and it induced defects.

The limitation of the hot-wire feeding speed changed when the different welding current for the first pass as 300 and 400 A was applied in Chapter 3. Figure 4.1 shows the schematic illustrations of cross-sections obtained in Chapter 3 when the welding current for the first pass was changed as 300 and 400 A. The bottom gap for the second pass, which is the same as the bead width of the first pass described in Fig. 4.1, is 7~8 mm on 300 A and 11~12 mm on 400 A. It is predicted that the balance of the molten metal volume, molten metal height, bead width (bottom width) and arc force affects on the molten metal precedence.

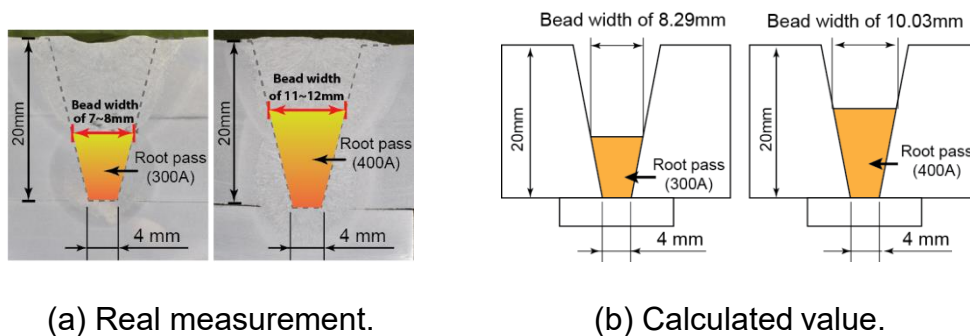


Fig. 4.1 Bead width of previous pass for thick steel plate of 20-mm.

The objective in this chapter is the application of hot-wire CO₂ arc welding for 36-mm heavy thick steel plate. In the first part of this chapter, the effect of the balance of the molten metal volume, molten metal height, bead width (bottom width) and arc force on the molten metal precedence was investigated. Phenomena of the molten pool formation and flow were discussed, and the limitation of the hot-wire feeding speed was obtained. In the second part, the optimizations of welding

conditions for the second to fourth passes of the 36-mm heavy thick joint were performed based on the results in the first part. Then, the joint properties were investigated using the suitable welding conditions. In the third part, the application of hot-wire CO₂ arc welding under a faster welding speed condition was carried out to widen the welding condition tolerance.

4.2 Effects of groove shape on molten metal precedence

Using the welding current on the root pass could increase the weld metal and give the wider bead width for welding the next pass. From experimental results of 20-mm thickness, they were used with the welding current of 300 and 400 A. There were the bead widths where were measured as mentioned above. Therefore, the bead width was determined for trying out with 7, 11, and 15 mm with thick plate of 20-mm. Then, these conditions were performed with the thick plate of 36-mm in each pass, respectively. It is shown the characteristic of root pass in various widths, as illustrated in Fig. 4.2.

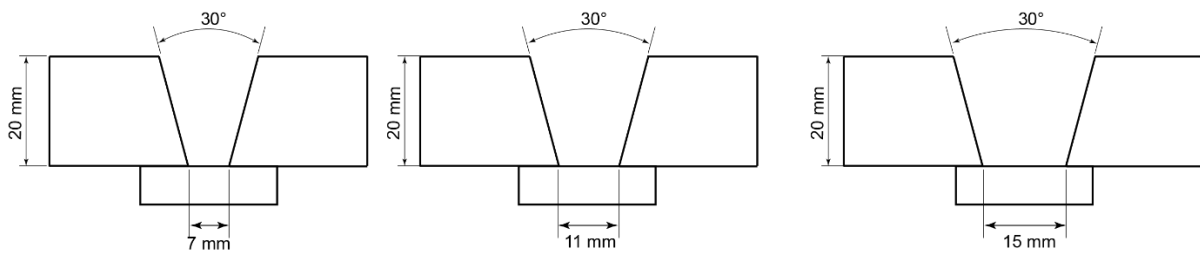


Fig. 4.2 Schematic illustrations of groove shapes with different groove widths.

4.2.1 Materials and specimen used

KE36 steel plates with a dimension of 20^t × 50^w × 400^l mm for finding the appropriate conditions were used as the base metal. The butt joint with a V-shaped groove having its angle of 30° and the root gap of 4 mm was employed, as shown in Fig. 4.3. The chemical compositions of base metal and filler wire and mechanical properties are shown in Tables 4.1 and 4.2.

Chapter 4

Investigation of welding phenomena and optimization of hot-wire CO₂ arc welding process for 36-mm heavy-thick steel plate

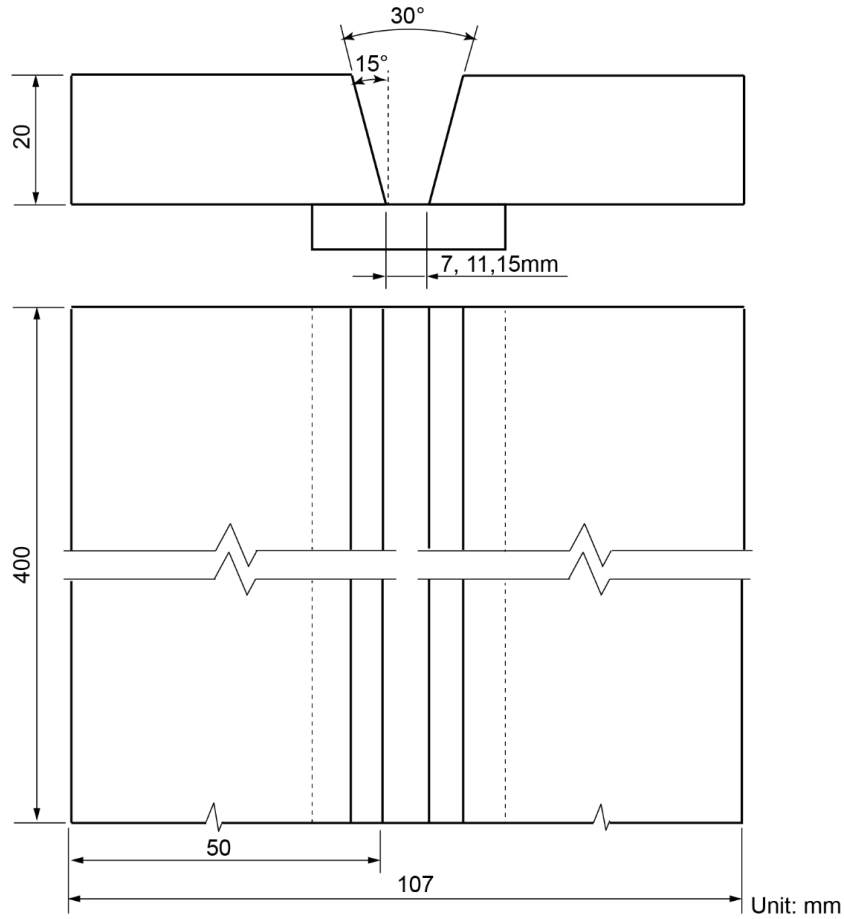


Fig. 4.3 Schematic illustrations of specimen.

Table 4.1 Chemical compositions of base metal and filler wire.

Contents	Base metal: K36E-TM	Filler wire: YGW11
C	0.12	0.02~0.15
Si	0.20	0.40~1.00
Mn	1.21	1.00~1.60
P	0.14	0.03 or less
S	0.04	0.03 or less
Cu	0.01	0.50 or less
Ni	0.01	-
Cr	0.02	-
Ti	-	0.02~0.15
Zr	-	

Table 4.2 Mechanical properties.

Grade	Target properties			
	TS (MPa)	YP (MPa)	EL (%)	vE ₀ (J)
KE36 (Base metal properties)	490~620	≥ 355	≥ 21	≥ 34 (Ave.) ≥ 24 (Each)

4.2.2 Experimental procedure

Figure 4.4 shows the front and side view of setting-up the conditions of the CO₂ hot-wire arc welding system, which was the combination between the CO₂ arc welding and hot wire. It is shown the appearance of the experimental setup in Fig. 4.5. The performance was welded on the first pass, especially at bead widths of 7, 11, and 15 mm, respectively, and used the weaving system with the MAG torch on the root pass as shown in Fig. 4.6. The hot-wire feeding speed was used differently with each bead width that is shown in Table 4.3.

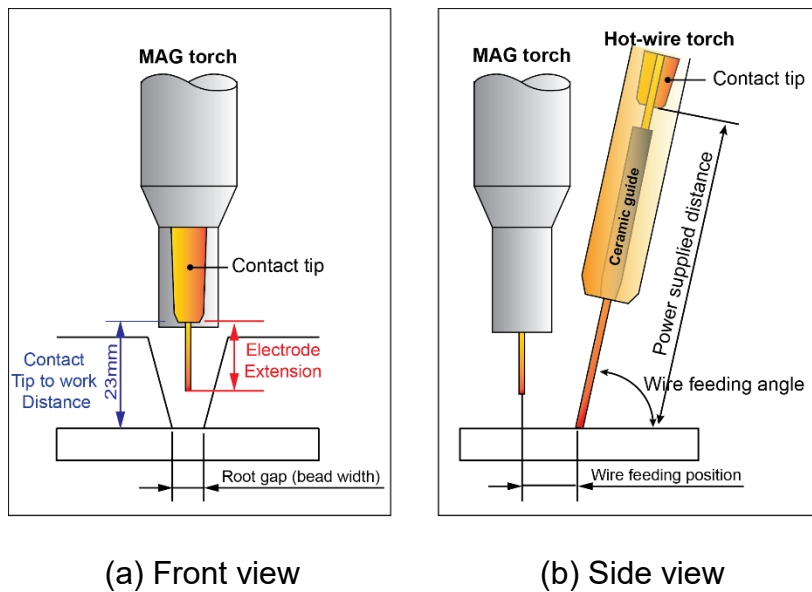


Fig. 4.4 Set up condition.

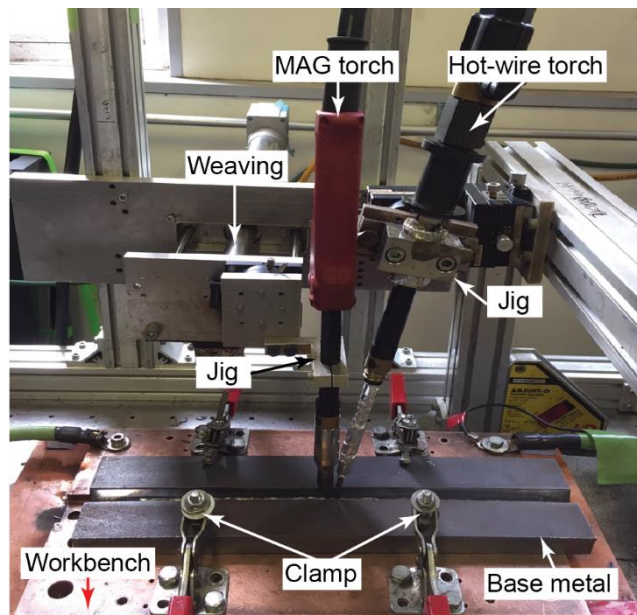


Fig. 4.5 Appearance of experimental setup.

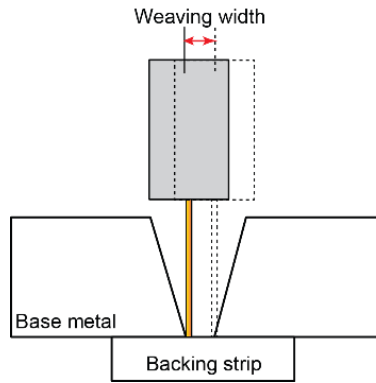


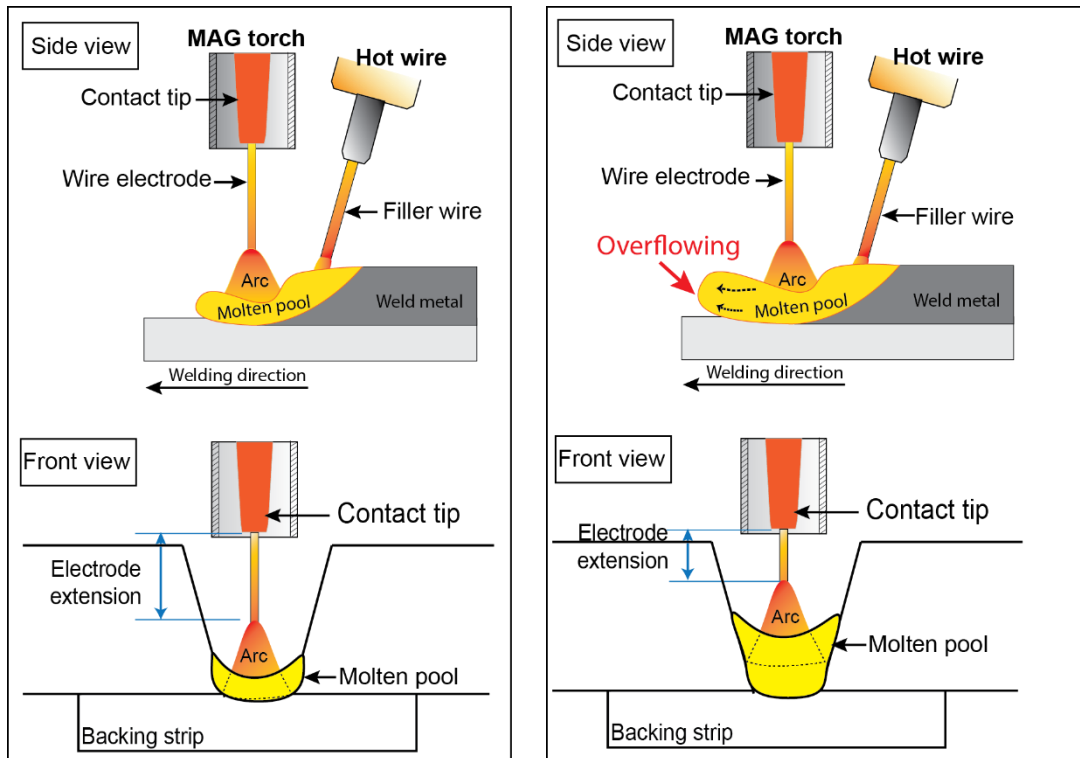
Fig. 4.6 Weaving method for CO₂ arc welding torch.

Table 4.3 Welding conditions

CO ₂ arc welding conditions			
Pass No.	Root pass		
Welding speed, m/min	0.3		
Welding current (Setting), A	400		
Arc voltage, V	41		
Wire feeding speed, m/min	19.9		
Volume, mm ³ /s	376		
Wire diameter, mm	1.2		
Extension length, mm	23		
Shielding gas, L/min	25		
Root pass (bead width), mm	5 (7)	8 (11)	13 (15)
Hot-wire conditions			
Bead width, mm	7	11	15
Wire feeding speed, m/min	5~7.5	10~12.5	10~12.5
Volume, mm ³ /s	167~251	335~417	335~417
Wire current, A	208~249	298~316	298~316
Wire diameter, mm	1.6		
Power supplied distance, mm	80		
Wire feeding angle, degree	70		
Wire feeding position, mm	10		
Duty, %	50		

4.2.3 Result and discussion

For this study, the experiment results are considered regarding the influence of the melting metal flow from filling hot wire's volume in each feeding speed, which were changed the welding speed and expanded the bead width. It was evaluated two conditions for judgment in one case studied. The considered factors in each welding condition were the stable molten pool without molten metal precedence and molten precedence, as presented in Figs. 4.7.



(a) Stable molten pool without molten metal precedence.

(b) Molten metal precedence

Fig. 4.7 Considered factors in each welding condition.

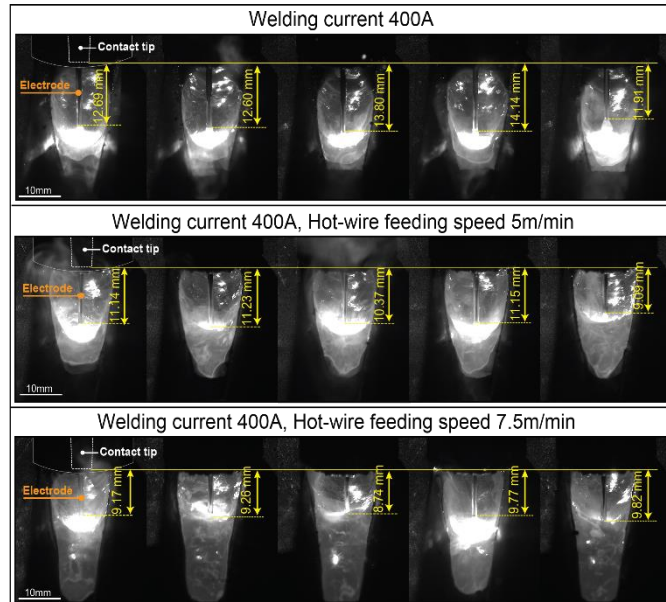
The essential welding variables were diagnosed from experimental results under the stable molten pool without molten metal precedence, which were applied with the bead width of 7, 11, and 15 mm. The welding current of 400 A was set up and used to combine with each hot-wire feeding speed, while the welding speed of 0.3 m/min was fixed. The results were discussed an unstable arc from changing the electrode extension length, which affected the molten pool phenomena as described below.

The high-speed video captured the phenomena of changing the electrode extension length during welding with a mimetic test specimen in each bead width of the filled pass. In this part, the bead width was used three widths as 7, 11, and 15 mm and the hot-wire feeding speeds of 5, 7.5, 10, and 12.5 m/min were applied respectively. The characteristics of changing the electrode extension and arc to work distance are shown in Figs. 4.8 in each bead width. For example, this case at the bead width of 7 mm (Fig. 4.8(a)) filled the hot-wire feeding speed of 5 and 7.5 m/min into the molten pool while the welding current of 400 A was constant. These are found that the electrode extension length decreases when compared with using the

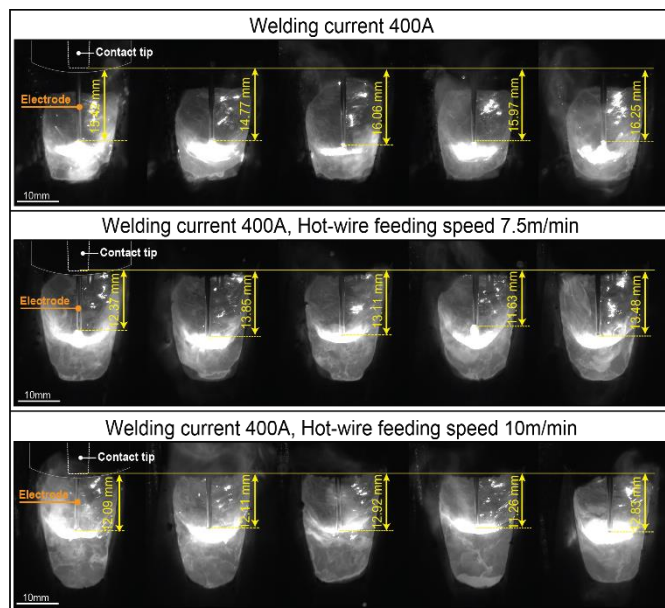
Chapter 4

Investigation of welding phenomena and optimization of hot-wire CO₂ arc welding process for 36-mm heavy-thick steel plate

arc welding of 400 A. The electrode extension length is shortened due to the molten metal of fed hot wire and increased weld metal height.

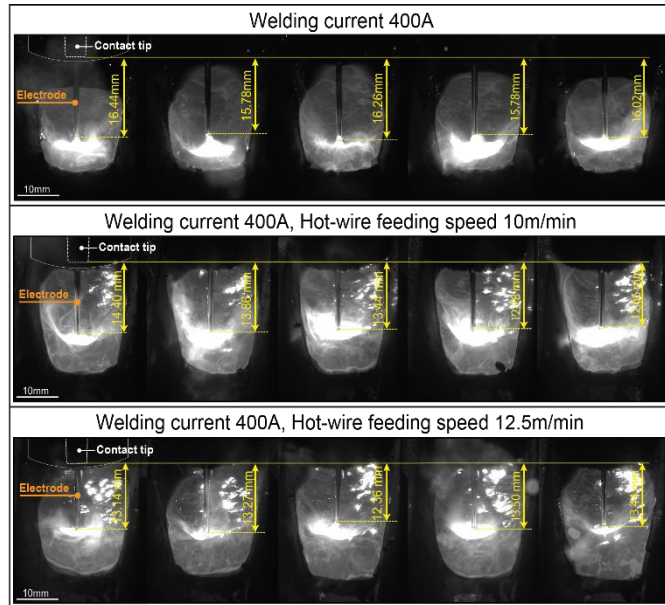


(a) Bead width of 7 mm.



(b) Bead width of 11 mm.

Fig. 4.8 High-speed images during welding.



(c) Bead width of 15 mm.

Fig. 4.8 High-speed images during welding (continued).

Figure 4.8(b) shows the molten pool phenomenon of the bead width as 11 mm. The results found that electrode extension length was shorted of about 3~4 mm from using the hot-wire feeding speed of 7.5 and 10 m/min, respectively when compared with only applying the welding current of 400 A. The molten pool was slightly unstable when it was fed the hot-wire feeding speed of 10 mm. However, when compared with all welding conditions of the bead width of 7 mm, it was found that the molten pool was stable when fed the hot wire as same value.

The bead width of 15 mm, welding current of 400 A, and combination of the CO₂ arc welding and hot-wire feeding speeds of 10 and 12.5 m/min were performed as shown in the molten pool phenomena in Figs. 4.8(c). Both hot-wire feeding speeds of 10 and 12.5 m/min, the molten pool is stable without the molten metal precedence when compared with both hot-wire feeding speeds. But it slightly risked to the molten metal precedence occurred when the hot-wire feeding speed of 12.5 m/min was fed. Thus, the extended bead width can obtain the higher deposit volume, and the molten pool is stable when is applied with the same hot-wire feeding. The electrode extension length and arc force are not disturbed by an additional hot wire when the bead width is more expansive.

Chapter 4

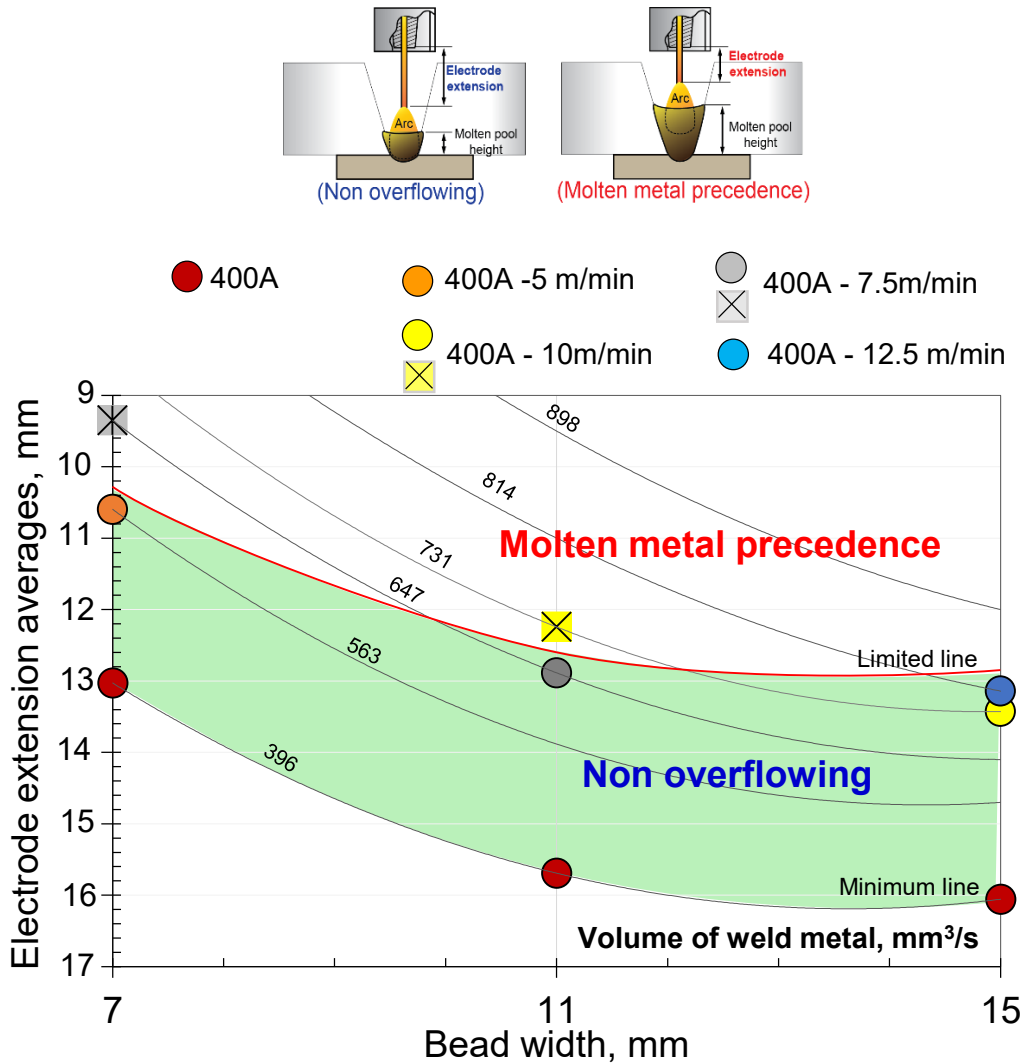


Fig. 4.9 Effects of bead width and electrode extension on molten metal precedence.

The molten pool was observed the flow behavior of molten metal and the change of electrode extension length in front of the molten pool. While the bead widths of 7~15 mm and hot-wire feeding speeds of 5~12.5 m/min were applied. The electrode extension length was measured during welding under the influence of the hot-wire feeding and changed electrode extension length, which affected the molten metal precedence. As a result, the wide bead width can obtain more volume by increasing the hot-wire feeding: for example, at the bead widths of 7~15 m/min, the molten pool shape can obtain the lowest weld metal volume of about 396 mm³/s from its CO₂ arc welding. The hot wire in each hot-wire feeding speed, which was inserted combining with CO₂ arc welding, while the bead width was changed as 7, 11, and 15 mm. The electrode extension average decreased almost linearly with the extension of the bead width and increase of weld metal volume, which the maximum volume of about 731 mm³/s (400 A-12.5 m/min) can be fed into the groove weld at the bead width of 15 mm by without the molten metal precedence occurred. Therefore, the influences of bead width and molten pool height affected the change

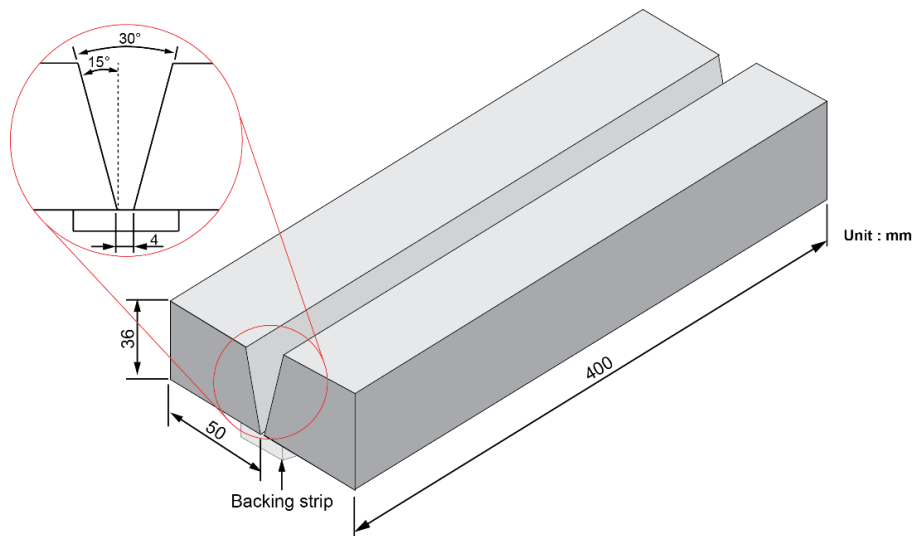
of electrode extension length, even though the same hot wire volume was applied. The available conditions are between the red line (limited line) and minimum line, or the green region in which the molten pool is stable without the molten metal precedence occurred.

The welding parameters such as bead width, and hot-wire feeding speed were performed and molten pool was observed using high-speed camera. The molten pool phenomenon and electrode extension length were investigated to determine the appropriate condition. These available conditions were selected for carrying out multi-pass welding for heavy-thick joint.

4.3 Optimization of multi-pass welding conditions for 36-mm heavy-thick joint

4.3.1 Materials and specimen used

The specimens of the experiment were the KE36 steel plate for using in this study, which is shown in Figs. 4.10. The dimension of the specimen was 36^t × 50^w × 400^l mm for finding the appropriate conditions. The butt joint with a V-shaped groove having its angle of 30 degree and a root gap of 4 mm was used. It is shown in Fig 4.10(a), and the specimen for joint properties evaluation is shown in Fig. 4.10(b).

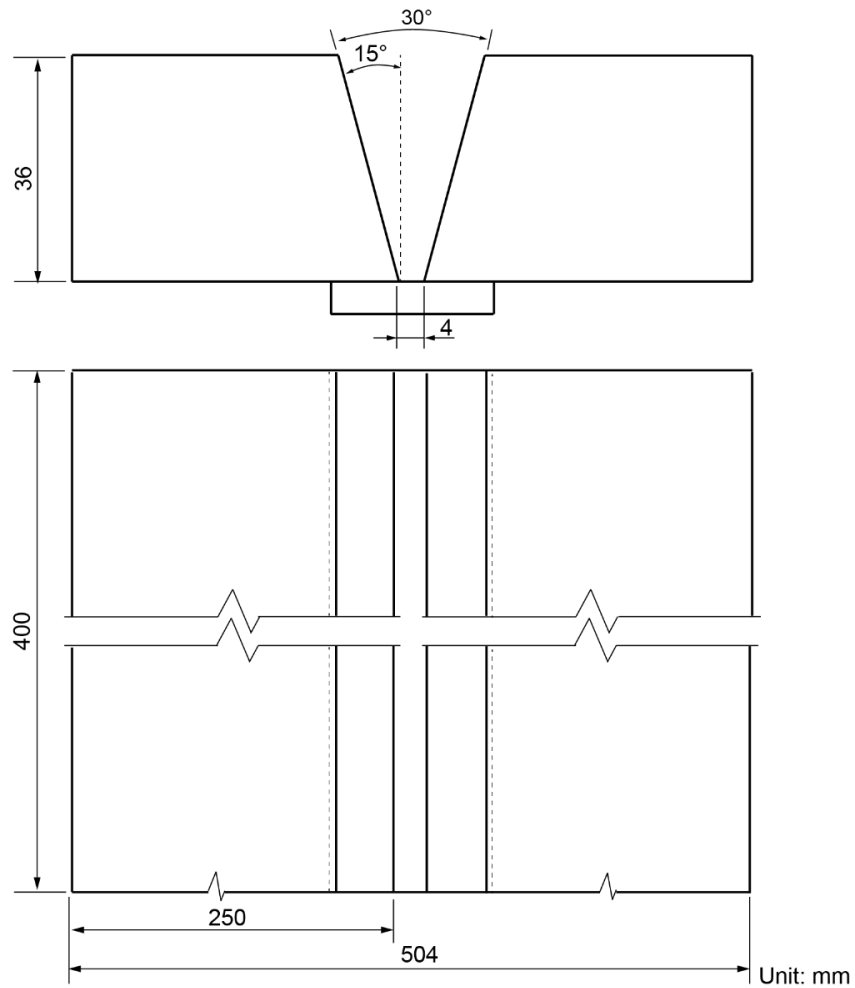


(a) Specimen for fundamental investigations.

Fig. 4.10 Schematic illustrations of specimen.

Chapter 4

Investigation of welding phenomena and optimization of hot-wire CO₂ arc welding process for 36-mm heavy-thick steel plate



(b) Specimen for joint properties evaluation.

Fig. 4.10 Schematic illustrations of specimen (continued).

The filler wire of MG-50 (JIS Z 3312 YGW11) for CO₂ arc welding with a diameter of 1.2 mm for CO₂ arc welding and 1.6 mm for hot wire were used. The chemical composition of base metal, and filler wire and mechanical properties are presented on Tables 4.4 and 4.5.

Table 4.4 Chemical compositions of base metal and filler wire.

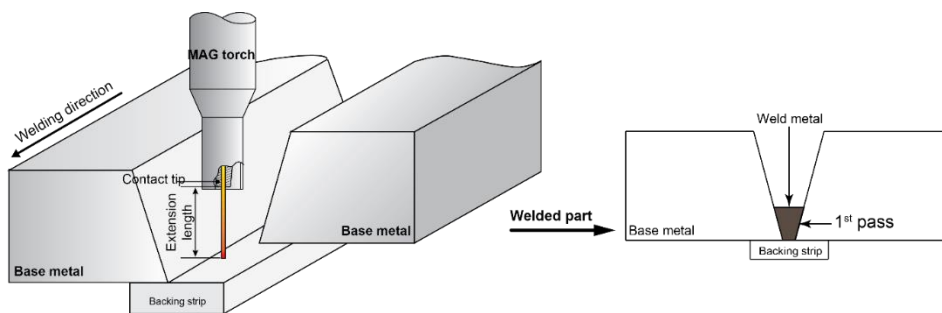
Contents	Base metal: K36E-TM	Filler wire: JIS Z 3312 YGW11
C	0.12	0.02~0.15
Si	0.2	0.40~1.00
Mn	1.21	1.00~1.60
P	0.14	0.03 or less
S	0.04	0.03 or less
Cu	0.01	0.50 or less
Ni	0.01	-
Cr	0.02	-
Ti	-	0.02~0.15
Zr	-	

Table 4.5 Mechanical properties.

Grade	Target properties			
	TS (MPa)	YP (MPa)	EL (%)	vE ₀ (J)
KE36 (Base metal properties)	490~620	≥ 355	≥ 21	≥ 34 (Ave.) ≥ 24 (Each)

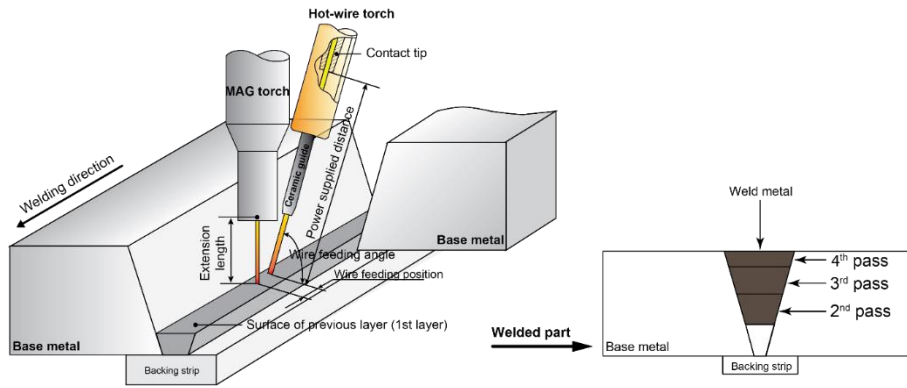
4.3.2 Experimental procedure

CO₂ welding machine equipment was used as YD-500CL4TA2 series (Panasonic) for the first pass welding with its filler wire of 1.2 mm diameter. For the second to fourth pass were combined between CO₂ arc welding and feeding hot wire. The hot wire was a diameter of 1.6 mm, which it was fed with each feeding speed. The characteristics of set-up in each pass are shown in Figs. 4.11.



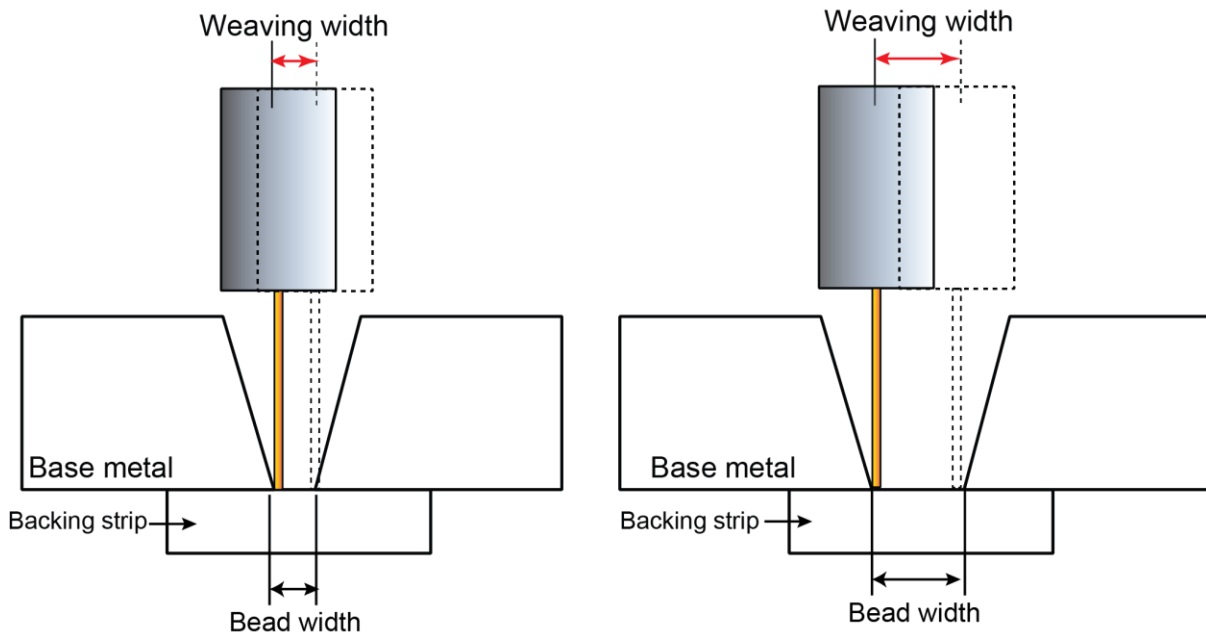
(a) First pass welding.

Fig. 4.11 Schematic illustrations of welding procedure.



(b) Second ~ fourth pass welding.

Fig. 4.11 Schematic illustrations of welding procedure (continued).



(a) Welding for 4 mm bead width. (b) Welding for 7, 11, 15 mm bead width.

Fig. 4.12 Weaving method for CO₂ arc welding torch.

Set up conditions for weaving width in each pass were used as the characteristic in Figs. 4.12. The thick steel plates of 36-mm were determined to weld with a root gap of 4 mm and performed using the welding current of 300 and 400 A. They are shown the welding condition as Tables 4.6 and 4.7. In a part of the root gap of 6 mm, the welding current of 400 A shows the welding condition in Table 4.8.

Chapter 4

Table 4.6 Welding conditions for 4 mm root gap and 300 A welding current on first pass.

CO ₂ arc welding conditions				
Pass No.	1 st	2 nd	3 rd	4 th
Welding speed, m/min	0.3	0.3		
Welding current (Setting), A	300	400		
Arc voltage, V	31	41		
Wire feeding speed, m/min	12.7	19.9		
Volume, mm ³ /s	241	376		
Wire diameter, mm	1.2	1.2		
Extension length, mm	24	22		
Shielding gas, L/min	25	25		
Weaving width, mm	2	7	11	14
Root gap, mm	4	7	14	17
Hot-wire conditions				
Pass No.	1 st	2 nd	3 rd	4 th
Wire feeding speed, m/min	/	5~7.5	10~12.5	10
Volume, mm ³ /s		167~251	335~417	335
Wire current, A		208~249	298~316	298
Wire diameter, mm		1.6		
Power supplied distance, mm		80		
Wire feeding angle, degree		70		
Wire feeding position, mm		10		
Duty, %		50		

Chapter 4

Table 4.7 Welding conditions for 4 mm root gap and 400 A welding current on first pass.

CO ₂ arc welding conditions				
Pass No.	1 st	2 nd	3 rd	4 th
Welding speed, m/min	0.3	0.3		
Welding current (Setting), A	400	400		
Arc voltage, V	41	41		
Wire feeding speed, m/min	19.9	19.9		
Volume, mm ³ /s	376	376		
Wire diameter, mm	1.2	1.2		
Extension length, mm	24	22		
Shielding gas, L/min	25	25		
Weaving width, mm	2	7	12	15
Root gap, mm	4	10	15	18
Hot-wire conditions				
Pass No.	1 st	2 nd	3 rd	4 th
Wire feeding speed, m/min	/	7.5~10	12.5~15	/
Volume, mm ³ /s		251~335	417~502	
Wire current, A		249~298	316~357	
Wire diameter, mm		1.6		
Power supplied distance, mm		80		
Wire feeding angle, degree		70		
Wire feeding position, mm		10		
Duty, %		50		

Table 4.8 Welding conditions for 6 mm root gap and 400 A welding current on first pass.

CO ₂ arc welding conditions				
Pass No.	1 st	2 nd	3 rd	4 th
Welding speed, m/min	0.3	0.3		
Welding current (Setting), A	400	400		
Arc voltage, V	41	41		
Wire feeding speed, m/min	19.9	19.9		
Volume, mm ³ /s	376	376		
Wire diameter, mm	1.2	1.2		
Extension length, mm	22	22		
Shielding gas, L/min	25	25		
Weaving width, mm	5	7	13	16
Root gap, mm	6	11.5	16	19
Hot-wire conditions				
Pass No.	1 st	2 nd	3 rd	4 th
Wire feeding speed, m/min	/	10~12.5	12.5~15	/
Volume, mm ³ /s		335~417	417~502	
Wire current, A		298~316	316~357	
Wire diameter, mm		1.6		
Power supplied distance, mm		80		
Wire feeding angle, degree		70		
Wire feeding position, mm		10		
Duty, %		50		

4.3.3 Macro specimen preparation and Initial measurements of weld metal

Specimens for metallography of weld metal achieved a complete join and obtained a sound weld bead appearance. The preparation was performed according to the detail in Chapter 3.

4.3.4 Results and discussions

From the previous experiment results, the essential welding parameters were considered for their effects on the molten pool phenomena as described below.

4.3.4.1 Influence of hot-wire feeding speed on molten pool phenomena

The welding phenomena were observed in the molten pool using the high-speed camera with the determined welding conditions. The root gap of 4 mm was welded by the welding currents of 300 and 400 A, and the welding current of 400 A was performed in the root gap of 6 mm. Both root gaps were welded without feeding the hot wire. The combination of CO₂ arc welding and hot-wire feeding was performed on the second to fourth pass while the CO₂ arc welding was fixed the welding current of 400 A and the hot-wire feeding speed was varied in each pass depending on the bead width of the previous pass.

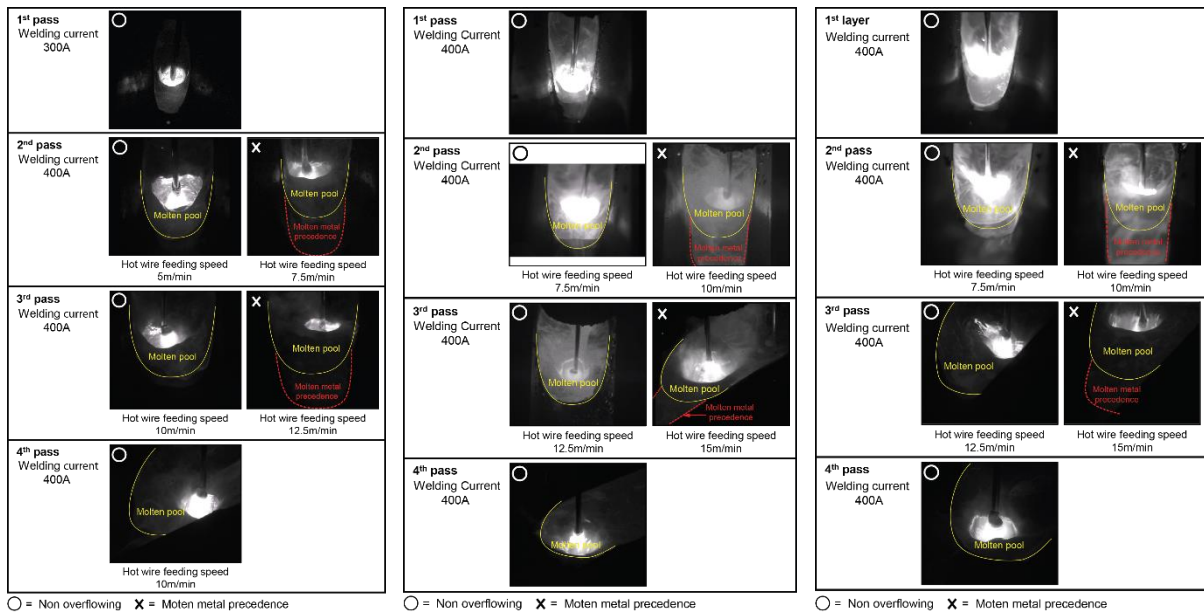
The results of experiment, as the root gap of 4 mm was welded with the welding current of 300 A as shown in Fig. 4.13(a). It is found that the second pass is filled with the hot-wire feeding speeds of 5 and 7.5 m/min. The occurred molten metal precedence since the hot-wire feeding speed of 7.5 m/min was fed when compared with the hot-wire feeding speed of 5 m/min having the stability of the molten pool. For the third pass was fed the hot-wire feeding speed of 10 and 12.5 m/min. The molten pool phenomenon of hot-wire feeding speed of 10 m/min shows to maintain the molten pool's stability better than using the hot-wire feeding speed of 12.5 m/min when was compared. On the fourth pass, it was fed the hot-wire feeding speed as 10 m/min which is sufficient for filling depth of groove weld.

Figure 4.13(b), the first pass was welded with the welding current of 400 A, while the root gap of 4 mm was fixed as 4 mm. The second pass was performed by the hot-wire CO₂ arc welding and fed as 7.5 and 10 m/min of hot-wire feeding speeds. The molten pool can maintain the stable arc and keep the higher hot-wire feeding as 10 m/min when compared with the second pass of the first pass welding current of 300 A. For the third pass, at the hot-wire feeding speed of 12.5 m/min, the molten pool is stable and without the molten metal precedence when compared with 15 m/min having the molten metal precedence occurred. The final pass (fourth pass) was welded by only CO₂ arc welding as the welding current of 400 A, which is adequate for filling depth without hot-wire feeding.

The first pass welding current of 400 A was used with the root gap of 6 mm, as shown in Fig. 4.13(c). In this case, according to a study about width bead, that could achieve the high deposited volume from feeding the hot wire in proper condition. As a result, the second to fourth pass is as successful as the first pass welding current of 400 A and root gap of 4 mm. Due to the extended root gap as 6 mm, there was a similarity in the previous bead width when compared with the root gap of 4 mm, as shown in Fig. 4.13(b).

Chapter 4

Investigation of welding phenomena and optimization of hot-wire CO₂ arc welding process for 36-mm heavy-thick steel plate



(a) First pass : 300 A,
root gap of 4 mm.

(b) First pass : 400 A,
root gap of 4 mm.

(c) First pass : 400 A,
root gap of 6 mm.

Fig. 4.13 High-speed images of molten pool during welding.

Therefore, each previous pass's width bead is the main reason that affects the arc force and stability of the molten pool while the hot-wire addition in each wire-feeding speed is used differently. The welding phenomenon of the molten pool was observed in the front of the arc. It can be inferred that the influence of the bead width and total volume of filler wires significantly affected the welding phenomenon.

4.3.4.2 Effects of groove-shape size on melting metal flow in molten pool

Both first passes were welded using the welding currents of 300 and 400 A, while the root gap of 4 mm was fixed with both welding currents. And the root gaps of 4 and 6 mm were applied with the welding current of 400 A. The obtained weld metal areas was measured the bead width (previous surface), where was varied according to welding in each pass as shown in Figs. 4.14 and 4.15. The bead width's measurement positions were the first, middle, and end of the welded part. Consequently, the welding conditions for the second and third pass were determined under the bead widths of the previous pass in each first pass welding current of 300 and 400 A and root gaps of 4 and 6 mm, respectively, as shown in Figs. 4.16.

Chapter 4

Investigation of welding phenomena and optimization of hot-wire CO₂ arc welding process for 36-mm heavy-thick steel plate

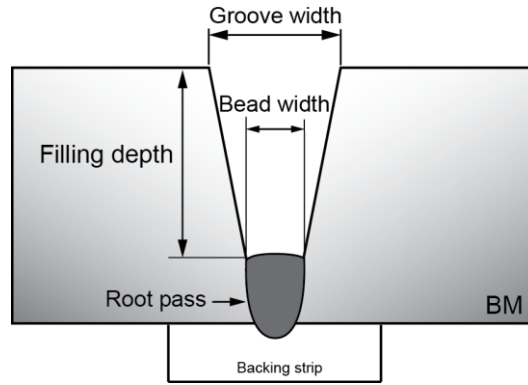


Fig. 4.14 Schematic illustration of first pass.

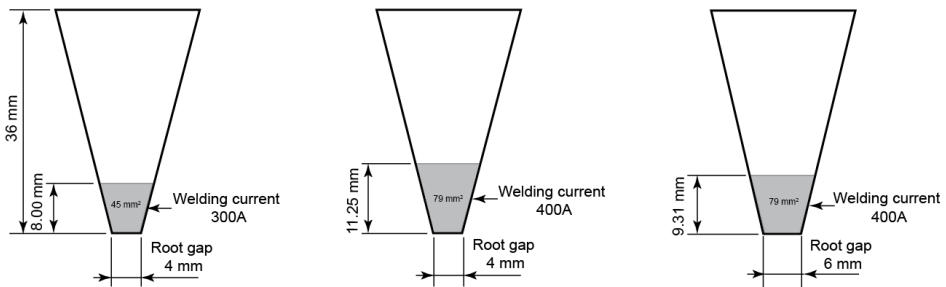
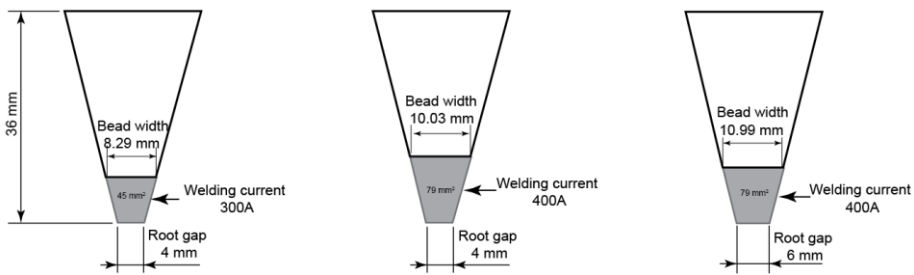
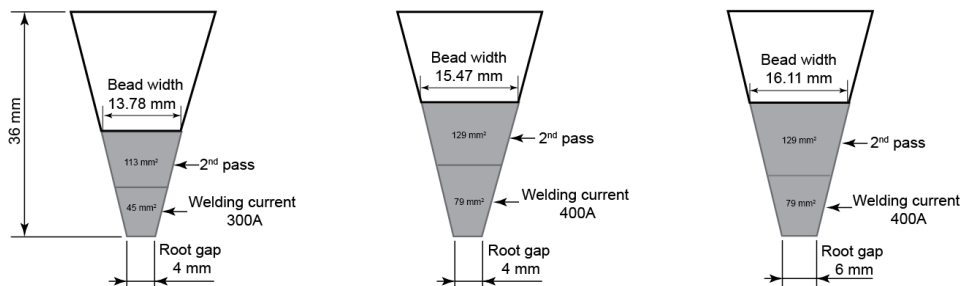


Fig. 4.15 Area of weld metal for each first pass.



(a) Bead width (bottom width) for second pass.

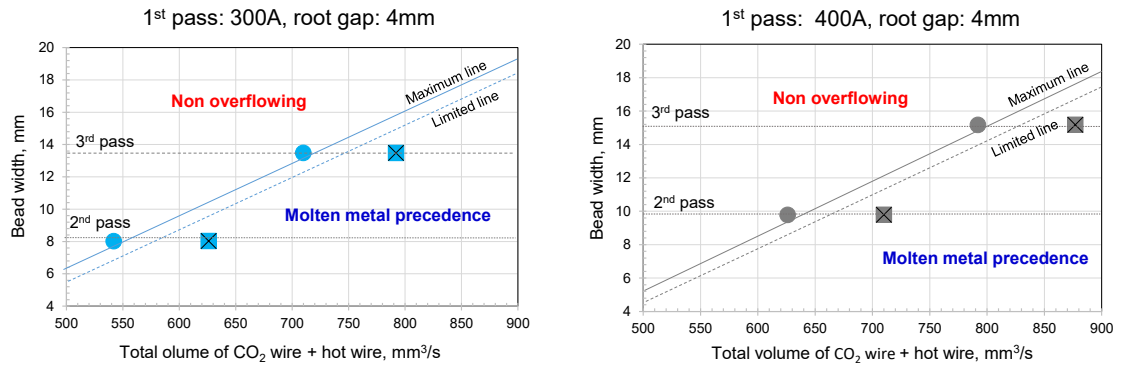


(b) Bead width (bottom width) for third pass.

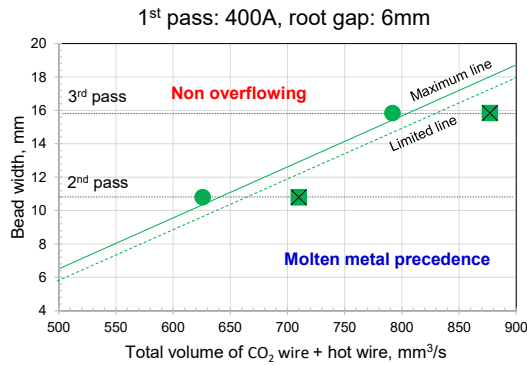
Fig. 4.16 Bead widths and deposited areas on each pass.

Chapter 4

Investigation of welding phenomena and optimization of hot-wire CO₂ arc welding process for 36-mm heavy-thick steel plate



(a) First pass: 300A, root gap of 4 mm. (b) First pass: 400A, root gap of 4 mm.



(c) First pass: 400A, root gap of 6 mm.

Fig. 4.17 Relationships between bead width and total volume of filler wires on each condition.

The experiment was performed according to the determined conditions. The results show the relationship between the total volume of filler wires and bead widths in each condition, as shown in Figs. 4.17. The blue circle marks above the blue line (maximum line) as shown in Fig. 4.17(a) and the grey circle marks above the grey line (maximum line) as shown in Fig. 4.17(b) had the stable molten pool and non-overflowing. The molten metal precedence occurred when the total volume of CO₂ wire and hot wire increased, which are shown in the cross marks under the dotted lines (limited line) of both first pass of 300 and 400 A welding currents at the root gap of 4 mm: for example, at the first pass welding current of 300 A, the molten pool can keep the stability of the arc when fed the hot-wire feeding speed of 5 m/min. However, the wider bead width from using 400 A of first pass welding current, It can avoid the molten metal precedence when inserted the hot-wire feeding speed of 7.5 m/min as well. The comparison between the root gaps of 4 and 6 mm, the first pass was welded at the welding current of 400 A as shown in Figs. 4.17(b) and (c). The status of the molten pool was similar when it was fed the same volume of hot wire because of the changed bead width of the previous surface slightly having the different width of about 2 mm. Therefore, the expansion of bead width from applying

the higher welding current and changing root gap size on the first pass affects the molten pool's stability, which can avoid the molten metal precedence occurred.

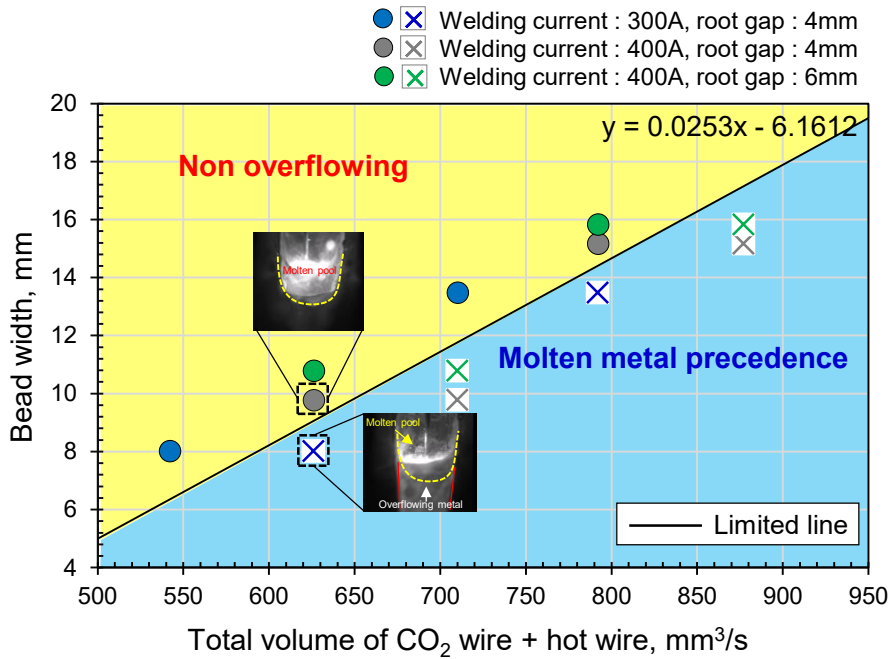


Fig. 4.18 Relationships between bead width and total volume of filler wires.

Figure 4.18 shows the evaluation of the filler wires' total volume for welding on the different bead widths. The hot wire volume was fed combining with the CO₂ arc welding by its welding current of 400 A. All welding conditions only were performed on the second and third pass. The circle symbols indicate the condition for the stable molten pool formation (non overflowing) without molten metal precedence. The cross symbols present the occurrence of molten metal precedence. It was found that the wider bead width can maintained the stable molten pool better than the narrower bead width. The yellow region in Fig. 4.18 shows the obtained conditions for welding under the limited bead width and deposited metal in each pass. The average trend of non-overflowing condition and molten metal precedence can be predicted from the total volume of filler wires and bead width. An average value between both conditions as shown the following equation, $y = 0.0253x - 6.1612$ is shown in graph (Fig. 4.18), which is the limit of deposited metal in each pass and bead width.

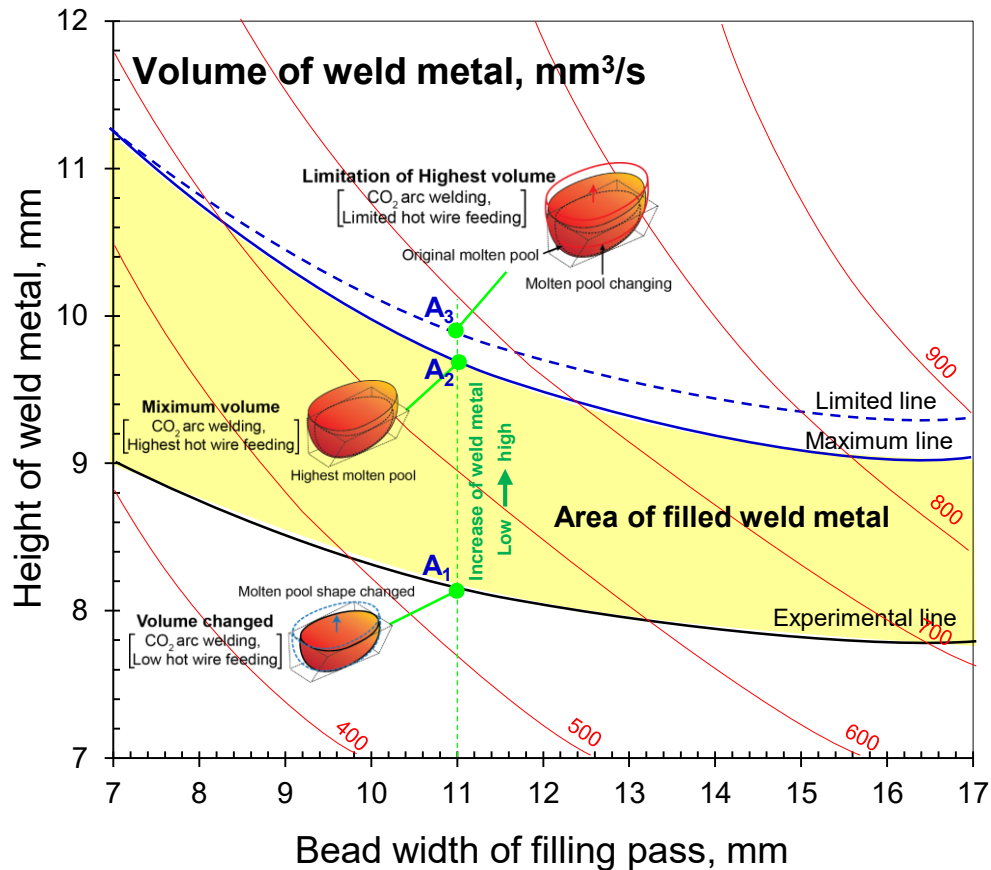


Fig. 4.19 Effects of combination between bead width and height of weld metal on molten metal precedence.

Figure 4.19 presents all parameters for the butt joint of 36-mm thick steel plate using the hot-wire CO₂ arc welding process. This relationship graph is summarized especially the available conditions on the second and third pass. It was performed under the combination between the CO₂ wire and hot wire volume. The bead width in each pass depends on the previous pass. The weld metal height corresponds to the filled weld metal, and the total deposited volume accredits from the bead width of the filled pass.

The total deposited volume of the weld metal can be predicted from each pass approximation. It clearly sees that the main effects of changing the molten pool shape were the changed bead width and fed hot-wire volume. For example, at 11 mm bead width of welded bead can be filled the highest deposited volume of about 658 mm³/cm as shown on position A₂ (maximum line) where is non-overflow metal. Moreover, in position A₃ (limited line) or over blue dash line, where has a risk to molten metal precedence occurred from filling more hot-wire volume under keeping its electrode extension and arc to work distance as mentioned above in part of investigating the effects of hot-wire feeding speed. Position A₁ (minimum line) shows the minimum of the total deposited volume of about 542 mm³/cm when the bead

width is 11 mm. The molten pool shape slightly is changed from the influence of the fed hot-wire volume. However, the molten pool still keeps the stable molten pool when the hot-wire volume is fed until position A₂ (maximum line). It is shown a range of filled weld metal as presented in the yellow region. Therefore, the weld metal can be filled in each bead width from welding on each pass and indicate the height of the welded bead by adding the hot wire in each feeding speed using the constant welding current. It gives the highest deposited volume under the maximum line in each bead width of the filling pass.

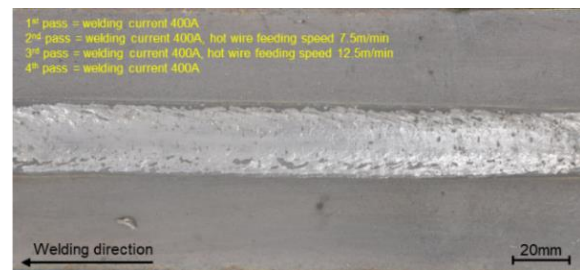
4.3.4.3 Evaluation of joint properties

The welding conditions, which were determined for welding each pass. It was selected according to the optimized condition from the difference of hot-wire feeding speed and bead width. Consequently, the sound weld joints were performed under the optimal conditions without the molten metal precedence occurred as shown in Figs. 4.13(a) and (b). Two weld beads achieved the filled-up sound bead without any defects and can avoid other problems as shown in Fig. 4.20.

Figure 4.21 shows the cross-sections obtained from welding under the appropriate condition which could avoid the molten metal precedence. Thus, both weld beads had the complete fusion and without any defects when was investigated.



(a) First pass: 300A.

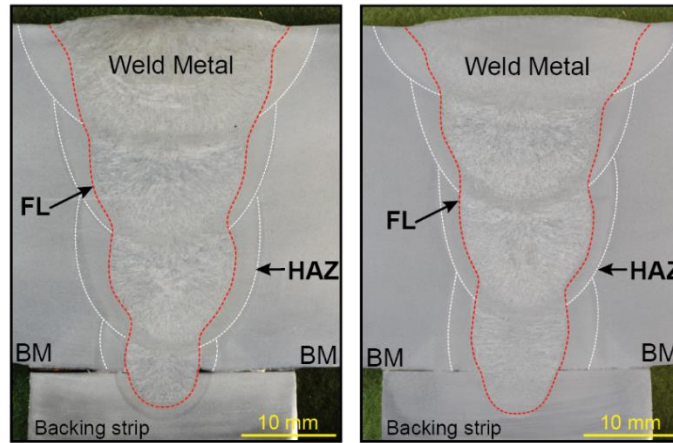


(b) First pass: 400A.

Fig. 4.20 Appearances of joints using suitable conditions on 4 mm root gap.

Chapter 4

Investigation of welding phenomena and optimization of hot-wire CO₂ arc welding process for 36-mm heavy-thick steel plate



(a) First pass: 300A. (b) First pass: 400A.

Fig. 4.21 Cross-sections of joints using suitable conditions on 4 mm root gap.

Optimized conditions

1 st pass	: welding current 300A
2 nd pass	: welding current 400A : hot wire feeding speed 5m/min
3 rd pass	: welding current 400A : hot wire feeding speed 10m/min
4 th pass	: welding current 400A : hot wire feeding speed 10m/min
1 st pass	: welding current 400A
2 nd pass	: welding current 400A : hot wire feeding speed 7.5m/min
3 rd pass	: welding current 400A : hot wire feeding speed 12.5m/min
4 th pass	: welding current 400A

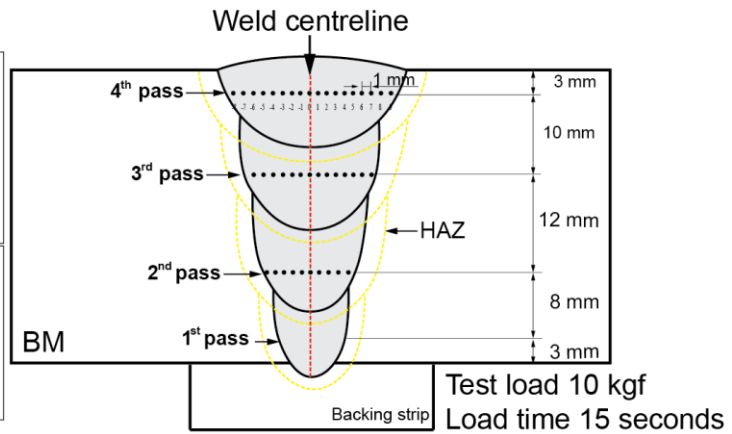
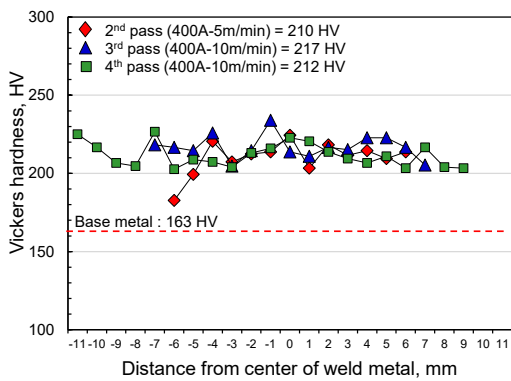
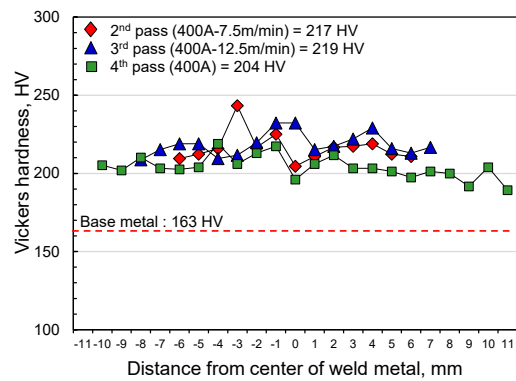


Fig. 4.22 Measurement point for Vickers hardness test.



(a) First pass: 300 A.



(b) First pass: 400 A.

Fig. 4.23 Vickers hardness distributions of weld metals on joints using suitable conditions on 4 mm root gap.

Two achieved weld beads were measured the hardness of weld metal on each pass as shown in Fig. 4.22 using the testing of 10 kgf and the load time of 15 s. The Vickers hardness of weld metal was welded by using the welding current of 300 A at the first pass, and the second to fourth pass were welded by the welding current of 400 A and fed the hot-wire feeding speeds of 5~12.5 m/min, respectively, as shown in Fig. 4.23(a). It was found that the hardness of weld metal depended on the value of the added hot-wire feeding speed into the arc. In this case, the second pass was filled with the hot-wire feeding speed of 5 m/min and 10 m/min for the third pass. The Vickers hardness of the second pass's weld metal is lower than the weld metal of the third pass when compared. They give the Vicker hardness average of the weld metal approximately 210~217 HV, respectively.

For the first pass welding current of 400 A is shown in Fig. 4.23(b). There is the highest hardness of weld metal in the third pass of about 219 HV, when compared with other passes because the hardness of weld metal was increased by filling the higher hot wire. Finally, the fourth pass was weld by using the welding current of 400 A without the hot-wire feeding having the hardness of weld metal of about 204 HV. In contrast, although the increase of hot-wire feeding speed give the slightly high hardness of weld metal, it can increase the volume of deposited metal and decrease the dilution ratio and HAZ width.

Charpy impact test was tested according to JIS Z 2242. The standard specimen size for Charpy impact test is 10 mm x 10 mm x 55 mm as shown the cutting plan and notch location of test pieces in Fig. 4.24. The Charpy test equipment has a heavy pendulum of 25.31 kg and arm length of 0.7 m in this test.

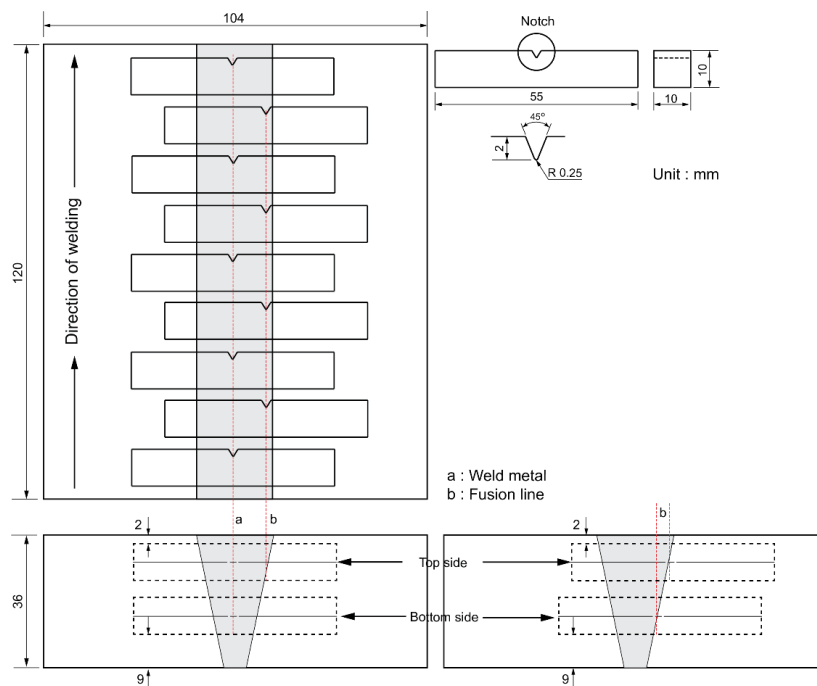
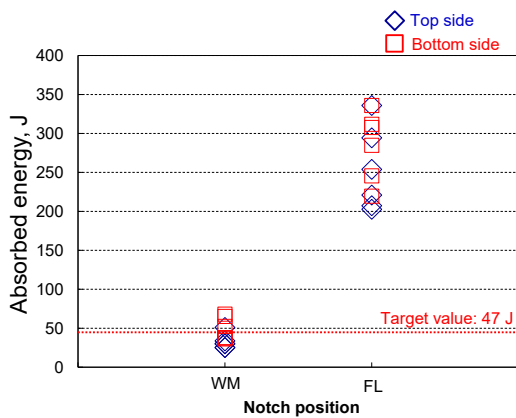


Fig. 4.24 Cutt-off plan for V-Notched Charpy specimen.

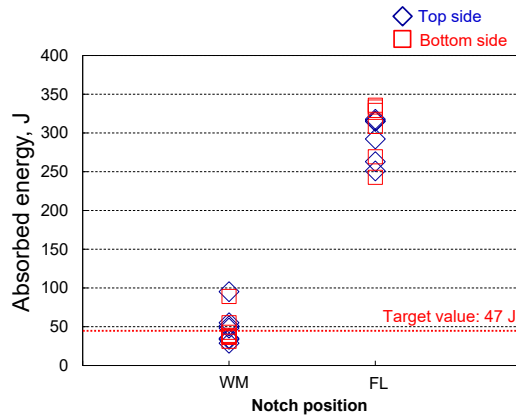
The evaluation of impact test is the absorbed energy of material for brittle fracture at 0° C only for obtaining to comply with the criterion test standard. The notch locations were at weld metal (WM) and fusion line (FL). Charpy V-notch impact test result is shown in Table 4.9.

Table 4.9 Result of absorbed energy.

Welding current on 1 st pass	Notch position	Absorbed energy, J	
		Weld metal	Fusion line
300A	Top side	98.4	291.3
		60.8	314.9
		63.7	300.3
	Bottom	68.8	333.9
		44.2	334.1
		59.4	334.3
400A	Top side	86.0	302.2
		89.1	275.5
		87.5	334.1
	Bottom	84.5	334.1
		71.0	334.1
		74.0	333.9



(a) First pass: 300A.

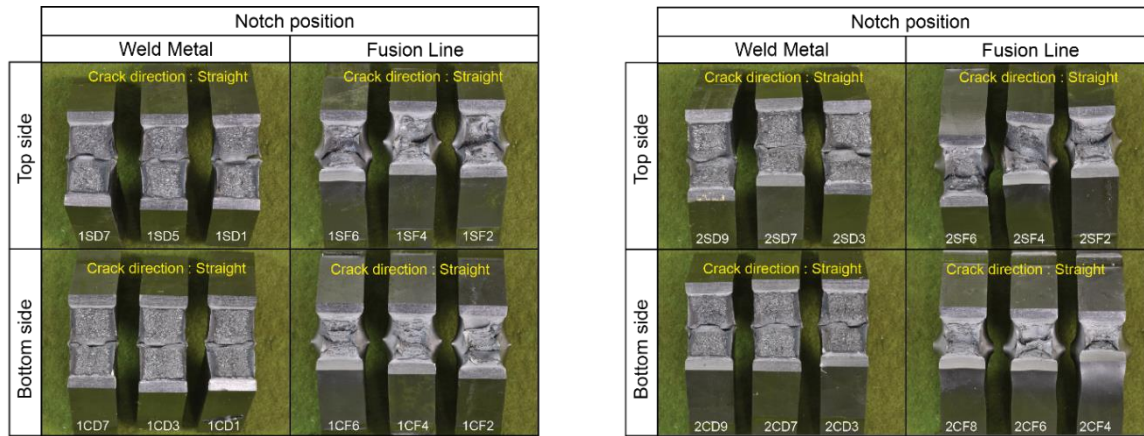


(b) First pass: 400A.

Fig. 4.25 Results of Charpy impact test.

Figure 4.25(a) shows the absorbed energy result at the first pass welding current of 300 A. The weld metal on top side gives the average of absorbed energy lower than the weld metal on bottom side. When both notch locations of weld metal (top and bottom side) were compared with both fusion line positions (top and bottom side) having the lower absorbed energy. Figure 4.25(b) shows the absorbed energy of the test pieces using the welding current of 400 A on the first pass. The toughness of weld metal and fusion line is adequate for the toughness property of the

specification requirement over 47 J at 0° C. These results are assumed that the low absorbed energy of weld metal influences by its structure because the hot-wire feeding affected the cooling rate within the molten pool and affected the obtained hardness.



(a) First pass: 300A.

(b) First pass: 400A.

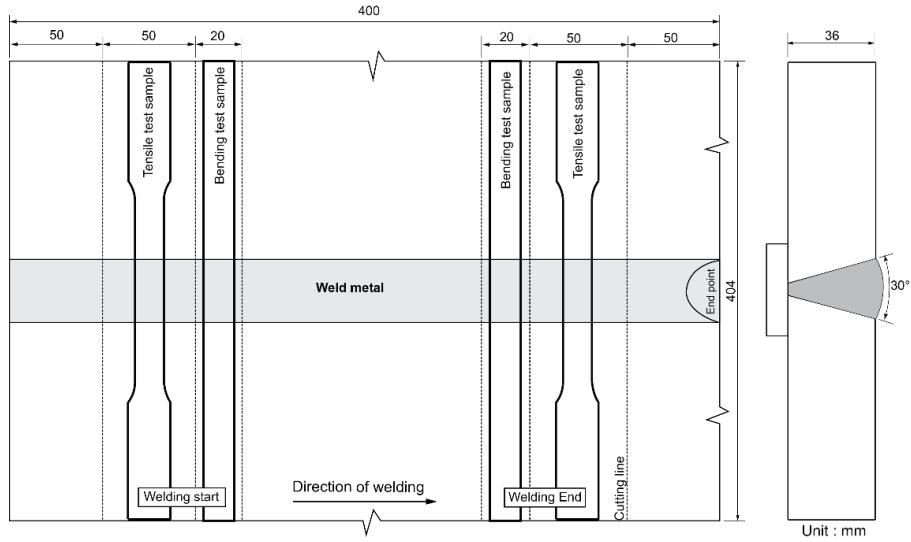
Fig. 4.26 Fracture surfaces of Charpy impact test specimens.

The fractured surface micrographs of the Charpy V-notch impact test specimens as shown in Figs. 4.26 (a) and (b) have the fracture modes of weld metal and fusion line region. In indications are different for both fractured surfaces that were split. In this case, these classification tests can be carried out on homogeneous or non-homogeneous between weld metal and heat affected zone leading to higher energy consumption at the fusion line zone. However, a relatively small value appears in the weld metal. That can select the different filler metals for improving its toughness.

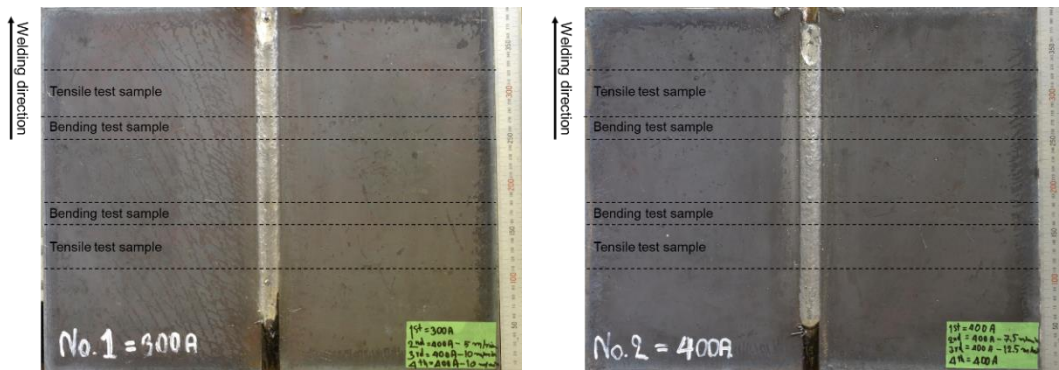
To check repeatability of sound welded joint, both the mechanical tests of bending test and tensile test were referred according to the mechanical testing of welded joint showing the layout of the test specimen and cut-off plan as displayed in Fig. 4.27. The bending test and tensile test specimens were subjected to different sizes. Both tests were performed coupons using two samples in each case.

Chapter 4

Investigation of welding phenomena and optimization of hot-wire CO₂ arc welding process for 36-mm heavy-thick steel plate



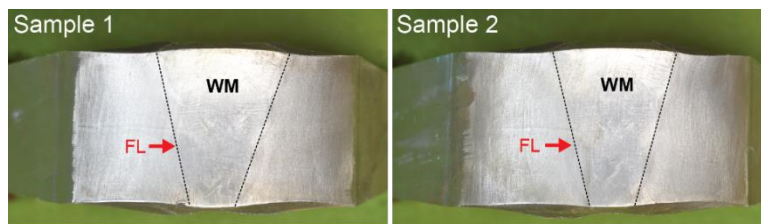
(a) Layout of test specimen.



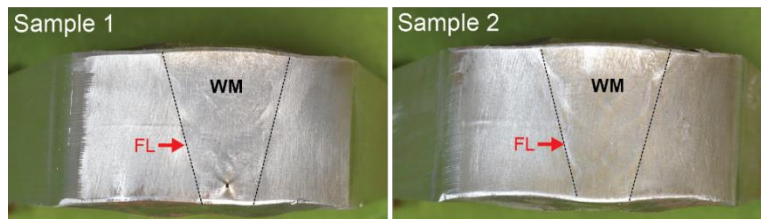
(b) First pass: 300A.

(c) First pass: 400A.

Fig. 4.27 Appearances of weld bead for bending and tensile test.



(a) First pass: 300A.



(b) First pass: 400A.

Fig. 4.28 Results of bending tests.

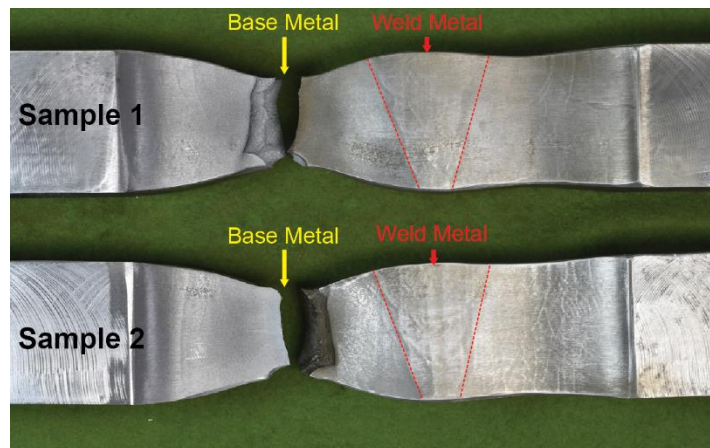
Chapter 4

The joint specimens were subjected to a guided bend test. The results are shown in Fig. 2.28. All bending specimens notice the absence of crack and fracture on the weld metal and fusion line surfaces. It is represented the good ductility of the welded joint under the different hot-wire feeding in each pass.

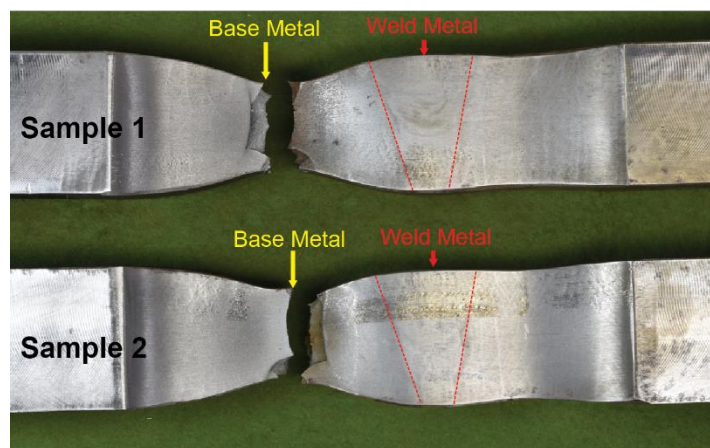
Table 4.10 Results of tensile testes.

Conditions	Tested position	Tensile strength [N/mm ²]	Breaking position
(a) Sample 1 Sample 2	Welding Start	500	Base metal part
	Welding End	501	Base metal part
(b) Sample 1 Sample 2	Welding Start	491	Base metal part
	Welding End	510	Base metal part

*Specified strength $\geq 400\text{N/mm}^2$



(a) First pass: 300A.



(b) First pass: 400A.

Fig. 4.29 Tensile test specimens after testing.

The tensile test was performed on the achieved joints, which was determined the sampling location on the welding start and end. The results of the tensile strength are shown in Table 4.10. The breaking positions of all tensile test specimens are located in the base metal region of both achieved joints as shown in Fig. 4.29. It clearly can be seen that all joints were welded under the proper conditions giving the tensile strength higher than the base material of 400 N/mm² of specified strength. All specimens that broke in the weld metal indicated the adequate tensile strength of about 491~510 N/mm² when compared with the value of the base material. The fracture in the base metal can be obtained with appropriate weld metal hardness and suppression of softening of HAZ from the hot-wire feeding.

4.4 Optimization of welding conditions for faster welding speed

4.4.1 Introduction

Nowadays, ship construction has been improved several welding processes for efficient and rapid manufacturing of large structural sizes. The conventional arc welding process still uses various welding speeds for multi-pass welding of heavy-thick joint. In order to increase the high-efficiency welding process without the need for a large increase in heat input to maintain joint quality and properties, it has been proposed to increase the welding speed and hot-wire feeding. The first part is to apply the welding speed of 0.3 m/min, welding current of 400 A, hot-wire feeding speed of 5~12.5 m/min in each pass with thick steel plate of 36-mm. The welded joint achieved the good joint under the determined welding conditions by controlling the filler wire's material volume. From the previous experiment, welding in bead width of 4 mm, welding speed of 0.3 m/min, and welding current of 400 A was employed. The molten pool slightly had the molten metal precedence, and cracking occurred from welding in a narrow gap groove.

In this part is designed to improve the weldment's high efficiency to study the feasibility of high-performance welding techniques. Also, it would be an alternative condition for fast welding of the thick steel plate using the hot-wire CO₂ arc welding process with hot-wire addition. The welding conditions were used the faster welding speed and higher hot-wire feeding. All of the welding conditions in each pass, the stability of the molten pool was observed by the high-speed camera. The sound welded joint was investigated the cross sectional profile and performed the mechanical property under the appropriate conditions using the low-heat-input CO₂ arc-welding process.

4.4.2 Predictions of heat input and additional material volumes under various welding speeds

The welding condition for this study, it was considered regarding the effects of hot-wire feeding in each welding speed while the bead width was varied. The weld metal area was evaluated under the determined welding condition, which can be predicted by the combination of heat input and additional material volume as shown in Fig. 4.30.

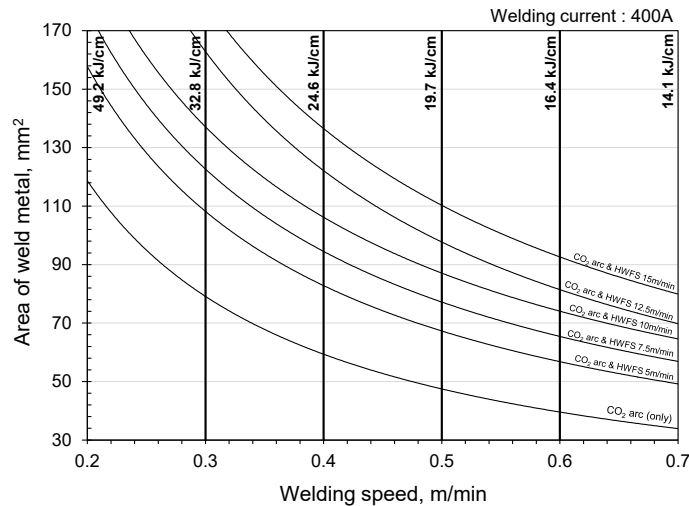


Fig. 4.30 Predicted combinations of heat input and additional material volumes.

4.4.3 Specimens and welding conditions

This study, the base metal was the steel plates of 490 MPa class (NK-KE36) with dimensions of 36^t × 50^w × 400^l mm. the butt joint with the V-shaped groove with the angle of 30° and bead widths of 4, 7, 11 and 15 mm was used, as shown in Figs. 4.31 and 4.32. The filler wire of JIS Z3312 YGW11 with 1.2 mm diameter was used for CO₂ arc welding and 1.6 mm diameter was used for hot wire.

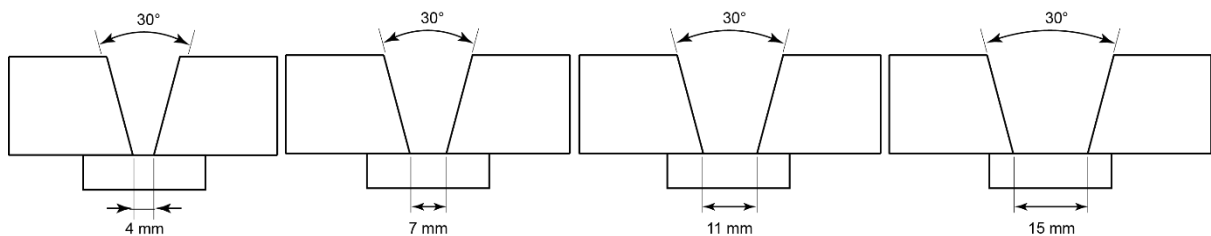


Fig. 4.31 Schematic illustrations of groove shape with different root gap.

Chapter 4

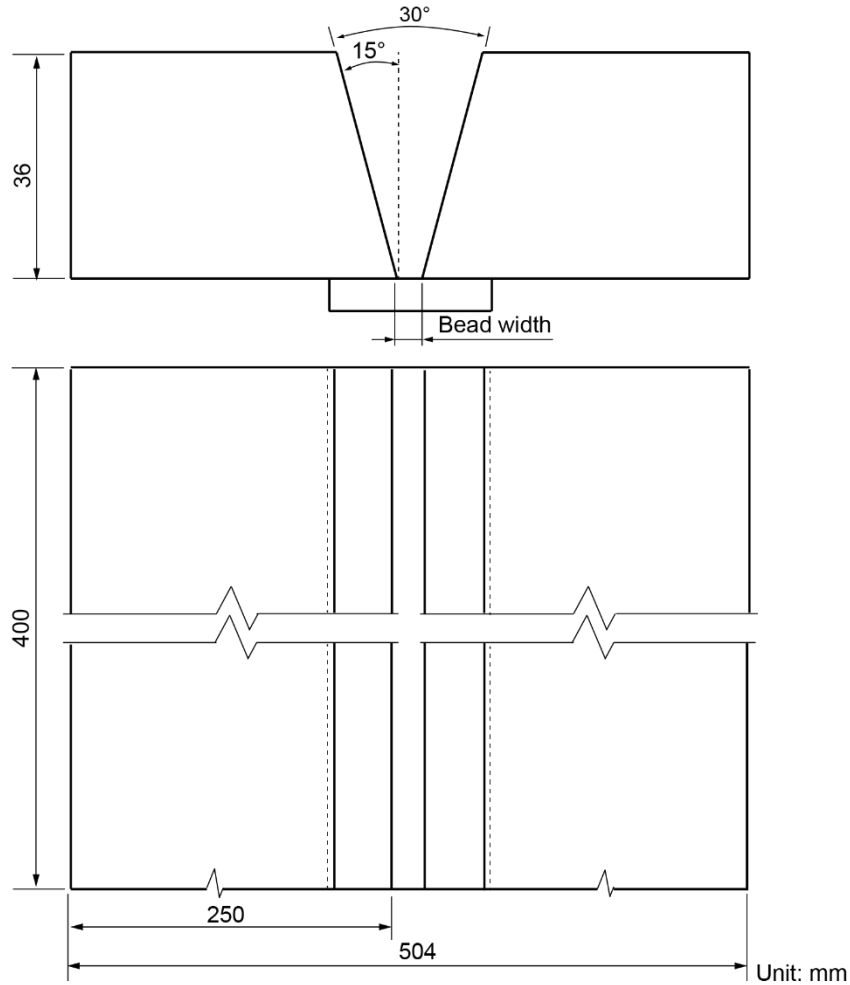


Fig. 4.32 Schematic illustrations of specimen groove shape.

The CO₂ welding machine equipment and hot-wire power source were used that is mentioned in Chapter 3. The filler wire for CO₂ arc welding was the diameter of 1.2 mm using with the bead width of 4 mm without the hot-wire feeding while 1.6 mm diameter belonged the hot wire, which was applied for welding on the bead widths of 7, 11, and 15 mm, the schematic illustrations of each bead width as shown in Figs. 4.33 and 4.34, respectively. The weaving width was used with the CO₂ arc welding torch according to the welding condition, which was performed using the hot-wire system, as shown in Fig. 4.35. High-speed imaging was shot to observe the stabilities of the arc, molten pool phenomena, and hot-wire feeding during welding.

Chapter 4

Investigation of welding phenomena and optimization of hot-wire CO₂ arc welding process for 36-mm heavy-thick steel plate

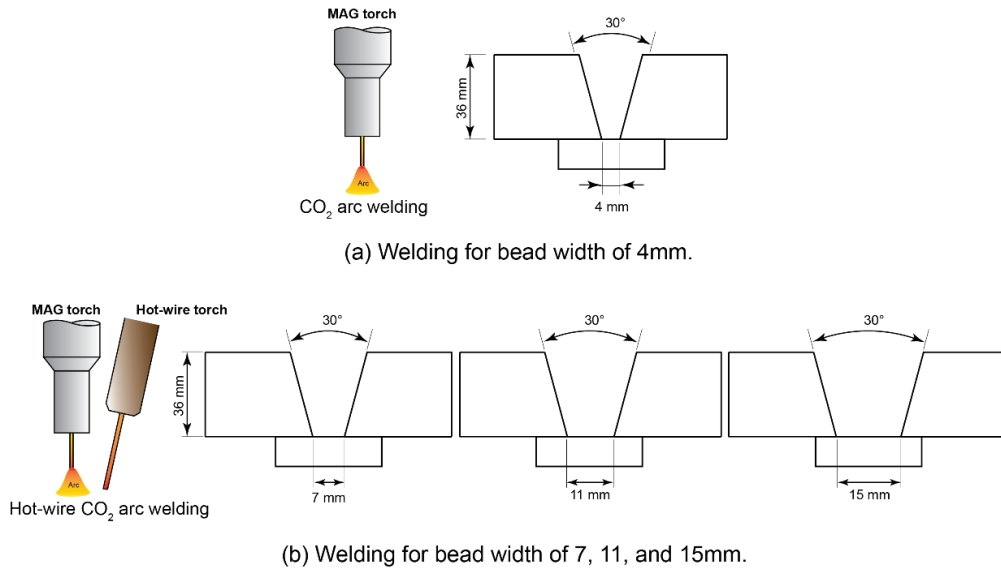


Fig. 4.33 Combinations of welding process and groove shape.

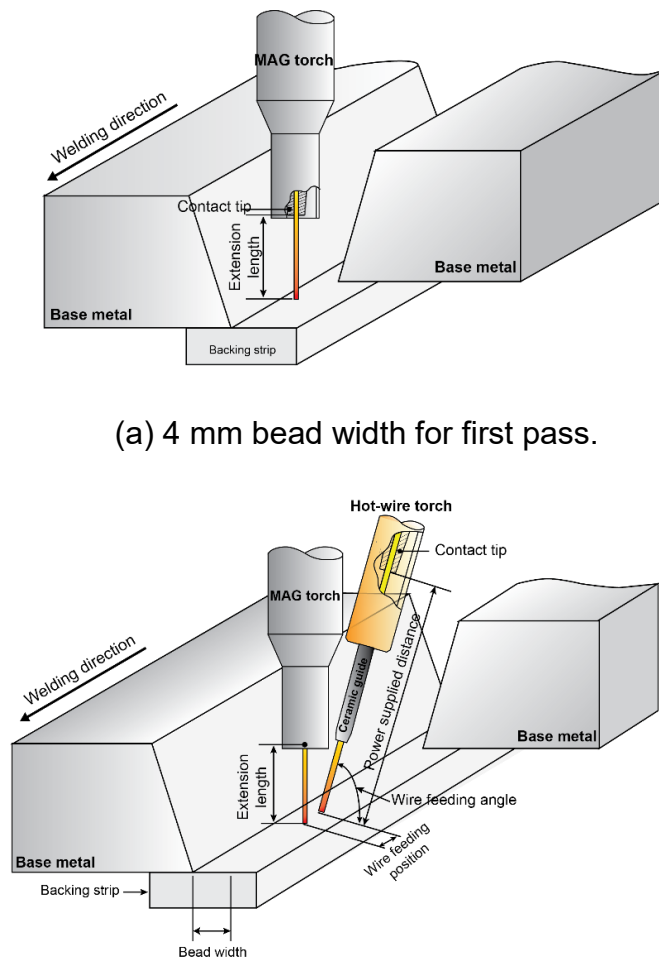


Fig. 4.34 Appearances of experimental setting-up.

Chapter 4

Investigation of welding phenomena and optimization of hot-wire CO₂ arc welding process for 36-mm heavy-thick steel plate

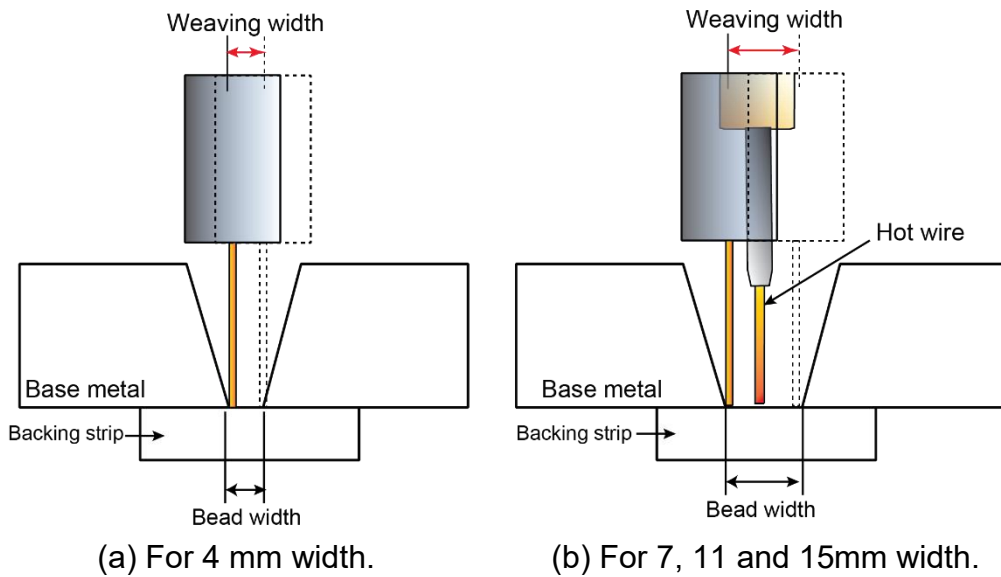


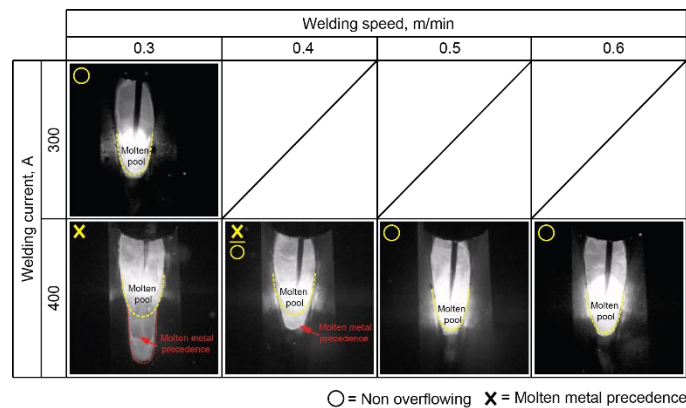
Fig. 4.35 Weaving method for CO₂ arc welding torch.

Table 4.11 Welding conditions.

CO ₂ arc welding conditions				
Bead width, mm	4 ~ 15			
Welding current (Setting), A	400			
Arc voltage, V	41			
Wire feeding speed, m/min	21			
Welding speed, m/min	0.3	0.4	0.5	0.6
Volume, mm ³ /s	396	330	264	198
Wire diameter, mm	1.2			
Contact tip to work distance, mm	23			
Nozzle standoff distance, mm	22			
Shielding gas, L/min	25			
Weaving width (Bead width), mm	2 (4)	4 (7)	8 (11)	11 (15)
Hot-wire conditions				
Bead width, mm	7 ~ 15			
Hot-wire feeding speed, m/min	5 ~ 15			
Welding speed, m/min	0.3	0.4	0.5	0.6
Volume, mm ³ /s	167 ~ 502	140 ~ 419	112 ~ 335	84 ~ 251
Wire current, A	Proper			
Wire diameter, mm	1.6			
Power supplied distance, mm	80			
Wire feeding angle, degree	70			
Wire feeding position, mm	10			
Duty, %	50			

From experimental results, the essential welding factors were considered for their effects on the molten pool phenomenon, and the quality of the bead appearances as described below.

The weldment without the hot-wire feeding was carried out at the bead width of 4 mm using the welding current of 300 A and welding speed of 0.3 m/min. It was welded with the low welding current and low welding speed. The molten pool and arc were stable without the molten metal precedence as shown in Fig. 4.36(a). At the bead width of 4 mm was set up while the welding speed was varied as 0.3 to 0.6 m/min, and the welding speed of 400 A was fixed. The results were found that using the high welding current and low welding speed can increase the deposited volume of weld metal on its wire feed rate: for example, at the welding speed of 0.3 and 0.4 m/min, the molten pool was observed, finding that had the molten metal precedence occurred. When the welding speed was varied as 0.5 and 0.6 m/min, it can decrease the deposited volume of weld metal as the molten pool size became smaller when compared with the low welding speed. Consequently, the increased welding speed's influence affects the decrease of heat input and molten pool size. There is the possibility of the molten metal precedence occurred for the narrow gap welding.

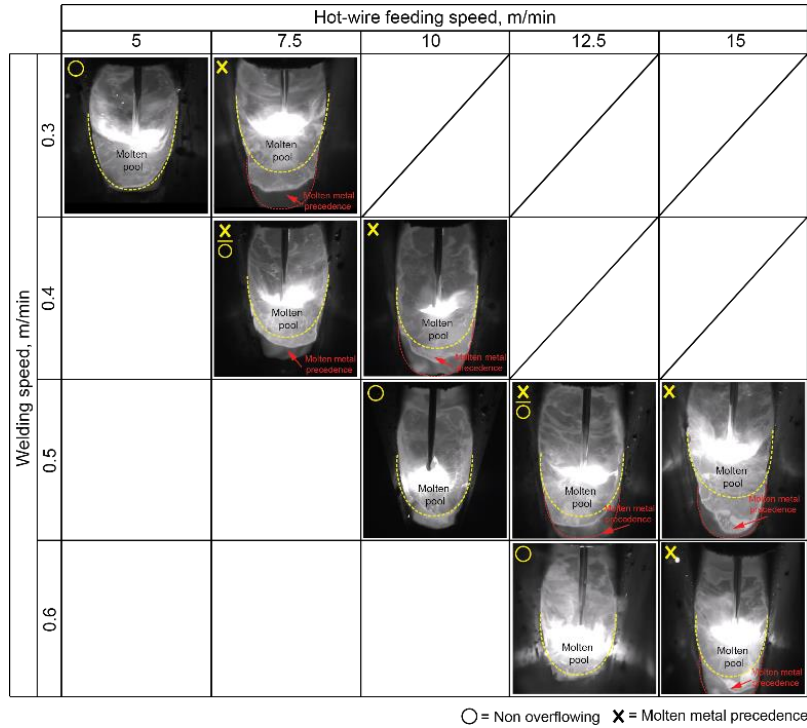


(a) 4 mm width.

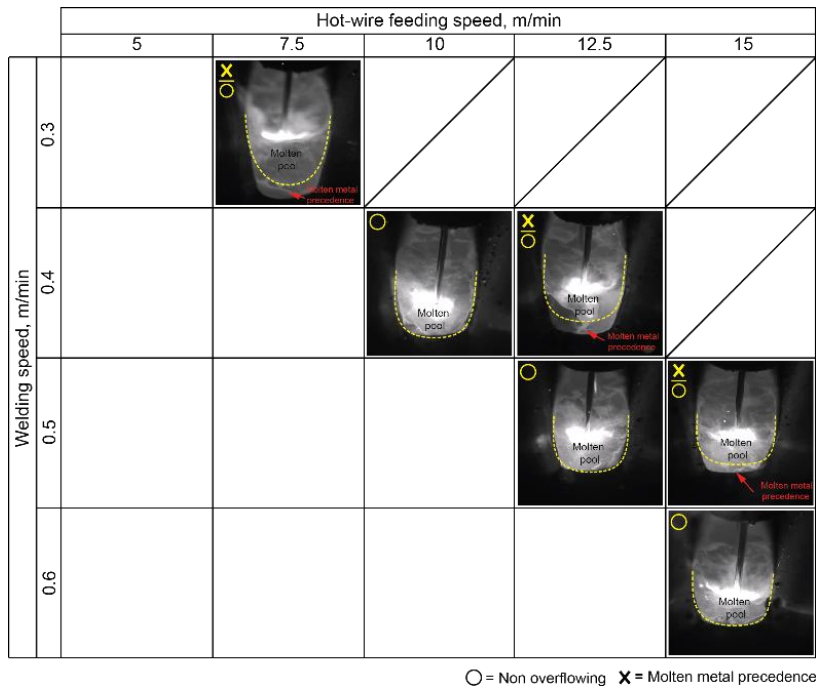
Fig. 4.36 High-speed images of molten pool during welding.

Chapter 4

Investigation of welding phenomena and optimization of hot-wire CO₂ arc welding process for 36-mm heavy-thick steel plate



(b) 7 mm width.

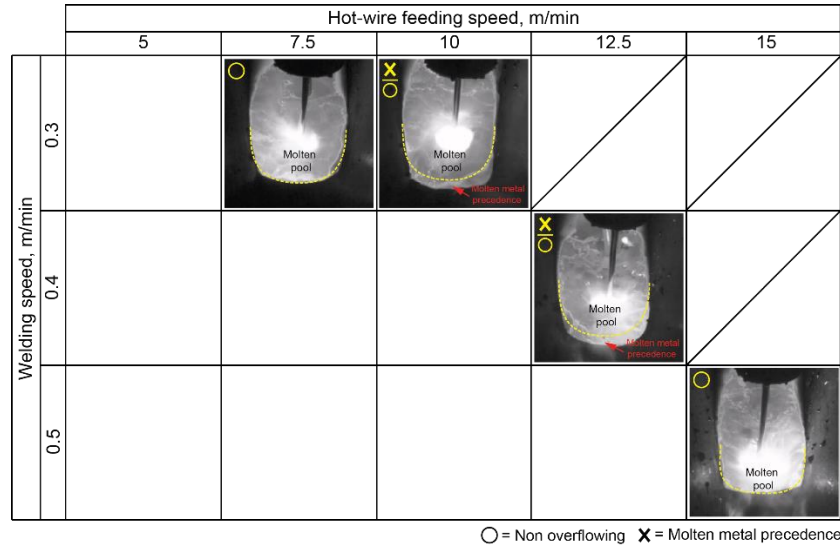


(c) 11 mm width.

Fig. 4.36 High-speed images of molten pool during welding (continued).

Chapter 4

Investigation of welding phenomena and optimization of hot-wire CO₂ arc welding process for 36-mm heavy-thick steel plate



(d) 15 mm width.

Fig. 4.36 High-speed images of molten pool during welding (continued).

Figure 4.36(b) demonstrates the molten pool phenomena, which were performed by CO₂ arc welding with hot-wire feeding. The bead width as 7 mm, welding speed was fixed while hot-wire feeding speed and welding speed were varied. As a result, it was found that at the welding speed of 0.3 m/min and hot-wire feeding speed of 7.5 m/min, the molten pool was unstable when compared with the hot-wire feeding speed of 5 m/min, the molten metal precedence did not occur, and the molten pool was stable.

When the bead width of 11 mm was applied in each welding condition as shown in Figs. 4.36(c). At the welding speeds of 0.4~0.6 m/min and hot-wire feeding speeds of 10~15 m/min were applied. The suitable conditions, the welding speed of 0.4 m/min and hot-wire feeding speed of 10 m/min, 0.5 m/min and 12.5 m/min, 0.6 m/min and 15 m/min, the molten pool could avoid the molten metal precedence and could not keep the stable arc, and molten pool when the hot-wire feeding speed was increased. Figure 4.36(d) shows the welding phenomena of the molten pool when it was performed with the bead width of 15 mm. The experimental results revealed that the extended bead width more than 7 and 11 mm bead width, the molten pool was stable and able to avoid the molten metal precedence when was used the higher hot-wire feeding speed. Accordingly, the wide bead width can maintain the stable molten pool under the hot-wire feeding speed and welding speed limit. Which significantly affects the deposited volume of weld metal and weldability.

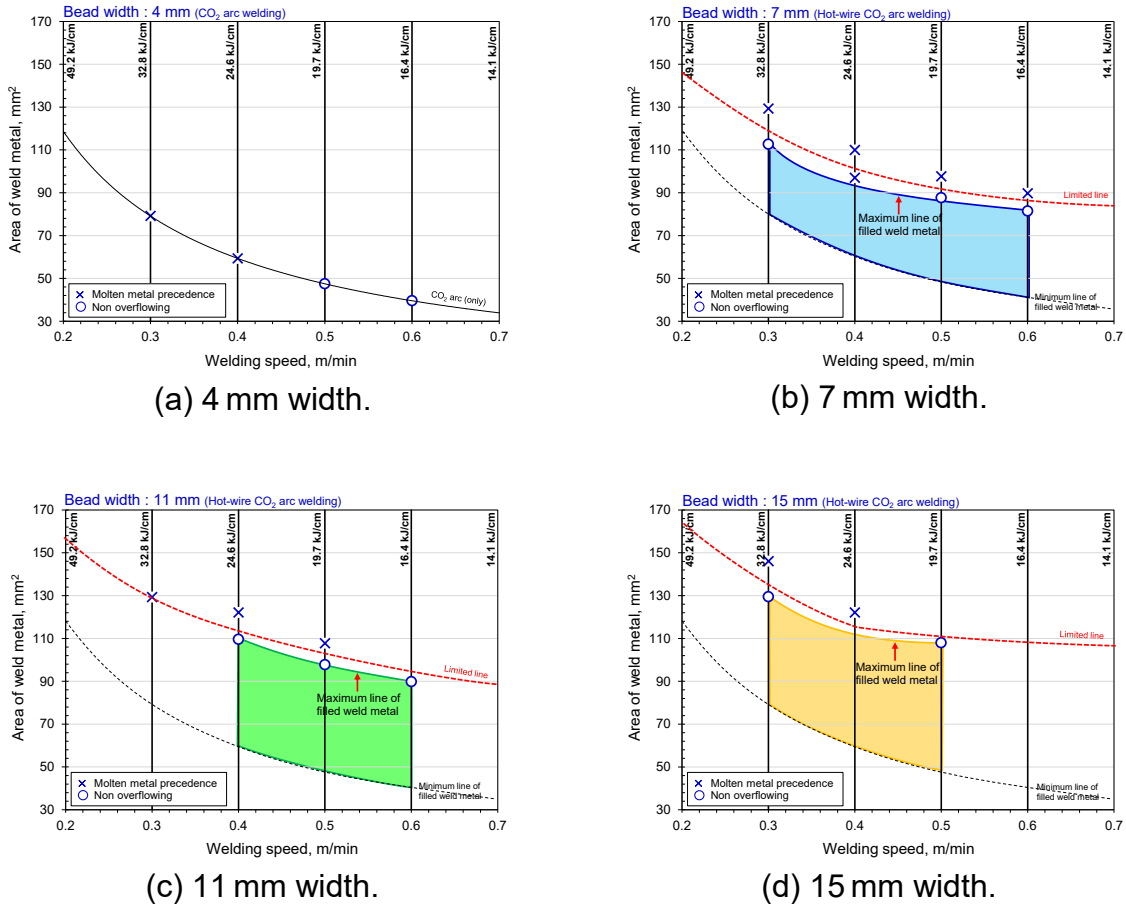


Fig. 4.37 Effects of welding speed and bead width on molten metal precedence.

From the observation of welding phenomena in each determined condition as (Fig. 4.36), It is summarized the appropriate conditions by welding on the bead widths of 4, 7, 11, and 15 mm as shown in Fig. 4.37. The blue circle and blue cross symbols indicate the stable molten pool (non overflowing) and molten metal precedence occurred, respectively. Figure 4.37(a) shows the obtained conditions from welding with the welding current of 400 A without feeding the hot wire by using the welding speeds of 0.3~0.6 m/min.

The weldment under the welding speeds of 0.3 and 0.4 m/min respectively gave the weld metal areas of about 79 and 59 mm², which were more than using the welding speeds of 0.5 and 0.6 m/min having the weld metal areas of about 47 and 40 mm² when were compared. Although the increase of the welding speed affected the decreasing of weld metal area, it can keep the stable arc in the molten pool and avoid the molten metal precedence. Figures. 4.37(b)~(d) show the results using the combination of CO₂ arc welding and hot wire at the welding speeds of 0.3~0.6 m/min, while the varied welding conditions were the bead widths of 7~15 mm and hot-wire feeding speeds of 5~15 m/min. For example, the constant welding conditions were the bead width of 7 mm, welding speed of 0.3 m/min while the hot-

wire feeding speed was varied as 5, and 7.5 m/min which gave the areas of weld metal of about 113 and 129 mm², respectively. As a result, there was molten metal precedence occurred when fed the hot-wire feeding speed of 7.5 m/min. Because the higher hot-wire feeding speed affected the height of weld metal which caused the unstable molten pool. Comparing the weld metal area between the welding speeds of 0.5 and 0.6 m/min were used as shown in Figs. 4.37(b), while the bead width was used at 7 mm. With the increased welding speed as 0.6 m/min, the molten pool size became small because of the decreased heat input compared to the welding speed of 0.5 m/min. At the bead widths of 11 and 15 mm and welding speed of 0.5 m/min, it can see that the area of weld metal was high from the high hot-wire feeding speed when the bead width was wide significantly. The achieved conditions were under the limited line; it was the weld metal area that can be fed the maximum hot wire and avoid the molten metal precedence.

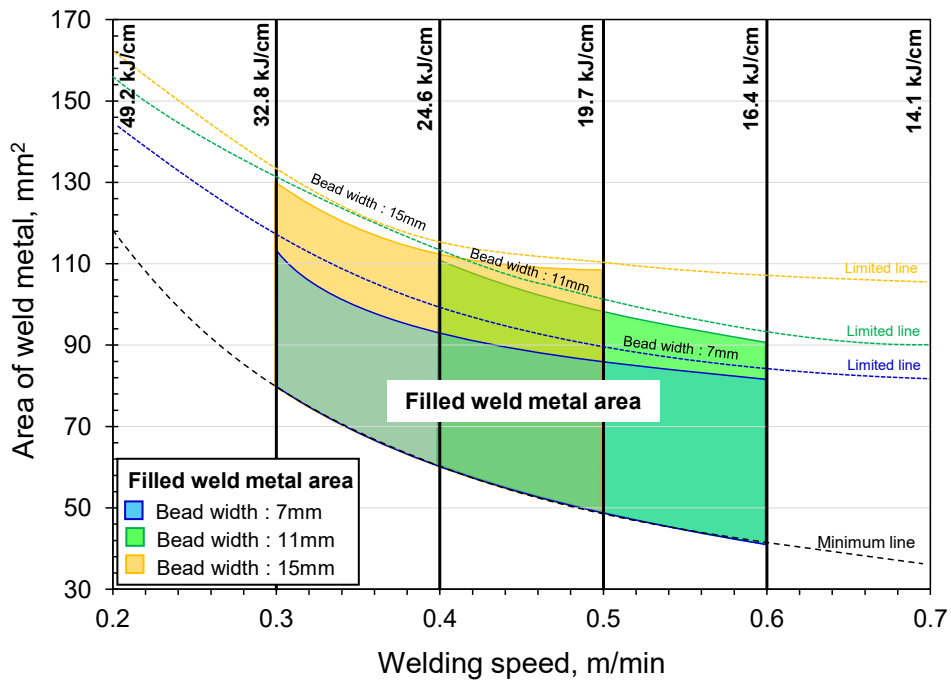


Fig. 4.38 Suitable conditions for each welding speed.

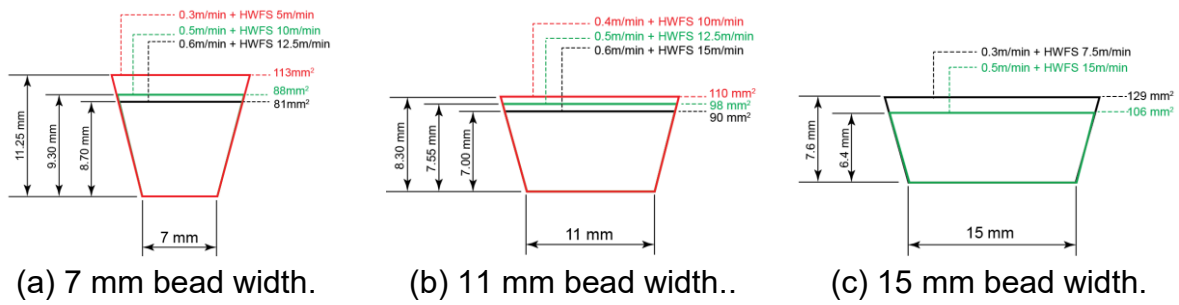


Fig. 4.39 Height, width and filing area of weld metal for each bead width.

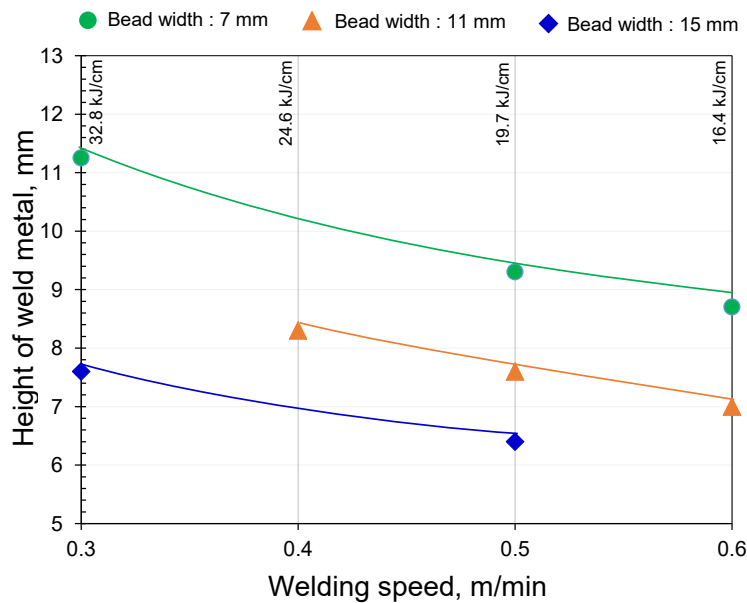


Fig. 4.40 Relationships between height and width of weld metal in each welding speed.

Available conditions in each bead width are summarized as shown in Fig. 38, which can use on the orange, green and blue areas under limited lines in each weeding speed until the minimum line of the filled weld metal. These achieved conditions had measured the height of weld metal, specifically applicable parameters from using the combination of CO₂ arc welding and hot-wire system, the measured value as shown in Fig. 4.39. The heights of weld metal from welding in each bead width and welding speed were measured, especially the suitable conditions. The molten pool's height changed according to the melting metal from the fed melting metal and extended bead width. In this case, at the bead width of 15 mm and welding speed of 0.3 m/min as shown in Fig. 4.39(c), the height of weld metal was higher when compared with the welding speed of 0.5 m/min. Thus, using the low welding speed and hot-wire feeding speed, it can maintain the molten pool's stability

by itself. Evaluating the main effects of the welding conditions revealed that the influences of the bead width, welding speed, and hot-wire feeding speed affected the stability of the molten pool and changed electrode extension. The relationships of the height and bead width of the weld metal under each bead width and welding speed were varied, as shown in Fig. 4.40. The height of the weld metal decreased almost linearly with the extension of the bead width, significantly.

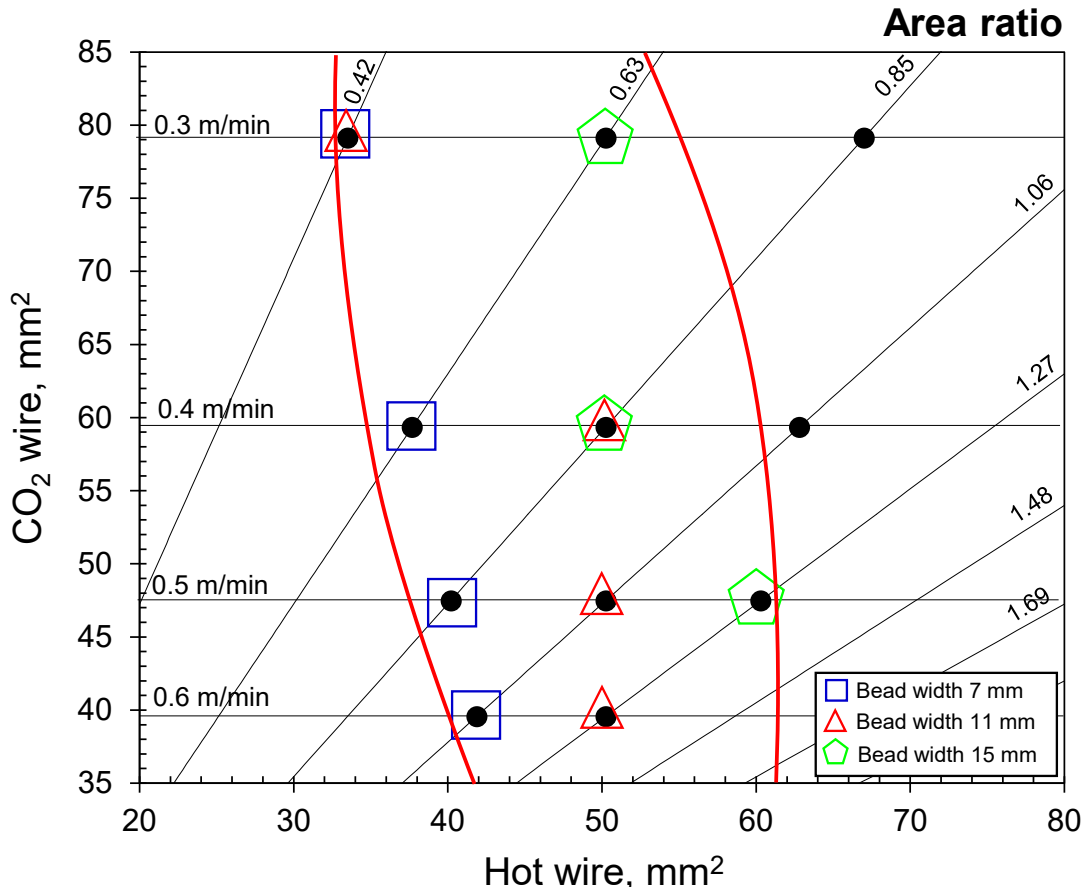


Fig. 4.41 Area ratio of weld metal in each bead width on filler metal volume combination from CO₂ arc welding and hot-wire feeding.

Figure 4.41 shows an area ratio of weld metal; it was carried out with several combinations between the CO₂ wire and hot wire in each welding speed and different bead width. The black points indicate all experimental conditions; the square, triangle, and pentagon symbols indicate the bead width as 7, 11, and 15 mm, respectively. The available ratios between CO₂ wire and hot wire are within the red curve; for example, at the welding speed of 0.3 m/min (heat input: 32.8 kJ/cm) was used while the bead widths of 7 and 11 mm were applied, having the area ratio of about 0.41 %. Both bead widths were compared with the bead width of 15 mm, it was found that the bead width of 15 mm giving the area ratio of about 0.63 % more

than both bead widths of 7 and 11 mm due to the extension of bead width and height of weld metal. On the other hand, the welding speed increase as 0.3 to 0.6 m/min affected the decrease of heat input and total deposited volume. For this reason, it is identified as the molten pool to be small from changing the high welding speed. Consequently, the changed welding speed and bead width affected the balance within the molten pool and area ratio of weld metal from the combination of CO₂ wire and hot wire.

4.4.4 Joint creation using appropriate welding conditions

From the experimental results in the first part, influence to keep the balance within the molten pool is pool shape size, and volume of molten metal by welding speed changed. Therefore, it was designed for high weldment efficiency in welding time, which can avoid the molten metal precedence in front of arc as shown in Fig. 4.36.

For this experiment, at the welding speed of 0.5 m/min was selected for welding all passes from the previous experiment. The specimen used for the butt joint was the thick steel plate (NK-KE36) of 36-mm with 36^t × 50^w × 400^l mm dimension. The V-shaped groove of 30°, root gap of 4 mm were used. The welding speed of 0.5 m/min was fixed, all passes. The first pass was welded by CO₂ arc welding without hot-wire feeding. The second to fifth pass were fed the hot-wire feeding speeds of 10~15 m/min in each passes combining with CO₂ arc welding at the welding current of 400A, and other conditions were set up as shown in Figs. 4.42~4.43 and Table 12.

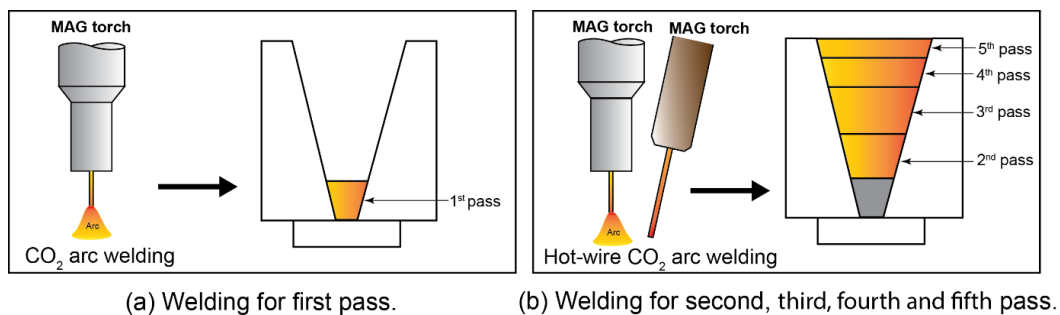


Fig. 4.42 Schematic illustration of welding pass plan.

Chapter 4

Investigation of welding phenomena and optimization of hot-wire CO₂ arc welding process for 36-mm heavy-thick steel plate

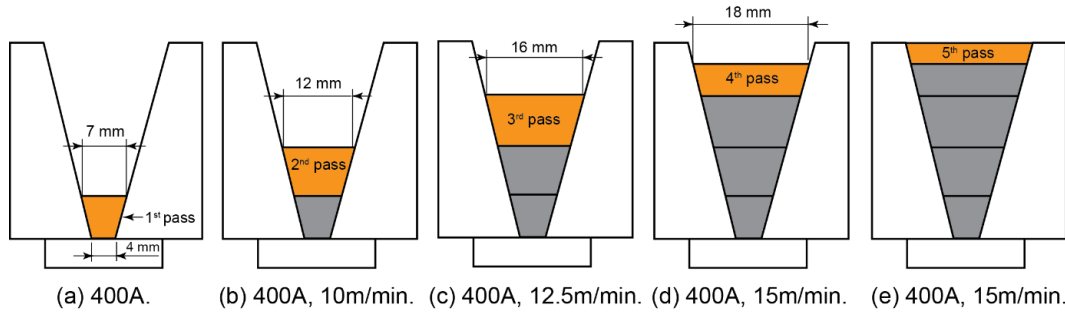


Fig. 4.43 Schematic illustrations of bead shapes on each pass at welding speed of 0.5 m/min.

Table 4.12 Welding conditions.

CO ₂ arc welding conditions					
Pass no.	1	2	3	4	5
Bead width, mm	4	7	12	16	18
Welding speed, m/min	0.5				
Welding current (Setting), A	400				
Arc voltage, V	41				
Wire feeding speed, m/min	21				
Volume, mm ³ /s	264				
Wire diameter, mm	1.2				
Contact tip to work distance, mm	23 (2 nd ~ 4 th pass), 26 (1 st , 5 th pass)				
Nozzle standoff distance, mm	22 (2 nd ~ 4 th pass), 25 (1 st , 5 th pass)				
Shielding gas, L/min	25				
Weaving width (Bead width), mm	2 (4)	4 (7)	8 (12)	12 (16)	15 (18)
Hot-wire conditions					
Pass no.		2	3	4	5
Wire feeding speed, m/min		10	12.5	15	15
Volume, mm ³ /s		223	279	335	335
Welding speed, m/min	0.5				
Wire current, A	proper				
Wire diameter, mm	1.6				
Power supplied distance, mm	80				
Wire feeding angle, degree	70				
Wire feeding position, mm	10				
Duty, %	50				

4.4.5 Results and discussion

From the experimental result above, the essential welding variables were analyzed according to factors affecting the welding phenomena on the front of the molten pool. It was indicated that welding on the narrow gap with the bead width of 4 mm couldn't feed the hot wire even though there was the height of filling depth. Then, welding on the first pass at the root part only should be used CO₂ arc welding without the hot-wire feeding. Likewise, the extended bead width could keep the stability of the molten pool and avoid the molten metal precedence from feeding the excess volume of CO₂ wire and hot wire. Therefore, the welded surface in each pass would be measured before performing on the next pass as presented in Figs. 4.43.

The first pass was welded with the welding current of 400 A without feeding the hot wire in the root gap of 4 mm. The second pass was applied with the welding current of 400 A and hot-wire feeding speed of 10 m/min on the bead width of 7 mm from measuring the previous pass. Then, the third to fifth pass were fed the hot-wire feeding speed of 12.5, 15, and 15 m/min, respectively. Each pass was welded on the bead width determined by the previous pass, the welding phenomena in each bead width as shown in Figs. 4.44. The molten pool phenomenon was considered under the stable molten pool and molten metal precedence condition. The results were found that the molten pools were stable without the molten metal precedence occurred when were observed all passes during welding.

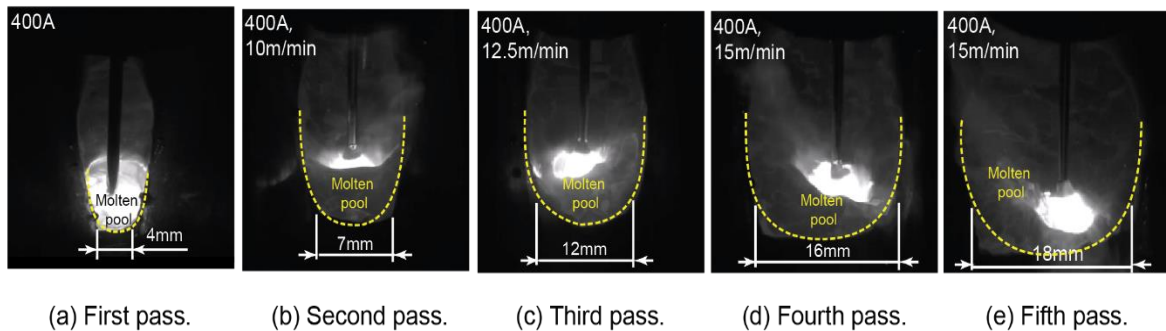


Fig. 4.44 High-speed images of molten pool on each pass during welding.

The complete weld pools from using the optimized conditions, the bead appearance achieved the complete deposition of the weld joint which was performed in five passes as presented in Fig. 4.45. The cross-section obtained as shown in Fig. 4.46, sound bead without any defects was obtained. The HAZ width became small when the hot-wire addition was increased on second to fifth pass, respectively.

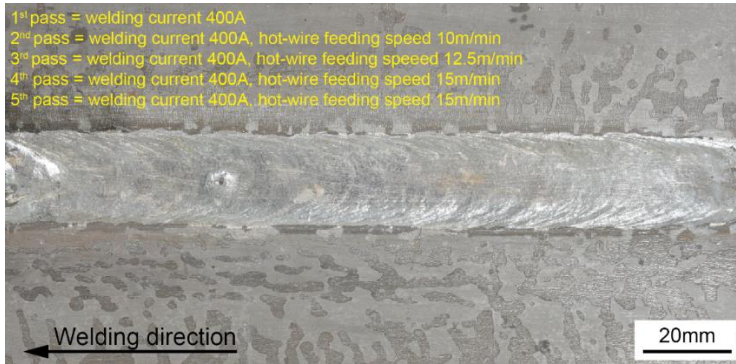


Fig. 4.45 Appearance of weld bead.

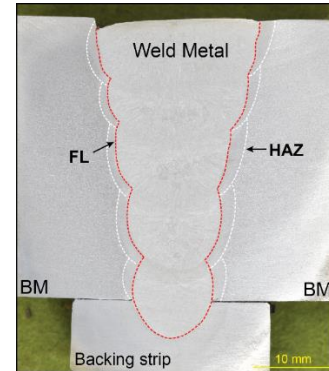


Fig. 4.46 Cross-section of weld bead.

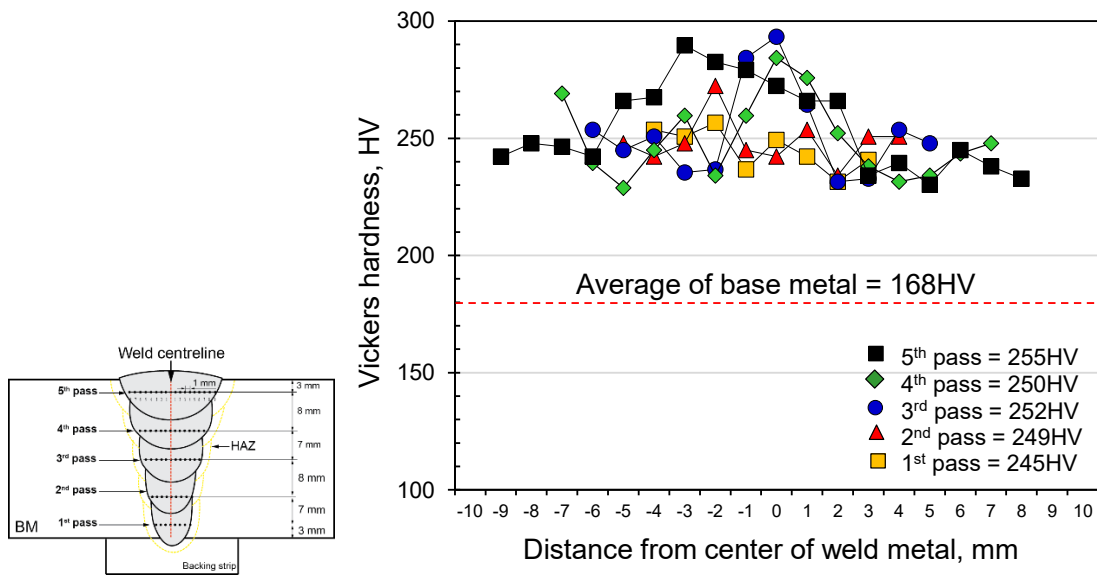
4.4.5.1 Property evaluations of the butt joint

The achieved weld bead was evaluated the property of the butt joint, which was welded with the appropriate conditions. The cross-sectional observation, hardness measurement of weld metal also was performed to investigate the effect of hot-wire addition on the joint characteristics.

Table 4.13 shows the result of Vickers hardness average of weld metal, which was used under the achieved parameters such as; the welding speed of 0.5 m/min, welding current of 400 A, hot-wire feeding speeds of 10~15 m/min. The Vickers hardness of weld metal is shown in Fig. 4.47, which clearly can indicate that the first pass only was used CO₂ arc welding at welding current of 400 A had the average hardness of weld metal of about 245 HV. The weld metal of the second to the fifth pass was fed the hot wire to increase deposited metal volume as much as necessary. The hardness averages had approximately 249~255 HV, which was higher than the average of base metal of about 168 HV. When compared with the welded bead using the welding speed of 0.3 m/min which gave the lower hardness average around 210~219 HV. Consequently, the combination of higher hot-wire feeding speed and welding speed is summarized as the increased weld metal hardness influenced by both low heat input and high hot-wire feeding speed. Because the high cooling rate and lower temperature from the hot-wire feeding were just under its melting point.

Table 4.13 Average hardness of weld metal.

Welding speed, (m/min)	1 st pass, Welding current, (A)	Welding current, Hot-wire feeding speed	Average hardness of weld metal, (HV)
0.5	400	1 st pass: 400A	245
		2 nd pass: 400A - 10m/min	249
		3 rd pass: 400A - 12.5m/min	252
		4 th pass: 400A - 15m/min	250
		5 th pass: 400A - 15m/min	255



(a) Measurement point.

(b) Vickers hardness of weld metal.

Fig. 4.47 Vickers hardness distribution of weld metal in each pass.

Charpy V-notch specimens were cut according to the standard full size of JIS Z 2242, the cutting plan as shown in Fig. 4.48. The brittle fracture was tested at the temperature of 0°C shall be over 47 J. Charpy impact machine has the heavy pendulum of 25.31 kg, and an arm radius of 0.7 m. The notch locations at Weld metal (WM), and Fusion line (FL) in top and bottom part of welded bead were evaluated the absorbed energy of butt joint.

Chapter 4

Investigation of welding phenomena and optimization of hot-wire CO₂ arc welding process for 36-mm heavy-thick steel plate

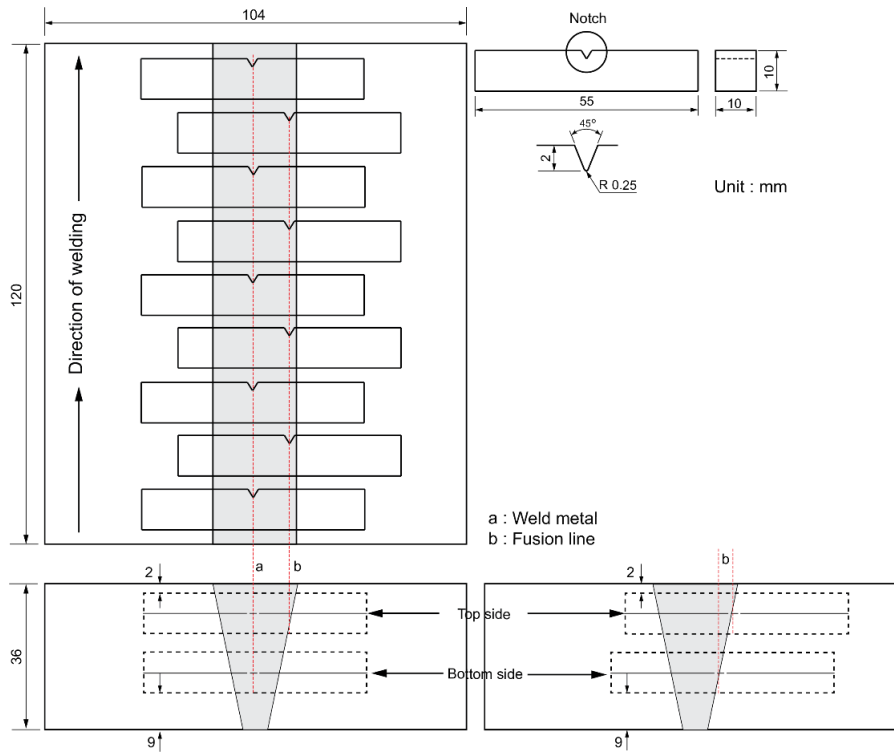


Fig. 4.48 Cut-off plan for V-notched Charpy specimen.

Table 4.9 Result of absorbed energy.

Welding current on 1 st pass	Notch position	Absorbed energy, J	
		Weld metal	Fusion line
400A	Top side	31.2	217.9
		23.9	186.8
		18.0	223.9
		21.5	204.1
		14.6	221.0
	Bottom	63.7	217.9
		68.1	204.1
		76.9	193.2
		59.4	216.4
		53.8	223.9

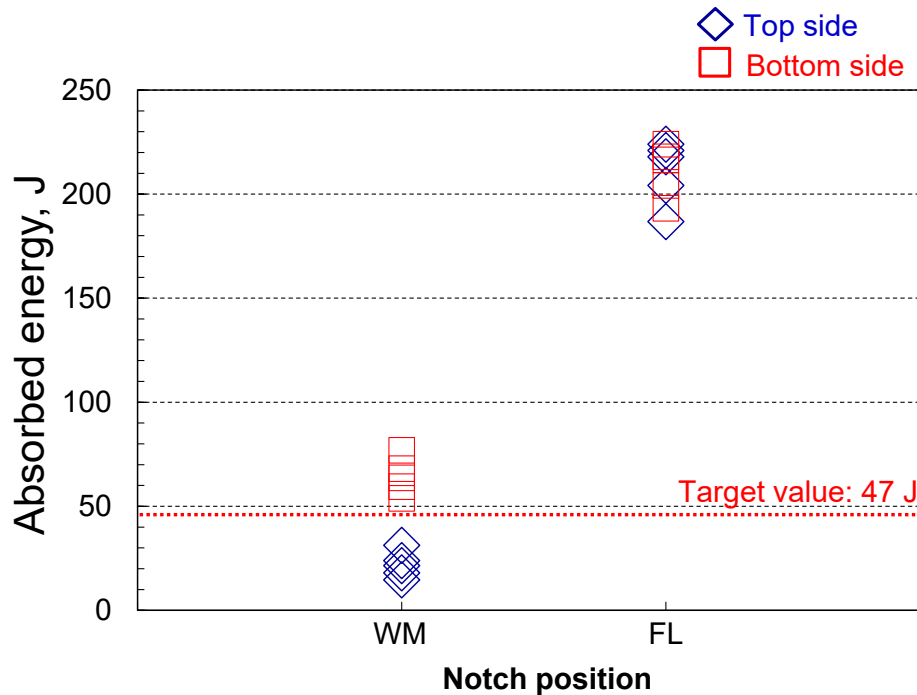


Fig. 4.49 Result of Charpy impact test.

V-notch Charpy impact test according to the standard specifies (JIS Z 3312) of the solid wire for MAG welding of mild steel and the Japan Marine Standard of ClassNK, the minimum average impact test value of the welded joint is 47 J. The Charpy impact test of the notch location at weld metal and fusion line is shown in Table 4.9 and Fig. 4.49.

The notch position of weld metal on the bottom side gave the higher absorbed energy of about 59.4~76.9 J when compared with the top side of the welded bead, which shows the low absorbed energy having the mean value of 47 J less than the specification requirement. Due to the notch position was on the fourth and fifth pass and having the higher hardness of weld metal, where influenced by reducing the heat input and the effect of hot-wire feeding speed increased. The toughness of the fusion line on the top and bottom side was approximately 186.8~223.9 J of absorbed energy which had the average impact test value higher than the toughness of weld metal. Because the notch location at fusion line zone was passed on the weld metal and heat-affected area that was referred to as homogeneous or non-homogeneous.

4.5 Summary

The butt joints of the thick steel plate of 36-mm were applied under the considered conditions by using the hot-wire CO₂ arc welding process.

Conclusions can be drawn as follows:

- 1) The stable arc and molten pool were observed in welding phenomena by the high-speed camera. The results clearly can be seen that the obtained conditions were primarily influenced by the bead width and total volume of filler wire. It can be selected according to the single V-groove dimensions and the appropriate volume of hot wire and its CO₂ wire.
- 2) The achieved conditions of weld beads, the butt joint was applied in four passes at the welding speed of 0.3 m/min, and getting in five passes was welded with the welding speed of 0.5 m/min. The total deposited metal volume, the area ratio of weld metal can be predicted under the changed bead width and welding heat input. It was the main factor that affected keeping the stable molten pool.
- 3) The sound beads without any defects were evaluated the mechanical properties performed by the Charpy impact test, tensile test, bending test of the weld joints. These test results complied with the criterion test standard.

Chapter 5

Development of hot-wire double lasers welding method for thick steel plate

5.1 Introduction

In Chapters 3 and 4, it became clear that the capability of hot-wire CO₂ arc-welding, and it had much potential to improve the efficiency and to reduce the heat input for joints of thick steel plates. In Chapter 3, the optimized conditions achieved sound joints using only two passes for a butt-joint with V-shaped groove of 20-mm thick steel plates. The hot-wire CO₂ arc welding obtained the sound joint without any defects and it also achieved a lower dilution ratio, narrower HAZ width, suitable hardness of weld metal, and appropriate mechanical properties.

A laser heat source also has the much potential to reduce heat input dramatically, and to improve efficiency and joint properties. The conventional laser welding and laser arc hybrid welding create a keyhole during welding to obtain a deep penetration. Although the laser arc hybrid welding has a larger gap tolerance than that of laser welding, it can not provide the enough tolerance on a thick steel plate welding. These welding process using a laser heat source for a thick joint also has problems, such as requirement of high-power laser, controllability of weld metal properties and so on.

However, the laser heat source can be controlled more precisely than an arc heat source, which means it has the potential to control melting phenomena more precisely and to improve the joint quality with higher strength and toughness especially for high strength and toughness steel plates. The hot-wire laser welding process has been developed as described in Chapter 2 to compensate the disadvantages of laser welding and laser arc hybrid welding described above. In the previous research, 12-mm thick joint with a narrow gap has been obtained using the combination of a 6 kW diode laser and hot-wire feeding.

In this study, the hot-wire laser welding process with a double laser beam system was proposed and examined for a narrow gap joint of 20-mm heavy thick steel plates. The total laser power of 12 kW is provided by two 6 kW diode laser oscillators, and two laser heads can produce two laser beams with different shapes and sizes respectively. This system can be also controlled a distribution of a power density and a positional relationships of two laser beams.

5.2 Materials and specimen used

In this experiment, the steel plate for using as the base metal was KE36. The dimension of workpiece were 20-mm thickness, 40-mm width and 160-mm length. The butt joint with the U-shaped groove with the root gap of 2-mm and the angle of 3° was employed as shown in Fig. 5.1 and shown the chemical composition in Table 5.1. The filler wire was used for this performant to be JIS Z3312 YGW11 with 1.6 mm diameter, a chemical property of filler wire as shown in Table 5.2.

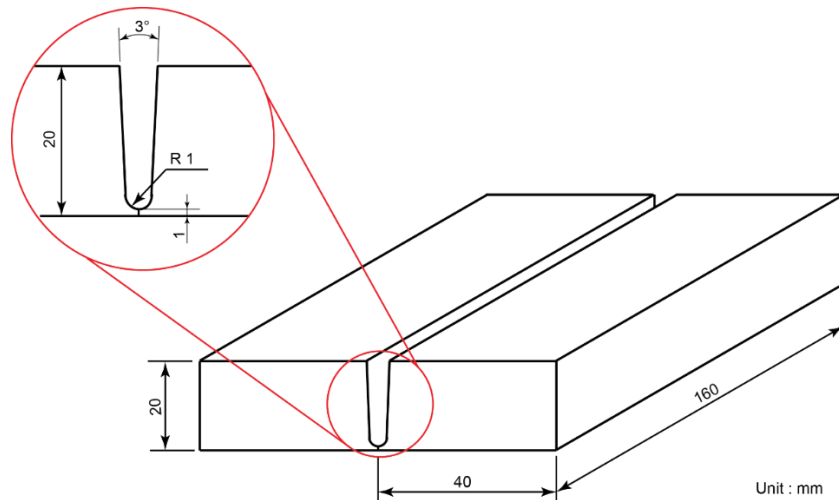


Fig. 5.1 Schematic illustration of specimen.

Table 5.1 Chemical composition of base material.

Element	C	Si	Mn	P	S	Cu	Ni	Cr
Base metal (KE36)	0.12	0.2	1.21	0.14	0.04	0.01	0.01	0.02

Table 5.2 Chemical composition of filler wire.

Filler wire	C	Si	Mn	P	S	Cu	Ti	Zr
JIS Z3312 YGW11	0.02 ~ 0.15	0.40 ~ 1.00	1.00 ~ 1.60	0.03 or less	0.03 or less	0.50 or less	Ti + Zr : 0.02~0.15	

5.3 Experimental procedure and equipment

Hot-wire double lasers welding method is a process of adding a hot wire for butt joint of thick steel plate especially a narrow gap joining which is energized and heated below the melting temperature by joule heat generation. A semiconductor laser with the high oscillation unit and optical equipment can change the laser spot into a rectangular shape. The base metal is melted by the heat from laser beam and formed the molten pool with the small heat input and low dilution. That's mean, the properties of weld metal depend on the type of additional hot wire filler metal. The schematic of experiment is shown in Fig. 5.2.

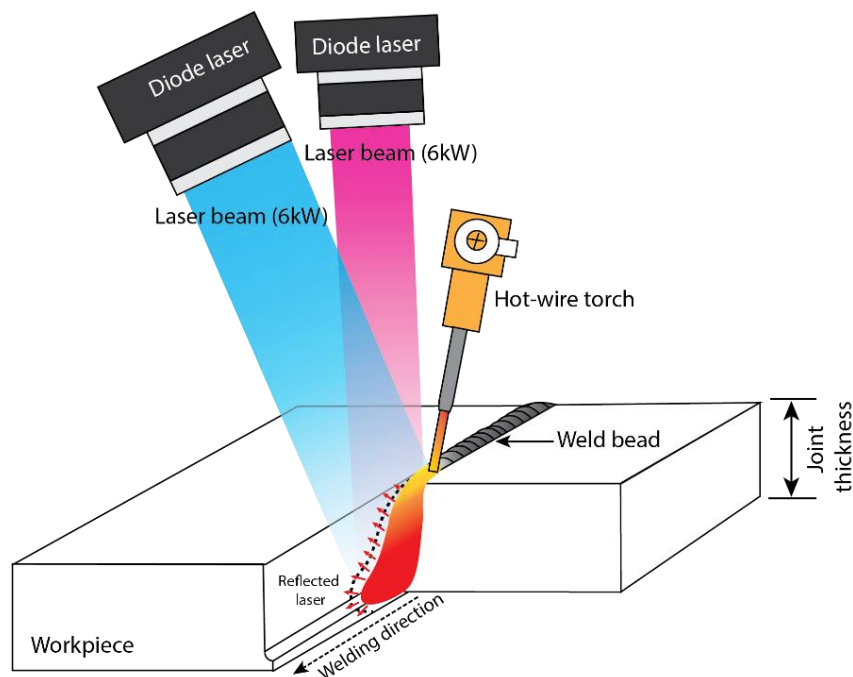


Fig. 5.2 Schematic illustration of double laser beam welding in narrow groove.

An equipment was shown their methods and typical set up, such as hot-wire power source, laser oscillator, hot-wire torch, and shielding gas system. The experimental setups were explained in each equipment as follow; the experimental setups included diode lasers (LD) welding equipment as shown in Fig. 5.3 which were used both power sources (6kW+6kW). The fiber core sizes of 400 and 1000 μm were connected (available) to wafer source and convey the output laser to the laser head and were used in each parameter. Figure 5.4 shows the typical assembly flow chart of laser head for joint thickness of 20-mm by using double laser beams.



Fig. 5.3 Laser oscillator.

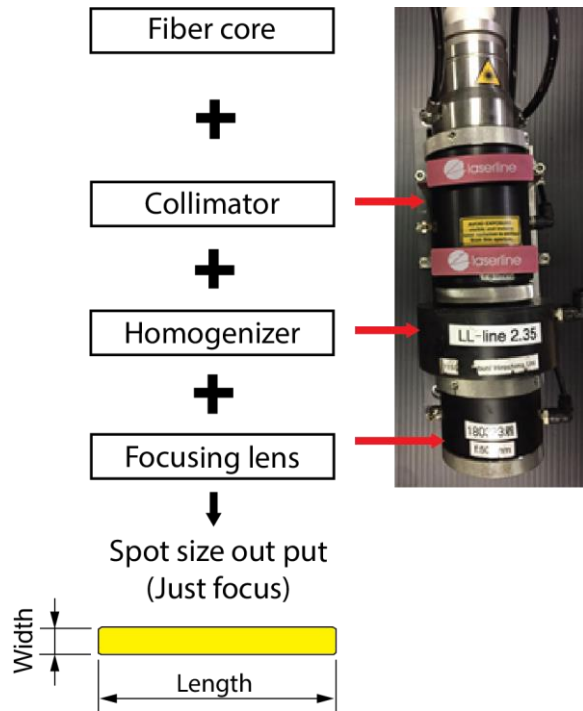


Fig. 5.4 Simplified chart of laser head.



Fig. 5.5 Hot-wire power source.



Fig. 5.6 Hot-wire torch.

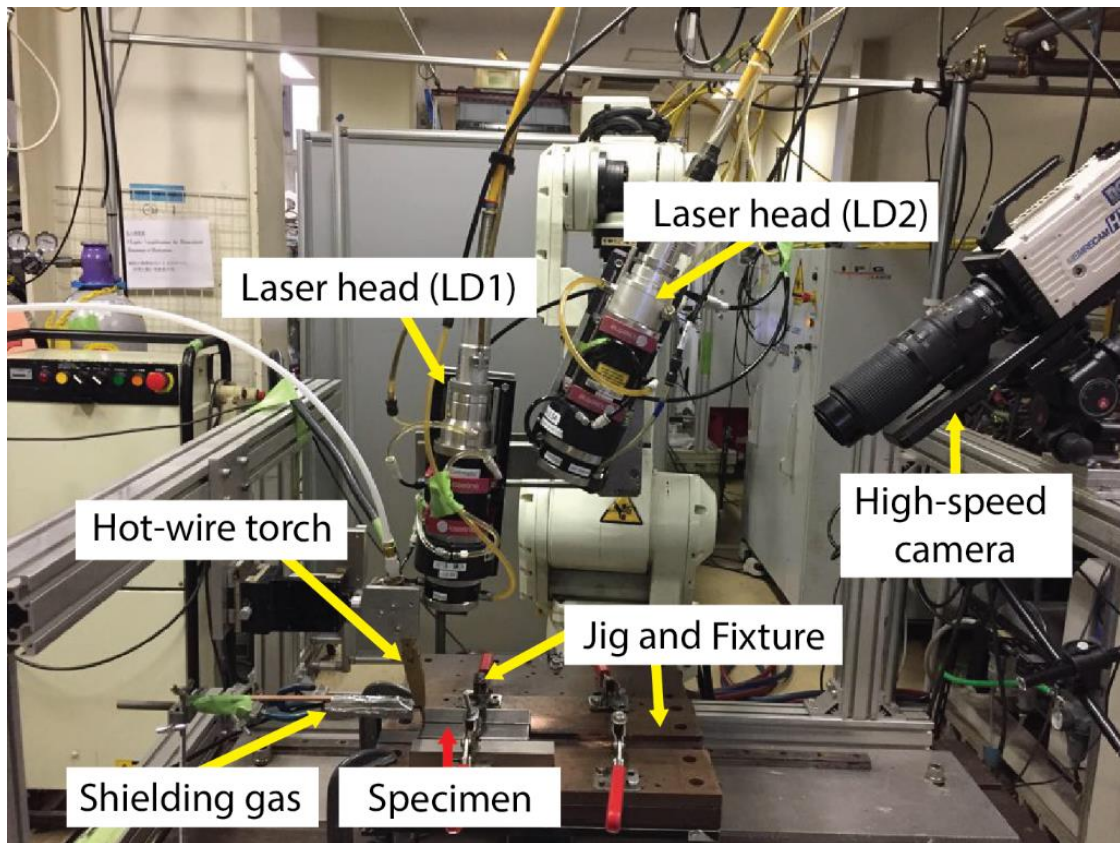


Fig. 5.7 Appearance of experimental.

Hot-wire system, Power Assist inverter IV1320 (Babcock Hitachi) is a hot-wire power source used as shown in Fig. 5.5 and shows a hot-wire torch has to be set as positive electrode on base metal as shown in Fig. 5.6. The appearance of experimental double laser welding for thick steel plate of 20-mm was observed the molten pool phenomenon of the laser irradiation by high-speed camera. The observed direction was the front of the molten pool for catching the video since the bottom to the top side, irradiation on the sidewall, stability of feeding hot wire. The shielding gas was set up on the back of the hot-wire torch where also was fixed in the same way as the laser head on the front of the hot-wire torch. In the experimental setup, the welding direction was moved by the horizontal work table, and the specimens were fixed by jig and fixtures as shown in Fig. 5.7.

The length and width of rectangular laser spots created by the combination of optical lenses and a fiber core diameter are shown in Table 5.3. The laser head was combined with the fiber core diameter, collimator lens and the chosen focusing lens. The laser spot length can be decided by changing the combination of homogenizing and focusing lenses. In this research, the laser beam was used a variety of laser spot size which was determined under each welding condition.

Table 5.3 Rectangular beam shapes with combinations of optical lenses and fiber core.

		Laser spot length, mm							
Homogenizer	Fiber core, μm	Distance of focus lens, mm							
		100	200	300	400	500	600	800	1000
LL 2.20	1000	11	23	34	45	56	68	90	113
LL 2.35 ⁽¹⁾		6	13	19	26	32	39	51	64
LL 2.54		4	8	13	17	21	25	34	42
LL 2.85	600	3	5	8	11	13	16	21	27
LL 2.146	400	1.5	3	5	6	8	9	12	15

		Laser spot width, mm							
Collimator, mm	Fiber core, μm	Focus distance of focus lens, mm							
		100	200	300	400	500	600	800	1000
100	1000	1	2	3	4	5	6	8	10
80		1.25	2.5	3.75	5.0	6.25	7.5	10.0	12.5
100	400	0.4	0.8	1.2	1.6	2.0	2.4	3.2	4.0
80		0.5	1.0	1.5	2.0	2.5	3.0	4.0	5.0

5.4 Investigation of molten pool formation and joint creation using stable laser beam combination

The laser welding process's main factor in applying the heavy-thick plate must be used as an adequate laser power due to creating the molten pool throughout the bottom until the sidewall's top side. Therefore, the hot-wire double lasers welding method was applied in the different beam sizes for suitability with the groove shape by the laser-power distribution and stable irradiation. Which are the advantages of creating the molten pool formation for welding in the narrow gap and the stable irradiation.

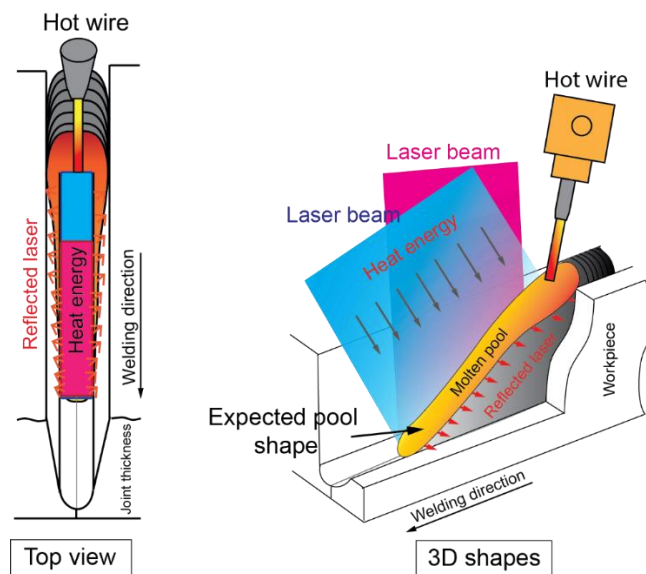


Fig. 5.8 Effects of double laser beam sizes on molten pool formation.

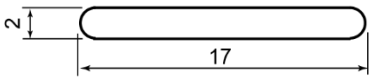
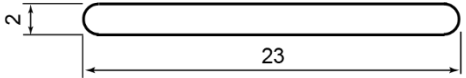
Furthermore, welding in narrow gap of thick steel plate can enormously decrease the feeder wire feeding rate compared with the conventional arc welding process, which creates a sizeable molten pool. The hot-wire laser welding process, It has to use laser power more than 12 kW to shape the larger molten pool on the root in particular and sidewall all along as shown in Fig. 5.8. To employ the laser power of 12 kW for finding the effect on the thick steel plate using the double lasers welding process was performed by determining the suitable laser beam size, beam position arrangement, welding speed, differently which influence to creating of the molten pool formation.

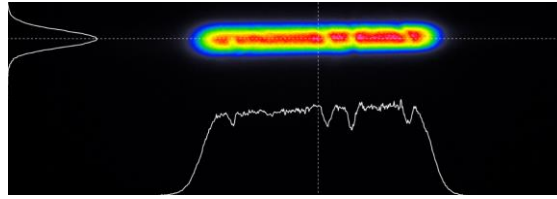
5.4.1 Fundamental investigation of molten pool formation and joint creation using stable laser beam combination of 23x2 mm and 17x2 mm

5.4.1.1 Welding conditions

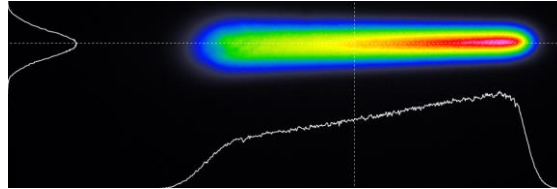
For the welding of the butt joint of thick steel plates in the narrow gap, it is normally well known that the heat input relates to creating the molten pool must be sufficient. The laser irradiation from the bottom until the molten pool's topside had to distribute power density consistently. The laser beam shapes contribute to combining the power density for giving the high laser power, and they were applied for welding to investigate the molten pool shape obtained. A rectangular spots, there was the same width to be 2-mm, but there were different lengths. Both rectangular spots of 17x2 mm and a longer rectangular spot of 23x2 mm had used the same laser power of 6 kW in all cases. Table 5.4 shows the energy density in each laser beam shape, which were calculated the power density. The difference in energy density indicates that the smaller beam size area has an increased power density more than the bigger laser spot area. The energy density distribution was investigated in each laser beam with the laser power of 6 kW as shown in Fig. 5.9.

Table 5.4 Energy density in each laser beam shape.

Laser beam shape (mm)	Laser spot area (mm ²)	Laser power (kW)	Power density (kW/mm ²)
	33.14	6	0.18
	45.14	6	0.13



(a) Laser beam profile of 17x2 mm.



(b) Laser beam profile of 23x2 mm.

Fig. 5.9 Measured laser beam profiles.

Table 5.5 Welding conditions (I).

Condition I.	A	B
Laser type	LD	LD
Welding speed, m/min	0.3 , 0.5	
Laser power, kW	6	6
Laser irradiation angle, deg	25	5
Defocus length, mm	0	0
Laser core, μm	1000	400
Focus lens	F200	F400
Collimator	100	80
Homogenizer	LL2.20	LL2.54
Spot size, mm	23x2	17x2
Wire feeding speed, m/min	9.9, 14.2	
Wire current, A	292, 357	
Wire feeding position (Top side), mm	0	
Wire feeding angle, deg	80	
Ar gas shielding, l/min	20	
Energization distance, mm	100	

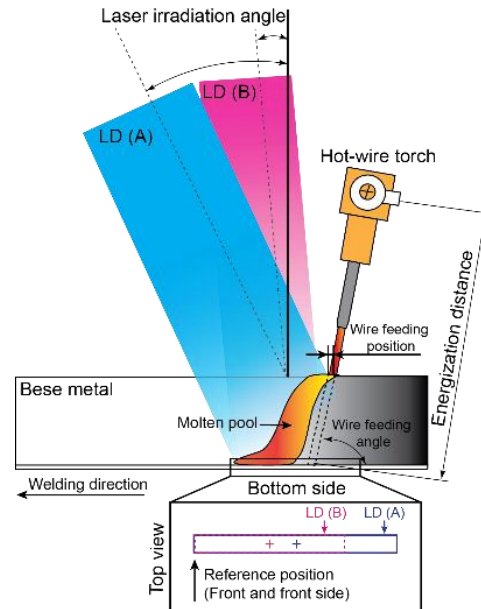


Fig. 5.10 Schematic illustration of experimental set-up (I).

The double lasers welding with thick steel plate of 20-mm in the narrow gap, this experiment was performed by using the combination of rectangular laser spot sizes of 23x2 mm and 17x2 mm, which was set up the irradiation angles of 25° and 5°. Both laser powers were provided by 6 kW and 6 kW diode laser oscillators, respectively. The welding speeds were used as 0.3 and 0.5 m/min, and all conditions were fixed as shown in Table 5.5. The hot wire was used with 1.6 mm diameter and set on the top of the groove weld at the wire feeding position of 0 mm. The laser beam position was set up on the bottom side. Both beams were arranged in the same reference position

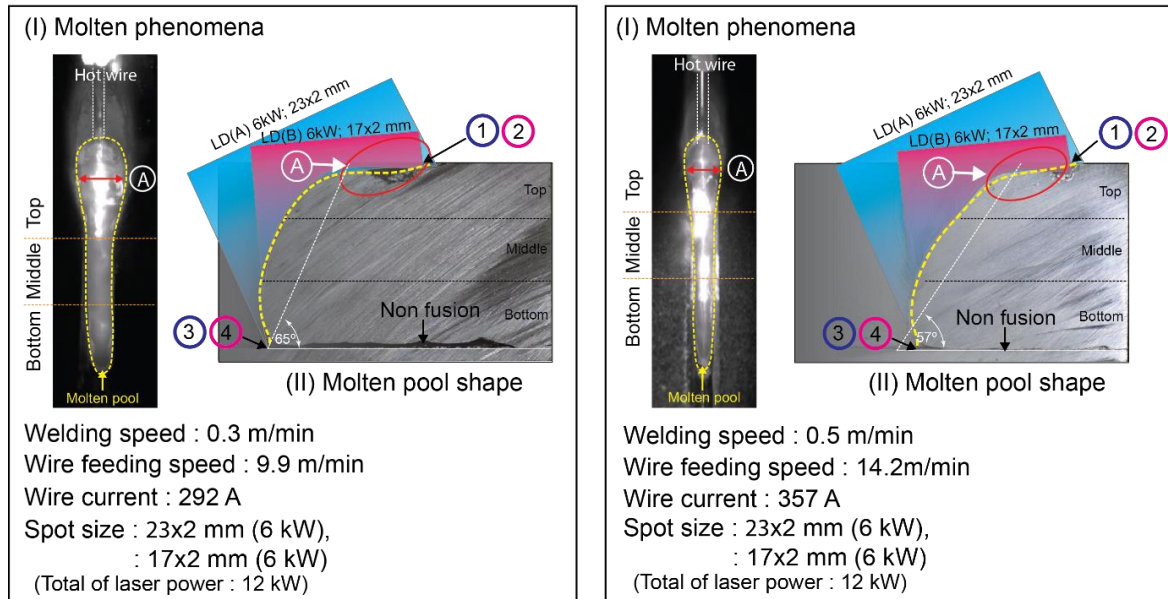
as shown in Fig. 5.10. The shielding gas was used to be Argon gas, which was set up behind the wire feeding position. During welding, the stability of the molten pool was observed by the high-speed camera.

5.4.1.2 Results and discussion

The essential welding parameters were diagnosed from experimental results for their effects on the molten pool phenomena by changing the welding speeds of 0.3 and 0.5 m/min. The combination of laser powers as 12 kW from applying double laser beams of 23x2 mm and 17x2 mm, the result of molten phenomena is shown in Fig. 5.11(a). The molten pool zone was divided to be three considered parts such as top, middle and bottom side of groove weld. The molten pool formation was necessary to apply the laser irradiation along the sidewall from the top to the bottom side of the groove weld. On the top side of the molten pool from using the welding speed of 0.3 m/min was observed on position A; there was a wider molten pool when compared with 0.5 m/min of welding speed as shown in Fig. 5.11(b). It demonstrated that the top area of the groove weld had a high accumulation of laser power. As shown in circles 1 and 2 from both irradiated positions affected by the excessive melting on the top side of the groove weld. This was assumed that the laser irradiation on the top side could be created to be better than other zones of groove weld.

At the welding speed of 0.3 m/min, the ends of the molten pool as shown on the yellow dotted line had a molten pool angle higher than 0.5 m/min of welding speed when was compared. Due to the excessively molten metal on the top side could not flow to the bottom side of the groove weld from creasing the shorter molten pool. Consequently, the laser's irradiation on the bottom side was hindered and not irradiated, which affected non-fusion on the bottom of the groove weld as shown on circles 3 and 4 in both welding speeds.

The molten pool shape was investigated on the end of weld bead which displayed the cross sectional profiles as shown in Figs. 5.11(a) and (b), picture (II). Comparing the molten pool formation from applying the different welding speeds, it was found that at the welding speed of 0.5 m/min had the molten pool angle less than the welding speed of 0.3 m/min. Because welding under the faster welding speed can create the molten pool shape longer than the slower welding speed. They can be observed the molten pool phenomena in picture (I) as shown in Figs. 5.11(a) and (b).



(a) Beam size of 23x2 mm and 17x2 mm, welding speed of 0.3 m/min.

(b) Beam size of 23x2 mm and 17x2mm, welding speed of 0.5 m/min.

Fig. 5.11 High-speed images of molten pool during welding and cross-sections of weld bead fronts in welding direction.

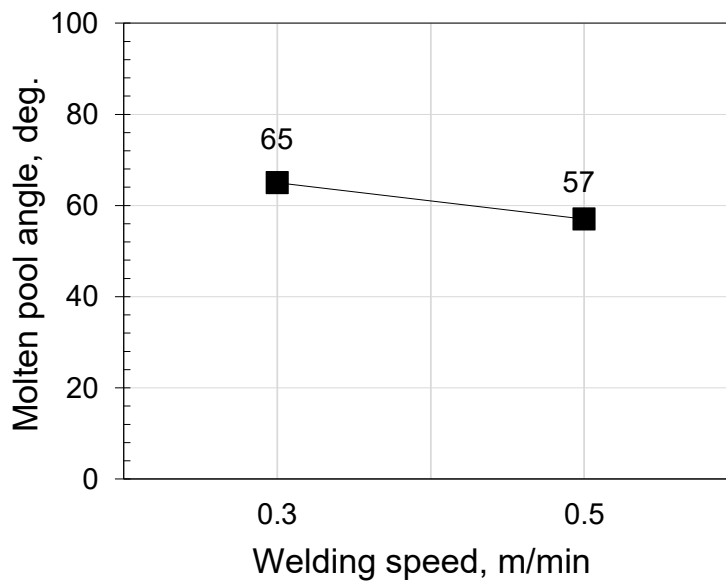
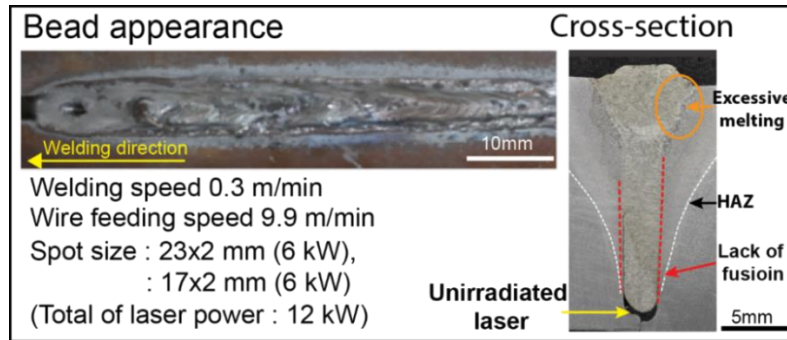


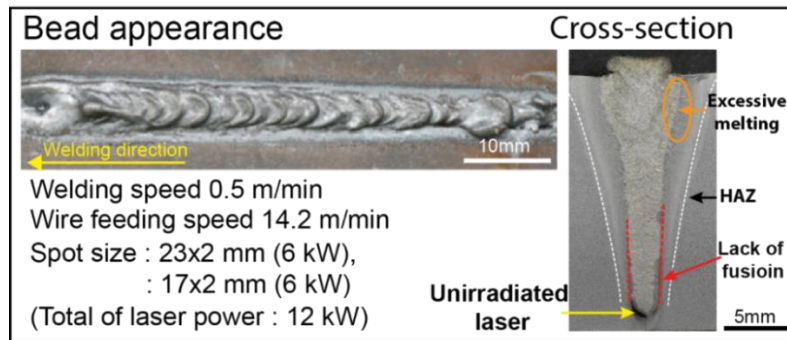
Fig. 5.12 Molten pool angle at welding speed of 0.3 and 0.5 m/min.

From the comparison between the welding speeds of 0.3 and 0.5 m/min is shown in Fig. 5.12. It indicated that the molten pool angle of the welding speed of 0.3 m/min having approximately 65°, which was more than the welded condition with the welding speed of 0.5 m/min giving the molten pool angle of about 57°. Both molten pool shapes could be created by changing the welding speed from using the stable double lasers.

Therefore, the molten pool length was changed by the influence of the welding speed on the ability of molten pool formation.



(a) Welding speed of 0.3 m/min



(b) Welding speed of 0.5 m/min

Fig. 5.13 Bead appearances and cross-sections.

Figure 5.13 shows the bead appearances and cross-sections under the stable double lasers welding and varied welding speed. The reduced welding speed of 0.3 m/min led to overheating on the weld bead and excessive melting, as shown in Fig. 5.13(a). When compared with the welding speed of 0.5 m/min as shown in Fig. 5.13(b).

The cross-section checked as shown in Fig. 5.13(a), it was found that the open groove area had the excessive melting of both welded conditions due to the influence of cumulative laser power on the top side of groove weld. It was seen on the HAZ width, and the fusion line occurred, especially the top till the middle side of the groove weld only. There was a lack of sidewall and unirradiated laser on the root in particular. When compared with the welded bead at the welding speed of 0.5 m/min, it was found that the bead width was smaller than using the welding speed of 0.3 m/min. Then, it can reduce the accumulation of laser power on the top side and the molten metal can rapidly flow when the welding speed increased. The molten pool was created on the groove's sidewall, where can be seen on the dilution and HAZ width of the cross-section.

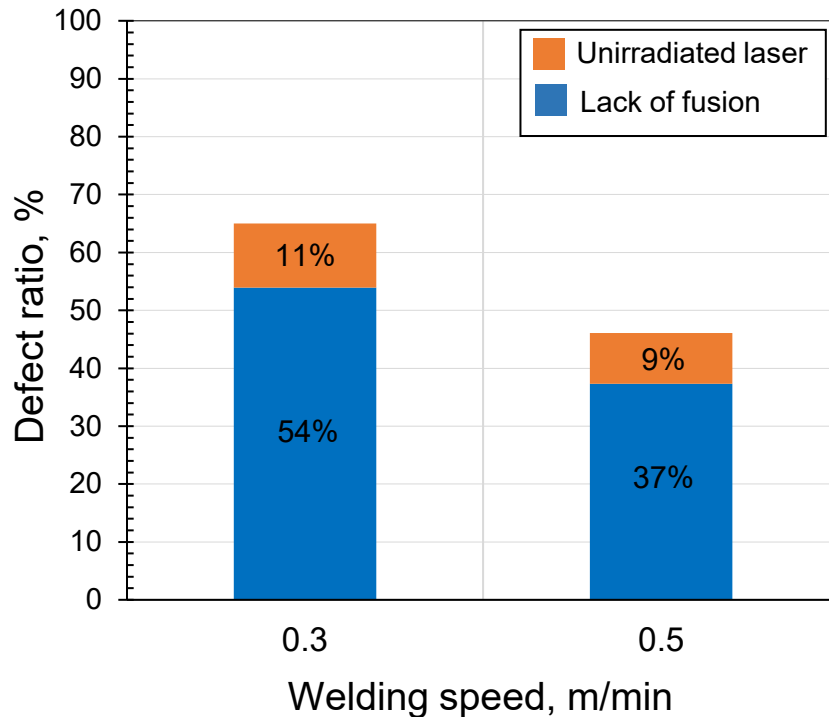


Fig. 5.14 Defect ratios in each welding speed.

The welding defects occurred; they were measured on the cross sectional profiles of both weld beads. The welding conditions were the constant double lasers beam, welding speeds of 0.3 and 0.5 m/min as shown in Fig. 5.13. Both conditions were compared regarding the defect ratios of the lack of fusion and unirradiated laser on the weld bead. From these results, at the welding speed of 0.3 m/min had the total defect ratio of about 65 %, which was more than at 0.5 m/min of welding speed having of about 46 %. Both weld beads had the lack of fusion more than the unirradiated laser as shown those value on the graph in Fig. 5.14.

Thus, applying the stable double lasers welding, which was combined with the stable laser beams of 23x2 mm and 17x2 mm using the total power laser of 12 kW for achieving the optimal condition. Sound weld bead without any defects is not visible, thus, this case was still being studied by using several laser beam combinations on molten pool formation.

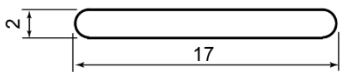
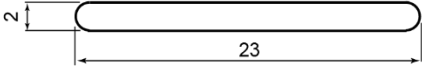
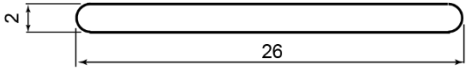
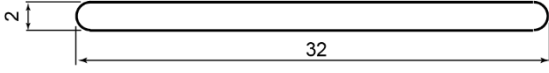
5.4.2 Effects of stable laser beam combination on molten pool formation and joint creation

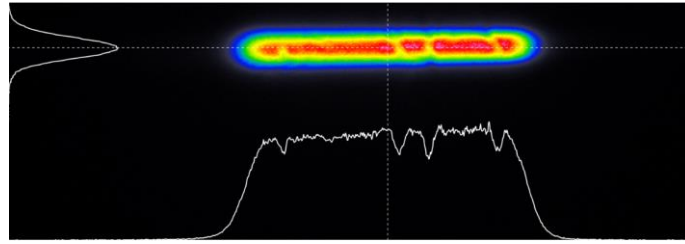
5.4.2.1 Welding conditions

The experimental results in the first part studied the influence of the molten pool formation by the varied welding speed. It was necessary to recognize the effect of the irradiation and appropriate laser power for the narrow gap joining. The joint creation for achieving sound bead and without any defects must be welded with sufficient laser power, which can reasonably create the molten pool's length.

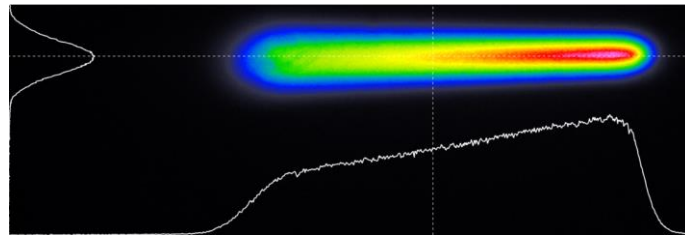
In this part, the experiment was performed by the differentiation of laser beams for studying the effect of molten pool shape by observing laser power's irradiation behavior. The laser beam's characteristic was the rectangle shape of 2 mm width, and 17~32 mm length. Each laser power was used with 6 kW (total laser power of 12kW) while the welding speed of 0.5 m/min was fixed. It can be seen that the smallest laser spot area has an increased power density. The power density is decreased when the laser spot area is significantly expanded, as shown in Table 5.6.

Table 5.6 Energy densities of each laser beam shape.

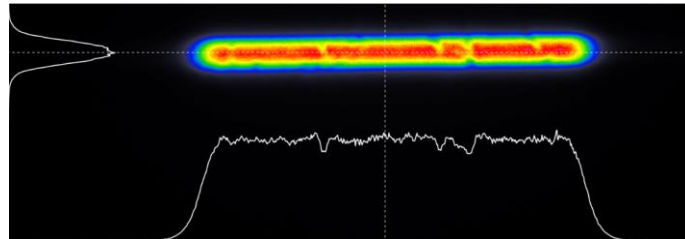
Laser beam shape (mm)	Laser spot area (mm ²)	Laser power (kW)	Power density (kW/mm ²)
	33.14	6	0.18
	45.14	6	0.13
	51.14	6	0.12
	63.14	6	0.10



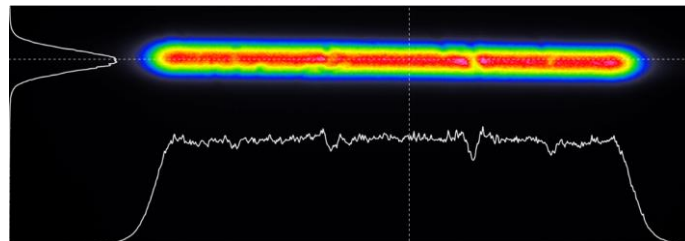
(a) Laser spot size of 17x2 mm, irradiation angle of 25°.



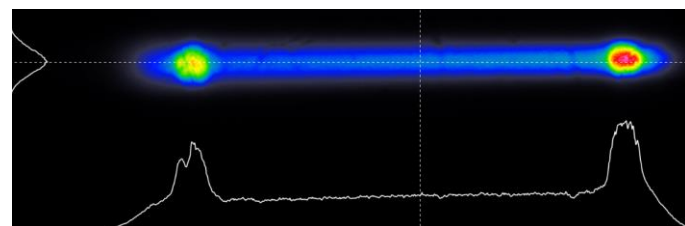
(b) Laser spot size of 23x2 mm, irradiation angle of 25°.



(c) Laser spot size of 26x2 mm, irradiation angle of 5°.



(d) Laser spot size of 32x2 mm, irradiation angle of 5°.



(e) Laser spot size of 32x2 mm (edge), irradiation angle of 23°.

Fig. 5.15 Measured laser beam profiles.

The laser power combination of different beam sizes was examined the energy density in each laser beam shape per the area affected. They can be seen the laser power distributions as shown in each laser beam profiles in Figs. 5.15 and displayed the graph of power density in each irradiation position used at different angles.

Therefore, each laser beam profile used in this research with the laser spot width of 2 mm, lengths of 17~32 mm shows the beam profile and power density of all beams at 6000 W as shown in Figs. 5.15(a)~(e), respectively. The operated laser's wavelength was 910, 940, 980, and 1030-nm irradiation for this laser power source. The fiber core sizes, collimator, homogenizer, and focusing lens used according to each condition experimented. These experimental conditions were determined three conditions as shown in Tables 5.8~5.10, respectively. The welding speed was used at 0.5 m/min and other welding conditions were fixed as shown in Table 5.7. The total laser power of 12 kW was provided by the combination of double laser beams. The laser irradiation angle of 17x2 mm beam size was 25° and 5° of 32x2 mm beam size. Focus length, laser core, focus lens, collimator and homogenizer of both laser heads were used and set up as shown in Fig. 5.16.

Table 5.7 Welding conditions for laser spot combination of 17x2 mm and 32x2 mm (II).

Condition II.	A	B
Laser type	LD	LD
Welding speed, m/min	0.5	
Laser power, kW	6	6
Laser irradiation angle, deg	25	5
Defocus length, mm	0	0
Laser core, μm	400	1000
Focus lens	F400	F200
Collimator	80	100
Homogenizer	LL2.54	LL2.20
Spot size, mm	17x2	32x2
Wire feeding speed, m/min	14.2	
Wire current, A	357	
Wire feeding position (Top side), mm	0	
Wire feeding angle, deg	80	
Ar gas shielding, l/min	20	
Energization distance, mm	100	

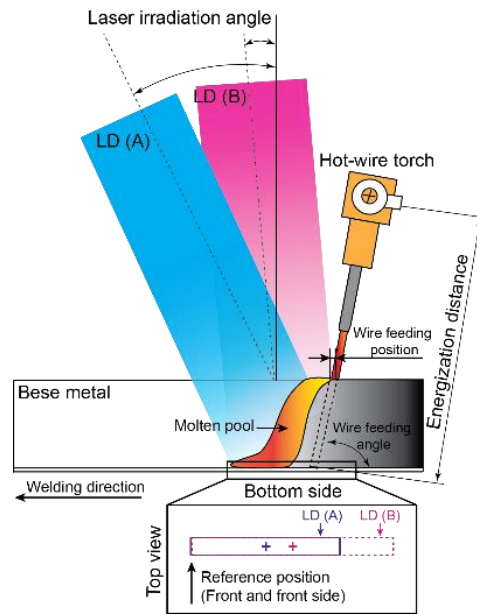


Fig. 5.16 Schematic illustration of experimental set-up (II).

Table 5.8 Welding conditions for laser spot combination of 23x2 mm and 26x2 mm (III).

Condition III.	A	B
Laser type	LD	LD
Welding speed, m/min	0.5	
Laser power, kW	6	6
Laser irradiation angle, deg	25	5
Defocus length, mm	0	0
Laser core, μm	1000	400
Focus lens	F200	F400
Collimator	100	80
Homogenizer	LL2.20	LL2.54
Spot size, mm	23x2	26x2
Wire feeding speed, m/min	14.2	
Wire current, A	328	
Wire feeding position (Top side), mm	0	
Wire feeding angle, deg	80	
Ar gas shielding, l/min	20	
Energization distance, mm	100	

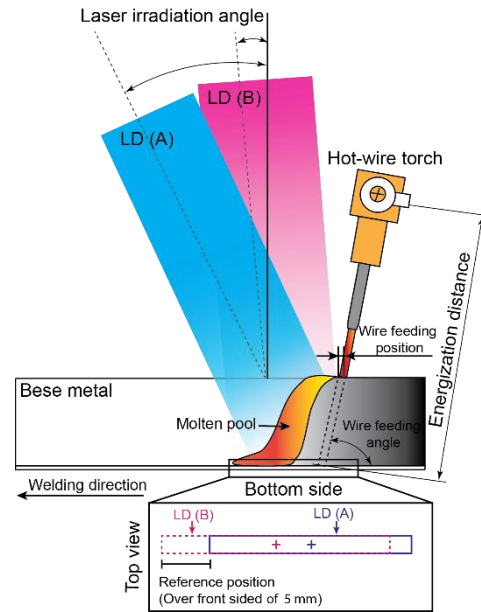


Fig. 5.17 Schematic illustration of experimental set-up (III).

Table 5.9 Welding conditions for laser spot combination of 32x2 mm and 26x2 mm (IV).

Condition IV.	A	B
Laser type	LD	LD
Welding speed, m/min	0.5	
Laser power, kW	6	6
Laser irradiation angle, deg	23	5
Defocus length, mm	0	0
Laser core, μm	400	400
Focus lens	F500	F400
Collimator	100	80
Homogenizer	LL2.35 (edge)	LL2.35
Spot size, mm	32x2	26x2
Wire feeding speed, m/min	14.2	
Wire current, A	328	
Wire feeding position (Top side), mm	0	
Wire feeding angle, deg	80	
Ar gas shielding, l/min	20	
Energization distance, mm	100	

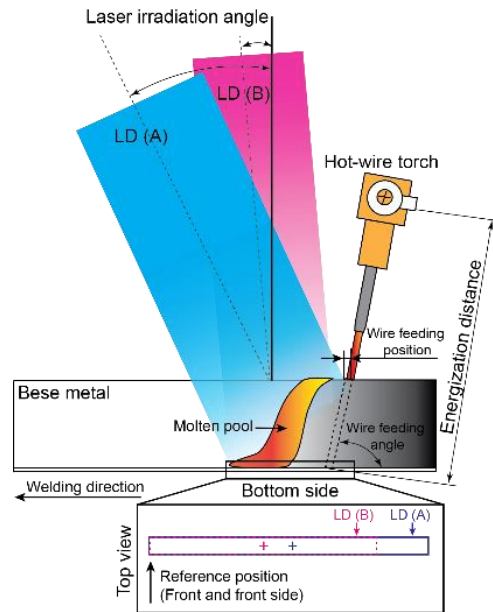


Fig. 5.18 Schematic illustration of experimental set-up (IV).

5.4.2.2 Results and discussion

Three welding conditions were carried out under the different combination of double lasers and observed the molten pool formation by high-speed camera. The molten pool phenomena was focused on the top, middle, and bottom of the groove weld for investigating the laser irradiation on the sidewall during welding as shown in Fig. 5.16 and shown the welding condition in Table 5.7. The laser irradiation was applied with the combination of 17x2 mm and 32x2 mm laser beams using the total laser power of 12 kW and welding speed of 0.5 m/min was fixed. The results reveal that the molten pool width was relatively small on the top side beside the hot-wire feeding position, but there was more expansive in the middle of groove weld showing in circle A as shown in Fig. 5.19(a). It was a beginning point of the combination of twin laser powers until the bottom side of groove weld. Which clearly can indicate as shown in Fig. 5.19(a), position (II) of molten pool shape. Because the molten pool's length was short, the molten metal could not keep flowing from the hot-wire feeding by applying the short laser beam of 17x2 mm combined with 32x2 mm of long laser beam.

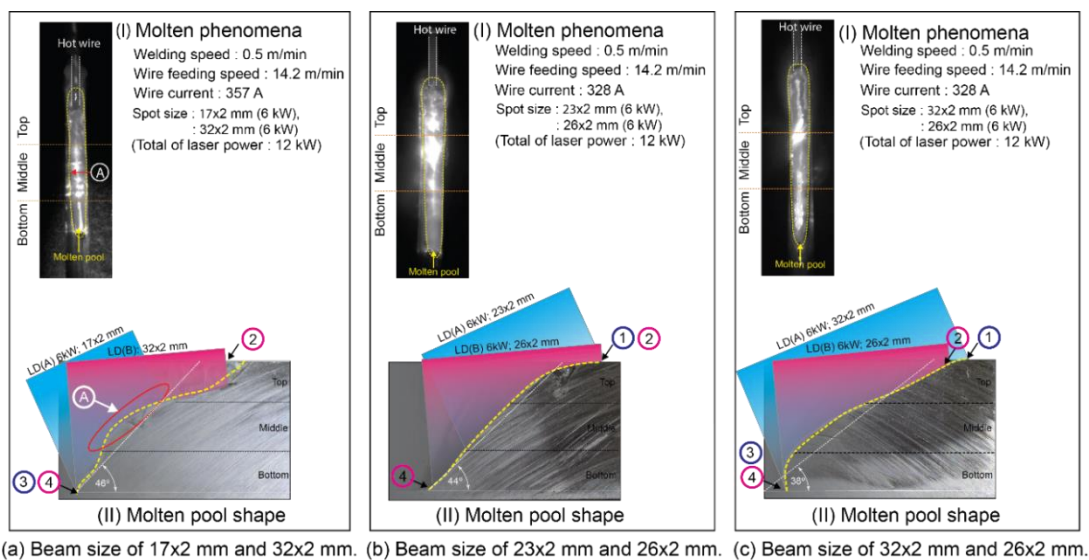


Fig. 5.19 High-speed images of molten pool during welding and cross-sections of weld bead fronts in welding direction.

Fig. 5.19(b) shows the result of using the combination of laser beams of 23x2 mm and 26x2 mm, laser irradiation angles of 25° and 5°, and other conditions were set up as shown in Table 5.8 and Fig. 5.17. As a result, Figure 5.19(b), picture (I) shows the molten pool formation on the top, middle and bottom side. It was found that the molten pool was relatively stable along the sidewall of groove weld. The molten pool shape was wider and longer than the combination of laser beams of 17x2 mm and 32x2 mm when was compared as shown in Fig. 5.19(a). The cross-section of the endpoint of the weld bead can be seen in Fig. 5.19(b), number (II). The molten metal

flow was invariable from the top until the bottom side of groove weld. The top side had the combination of both power densities, but the bottom side had only the laser irradiation of laser beam of 26x2 mm, where is presented the irradiated position in circle 4.

The final condition was experimented as shown in Fig. 5.19(c), which was used the combination of double laser beams of 32x2 mm and 26x2 mm. The laser beam of 32x2 mm was adjusted to the laser irradiation angle at 23°, and the laser beam of 26x2 mm was applied at 5°. Other conditions were set up in the following condition as shown in Table 5.9 and Fig. 5.18. The combination of energy from double laser beams was observed in the molten metal behavior on the top till bottom side of groove weld. The flow of molten metal within the groove was longer than both conditions (condition II and III) and was stable on the top of sidewall until the bottom side. Due to the combination of both laser powers was sufficient to create the molten pool formation from the top to bottom side of groove weld. It clearly defined the irradiation position of laser beam where was observed from the melting phenomena and examined molten pool shape as shown in Fig. 5.19(c). The circles 1, 2 show the laser irradiation positions of both on the top side. The circles 3, 4 show the irradiated bottom area of both laser beams. Thus, the combination of double laser beams of 32x2 mm and 26x2 mm can create the least molten pool angle when was compared with all experimental conditions.

Therefore, the molten pool angle of three conditions was measured on the cross sectional profile of the weld bead's endpoint and compared in each condition as shown in Fig. 5.20. It was found that the molten pool angle was created by using total laser power of 12 kW from both long laser beams of 32x2 mm and 26x2 mm. There was the molten pool angle of about 35° when compared with the shorter laser beam as shown in Figs 5.19(a) and (b), which had the molten pool angles of about 45° and 44°, respectively.

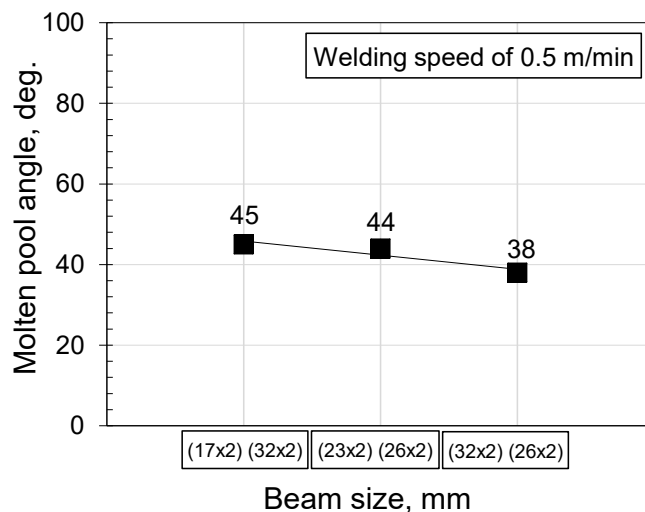
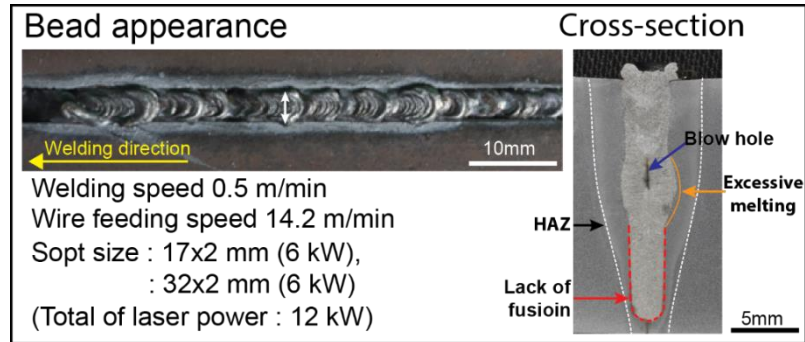
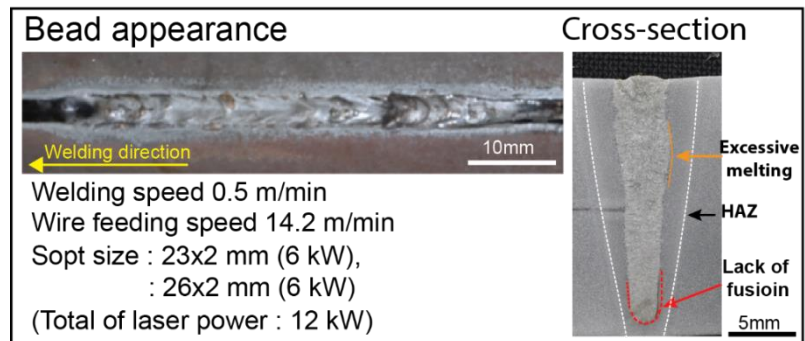


Fig. 5.20 Molten pool angles in each laser beam combination.

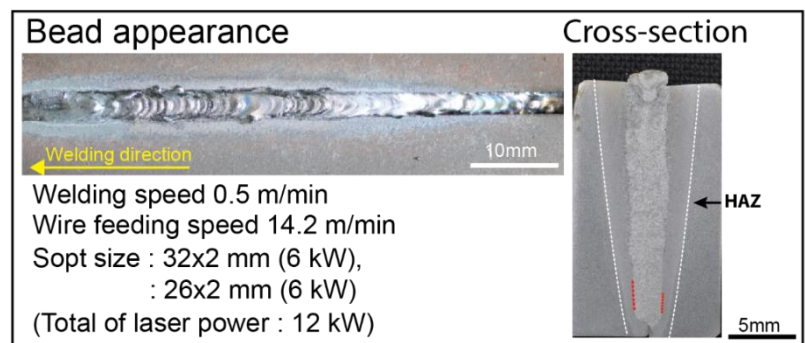
Therefore, the influence of laser spot length from stable laser beam combination affected the molten pool formation. The sufficient laser power could create the molten pool shape from overlapping irradiation. Both laser beam lengths must be similar to the same spot size for obtaining the optimal condition.



(a) Beam size of 17x2 mm and 32x2 mm.



(b) Beam size of 23x2 mm and 26x2 mm.



(c) Beam size of 32x2 mm and 26x2 mm.

Fig. 5.21 Bead appearances and cross-sections.

From diagnosing the joint creation under the welding conditions of different beam sizes and adjusting the laser irradiation position, the results of experiment show the bead appearances and cross-sections as shown in Figs. 5.21. All of bead appearances had an undercut from irradiation of long laser beam on the top side of groove weld. The bead cross-section profile obtained from applying the combination

of laser beams of 17x2 mm and 32x2 mm as shown in Fig. 5.21(a), there was an excessive melting, blowhole, and lack of fusion. For using the laser beams of 23x2 mm and 26x2 mm were combined. The welded bead slightly had the excessive melting on the top of groove weld as shown in Fig. 5.21(b). The welding defects occurred; there was the lack of fusion on the bottom side less than applying the laser beam combination of 23x2 mm and 26x2 mm when was compared. Figure 5.21(c) shows the results using the combination of laser beams of 32x2 mm and 26x2 mm. Both laser beams had the long rectangle shape. Consequently, it could irradiate on the top until the bottom side of groove weld better than carrying out by the short laser beam due to the combination of both long laser beams that could irradiate along the sidewall of groove weld invariably.

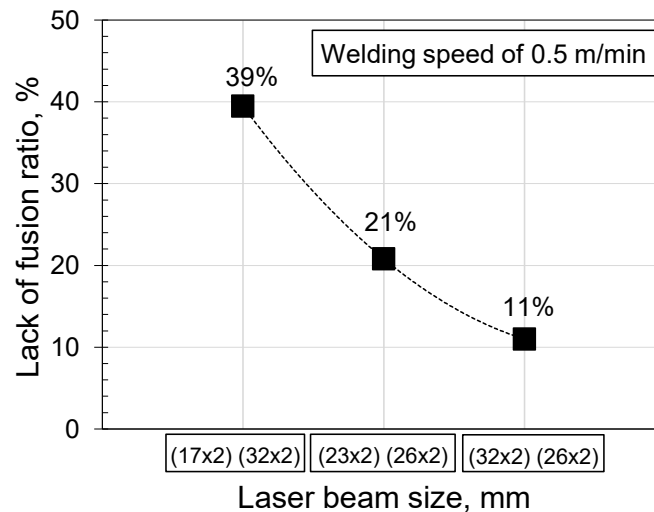


Fig. 5.22 Lack of fusion ratios in each laser beam combination.

Figure 5.22 shows the lack of fusion ratios on the weld bead in each laser beam size from measuring the cross-section under the defined conditions. It can be seen that the lack of fusion occurred in each welding condition specifically from the middle till bottom side of groove weld as shown in Fig. 5.21. The highest lack of fusion ration of about 39 % belonged using the short laser beam combination (17x2 and 32x2 mm), when compared with the combination of longer laser beam giving the lack of fusion of about 21 % (23x2 and 26x2 mm) and 11 % (32x2 and 26x2 mm), respectively.

Therefore, the weldment with double lasers using the combination of total laser power of 12 kW, laser beam combination of 32x2 mm and 26x2 mm, and welding speed of 0.5 m/min, it can create the longest pool shape and the least molten pool angle compared to all welding conditions. Thus, this section aims to investigate the effect of different combinations of laser beam sizes to the molten pool formation. It succeed by changing the stable double laser beams which can obtain the suitable joint creation under low laser power.

5.4.3 Joint creation using stable laser beam combination of 32x2 mm and 26x2 mm and evaluation of joint properties

5.4.3.1 Welding conditions

From study the effect of laser beam size by using the several combinations of laser bead size, it was found that the laser beam sizes of 32x2 mm and 26x2 mm, the welding speed of 0.5 m/min can create the least molten pool angle and give the lowest lack of fusion. This condition was selected for carrying out with varying of the welding speeds and beam position arrangements for investigating the influence of the mentioned conditions.

This part, study the effect of stable laser beam combination of 32x2 mm and 26x2 mm, welding speeds of 0.3, 0.4, and 0.5 m/min, beam position arrangements as the bottom and top side of groove weld were performed. The welding conditions and experimental set-up are shown in Table 5.10 and Figs. 5.23, respectively.

Table 5.10 Welding conditions (V).

Condition V.	A	B
Laser type	LD	LD
Welding speed, m/min	0.3, 0.4, 0.5	
Laser power, kW	6	6
Laser irradiation angle, deg	23	5
Defocus length, mm	0	0
Laser core, um	400	400
Focus lens	F500	F400
Collimator	100	80
Homogenizer	LL2.35 (edge)	LL2.35
Spot size, mm	32x2	26x2
Wire feeding speed, m/min	8.4~14.2	
Wire current, A	252~328	
Wire feeding position (Top side), mm	0	
Wire feeding angle, deg	80	
Ar gas shielding, l/min	20	
Energization distance, mm	100	

beam position arrangement on the bottom side of groove weld. The results show that the molten pool formation and joint creation have the complete fusion along the groove weld to achieve the sound joint using the stable laser beam combination.

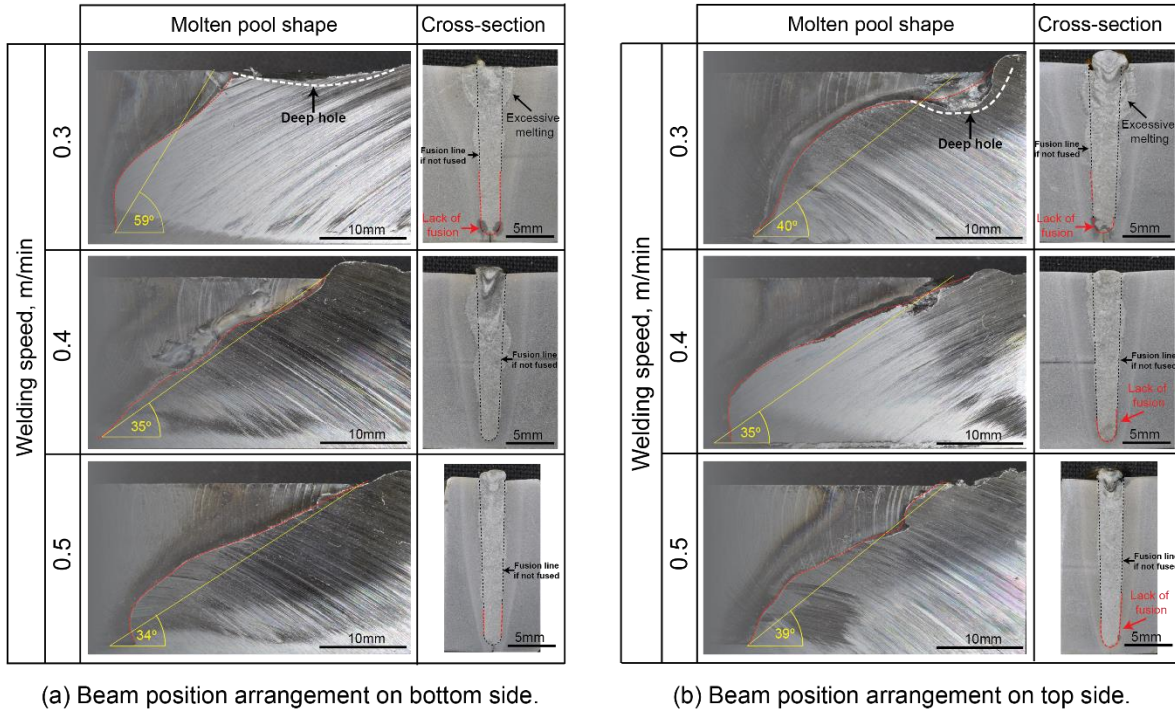


Fig. 5.24 Cross-sections of weld bead fronts in welding direction and cross-sections of joints.

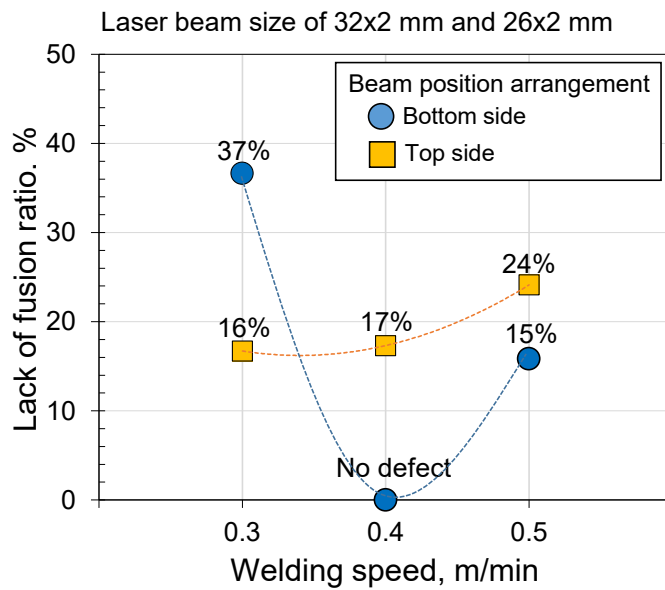


Fig. 5.25 Lack of fusion ratio.

Comparing the lack of fusion ratio of the weld bead, both beam position arrangements and each welding speeds of 0.3~0.5 m/min is shown in Fig. 5.25. The results found that setting up the beam position on the bottom side of groove weld, welding speed of 0.3 m/min had the lack of fusion ratio of about 37 %, which was more than 0.5 m/min of welding speed having of about 15 % lack of fusion when was compared. The weld bead without any defect, when the welding speed of 0.4 m/min was used. The beam position arrangement on the top side of groove weld and welding speeds of 0.3~0.5 m/min were employed. The examination of the lack of fusion ratio exhibited of about 16 % to 24 %, respectively. Thus, the high welding speed affected the reduction of the power density and could not create the complete molten pool at the root in the particular and sidewall of groove weld.

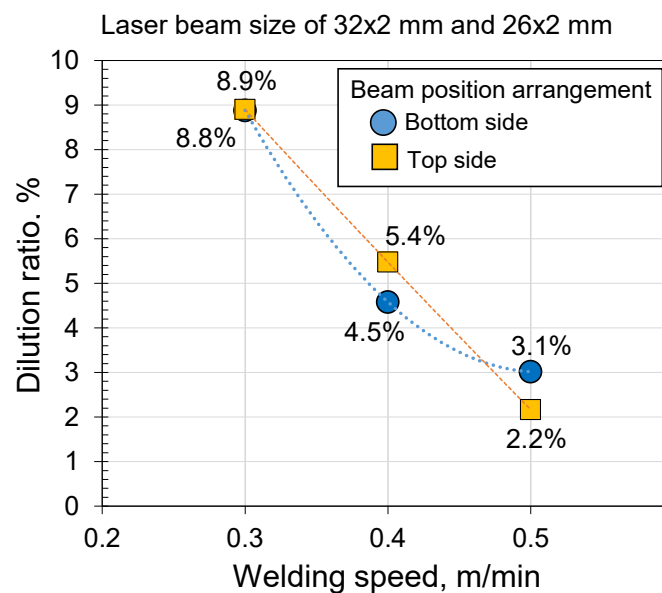


Fig. 5.26 Dilution ratio.

The result of dilution ratio is shown in Fig. 5.26. The dilution ratios decreases almost linearly with the increase of welding speed under all welding conditions. The effect of heat input on the dilution ratio became smaller as the hot-wire feeding according to the welding speed increased and beam position arrangement changed as well: for example, dilution ratios for the beam position arrangement on the top of groove at the welding speeds of 0.3~0.5 m/min were 8.9 %, 5.4 %, and 2.2 %, respectively.

In this section, the obtained condition achieved by using the stable laser beam combination of 32x2 mm and 26x2 mm, welding speed of 0.4 m/min, beam position arrangement on the bottom side. The weld bead without any defect had deep penetration throughout the sidewall and un-melty on the open groove. Hence, the sound bead obtained was tested the mechanical properties with the Vickers hardness

test, tensile test, Charpy impact test for assessment of the butt joint using the stable double lasers welding by the low laser power.

2) Joint properties

Evaluations of butt joints were tested the mechanical property under the welding condition achieved using the stable laser beam combination of 32x2 mm and 26x2 mm, welding speed of 0.4 m/min and beam position arrangement on the bottom side was carried out. Sound weld joining was evaluated the Vickers hardness test, tensile test, and Charpy impact test for this experiment as listed below.

The Vickers hardness distribution was measured across the middle side of the welded part on the cross-section, where the measurement position was determined as shown in Fig. 5.27(a). The measurement condition was used the testing load of 10 kgf and the load time of 15 s. There was the distance from the center of weld metal as 3 mm on both sides, each investigating point of 0.5 mm.

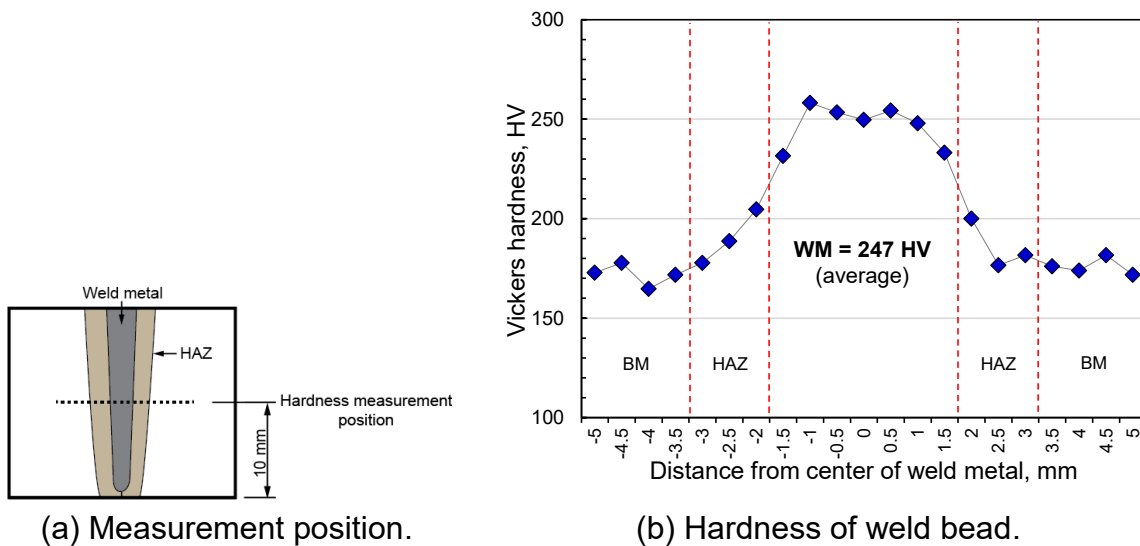


Fig. 5.27 Result of Vickers hardness test.

Vickers hardness is shown in Fig. 5.27(b), which had the hardness average of weld metal approximately 247 HV. On the other hand, the HAZ area had the lower hardness value that there was the trend decreased to be similar to the base metal of about 170 HV. The comparison for Vickers hardness of weld metal between the hot-wire laser welding and the hot-wire CO₂ arc welding process had the hardness average of the weld metal more than the welded part by using the double lasers welding method as same material with the thickness of 20-mm, and filler wire. In the hot-wire CO₂ arc welding method, the hardness average of weld metal was lower than the weld metal from using the double lasers welding of about 50 HV when was

compared. Besides, the heat input used in the part of hot-wire double lasers welding method had lower power and higher cooling rate that is assumed. It affected the high hardness of weld metal for this process but can deduce HAZ width when compared with the cross-sections which welded by hot-wire CO₂ arc welding method as shown in Fig 5.24.

The tensile test was conducted to evaluate the strength of the butt joint from using the obtained condition. The tensile test specimens and the testing locations are shown Fig. 5.28. They were tested according to JIS Z 2241 No.14B as shown in Fig. 5.29.

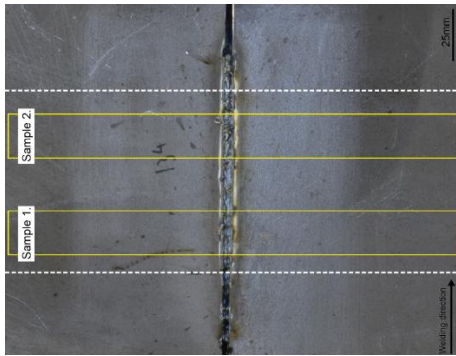


Fig. 5.28 Cut-off plan for tensile test specimen.

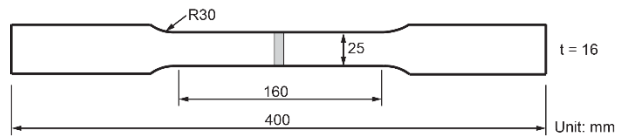


Fig. 5.29 Tensile test specimen.

The result of the tensile test is shown in Table 5.11. The appearance of test specimens is displayed as shown in Fig. 5.30, which found that sample 1 was broken on the welded metal part and had yield point and tensile strength of about 375.7 and 522.3 MPa. It can see the stress-strain curve which is shown in Fig. 5.31, and found that there was the percent of strain less than the values of sample 2 giving the yield point approximately 382.6 and 552.1 MPa of tensile strength. The breaking point was fractured at the base metal, which suggested that the weld metal zone was stronger than the base metal. When inspected the welded samples after testing found that the fracture surface was on top of the weld bead as shown in sample 2. It was suspected due to the failed fusion zone appeared on the fusion line position. Comparing the yield point and tensile strength of test pieces had the breaking point on the weld metal and base metal. The fracture surface of the tensile test specimen (sample 1) is shown in Fig. 5.32 which was the breaking position on the weld metal.

Table 5.11 Results of tensile test.

Specimens	Yield point (MPa)	Tensile strength (MPa)
Sample 1	375.7	522.3
Sample 2	382.6	552.1

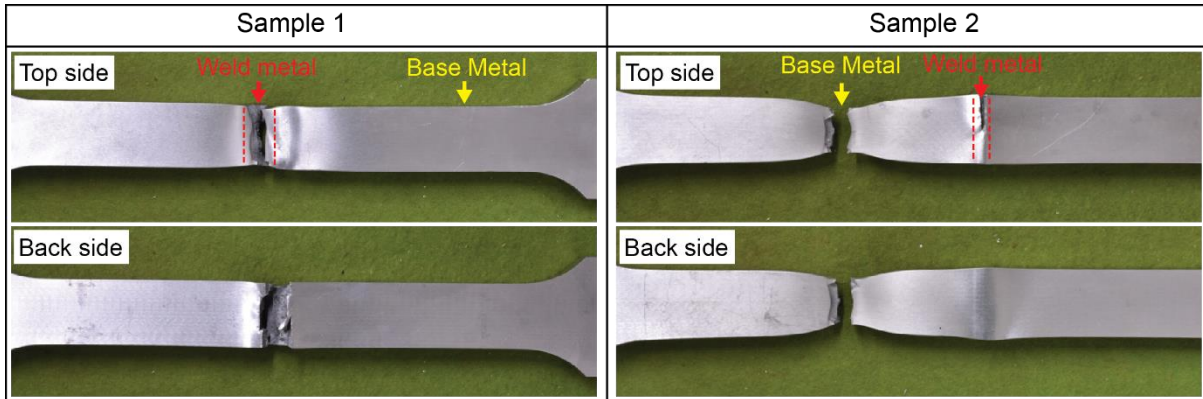


Fig. 5.30 Appearances of tested specimens.

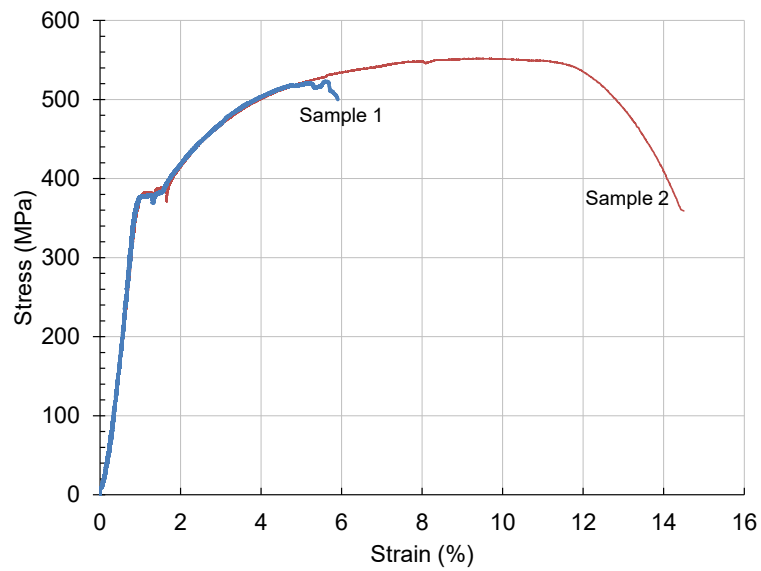


Fig. 5.31 Stress-strain diagrams.

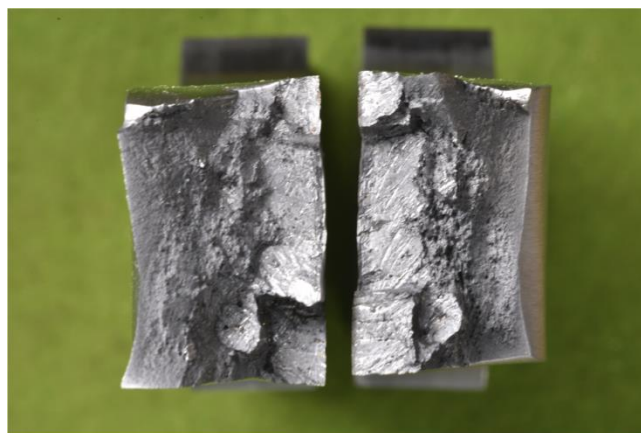


Fig. 5.32 Fracture surface of tensile test specimen (Sample 1).

From these results, it was found that using the stable laser beam with the laser power of 12 kW can create the butt joint of 20-mm thickness steel plates. It gave sufficient strength in narrow gap joining, which can replace the conventional welding process.

To evaluate the toughness of the welded joint, Charpy impact test was performed according to JIS Z 2242 with the specimen size of 10 mm x 10 mm x 55 mm as shown in Fig. 5.33. The Charpy test equipment was used with a heavy pendulum of 25.31 kg and arm length of 0.7 m. The welded joint was evaluated the absorbed energy of weld metal (WM) and fusion line (FL) zone at a test temperature of 0°C. The Charpy impact test specimen was welded with the obtained condition and determined the location according to the welded part's sampling position as shown in Fig. 5.34.

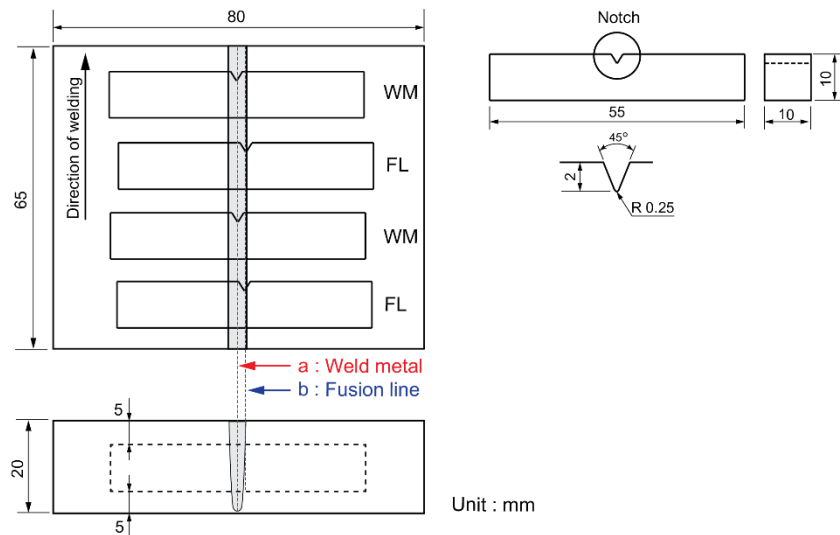


Fig. 5.33 Cut-off plan and notch locations for V-notched Charpy impact.

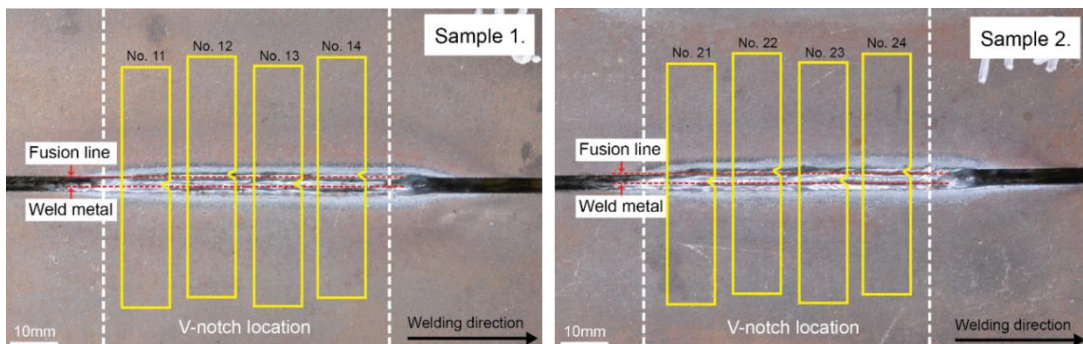


Fig. 5.34 Cut-off locations for specimen.

The impact test specimens were inspected on the fracture surface of the test piece after the test. They were found that there was some lack of fusion on V-notched specimens, as shown in Table 5.12. The absorbed energy value is shown especially without any defect as presented in Fig. 5.35. The fusion line (specimen number: 12, 21 and 22), almost all specimens had the defect and genuinely cannot confirm the value of absorbed energy because of the failed fusion line occurred, but they gave the high absorbed energy more than the specification requirement.

Table 5.12 Results of Charpy impact tests.

Specimen number	Notch position	Absorbed energy, J	Defect detection
11	WM	211.4	Lack of fusion
12	FL	51.8	Lack of fusion
13	WM	282.8	-
14	FL	33.1	Lack of fusion
21	WM	60.3	Lack of fusion
22	FL	19.6	Lack of fusion
23	WM	239.4	-
24	FL	54.6	-

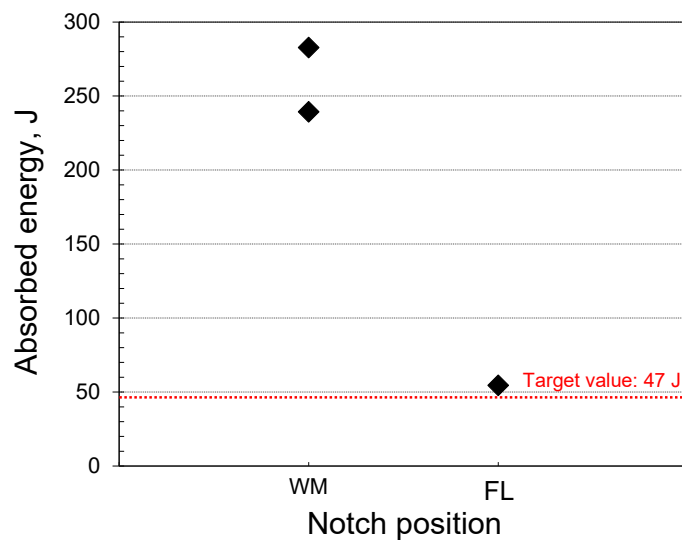


Fig. 5.35 Results of Charpy impact tests.

Figure 5.35 shows the value of absorbed energy of the weld metal and fusion line without any defect after performing and was examined on the impact test specimen. The mean value was higher than the minimum average impact test value of the welded joint, which was 47 J at 0° C. The result of V-notch Charpy impact test

clearly displays that this process can perform with 20-mm thick steel plate, and without suspicions on the weld bead.

Thus, the development of hot-wire welding process using stable double laser beams for joining the thick steel plate was studied with the thickness 20-mm in the narrow gap. From the achieved welding condition, the root gap of 2 mm, stable laser beam combination of 32x2 mm and 26x2 mm, total laser power of 12 kW, beam position arrangement on the bottom side set up, welding speed of 0.4 m/min was performed. It completely achieved under adequate weld penetration and without any defects when the weld bead was investigated on the bead appearance and cross-section. The welded joint was tested the Vickers hardness of the weld bead. As a results of the hardness of weld metal was much higher than the base metal and HAZ. The tensile strength and V-notch Charpy impact test result provided the specification requirement even though met the failed fusion on the test piece.

The results of experiment, as mentioned above, it can be proposed using a weaving system to distribute the laser power beam for creating the molten pool on the sidewall and avoiding defects occurred. The top till bottom zone of groove weld can be irradiated by combining both laser beams using low power laser.

5.5 Investigation of molten pool formation and joint creation using weaving and stable laser beam combination

From The previous experiment could confirm that using the stable laser irradiation still had some lack of fusion on the bottom side of groove weld due to low power density could not create the molten pool during melting metal flow. Therefore, it was conducted by using the weaving laser head to give irradiation on the sidewall and bottom side of groove weld, which can control the weaving width under the command voltage from the function generator. In this part, it was interested in adjusting a laser irradiation angle of fixed head and weaving head to study the effect of weaving system in hot-wire double lasers welding method.

5.5.1 Materials and specimen used

Steel plate of base metal was KE36 with dimensions of 20-mm thickness, 40-mm width, and 160-mm length. U-shaped groove for butt joint with an angle of 6° and root gap of 3-mm were employed as shown in Fig. 5.36. The chemical composition of base metal as shown in Table 5.13. The filler wire of JIS Z3312 YGW11 with 1.6 mm diameter was used as shown a chemical property of filler wire in Table 5.14.

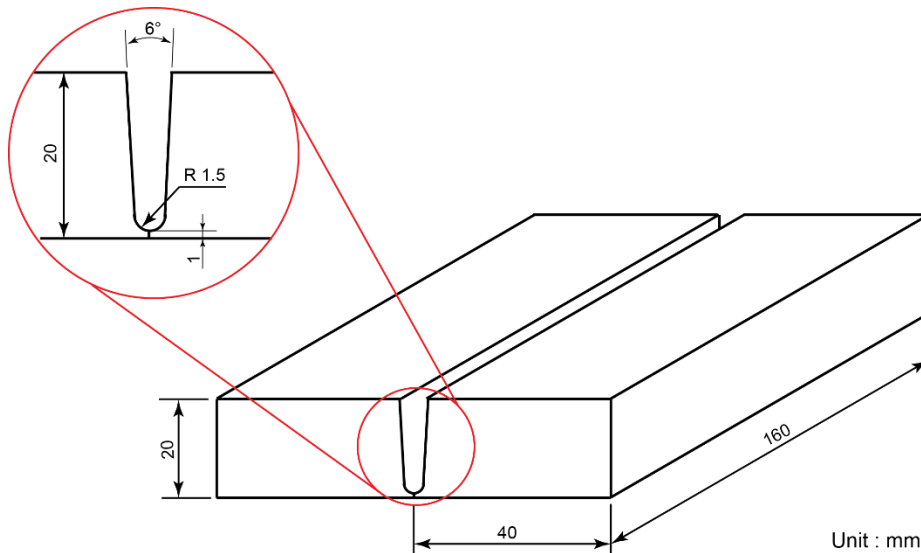


Fig. 5.36 Schematic illustration of specimen.

Table 5.13 Chemical composition of base material.

Element	C	Si	Mn	P	S	Cu	Ni	Cr
Base metal (KE36)	0.12	0.2	1.21	0.14	0.04	0.01	0.01	0.02

Table 5.14 Chemical composition of filler wire.

Filler wire	C	Si	Mn	P	S	Cu	Ti	Zr
JIS Z3312 YGW11	0.02	0.40	1.00	0.03 or less	0.03 or less	0.50 or less	Ti + Zr : 0.02~0.15	
	~	~	~					
	0.15	1.00	1.60					

5.5.2 Welding conditions

The experiment was performed under the welding conditions as shown in Table 5.15. The laser spot size was fixed and weaved of 32 x 2.5 mm and 25 x 2.4 mm, they were adjusted the fixed laser irradiation angle and weaving head of 25° and 5°, 30° and 5°, 30° and 10°, respectively. Both laser powers were used with 6 kW (total laser power of 12 kW) and was arranged the laser beam position on the bottom of groove at the front and front sides of groove weld. Table 5.16 shows the main condition selected for studying the influence of weaving width on laser irradiation on the sidewall's bottom side using the weaving width of 0.65, 1.0, and 1.3 mm, respectively. Arrangement of the laser beam position, configuration of hot-wire double lasers welding, and all conditions set up using weaving system are shown in Fig. 5.37 and Fig. 5.38.

Table 5.15 Welding conditions.

Conditions	A		B	
Welding speed, m/min	0.3			
Laser type	LD (Fixed head)		LD (Weaving head)	
Weaving width, mm			0.65	
Frequency of weaving, Hz			5	
Weaving waveform			Exponential	
Laser power, kW	6		6	
Laser irradiation angle, deg.	25	30	5	10
Defocus length, mm	0		0	
Laser core, μm	400		400	
Focus lens	500		600	
Collimator	80		100	
Homogenizer	LL2.35		LL2.54	
Spot size, mm	32 x 2.5		25 x 2.4	
Wire feeding speed, m/min	11.1			
Wire current, A	283			
Wire feeding position, mm	0			
Wire feeding angle, deg.	80			
Ar gas shielding, l/min	25			
Energization distance, mm	110			
Laser spot position	Front and Front side			
Root gap, mm	3			

Table 5.16 Welding conditions.

Conditions	A	B
Welding speed, m/min	0.3	
Laser type	LD (Fixed head)	LD (Weaving head)
Weaving width, mm	0.65, 1.0, 1.3	
Frequency of weaving, Hz	5	
Weaving waveform	Exponential	
Laser power, kW	6	6
Laser irradiation angle, deg.	30	10
Defocus length, mm	0	0
Laser core, μm	400	400
Focus lens	500	600
Collimator	80	100
Homogenizer	LL2.35	LL2.54
Spot size, mm	32 x 2.5	25 x 2.4
Wire feeding speed, m/min	11.1	
Wire current, A	283	
Wire feeding position, mm	0	
Wire feeding angle, deg.	80	
Ar gas shielding, l/min	25	
Energization distance, mm	110	
Laser spot position	Front and Front side	
Root gap, mm	3	

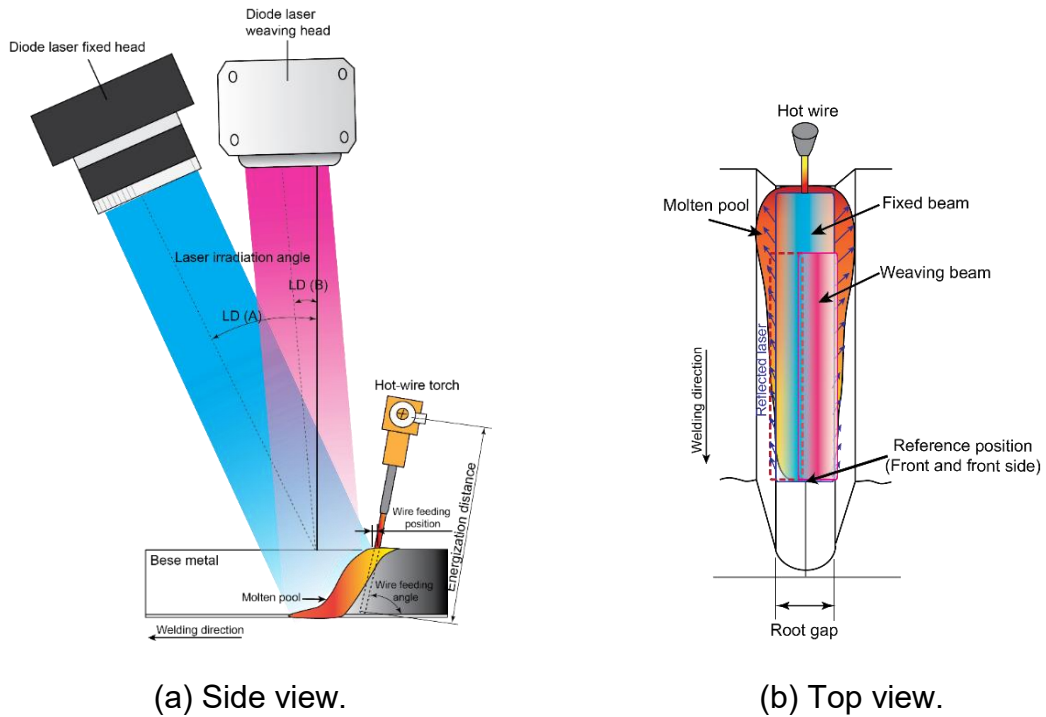


Fig. 5.37 Schematic illustration of experimental set-up.

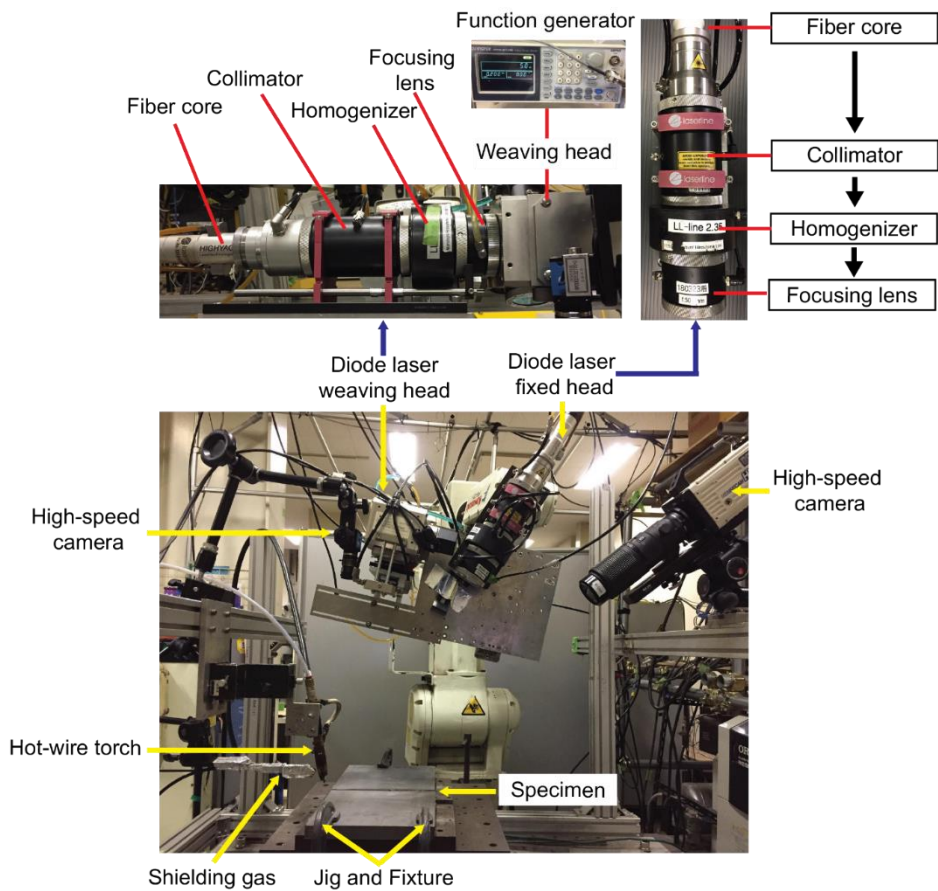


Fig. 5.38 Appearance and equipment for hot-wire laser welding using weaving system.

Laser-irradiating conditions of the laser spot size, laser weaving spot and laser power density were examined on the molten pool formation and weld bead created. There were two laser spot sizes of 25x2.4 mm and 32x2.5 mm used for welding in the narrow gap using the weaving system combined with the fixed laser beam. Both laser spot sizes, which were applied in this experiment to be the rectangle shape and each laser power was used with 6 kW (total laser power of 12 kW). It can be seen that the smallest laser spot area has more power density than the bigger laser spot area expanded as shown in Table 5.17.

Table 5.17 Energy density in each laser beam.

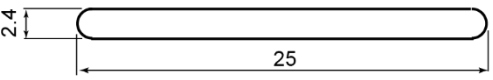
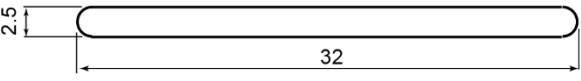
Laser beam shape (mm)	Laser spot area (mm ²)	Laser power (kW)	Power density (kW/mm ²)
	59.72	6	0.10
	79.90	6	0.08

Figure 5.39 displays the laser beam profiles of narrow beam applied in this study found that adjustment of laser irradiation angle tilted up can decrease the power density on the top area of groove weld such as the laser spot size of 25x2.4 mm, laser irradiation angle of 10° having lower power density than 5° of irradiation angle adjusted.

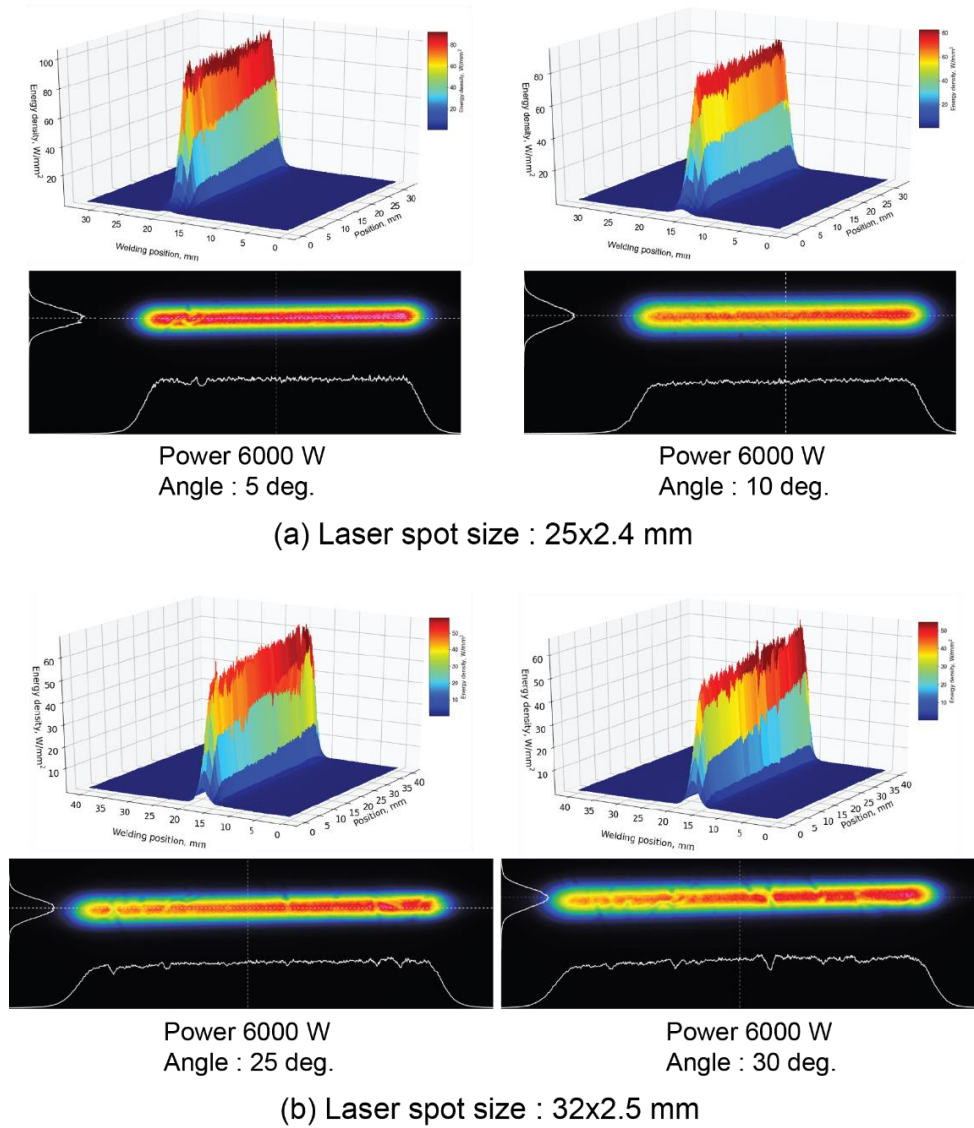


Fig. 5.39 Laser beam profiles.

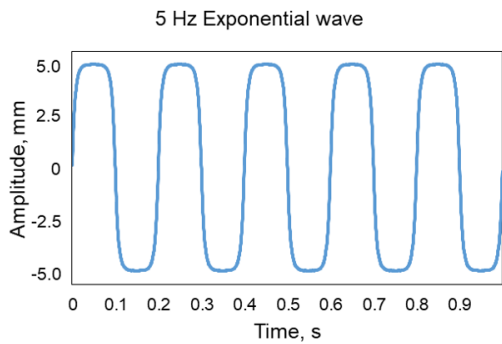


Fig. 5.40 Exponential weaving waveform at 5-Hz.

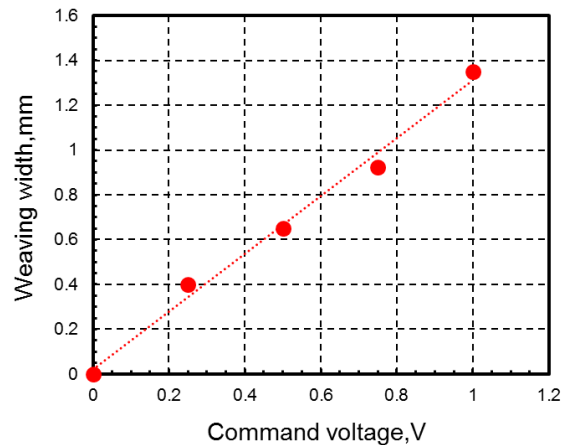


Fig. 5.41 Relationship between command voltage and weaving width.

Laser weaving head was used under a weaving motion of laser beam throughout a groove weld. The laser energy density was transmitted through the laser beam movement while moving, and the laser energy density was changed over time because of distinctive interaction time. The weaving frequency and weaving waveform was 5-Hz exponential wave as shown in Fig. 5.40. For used weaving width was determined under adjusting a command voltage and controlled by the function generator as shown the relationship between command voltages set and weaving width obtained in Fig. 5.41.

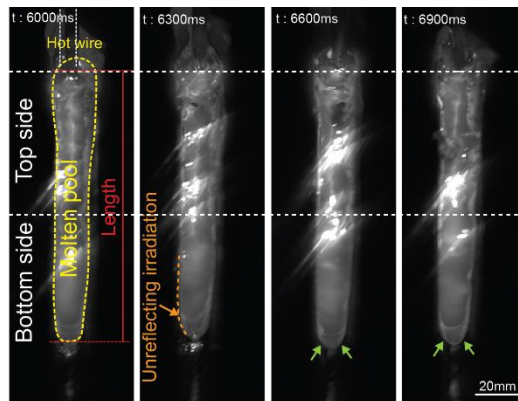
5.5.3 Results and discussion

5.5.3.1 Molten pool and bead formations

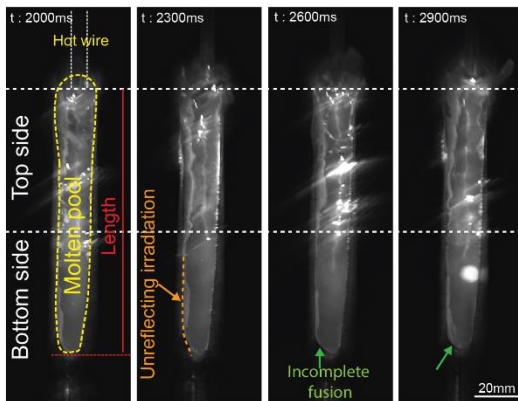
The results of experiment by adjusting the laser irradiation angle of weaving and fixed head, high-speed images during welding of one second with using weaving frequency of 5-Hz, weaving width of 0.65 mm was set. It was found that the middle till bottom side of groove weld was not the unreflecting irradiation when used according to the welding condition as shown in Fig. 5.42(a). Adjusting the angle of laser weaving and fixed heads as shown in Figs 5.42(b) and (c) still had the incomplete fusion and unreflecting irradiation on the bottom side. However, both conditions could create the longer molten pool when compared with using both low laser angles as shown in Fig. 5.42(a). Preliminary results using the different laser beam size from observation of all welding phenomena can be seen in Fig. 5.42. The sizeable molten pool shape was created using the laser weaving head of 25x2.4 mm and angle of 10°, and laser fixed head of 32x2.5 mm and 30° when compared with other conditions as shown in Figs. 5.42(a) and (b).

Chapter 5

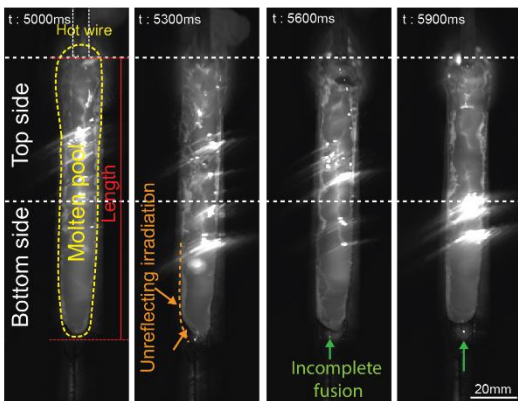
Development of hot-wire double lasers welding method for thick steel plate



(a) Diode laser weaving head : 25x2.4 mm (6 kW), Angle : 5 deg.
Diode laser fixed head : 32x2.5 mm (6 kW), Angle : 25 deg.
Weaving width 0.65 mm.



(b) Diode laser weaving head : 25x2.4 mm (6 kW), Angle : 5 deg.
Diode laser fixed head : 32x2.5 mm, Angle : 30 deg.
Weaving 0.65 mm.



(c) Diode laser weaving head : 25x2.4 mm (6 kW), Angle : 10 deg.
Diode laser fixed head : 32x2.5 mm, Angle : 30 deg.
Weaving 0.65 mm.

Fig. 5.42 High-speed images on several laser irradiation angles.

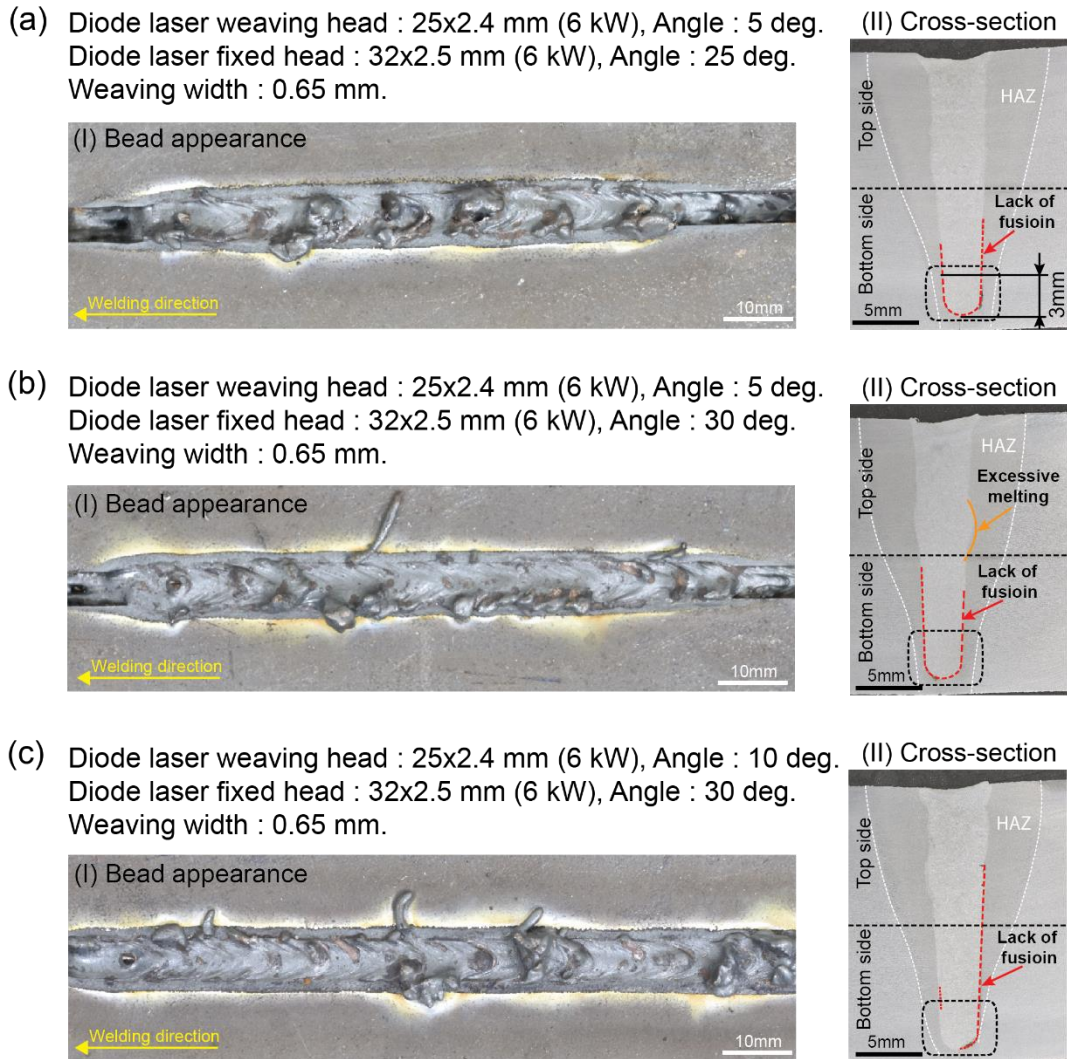
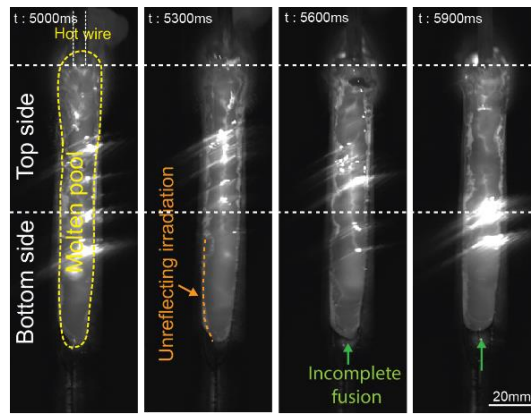


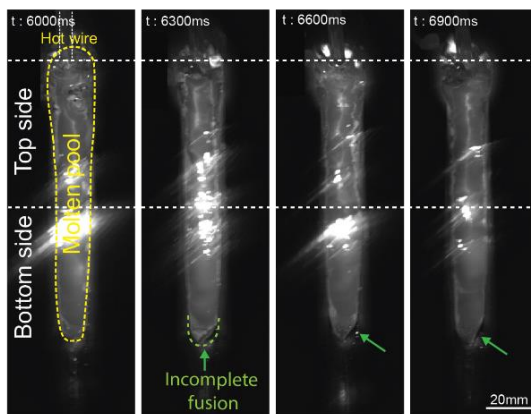
Fig. 5.43 Weld bead and cross-section on several laser irradiation angles.

Figure 5.43 shows the bead appearances and cross sectional views which were performed in each condition. The weld beads could be adequately fed the hot wire on the top side of groove weld and seen the characteristics of weld bead as shown on the cross-sections (II). The laser irradiation angle had a substantial effect on the stable reflecting irradiation on the bottom side. The welded bead with the laser irradiation angle according to as shown in Fig. 5.43(c) was found that the incomplete fusion was least at the root in particular when compared with the other conditions as shown in Figs 5.43(a) and (b).

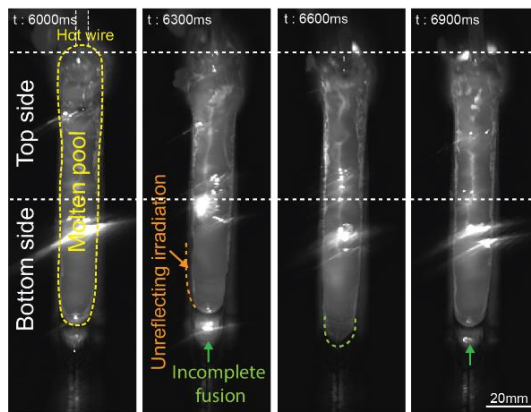
This experiment was carried out to investigating the effect of the laser irradiation angle on the welding phenomena. The weaving head angles of 25x2.4 mm laser beam were set as 10°, and 30° of laser fixed head of 32x2.5 mm, while the constant welding condition was the weaving width of 0.65 mm. Therefore, the changed laser irradiation angle had a substantial effect on the incomplete fusion at the root in particular as shown in the dotted line where represents the region affected in each welding condition as shown in Fig. 5.43.



(a) Weaving width : 0.65 mm.
 Diode laser weaving head : 25x2.4 mm (6 kW), Angle : 10 deg.
 Diode laser fixed head : 32x2.5 mm (6 kW), Angle : 30 deg.



(b) Weaving width : 1.0 mm.
 Diode laser weaving head : 25x2.4 mm (6 kW), Angle : 10 deg.
 Diode laser fixed head : 32x2.5 mm (6 kW), Angle : 30 deg.



(c) Weaving 1.3 mm.
 Diode laser weaving head : 25x2.4 mm (6 kW), Angle : 10 deg.
 Diode laser fixed head : 32x2.5 mm (6 kW), Angle : 30 deg.

Fig. 5.44 High-speed images on several weaving width.

From previous welding phenomena, the angles of laser weaving head of 10° , and 30° of laser fixed head were carried out with the weaving width of 0.65 mm which slightly had some defect. It was determined for investigating the effect of laser irradiation by using wider weaving beam width, the molten pool phenomenon as shown in Fig. 5.44.

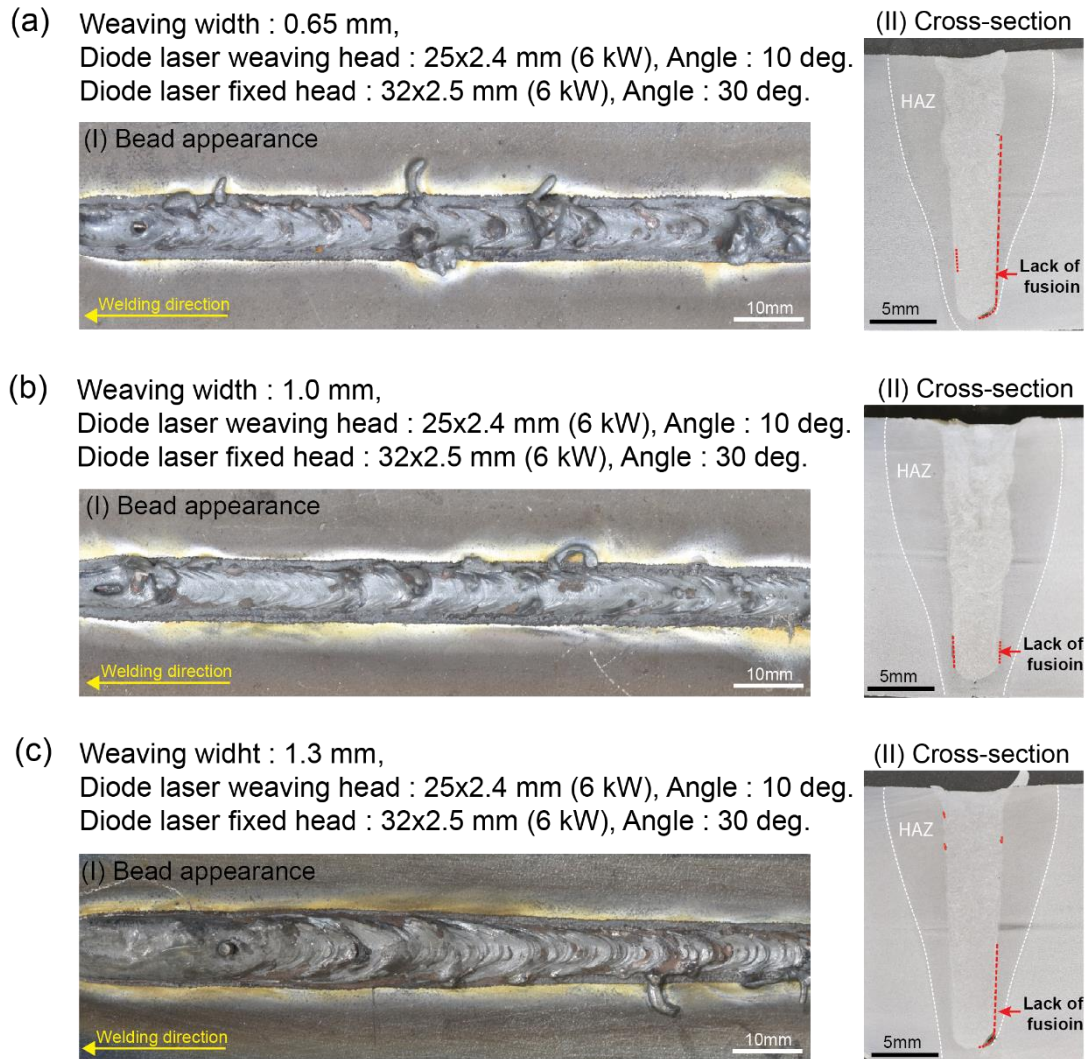


Fig. 5.45 Weld bead and cross-section on several weaving width.

Figure 5.44 shows the welding phenomena from varying the weaving width as 0.65, 1.0, and 1.3 mm, respectively. The results were found that using the weaving beam width of 1.0 mm as shown in Fig. 5.44(b) could create the molten pool on the bottom side of groove weld better than using the weaving width of 0.65 and 1.3 mm as shown in Figs. 5.44(a) and (c), respectively. Due to using the narrow and wide weaving width could not irradiate and reflect on the sidewall and root in particular when viewed the cross sectional profile as shown in Figs. 5.45(a) and (c) because of the incomplete fusion from using both weaving widths. Therefore, when the weaving width

was applied as 1.0 mm, the molten pool formation was stable from the top till bottom side when the cross-section was investigated as shown in Fig. 5.45(b) and found that it slightly had some lack of fusion on the sidewall of groove. Moreover, when the weaving width was adjusted as 1.3 mm, it could irradiate on the top side of groove weld more than the bottom side where can be seen as shown in Fig. 5.45(c), on bead appearance (I) and cross sectional profile (II). Thus, the weaving width adjustment directly affected the molten pool formation, especially in the groove weld's bottom side and sidewall.

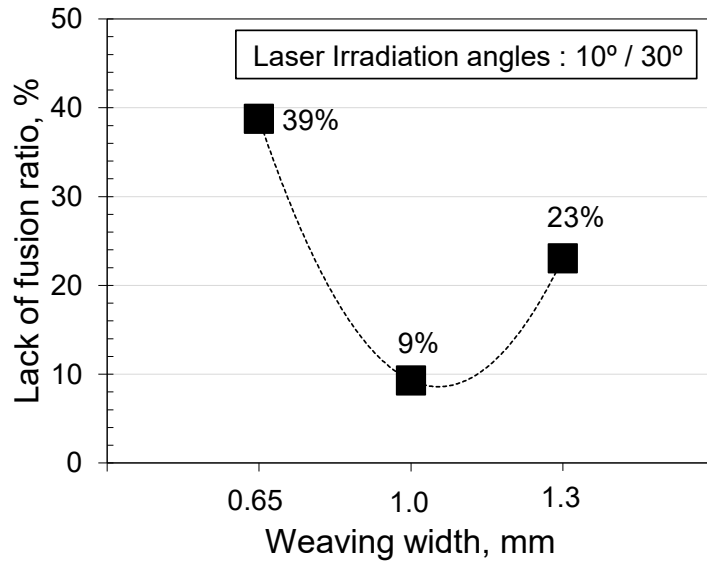


Fig. 5.46 Lack of fusion.

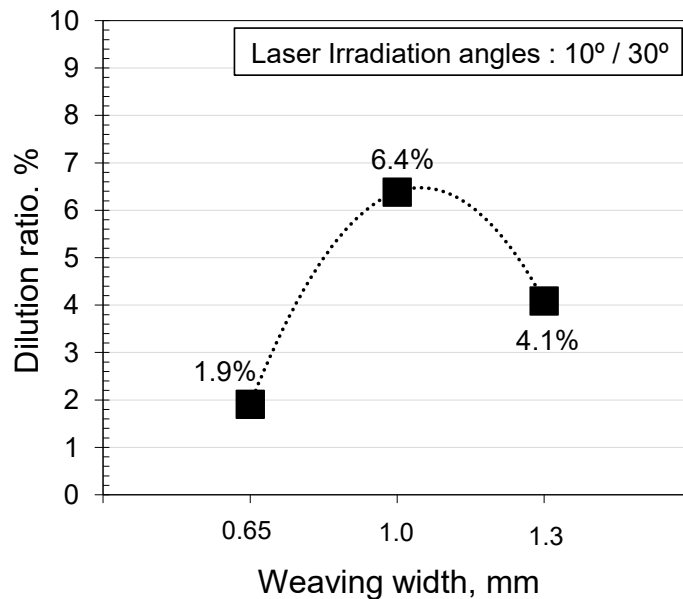


Fig. 5.47 Dilution ratio.

The weld joints and cross-sections were conducted with the determined welding conditions using the weaving system in the narrow gap joining. All welded beads were checked the cross sectional profile to investigate the complete joint creation and fusion under changing the weaving widths of 0.65, 1.0, and 1.3 mm, respectively. Some lack of fusion defects remained on the sidewall, which shows the lack of fusion ratio as shown in Fig. 5.46. The lack of fusion appeared of about 39 %, 9 % and 23 %, respectively. The dilution ratio as shown in Fig. 5.47, it was found that using the weaving widths of 1.0 mm had the highest dilution ratio approximately 6.4 %. Compared with the weaving width of 0.65 and 1.3 mm, they gave the value of dilution ratios of about 1.9 % and 4.1 %, respectively.

5.5.3.2 Evaluation of joint properties

The successful condition of the welded joint was carried out under the combination of laser beams of 32x2.5 mm and 25x2.4 mm, laser irradiation angles of 30° and 10°, weaving width of 1.0 mm, and beam position arrangement on the bottom side were used. The evaluation of the joint property was Vickers hardness test, and Charpy impact test for this experiment as listed below.

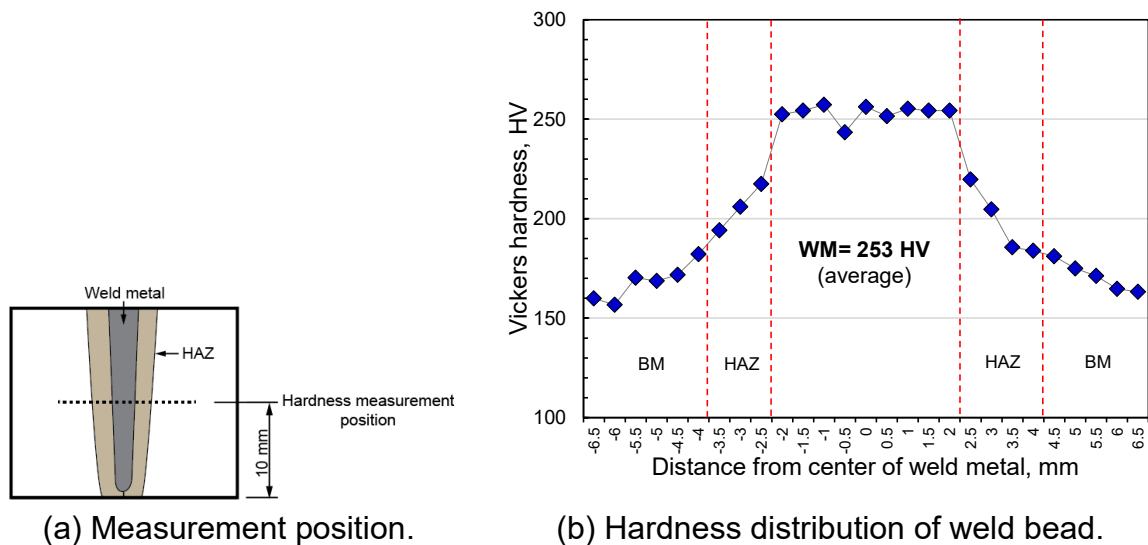


Fig. 5.48 Vickers hardness distribution of welded metal.

Hardness test of the welded part was determined the examined position as shown in Fig. 5.48(a). The result of Vickers hardness distribution of weld metal had a high hardness level and gave the average of weld metal approximately 253 HV which was harder than the base metal of about 80 HV as shown in Fig. 5.48(b). It is assumed that the filler wire used gave the high hardness of weld metal zone and suggested that

the weld metal can be improved the hardness when is selected the appropriate filler wire.

Charpy impact test was performed according to standard specimen size to be JIS Z 2242 as shown in Fig. 5.49. The V-notched specimens were cut-off from the joints welded with specimen size of 10 mm x 10 mm x 55 mm. The toughness property of welded joint was determined the location according to sampling position of the welded part as shown in Fig. 5.50.

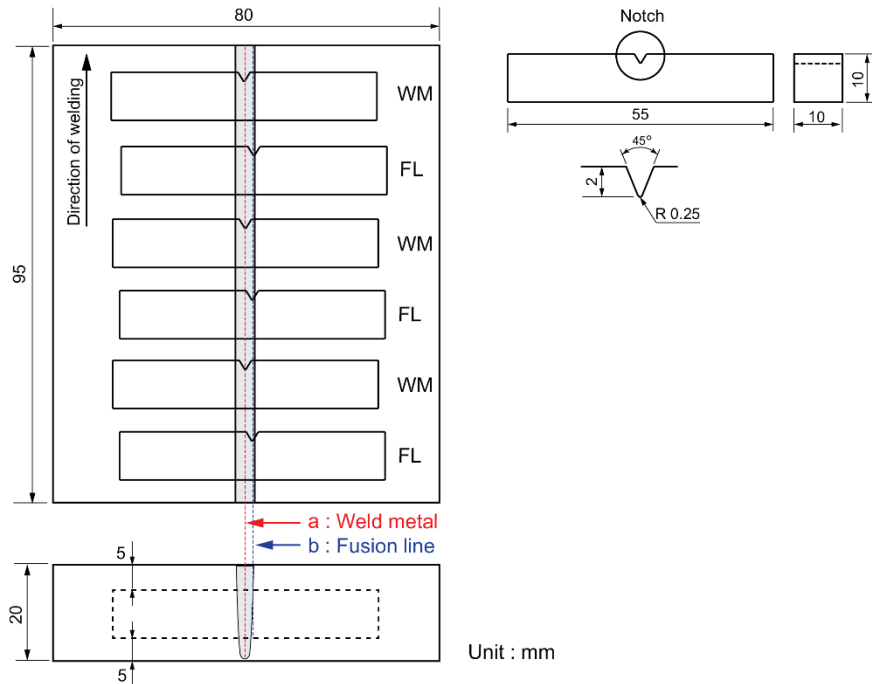


Fig. 5.49 Cutting layout and notch locations.

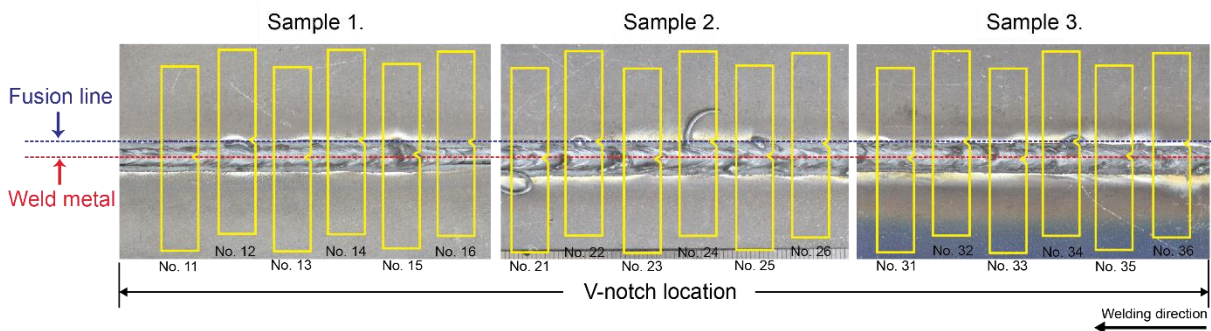


Fig. 5.50 Cut-off plan and notch locations for V-notched Charpy impact test specimen.

Table 5.18 Results of Charpy impact tests.

Specimen number	Notch position	Absorbed energy, J	Defect detection
11	WM	37.6	-
14	WM	25.1	-
22	FL	22.7	-
23	WM	20.3	-
24	FL	20.3	-
26	FL	42.9	-
36	FL	18.0	-
37	WM	18.0	-

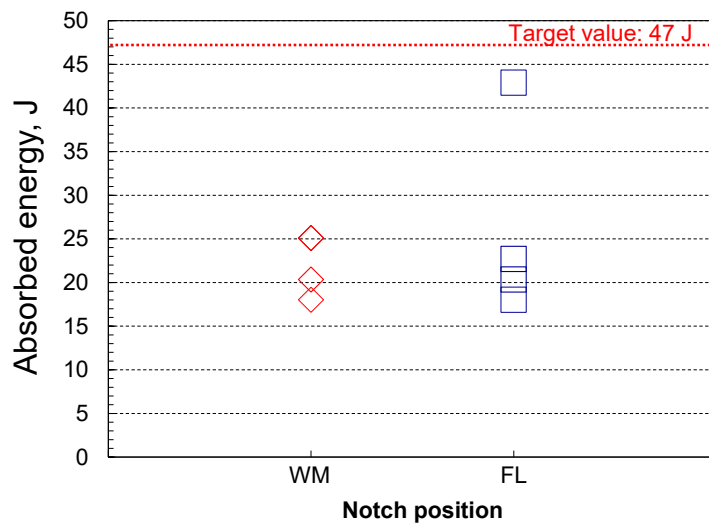


Fig. 5.51 Result of Charpy impact test.

The tested result of Charpy test was shown in Table 5.18. The toughness levels of the two cases, the absorbed energy of weld metal, and the fusion line zone had the low trend of toughness property, as shown in Fig. 5.51. Which had the brittle behavior and gave the value of absorbed energy lower than the minimum average impact test value of the specification requirement of 47J at 0°C test temperature. It was influenced by the high hardness of weld metal, and type of filler wire was used, which had the effect on the mechanical properties of butt joint made by the hot-wire double lasers welding method.

5.6 Summary

The hot-wire double lasers welding method for thick steel plate was studied with thickness 20-mm in the narrow gap. They were performed with both stable laser beams and was used the weaving head system combined with the stable laser beam. The results of optimizing the laser spot size and investigating the butt joint properties can be drawn as follows:

- 1) The optimal welding conditions of stable laser beam combination on molten pool formation and joint creation, stable laser beam combination of 32x2 mm and 26x2 mm, beam position arrangement on the bottom side, and welding speed of 0.4 m/min, etc. were applied for 20-mm thick steel plate. It could create the longest molten pool shape, and the least molten pool angle. The obtained weld bead was fulfilled under the mentioned condition and performed to evaluate the mechanical properties by the tensile test, Charpy impact test, and Vickers hardness test. The results found that both tensile strength and absorbed energy provided the specification's requirement but the hardness of weld metal was higher than the base metal.
- 2) The combination of stable and weaving laser beam was applied to study the effects of molten pool formation and joint creation. It was found that the optimal condition from the combination of double laser beams was 32x2.5 mm and 25x2.4 mm, and angle of fixed and weaving head as 30°, and 10°. While weaving width of 0.65 mm was used. It could be fulfilled in groove weld but slightly had some lack of fusion on the bottom side due to the insufficient power density to reflect in the root in particular. The weld metal gave the high hardness value. Therefore, it affected the low toughness property on the weld and fusion zone.

Chapter 6

Summary and future work

This research aims to develop a high-efficiency and low-heat-input welding process by using a hot-wire system. The hot-wire CO₂ arc welding method is applied to a thick weld joint of 20-mm and 36-mm. The hot-wire double lasers welding method is carried out with 20-mm thickness to increase the weldability and reduce the heat input by feeding the hot wire and using the low laser power. Both were studied under different conditions for obtaining the filled-up sound beads without any defects and compared the mechanical properties evaluation for the welded joint in each achieved condition.

The first part of study, the background of research, and aim and construction of thesis were discussed. Then, the present research on the hot-wire CO₂ arc welding process for the butt joint of 20-mm thickness was reviewed and summarized. For this method has been developed for improvements in productivity, and quality especially in the welding process for the thick steel plates. The welding conditions have been optimized to improve the high-efficiency welding without the requirement for a large increase in heat input to control joint properties. The optimization of welding conditions using the several combinations of hot-wire feeding speed and welding current, they were determined under maintaining the stable arc and balancing the total wire feeding speed in each condition. The achieved weld bead was fully filled by deposited metal in the two passes. The dilution ratio and heat affected zone were influenced by the low welding current and high hot-wire feeding speed due to changed heat input and blocked arc force from the hot-wire feeding. In the mechanical properties of joint, Vickers hardness of weld metal gave the lower value when was applied to the high welding current and low hot-wire feeding speed. The Charpy impact test, tensile test, and transverse side bending test were obtained on welded joints created with the optimized combinations of welding current and hot-wire feeding speed.

In the second part, the hot-wire CO₂ arc welding process was applied with the thickness of 36-mm of steel plate by the determined conditions under each changed bead width of the previous pass. All passes of weld metal were observed the welding phenomena by high-speed camera image for confirming the appropriate condition from the combination of CO₂ wire and hot-wire volume. Therefore, the influence of hot wire and its arc affected the stable molten pool when were used below the limitation of total filler wire feeding in each bead width on the next pass. The wider bead width could keep the high volume of CO₂ wire and hot wire better than the narrower bead width. Thus, the sound joints were achieved under using the optimized conditions. The sound beads were investigated on the cross-section and

evaluated the mechanical properties. Experimental results showed that Vickers hardness of weld metal gave the high value when fed the higher hot-wire feeding speed due to high cooling rate, which affected the molten pool's temperature. For Charpy impact test, tensile test and bending test met the standard requirements without any defects.

Finally, the hot-wire double lasers welding method for thickness 20-mm of steel plate was performed with the total laser power of 12 kW and differently was used under two conditions. In the first part, it was fixed both laser beads for welding in the root gap of 2 mm. The second part, it was used with the weaving head system and stable laser beam for welding in the root gap of 3 mm. Using both welding systems, the main factor was found that the combination of long laser beams could create the longest molten pool. At the first study, the obtained condition achieved by using stable laser beam combination of 32x2 mm and 26x2 mm, welding speed of 0.4 m/min, beam position arrangement on the bottom side. The weld bead without any defect, it had the deep penetration throughout the sidewall and un-melty on the open groove. Hence, the sound bead obtained was tested the mechanical properties with the Vickers hardness test, tensile test, Charpy impact test for assessing the butt joint using double lasers welding method by the low laser power. Those test results complied with the standard value and without any defects when they were investigated. In the studied second part, the laser beam combination of 32x2.5 mm and 25x2.5 mm was used with weaving head system. While the both laser irradiation angles of 30° (fixed head) and 10° (weaving head), weaving width of 0.65 mm, beam position arrangement on the bottom side of groove weld and welding speed of 0.3 m/min were applied. In the Charpy impact test's joint property, the absorbed energy was lower than the specification requirement due to the weld metal's high hardness and some defects on the groove sidewall.

The high-efficiency welding technology for heavy-thick steel plates using hot-wire CO₂ arc welding and hot-wire double lasers welding method have been successfully developed. Therefore, the future work is to balance the mechanical properties of the hardness and toughness of the weld metal by using various filler wires. For the development of the hot-wire double lasers welding method, the increase of higher laser power on narrow gap welding for the thickness of 20-mm should be studied using adequate laser power for joint creation and molten pool formation. Both proposed welding methods would be alternative method for thick steel plate, it can increase productivity and reduce welding consumable.

Acknowledgements

Firstly, I would like to express my sincere gratitude to my advisor Prof. Motomichi Yamamoto for his guidance, encouragement and insight throughout this study. He gave me full support not only with my research, but also with my life and career, and has played an important role in both my academic and personal development.

I would like to thank Prof. Kenji Shinozaki. He gave me so much positive help and instructive discussion in my study, and I have learned so much from him. Additionally, I extend many thanks to Prof. Kazuhiro Matsugi, Assoc. Prof. Ryutaro Hino, Assoc. Prof. Eiji Shintaku, and Assoc. Prof. Yoshikazu Tanaka for their insightful comments and encouragement, but also for the hard question which incited me to widen my research from various perspectives.

I would like to thank TSUNEISHI SHIPBUILDING Co., Ltd.: Mr. Shinichiro Shinohara, and Mr. Hisao Narimatsu. They gave the financial support, materials and specimen for this research in the “Joint R&D with Industries and Academic Partners” research program.

I would like to thank the past members of my research group: Mr. Yutaro Yamada, Mr. Hisato Ogasawara, Mr. Shota Imoto, and Mr. Hirofumi Yamada. I would also like to thank all the past and present members of the Materials Joining Science and Engineering Laboratory, in the Department of Mechanical Science and Engineering, Hiroshima University, for their enthusiastic help to both my life and study.

I would like thank my parents for their support and encouragement from my youth to my time as a doctoral student. Their teaching is gratefully appreciated and has been invaluable in my life.

Reference

- 1) Y. Okumoto: "Applications of welding and joining technology (Shipbuilding)", Journal of the Japan Welding Society, 79-6 (2010), 593-598. (in Japanese)
- 2) T. Miyazaki: "Advances in production technology of shipbuilding and the guidance for future development", Journal of the Japan Welding Society, 70-1 (2001), 21-27. (in Japanese)
- 3) Image courtesy of Tsuneishi shipbuilding Co., Ltd. (in Japan)
- 4) N. Oda: "New technical trend of shipbuilding steel", Journal of the Japan Welding Society, 86-2 (2017), 80-84. (in Japanese)
- 5) T. Inoue, J. Otani: "New technical trend of shipbuilding steel", Journal of the Japan Welding Society, 79-8 (2010), 714-716. (in Japanese)
- 6) S. Okano, Y. Obana, K. Abe, K. Hosoi: "Latest technical trends in steel plate and action in kobe steel", Kobe Steel Eng. Reports, 58-1 (2008), 2-7.
- 7) R. Uemori, M. Fujioka, T. Inoue, M. Minagawa, H. Shirahata, T. Nose: "Steels for marine transportation and construction", Nippon Steel Technical Report, 391 (2011), 37-47.
- 8) K. Ito, S. Nagaoka, T. Hashimoto, T. Kurokawa: "Newly developed and high quality flux-cored wire for shipbuilding and bridge construction", Kobe Steel Engineering Reports, 54-2 (2004), 15-19.
- 9) B. K. Sprovastava, S. P. Tewari, J. Prakash: "A review on effect of arc welding parameters on mechanical behaviour of ferrous metals/alloys", International Journal of Engineering Science and Technology, 2-5 (2010), 1425-1432.
- 10) H. baba, T. Era, T. Ueyama, M. Tanaka: "Single pass full penetration joining for heavy plate steel using high current GMA process", Welding in the World, 61 (2017), 963-969.
- 11) H. Sumi, T. Kataoka, Y. Kitani: "Application of narrow gap welding process with "J-STAR Welding" to shipbuilding and construction", JFE technical report, 34 (2014), 44-49.

- 12) I. Kimoto, R. Mtomatsu: "CO₂ gas shielded one-side welding process two electrodes "NS-Oneside MAG"", Nippon Steel Technical Report, 95 (2007), 11-16.
- 13) G. E. Riding, R. C. Thomson, G. Thewlis: "Prediction of multiwire submerged arc weld bead shape using neural network modeling", Science and Technology of Welding and Joining, 7-5 (2002), 265-279.
- 14) K. Nagatani, M. Komura: One-side Submerged Arc Welding "the key to modern ship construction", Kobe Steel Engineering Reports, 50-3 (2000), 70-73.
- 15) N. Okui: "Active control of welding parameters in deviating weld groove-automatic control system for 3-electrode One-side Submerged Arc Welding with flux copper backing (Report 1)"-, Quarterly Journal of The Japan Welding Society, 18-2 (2000), 288-294. (in Japanese)
- 16) Dae-Won ch., et al.: "Molten pool behavior in the tandem submerged arc welding processDae", Journal of Materials Processing Technology, 214 (2014), 2233-2247.
- 17) T. Yokura: Practical Lecture "A class in joining & Welding-shipbuilding (Process & Construction)", Journal of the Japan Welding Society, 81-6 (2012), 43-50. (in Japanese)
- 18) Y. Lu, J. Chena, Y. Zhanga, L. Kvidahl: "Predictive control based double-electrode submerged arc welding forfilet joints". Journal of Manufacturing Processes, 16 (2014), 415-426.
- 19) Welding Science and Technology, (Hand book).
- 20) K. Isamu, M. Ryuichi: "CO₂-gas-shielded one-side welding process two-electrode "NS-Oneside MAG®"", Nippon Steel Technical Report, 95 (2007), 11-16.
- 21) F. Chen-fu, H. Bin, Z. Zhong-chao, H. Xiao-guang, et al.: "Comparative study on processing property between CWW CO₂ gas shielded welding and SAW". Journal of Iron and Steel Research, International (2013), 20(4), 81-86.
- 22) Z. Yang, et al.: "Arc behavior and droplet transfer of CWW CO₂ welding". Journal of Iron and Steel Research, International (2016), 23 (8), 808-814.

- 23) K. Shinozaki, M. Yamamoto, K. Mitsuhashi, T. Nagashima, T. Kanazawa, H. Arashin: "Bead formation and wire temperature distribution during ultra-high-speed GTA welding using pulse-heated hot-wire", *Welding in the World*, 55 (2011), 12-18.
- 24) R. Phaoniam, K. Shinozaki, M. Yamamoto, K. Kadoi, S. Tsuchiya, A. Nishijima: "Development of a highly efficient hot-wire laser hybrid process for narrow-gap welding -welding phenomena and their adequate conditions", *Welding in the World*, 57 (2013), 607-613.
- 25) T. Tsuyama, K. Nakai and T. Tsuji: "Development of submerged arc welding method using hot wire", *Welding in the World*, 58 (2014), 713-718.
- 26) T. Tsuyama, M. Yuda, K. Nakai: "Effects of hot wire on mechanical properties of weld metal using gas-shielded arc welding with CO₂ gas", *Welding in the World*, 58 (2014), 77-83.
- 27) M. Yamamoto, K. Shinozaki, K. Kadoi, D. Fujita, T. Inoue, M. Fukahori, Y. Kitahara: "Development of hot-wire laser welding method for lap joint of steel sheet with wide gap", *Quarterly Journal of the Japan Welding Society*, 29-3 (2011), 58-61.
- 28) K. Kadoi, K. Shinozaki, M. Yamamoto, K. Owaki, K. Inose, D. Takayanagi: "Development of high-efficiency/high-quality hot-wire laser fillet welding process", *Quarterly Journal of the Japan Welding Society*, 29-3 (2011), 62-65.
- 29) S. Takaya, M. Yamamoto, K. Shinozaki, H. Matsuda and R. Ikeda: "Hot-wire brazing technology for steel/aluminum alloy dissimilar joint", *Quarterly Journal of the Japan Welding Society*, 35-2 (2017), 155-159.
- 30) K. Günther, J. P. Bergmann, D. Suchodoll: "Hot wire-assisted gas metal arc welding of hypereutectic FeCrC hardfacing alloys -Microstructure and wear properties", *Surface & Coatings Technology*, 334 (2018), 420-428.
- 31) H. Emi: "Illustrations of hull structures", Seizando-Shoten Publishing (2006), 123.
- 32) H. Yamamoto: "Production site capabilities related to welding and joining technology for construction machinery", *Journal of the Welding Society*, 76 (2007), 35-38. [in Japanese]

- 33) Yokota, Kibata, Nakao: "Tandem arc welding system". Kobe Steel Technical Report, 54, 2, (2004), 81-85. [in Japanese]
- 34) H. Tamata, M. Yamamoto, K. Shinozaki, N. Fukushima, H. Yamamoto, T. Nakajima, T. Takahashi: "Investigation of proper process conditions of hot-wire MAG welding for butt joint of high-tensile strength steel plate -(Development of high-efficiency and high quality welding technique for high-tensile strength thick-steel plate using hot-wire MAG welding method (4th Report)-", National conference of the Japan Welding Society, 105 (2017-9). [in Japanese]
- 35) ASM INTERNATIONAL, ASM Handbook: "Welding brazing and soldering", Vol.6, US, 1993.
- 36) American Welding Society: "Welding Hand Book", Vol. 1. Welding Science and technology. 9th ed., American Welding Society, USA (2001).
- 37) Dodko, D.A et al.; "Multi-pass welding of thick metal in the shield of carbon dioxide", Automation Welding, 3, (1957), 58-59.
- 38) R. P. Meister and D. C. Martin: "Narrow gap welding process", British Welding Journal, 13 (1966), 252-257.
- 39) M. Ushio, F. Matsuda, I. Masumoto: "Narrow gap welding. Review on NGW in Japan. (Part 2)". Journal of the Japan Welding Society, 54 (1985), 8, 451-455. [in Japanese]
- 40) Cicero M. D. Starling, Paulo V. Marques, Paulo J. Modenesi: "Statistical modeling of narrow-gap GTA welding with magnetic arc oscillation". J. Materials Processing Technology, 51 (1995), 37-49.
- 41) I. Shinji, M. Masatoshi, K. Yuji: "Application of narrow gap welding process with high speed rotating arc to box column joints of heavy thick plates". JFE Technical Report, 14 (2009), 16-21.
- 42) M. Ushio, F. Matsuda, I. Masumoto: "Narrow-gap welding review on NGW in Japan (Part 1)". Journal of the Japan Welding Society, 54 (1985), 6, 358-365. [in Japanese]
- 43) G. A. Hutt: "Narrow gap welding", Metal Construction, June (1984), 355.

- 44) Miikka Karhu, Veli Kujanpää I: "Experimental test set-up for studying hot cracking in multi pass laser hybrid welding of thick section austenitic stainless steel". Laser Materials Processing Conference, ICALEO (2008), 535-544.
- 45) M. Ono, Y. Shinbo, A. Yoshitake, M. Ohmura: "Development of Laser-arc Hybrid Welding". NKK technical review, 86 (2002), 9-12.
- 46) Claus Bagger, Flemming O. Olsen: "Review of laser hybrid welding", Journal of Laser Applications", 17 (2005), doi: 10.2351/1. 1848532
- 47) D. Bajic, G. Vladimirovich Kuzmenko, I. Samardzic: "Welding of rails with new technology of arc welding", Journal of Metalurgija, 52 (2013), 399-402.
- 48) T. Shinoda, K. Hoshino; R. Yamashita, H. Ono: "Development of solidification cracking test for MAG narrow gap welding. Effect of boron contents on solidification cracking". Quarterly Journal of the Japan Welding Society (1990), 8, 1, 21-25.
- 49) S. Tsushima, Y. Horii, N. Yurioka: "Development of AC-MIG welding process (Report 5). Application of AC-MIG narrow gap welding process for butt joints of 980MPa high strength steels". Quarterly Journal of the Japan Welding Society (1994), 12, 1, 51-57.
- 50) K. HORI and M. HANEDA: "Narrow gap arc welding", Journal of the Japan Welding Society (1999), 68, 3, 41-62. [in Japanese]
- 51) V.Y. MALIN: "The State of the art of narrow gap welding", Welding Journal, April (1983), 22 and June (1983), 37.
- 52) M. Persson: " Fully automation welding of thick walled pressure vessel by the narrow gap subaer process", J. Materials and Design (1985), 6, 5, 244-247.
- 53) Chandel, R.S Bala, S.R: "Effect of welding parameters and groove angle on the soundness of root beads deposited by SAW process, Advance in Welding Science and Technology", ASM (1983), 379-385.
- 54) www.ametinc.com/.../AMET_Narrow_Gap_SAW

- 55) K Hori, H Watanabe, K Kusano, T Myoga: "Development of hot wire TIG welding methods using pulsed current to heat filler wire- research on pulse heated hot wire TIG welding processes". *Journal of Welding International* (2004), 18, 6, 456-468.
- 56) Cicero M.D. Starling, et al.: "Statistical modelling of narrow-gap GTA welding with magnetic arc oscillation", *Journal of Materials Processing Technology* 51 (1995), 37-49.
- 57) S. Pike, C. Allen, C. Punshon, P. Threadgill, M. Gallegillo, B. Holmes, J. Nicholas: "Technical Report 09-05. "Critical review of welding technology for canisters for disposal of spent fuel and high level waste", TWI, Ltd., (2010).
- 58) S. Tsubota, T. Ishide, M. Nayama, Y. Shimokusu, S. Fukumoto: "Development of 10kW class YAG Laser Welding Technology", *ICALEO* (2000), 219-229.
- 59) S. Katayama, A. Yohei, M. Mizutani, Y. Kawahito: "Development of deep penetration welding technology with high brightness laser under vacuum", *Physics Procedia*, 12 (2011), 75-80.
- 60) J. Frostevarg: "Factors affecting weld root morphology in laser keyhole welding", *Optics and Lasers in Engineering*, 11 (2018), 89-98.
- 61) Y. Qi, G. Chen: "Root defects in full penetration laser welding of thick plates using steady electromagnetic force", *Journal of Materials Processing Tech.*, 260 (2018), 97-103.
- 62) M. Karhu, V. Kujanpaa, M. Pesari, B. Ievesy: "Comparison of laser welding methods in position welding edge joint of austenitic stainless steel", *NOLAMP 14, Gothenburg* (2013), 46-58.
- 63) B. Chang, Z. Yuan, H. Pu, H. Li, H. Cheng, D. Du, J. Shan: "A comparative study on the laser welding of Ti6Al4V alloy sheet in flat and horizontal positions", *Appl. Sci.*, 7, 376 (2017), 1-12.
- 64) B. Chang, Z. Yuan, H. Pu, H. Li, H. Cheng, D. Du, J. Shan: "Study of gravity effects on titanium laser welding in the vertical position", *Materials*, 10, 1031 (2017), 1-12.

- 65) R. Phaoniam: "Evaluation and prediction method for solidification cracking during hot-wire laser welding with a narrow gap joint and GMAW process using computational simulation", Doctoral dissertation, Hiroshima University, 2014.
- 66) R. Phaoniam: "Evaluation and prediction method for solidification cracking during hot-wire laser welding with a narrow gap joint and GMAW process using computational simulation". Hiroshima University, Doctoral thesis (2014).
- 67) K. Shinozaki, M. Yamamoto, Y. Nagamitsu, T. Uchida, K. Mitsuata, T. Nagashima, et al: "Melting phenomena during ultra-high-speed GTA welding method using pulses-heated hot-wire", Quarterly J. JWS, 27, 2 (2009), 22-26.
- 68) S. Ueguri, Y. Tabata, T. Shimizu, T. Mizuno : "A Study on control of deposition rate in hot-wire TIG welding", Quarterly J. JWS, 4 (1986), 24-30.
- 69) K. Hori, H. Watanabe, T. Myoga, K. Kusano: "Development of hot wire TIG welding methods using pulsed current to heat filler wire", Welding International, 18, 6 (2004), 456-468.
- 70) R. Phaoniam, K. Shinozaki, M. Yamamoto, K. Kadoi, S. Tsuchiya, A. Nishijima: "Development of a highly efficient hot-wire laser hybrid process for narrow-gap welding-welding phenomena and their adequate conditions", Weld World, 57 (2013), 607-613.
- 71) R. Phaoniam, M. Yamamoto, K. Shinozaki, M. Yamamoto, K. Kadoi: "Development of a heat source model for narrow-gap hot-wire laser welding", Quarterly J. JWS, 31, 4 (2013), 82-85.
- 72) K. Kadoi, K. Shinozaki, M. Yamamoto, K. Owaki, K. Inose, D. Takayanagi: "Development of high-efficiency/high-quality hot-wire laser fillet welding process", Quarterly J. JWS, 29, 3, 62-65.
- 73) D. Okita, T. Kado, M. Yamamoto, K. Shinozaki, K. Kadoi: "Weld defect prevention for fillet welded joints on steel plates coated with shop primer using hot-wire laser welding", Quarterly J. JWS, 33, 2, 98-101.
- 74) M. Yamamoto, K. Shinozaki, K. Kadoi, D. Fujita, T. Inoue, M. Fukahori, et al.: "Development of hot-wire laser welding method for lap joint of steel sheet with wide gap", Quarterly J. JWS, 29, 3 (2011), 58-61.

- 75) E. Warinsiriruk, K. Hashida, M. Yamamoto, K. Shinozaki, K. Kadoi, T. Tanino, et al.: "Welding phenomena during vertical welding on thick steel plate using hot-wire laser welding method", Quarterly J. JWS, 33, 2 (2015), 143-147.
- 76) E. Warinsiriruk, K. Hashida, M. Yamamoto, K. Shinozaki, H. Yajima, T. Tanino, et al.: "Oblique laser irradiation technique for vertical welding of thick steel plates employing hot-wire laser welding", Quarterly J. JWS, 33, 4 (2015), 326-331.
- 77) E. Warinsiriruk: "Development of vertical welding technology on thick steel plate using hot-wire laser welding method", Doctoral Dissertation, Hiroshima University, (2015).
- 78) M. Kouhei: "Development of vertical welding process for thick steel plate using hot-wire laser welding method", Master thesis, Hiroshima University, (2016).
- 79) S. Charunetratsamee: "Development of vertical welding technology for heavy-thick and Ni steel plate using hot-wire laser welding method". Doctoral Dissertation, Hiroshima University, (2019).
- 80) Shiga, Ota, Hiraoka, Tsukamoto: "Welding of frontier structural materials". Journal of the Welding Society, 66, 8 (1997), 609-614.
- 81) D. Okida: "Development of thick plate butt welding technology by hot wire laser welding". Hiroshima University, Master's Thesis (2014).
- 82) M. Yudai: "High-strength steel plate hot wire/laser welded part effect of fitting conditions on mechanical properties". Hiroshima University, Master's Thesis (2016).
- 83) R.-S. Huang, L.-M. Liu, G. Song: "Infrared temperature measurement and interference analysis of magnesium alloys in hybrid laser-TIG welding process". Materials Science and Engineering, 447 (2007), 239-243.
- 84) C. Chen, et al.: "Effect of beam oscillation on microstructure and properties of laser-TIG hybrid welding of D406A ultra-high strength steel". Journal of Manufacturing Processes, 57 (2020), 798-805.
- 85) A.-V. Bîrdeanu, C. Ciucă, A. Puicea: "Pulsed LASER-(micro)TIG hybrid welding: Process characteristics". Journal of Materials Processing Technology, 212 (2012), 890-902.

- 86) L. Liu, X. Hao, G. Song: "A new laser-arc hybrid welding technique based on energy conservation". *Materials Transactions*, 47, 6 (2006), 1611-1614.
- 87) H. Koga, et al.: "First application of hybrid laser-arc welding to commercial ships". *Mitsubishi Heavy Industries Technical Review*, 47, 3 (2010), 59-64.

Published or Submitted Papers in Regard to This Thesis

1. **S. Wonthaisong**, Y. Yamada, M. Yamamoto, K. Shinozaki, S. Shinohara :
“Development of High-efficiency Welding Technology for Thick steel Plate using Hot-wire CO₂ Arc Welding Method”, Proceedings of The 8th Asia-Pacific IIW International Congress, Thailand, 2019, p.49-52. (Chapter 3)
2. **S. Wonthaisong**, S. Shinohara, K. Shinozaki, R. Phaoniam, M. Yamamoto :
“High-Efficiency and Low-Heat-Input CO₂ Arc-welding Technology for Butt Joint of Thick Steel Plate Using Hot Wire”, Quaterly J. JWS, Vol. 38(3), 2020, p.199-205. (Chapter 3)

Presentations

1. **S. Wonthaisong**, Y. Yamada, M. Yamamoto, K. Shinozaki, S. Shinohara :
“Development of High-efficiency Welding Technology for Thick Steel Plate using Hot-wire CO₂ Arc Welding Method”, National Conference of JWS, Japan, Vol.103(2018-9), p.388-389. (Chapter 3)
2. **S. Wonthaisong**, H. Ogasawara, M. Yamamoto, K. Shinozaki, S. Shinohara :
“Property Evaluation of Butt Joint made by Hot-wire CO₂ Arc Welding Method”, National Conference of JWS, Japan, Vol.105(2019-9), p.322-323. (Chapter 3)
3. **S. Wonthaisong**, Y. Yamada, M. Yamamoto, K. Shinozaki, S. Shinohara :
“Development of High-efficiency Welding Technology for Thick steel Plate using Hot-wire CO₂ Arc Welding Method”, Proceedings of The 8th Asia-Pacific IIW International Congress, Thailand, 2019, p.49-52. (Chapter 3)